FINGER FLEXOR TENDON ORIENTATION AND LOCATION AS A FUNCTION OF POSTURAL CHANGES OF THE WRIST AND FOREARM: THE QUANTIFICATION OF MUSCULOSKELETAL LOADING IN JOBS WITH DEVIATED FOREARMS

ELIZABETH A. SALAS

A DISSERTATION SUBMITTED TO
THE FACULTY OF GRADUATE STUDIES
IN PARTIAL FULFILLMENT OF THE REQUIREMENTS
FOR THE DEGREE OF
DOCTOR OF PHILOSOPHY

GRADUATE PROGRAM IN KINESIOLOGY
AND HEALTH SCIENCE
YORK UNIVERSITY
TORONTO, ONTARIO

May 2017

ABSTRACT

Forearm pronation/supination is common during manual activities, and has been linked to upper limb disorders in the workplace (Hughes et al. 1997). Forearm deviations from neutral (palm of the hand facing medially) can increase discomfort and forearm musculature activity (EMG) (Khan 2009a; Domizio & Keir, 2010), particularly when combined with wrist postures deviated from neutral. Yet ergonomic tools commonly used to assess the risk of developing distal upper limb disorders (e.g., Strain Index and RULA), often disregard or only minimally account for forearm pronation/supination posture. As a result, the risk of injury may be underestimated.

This dissertation first examined methods of measuring pronation in the workplace by testing instantaneous agreement of forearm posture measurements between Inertial Motion Units (Xsens, Netherlands) and a laboratory-based motion capture system (Vicon, UK). Participants turned metallic and non-metallic handles in front of them, in order to quantify the effect of magnetic disturbance and sensor orientation on the Xsens. On average, RMSE errors of 12.6° around metal, and 8.6° around plastic were observed on instantaneous measures. Higher rotational velocities appeared associated with larger errors. Summarized data revealed smaller discrepancies. Second, this dissertation examined the effect of forearm pronation/supination coupled with wrist flexion/extension on the orientation and location of finger flexor tendons with respect to a radial coordinate system, using MRI of 4 healthy wrists. Pronation/supination caused movement almost exclusively in the frontal plane. Radial tendons exhibited larger angular deviations in pronation, whereas ulnar tendons were nearly straight, and the opposite was observed in supination. Larger angular deviations were thought to increase contact forces within the tunnel in the direction of the bend, which combined with finger movement could increase the

risk of tenosynovitis. Finally the results of these studies were combined to measure tendon movement during a repetitive task. The three tendons with the greatest angular movement in the tunnel were: FDP2 (0.16°/pronation/supination degree), FDS3 (0.15°/ pronation/supination degree), and FDS4 (0.17°/ pronation/supination degree).

DEDICATION

I would like to dedicate this work to my family. This work would not have been possible if I did not have the support of those who surround me. I want to thank my family members and friends for their encouragement in different ways, as each one served a very special purpose. I am grateful to my husband for patiently being by my side throughout this challenging but amazing journey, and for his continuous love and encouragement. Thank you to my boy for his unconditional love and admiration, because it is him who motivates me every day to be the best role model I can be. Special gratitude to my parents: to my mom for her sporadic by powerful words of encouragement, and to my dad for instilling the passion for science and health which I carry with me since I was a little girl – and most importantly, for believing in me so much that I learned to believe in myself.

ACKNOWLEDGEMENTS

I wish to express my appreciation to my committee members for contributing to this work with their guidance and support. I am extremely grateful to my supervisor Dr. Anne Moore for her patient and insightful guidance throughout the years. Thank you for offering additional support without hesitation when I needed it. I have learned so much from you and I admire you deeply, not only as an academic but also as a person. A special thanks to Dr. William Gage for his guidance. Thank you for pushing me to strive for greatness, and motivating me to persevere. Thank you Dr. Keith Schneider, Dr. Jennifer Steeves, and Dr. Michele Oliver for your commitment to participate in my committee, and for your insightful contributions.

I also would like to thank my lab mates and volunteers, particularly Andrew Dang, Andrew Lagree, and Anthony Tse, who contributed greatly to various stages of this research. Their excitement to learn and willingness to help made this project more enjoyable. Special thanks to my friend Dr. Tina Mayberry, who worked with me through countless hours of proofreading, while helping me to stay focused.

Finally, I would also like to thank each one of my university lecturers, who helped me build my academic foundations to successfully complete this dissertation. Thank you.

TABLE OF CONTENTS

LIST OF TABLES

LIST OF FIGURES

ABREVIATIONS

List of Common Abbreviations in this Thesis			
Common		**Anatomical**	
CS	Coordinate System	*CT*	Carpal Tunnel
CTS	Carpal Tunnel Syndrome	*DRUJ*	Distal Radio-ulnar Joint
EMG	Electromyography	*ECRB*	Extensor Carpi Radialis Brevis
IMUs	Inertial Motion Units	*ECRL*	Extensor Carpi Radialis Longus
MSD	Musculoskeletal Disorders	*ECU*	Extensor Carpi Ulnaris
MSK	Musculoskeletal Loading	*EDC*	Extensor Digitorum Communis
NM	Neutral-mid Reference trial in MRI studies	*EDM*	Extensor Digitorum Minimi
ROM	Range of Motion	*FCR*	Flexor Carpi Radialis
		FCU	Flexor Carpi Ulnaris
		FDP	Flexor Digitorum Profundus
		FDS	Flexor Digitorum Superficialis
		FPL	Flexor Pollicis Longus
		IP	Interphalangeal Joints
		MP	Metacarpophalangeal Joints
		MS	Metacarpal Styloid of 3rd Metacarpal
		PL	Palmaris Longus
		PRUJ	Proximal Radio-ulnar Joint
		RS	Radial Styloid of Radius
		SSCT	Sub-synovial Connective Tissue
		TFCC	Triangular Fibro-cartilage Complex
		UN	Ulnar Notch of Radius

1 CHAPTER 1. INTRODUCTION

Musculoskeletal disorders (MSDs) is an umbrella term used to describe injuries and disorders of the musculoskeletal (MSK) system, which may involve damage to the muscles, nerves, ligaments, joints, cartilage, and/or spinal discs (OHSCO, 2008). There were nearly 1,200,000 MSDs reported in 2014 in the United States in all sectors, and approximately 30% affected the upper limb (arm, wrist, and hand), making upper extremities the leading injured body part (BLS, 2015). Upper limb injuries require approximately 15 days away from work, and it was estimated that employers spent as much as $20 billion a year on direct costs for MSD-related workers' compensation, and up to five times that for indirect costs, such as hiring and training replacement workers (BLS, 2015).

Common examples of these injuries include carpal tunnel syndrome (CTS), tenosynovitis, tendinitis, and epicondylitis, among others. These disorders have been linked to a variety of risk factors, including high or sustained force, awkward postures, and repetitive activities (Armstrong, et al. 1982). Current guidelines for injury prevention may oversimplify the of risk involved in upper limb injuries, because the potential for harm associated with different work tasks depends on a number of contributing risk factors, such as work exposure, and individual variability. Wells et al. (1990) proposed a model to depict the interrelationships of these factors on the development of tenosynovitis (Figure. 1.1).

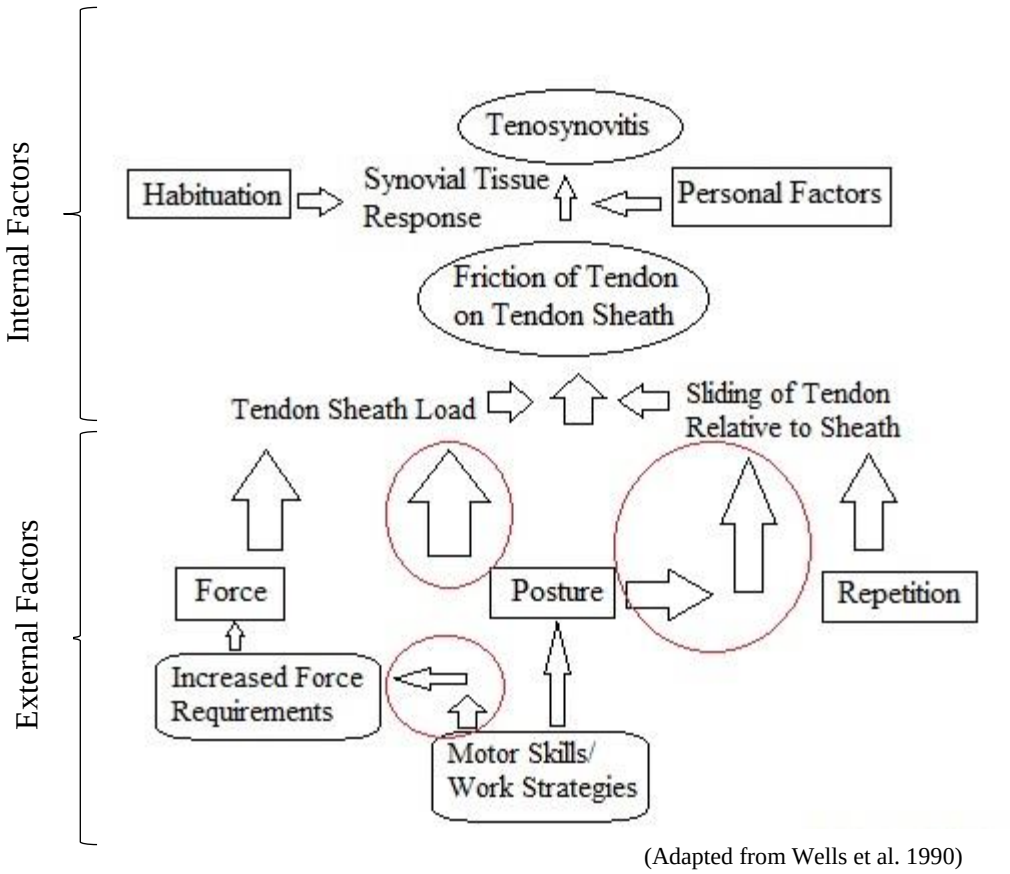

(Adapted from Wells et al. 1990)

Figure 1.1. Depiction of complex inter-relationships between external risk factors and individual factors, in the development of musculoskeletal disorders, using tenosynovitis as an example.

This model shows the injury mechanism of tenosynovitis (beginning with the external risk factors at the bottom), and explaining the effect of posture under loading conditions, and of postural changes (e.g. repetition) on frictional forces at the tendon and tendon sheaths. While individual factors also influence the response to mechanical loading, it is evident that external risk factors should merit further study because of their modifiability.

Although posture alone has been reported to not have as much of an effect as force on MSD risk (Schoenmarklin, et al. 1994), its contribution to injury should not be underestimated, because it magnifies the effects of force and repetition on MSK loading. For instance, Moore et al. (1991) presented a compilation of injury mechanisms for some of the most common

cumulative trauma disorders in the literature at the time, and their respective external risk factors. They reported that sustained posture and/or repetitive postural changes contributed to all injury mechanisms presented for CTS, tenosynovitis, muscle fatigue and overuse. The Bureau of Labor Statistics has long recognized worker postures and motions as the second most common source of exposure resulting in injury at the workplace (BLS, 2015), further supporting the position that posture is a large contributing factor to MSD risk.

Current research has suggested a link between upper limb injuries and forearm postures and motions. Epidemiological evidence shows that years of repetitive pronation and supination can be a predictor of elbow/forearm and hand/wrist disorders in aluminum smelters (Hughes, et al. 1997). Forestry workers requiring pronated forearm postures to operate machinery controls have been reported more often on sick leave due to upper limb injury than those requiring semi-pronated forearm postures (Grevsten & Sjögren, 1996). Other researchers have provided evidence of increased MSK loading associated with forearm postures away from neutral. Forearm EMG increases with pronated forearm during push/pull tasks, and intermittent pronation torques (Domizio & Keir, 2010; Mukhopadhyay, et al., 2007), and increases in carpal tunnel (CT) pressure in full supination with metacarpophalangeal joints (MP) at 90° (Rempel, et al., 1998) have been shown. Others have reported increasing discomfort ratings with forearm postures away from neutral during intermittent pronation torques and, static wrist flexion tasks (Khan, O'Sullivan, & Gallwey, 2009a, 2009b; Mukhopadhyay et al., 2007), and an additive effect on discomfort when combined with wrist postures away from neutral (Khan et al., 2009a, 2009b). Despite evidence showing that forearm pronation/supination contributes to MSK loading, little is known about the role of forearm rotation in injury development, which is need to take steps to minimize injuries at work.

First, it is important to have feasible methods for quantification of forearm pronation/ supination in the workplace. Reliable and portable methodologies to continuously quantify forearm pronation/supination in the workplace have not been validated. Pronation and supination involve rotation around the forearm's long axis (internally and externally, respectively), rather than a movement of one segment with respect to another. This movement can be very fast, reaching higher angular velocities than wrist flexion/extension or radial/ulnar deviation; thus it can be difficult to measure. In spite of this, forearm pronation/supination data are needed for a variety of jobs, in order to understand their forearm postural demands.

Second, little is known about the effect of forearm pronation/supination on the location, orientation, and physical interaction of the MSK structures within the wrist (e.g. finger flexor tendons); this information is relevant for understanding the mechanism of injury associated with postural change. Previous research to investigate the effects of wrist posture on the physical interactions of anatomical structures within the wrist includes: wrist posture effects on flexor tendon deviations at the CT (Keir & Wells, 1999), CT area:tunnel contents ratio (Bower, et al., 2006), and the relative motion between the flexor digitorum superficialis (FDS) tendons and the adjacent paratenon (Kociolek & Keir, 2016). Two main areas that should be targeted are 1) finding reliable ways to measure forearm pronation/supination in the workplace, 2) understanding the role of forearm pronation/supination on the injury mechanisms of the upper limb.

1.1 Thesis Overview

This work will be presented in seven chapters, three of which will be different studies addressing the two goals of this thesis. The goals are:

1) To determine a user-friendly, portable, and reliable method to quantify forearm pronation and supination in the workplace.
2) To study the effects of various forearm pronation/supination and wrist flexion/extension posture combinations on the orientation and location of the FDS and FDP tendons, proximal and distal to the CT.

1.2 Chapters of this Thesis

1.2.1 Chapter 2. Review of Literature

The first section briefly explains the importance of upper limb posture in the development of injury, followed by an epidemiological review to illustrate which features of forearm pronation/supination have been linked to injury. Evidence of biomechanical measures are presented to demonstrate that forearm pronation/supination postures, along with wrist postures away from neutral, seem to increase MSK loading of the upper limb.

The second section of this chapter addresses the first goal, measuring forearm pronation/supination in the workplace. It briefly describes current methods used by ergonomists, and highlights how forearm pronation/supination is often not considered. Challenges of measuring forearm pronation/supination in the workplace are presented, as well as advantages and disadvantages of technologies currently available.

The last section reviews literature associated with the second goal of the study, evaluating the effect of forearm and wrist posture on the orientation and location of the finger flexor tendons. This section begins with a brief description of wrist anatomy and the mechanics of forearm pronation/supination. Current literature about the effects of posture on internal MSK loading, including both cadaveric and in-vivo data, follows. The next piece describes the usability of this particular study, and the challenges currently encountered when attempting to transfer external exposures to internal loading. The section ends by describing the histological impact of internal loading.

1.2.2 Chapter 3. Assessing Forearm Pronation/Supination in the Workplace: A Comparison between Xsens and Vicon Measurements during a Handle-Turning Task.

Forearm pronation/supination is often neglected in evaluations of occupational physical postural exposures. In fact, classic ergonomic tools do not usually take forearm pronation/supination into account (e.g. Strain Index by Moore and Garg, 1995), or evaluate it as a binary variable (i.e. rate it as high-risk only if the forearm is at or near the end of the range of motion (ROM)) (e.g. RULA by McAtamney & Corlett, 1993). However, higher discomfort has been reported when the forearm deviates from neutral by 60% of ROM than when it deviates by 30% (Khan et al., 2009a), which suggests that the amount of forearm deviation from neutral is correlated with MSK loading. Further, the additive effects of forearm and wrist posture on discomfort (Khan et al., 2009a) suggest that simultaneous quantification of forearm and wrist postural requirements is more logical when assessing the risk associated with the postural requirements of work tasks. However, in order to do this, a portable and reliable method is needed to quantify forearm pronation/supination in the workplace.

Widely accepted motion capturing systems such as Vicon (Vicon Motion Systems Inc., Oxford, UK) are commonly used in laboratory settings to quantify posture. However, the use of this system in a workplace setting is not feasible due to logistical challenges (e.g. reflective surfaces, potential interference of people in the collection area, lack of safety of very expensive equipment, and lengthy calibration). Instead, portable systems, such as the Xsens inertial motion units (IMUs) (Xsens Technologies B.V., Enschede, Netherlands), can be used for motion capture in work environments. These IMUs, containing triaxial magnetometers, gyroscopes, and accelerometers, can be attached to different body segments to measure their orientation in space

and thus estimate posture. The data logger carried by the participant records the information and sends it over relatively large distances to a computer via Bluetooth. This technology is practical for field research, as it allows workers mobility in their own environment. Additionally, the Xsens IMUs do not require lengthy calibration procedures, making data collection time-efficient.

Nevertheless, their reliability when measuring forearm pronation/supination in the workplace has not been evaluated, nor has their capability to adjust to common ferromagnetic disturbances at work (e.g. tool use) given that they use magnetometers. Thus, the goal of this study was to evaluate the agreement of forearm pronation/supination measurements made with and without metal in hand, in a handle turning task. It was hypothesized that Vicon and Xsens measurements would have good agreement and that agreement would vary in the presence of metal.

1.2.3 Chapter 4. Evaluation of Finger Flexor Tendon Trajectories at the Wrist as a Function of Forearm and Wrist Postural Change, Using MRI: Introduction and Methods.

This chapter presents the introduction and methodology sections shared by two manuscripts relating to the evaluation of finger flexor tendon trajectories with wrist and forearm postural change. Magnetic resonance imaging (MRI) is shown to successfully reveal the anatomical changes that occur with postural changes and different loading conditions, thus increasing our understanding of mechanisms of injury. For instance, Keir & Wells (1999) were able to demonstrate changes in the path of finger flexor tendons as a function of flexion and extension of the wrist, and Bower et al. (2006) evaluated the effects of wrist flexion/extension and loading conditions (e.g. pinch grip) on the ratio between the CT contents and the tunnel

dimensions. Findings from these two studies helped understand contact forces experienced by the median nerve, and thus the effect of wrist posture on the risk of CTS development.

Because MRI allows visualization of internal structures in a non-invasive manner, it can facilitate great insights by highlighting the internal anatomical changes that accompany postural changes, which can result in increased MSK loading among tissues. The current work used MRI to accomplish its goal of evaluating changes in the finger flexor tendon orientations and locations as a function of the combination of 3 forearm pronation/supination postures (40° pronated, neutral, 60° supinated) and 3 wrist flexion and extension postures (30° flexion, neutral, 30° extension).

This chapter ends by explaining the methodologies used to determine tendon locations proximal and distal to the CT as well as relative angular trajectories between proximal and distal portions of the finger flexor tendons.

1.2.4 Chapter 5 Finger Flexor Tendon Trajectories Proximal to the Carpal Tunnel as a Function of Forearm and Wrist Posture: Results and Discussion.

This chapter delivers findings on tendon locations and angular trajectories proximal to the CT as a function of forearm and wrist posture; the aim is to determine whether finger flexor tendons exhibit greater displacements and angular deviations with larger forearm and wrist posture deviations from neutral. It also presents the amount of tendon displacement and tendon "sweep" (angular movement of the tendon) proximal to the CT, as a function of forearm pronation/supination and wrist flexion/extension. The chapter ends by noting loading implications (at the measurement site and on the forearm) associated with some forearm and wrist posture combinations.

1.2.5 Chapter 6 Finger Flexor Tendon Trajectories Distal to the Carpal Tunnel as a Function of Forearm and Wrist Posture: Results and Discussion.

This chapter introduces findings on tendon locations distal to the CT, and the tendon trajectories through the wrist, as estimated from angle measurements of tendon portions proximal and distal to the tunnel. The aim is to determine whether tendon angular trajectories through the wrist and tendon locations distal to the CT were affected by postural changes of the forearm and wrist. This chapter includes a description of tendon displacement distal to the tunnel, and tendon sweep through the wrist, as a function of forearm pronation and supination, and wrist flexion/extension. The chapter ends by noting the implications of certain forearm and wrist

posture combinations on MSK loading of the wrist, via changes in finger flexor tendon's location and orientation.

1.2.6 Chapter 7 Frontal Tendon Angles Estimates During a Handle Turning Task.

This chapter presents a regression model to estimate frontal angles of the FDP2, FDS3 and FDS4, the tendons with the largest angular sweep observed in the MRI studies, during a continuous task, requiring repetitive pronation/supination. This model was based on the observed relationship between forearm posture and each tendon angle. Descriptive statistics are presented to highlight the estimated tendon angles during two different conditions of the manual task. A discussion explains the potential use of the predicted tendon angles in modelling contact force.

1.2.7 Chapter 8 Summary

This chapter summarizes the findings of each of the three studies in this dissertation. It discusses and compares findings of the two MRI studies. It presents the individual MSK loading implications based on tendon movement from posture at both the wrist and forearm, while distinguishing between the effects of sustained postures and repetitive motions. It illustrates suggested loading mechanisms with diagrams of various wrist-forearm posture combinations, along with sample activities. Finally, it ends by outlining future directions and proposes potential applications of the findings.

2 CHAPTER 2. REVIEW OF THE LITERATURE

2.1 General Overview

2.1.1 Importance of Postural Change in the Development of Injury

Although force is often considered the major loading factor in injury (Descatha, et al., 2003; Goldstein, et al., 1987; Kroemer, 1989; Silverstein, et al., 1986), it is important to recognize that postural change greatly affects the way force is experienced by internal structures. For a given externally applied force, the internal force experienced by finger flexor tendons, as well as the normal forces per unit area between tendons and nearby structures (such as the flexor retinaculum), vary with postural change (Keir & Wells, 1999; Moore et al., 1991). Changes to these loading conditions affect tissue fatigue, and can thus affect the risk of developing an injury. Additionally, the ability to produce gripping force can also be affected by postural change, because of its effects on muscle length of the hand's extrinsic muscles. Thus postural changes have a direct effect on the level of exertion and the resulting risk of developing muscle fatigue and injury; quantifying postural demands during job analyses is as important as quantifying force.

Summary: Although force is considered the major risk factor in injury development, posture can largely affect internal loading experienced in job activities. Thus, investigating posture change is as important as force evaluation during job analyses.

2.1.2 Epidemiological Links between Forearm Pronation/Supination Postures and MSDs

Forearm pronation/supination has been epidemiologically linked to the development of upper limb injuries of both the wrist/hand, and the forearm/elbow. For example, Hughes et al. (1997) studied several risk factors associated with the development of injury in 104 aluminum smelters, most of whom were carbon setters and crane operators. The relationships between various physical and psychosocial factors on health status were modeled using a multiple logistic regression. It was determined that years of repetitive forearm pronation/supination, was a significant predictor of hand/wrist disorders (Odds ratio or OR =17) and elbow/forearm disorders (OR=37). Similarly, Grevsten & Sjögren (1996) found that forestry machine operators who used controls that required postures with a pronated forearm were more often on sick leave due to upper limb injury than those who used controls requiring semi-pronated postures.

Forearm pronation/supination postures and motions have been associated with the development of several disorders (Descatha et al., 2003; Kroemer, 1989; B A Silverstein, et al., 1986). For example, forearm postures/actions contribute to mechanical loading of the upper limb, as reported in a review of physical factors associated with common upper limb disorders (Kroemer, 1989). Lateral and medial epicondylitis, CTS, wrist tenosynovitis, DeQuervain's disease, ganglion cysts, as well as radial tunnel and pronator teres syndromes, were all found to be related to forearm pronation/supination postures and motions. Silverstein et al. (1986) studied the association between several physical exposures and lateral epicondylitis in workers with a variety of jobs in the private and manufacturing sector. The following were identified as significant predictors of lateral epicondylitis: forearm pronation $\geq$45° for $\geq$40% of the time in combination with forceful exertions and forearm supination $\geq$45° for $\geq$5% of the time when combined with any two types of forceful exertion (e.g. power grip and lifting $\geq$3% of the time).

Similarly, Descatha et al. (2003) investigated the associated factors that may contribute to the development of medial epicondylitis in a working population (N=1757 workers), using surveys and physician assessments. Workers who tended to hold tools in place, use tools forcefully, or turn and screw (OR=1.64 (0.99 –2.71), 1.47 (0.82–2.64), and 1.24 (0.72–2.14) respectively) had a higher risk of developing epicondylitis than those who did not. It is worth noting that epidemiological studies allow us to recognize a relationship between forearm postural demands and injury; however, more work is needed to understand the implications of forearm posture on mechanical loading, and how loading may affect the risk of developing injury.

Epidemiological evidence has identified forearm pronation/supination as a factor in upper limb MSDs; however, more research is needed to elucidate its role.

2.1.3 Biomechanical Evidence Relating Forearm Pronation/Supination Postures and MSK Loading

Recently, several researchers have evaluated the effect of forearm posture, often in combination with wrist and/or finger posture, on a variety of biomechanical measures (Tables 2.1 and 2.2) (Domizio & Keir, 2010; Khan et al., 2009a; Mogk & Keir, 2003; Mukhopadhyay et al., 2007; Rempel et al., 1998; O'Sullivan & Gallwey, 2005; O'Sullivan & Gallwey, 2002; Werner et al., 1997). This section will discuss the effect of forearm pronation/supination on each of these variables.

2.1.3.1 Effect of Forearm and Wrist Posture on Discomfort

The relationship between discomfort and forearm pronation/supination has been previously studied (O'Sullivan and Gallwey, 2005; Mukhopadhyay et al. 2007; Khan et al. 2009). O'Sullivan and Gallwey (2005) studied the effect of eleven forearm postures (75%, 60%, 45%, 30%, 15% and 0% of pronation and supination ROM) on discomfort and torque strength in both directions, while participants performed 1 s, 20% MVC, intermittent pronation and supination torques with a frequency of 10 exertions/min. Pronation torques were more uncomfortable overall than supination torques (5.76 and 4.26 standardized discomfort scores (SDS), respectively, averaged across all forearm postures). Discomfort increased as the forearm moved away from neutral (up to 2.65 SDS points higher at 75% supination ROM compared to neutral, during the supination torque exertion).

Similarly, Mukhopadhyay et al. (2007) studied the effect of three forearm pronation/supination postures (neutral and 60% ROM for pronation and supination), three elbow angles (45°, 90°, and 135° of flexion), two exertion frequencies (10 and 20 exertions/min), and two torque intensities (10 and 20% MVC pronation torque) on discomfort and forearm EMG, while participants performed repetitive pronation torques. Discomfort was rated using a visual analogue scale. Their measurements were taken while the arm was abducted 90° in the coronal plane. Discomfort increased when the forearm moved away from neutral; discomfort (SDS) was higher in pronated postures than in supine.

Additionally, Khan et al. (2009) studied the combined effect of five wrist ulnar and radial deviations (0%, 35% and 55% of radial and ulnar deviation ROM) and five forearm pronation/supination postures (0%, 30% and 60% of pronation and supination ROM) on discomfort during a repetitive, 1-second isometric wrist flexion task, with a frequency of 15

exertions/min and a force of 10N ±1N. The elbow was flexed at 90°, and the upper arm externally rotated approximately 45°. The reported SDS revealed that discomfort increased when either the wrist or the forearm were deviated away from neutral. Importantly, deviations away from neutral in both joints had an additive effect on discomfort much larger than a deviation in only one joint (Figure 2.1).

Summary: There may be anatomical changes with forearm deviation postures away from neutral which increase discomfort in the upper limb; the discomfort is magnified when wrist postures also deviate from neutral in the frontal plane.

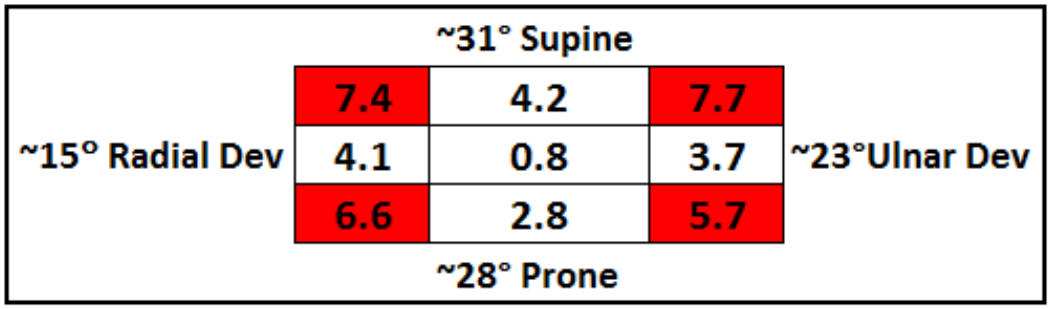

Figure 2.1. Additive effects of both forearm pronation/supination and wrist radial/ulnar deviation on perceived discomfort. Note higher discomfort ratings when combining postures deviated from neutral at both the wrist and forearm. Adapted from Khan et al. 2009.

2.1.3.2 Effect of Forearm Posture on Forearm EMG and Strength

Forearm rotation postures have been shown to affect forearm EMG and force generation ability. Domizio and Keir (2010) evaluated the effect of three forearm postures (pronation, neutral, and supination) on forearm EMG during a variety of isometric tasks, including: gripping (15%, 30% and 50% of maximum grip force), push/pull actions (30N push, 30N pull), or a combination of the two (30N push with 15% gripping force, 30N pull with 15% gripping force). It was reported that forearm extensor EMG generally increased as the forearm moved from supination to pronation while gripping, with or without pushing/pulling force.

Mukhopadhyay et al. studied the effect of forearm and elbow posture, exertion frequency, and torque intensity on EMG of the extensor carpi radialis brevis (ECRB) during repetitive pronation torques. The ECRB EMG increased when the forearm was prone, and decreased when it was supine, compared to neutral. No effect of elbow flexion angle was reported when 45° and 135° angles were compared to 90°. A supplementary experiment was carried out to determine the effect of elbow and forearm posture on pronation torque strength, using the same postures as in the main experiment. Pronation torque strength was highest when the forearm was supine and lowest when it was prone, independent of elbow angle. These findings were echoed by the discomfort scores (i.e., there was more discomfort at lower pronation torque strengths).

Similarly, O'Sullivan and Gallwey (2005) found weaker pronation torque strength in more pronated forearm postures (75% ROM prone) compared to neutral or supinated ones (75% ROM supine). Additionally, their study reported steep linear decreases in supination torque strength as the forearm deviated from neutral to 75% ROM supine (14.8Nm to 10.7Nm of maximum torque strength in neutral and supine, respectively).

In another study, O'Sullivan and Gallwey (2002) studied maximum pronation and supination torques at different elbow angles (0°, 45°, 90°, and 135°) and forearm angles (75% prone, neutral, and 75% supine). They collected torque strength data in different postures that are common in the industry, as well as EMG data of muscles that could potentially be at risk of injury. It was determined that supination torque strength was higher than pronation torque strength. Supination torque strength was more affected by forearm pronation/supination, decreasing consistently from 75% ROM prone to 75% ROM supine posture, across all elbow postures. Pronation torque strength did not seem to be as affected by forearm pronation/supination, although lower pronation torques were seen in 75% ROM pronation compared to neutral or 75% ROM supination.

Mogk and Keir (2003) studied the effect of wrist and forearm postures on gripping force. Their results showed a consistent trend of decreasing maximal grip force with pronated forearm, but the differences were only significant while the wrist was flexed. This evidence suggests that forearm pronation/supination changes orientation of muscles and tendons in the forearm/wrist area in a manner which could affect internal forces among tissues, potentially resulting in increased exertion and discomfort; thus further evaluation is necessary.

Summary: Forearm pronation/supination posture has been found to affect forearm EMG, as well as torque and grip strength. Reported results include: EMG increases in the forearm extensors in pronated posture, lower pronation torque strength with pronated forearm, and higher supination torque strength with supinated forearm.

Table 2.1. Summary of biomechanical evidence demonstrating the effect of forearm pronation/supination posture on discomfort, forearm EMG, and strength.

Paper	Posture	Discomfort	EMG	Strength	Actions
Khan et al. (2009) Goal: Study the effect of forearm and wrist ulnar/radial deviation on discomfort	-0%, 35%, and 55% ROM wrist U/R dev'n -0%, 30%, and 60% ROM forearm P/S -90° elbow flexion -Upper arm rotated 45°	- Higher discomfort with forearm postures deviated from neutral -Higher discomfort in supine than prone postures -Additive effect of combined wrist and forearm deviations from neutral posture	N/A	N/A	Repetitive, 1-sec, isometric wrist flexion task at 15 exertions/min, with a force of 10N
Dominizio and Keir (2010) Goal: Study effect of forearm posture on forearm EMG	Forearm in -Pronation -Neutral -Supination	N/A	Increased EMG of forearm extensors in pronated postures for grip alone and with pull/push	N/A	Combinations of Pull/push and grip tasks: 1) Isolated grip (15, 30, 50% of max force) 2)30N push, 3) 30N pull 4) 30N push/pull with 15% grip
Mukhopadhyay et al (2007) Goal: Study the effect of elbow, forearm posture, exertion frequency and intensity on discomfort and forearm EMG. Note the supplementary study studied the effect of variables on torque strength and discomfort	-Neutral, 60% ROM forearm P/S. -Elbow at 45°, 90°, 135°. -Shoulder abducted 90°	-Increased with forearm deviated postures, but greater discomfort in pronated postures than supinated. - Higher discomfort at 45° than 90° elbow not sig differences between 90° and 135° Supplementary study found highest discomfort in prone lowest in supine	ECRB EMG increased in pronation and supination compared to neutral regardless elbow posture	From supplementary study: Despite elbow angle, pronation torque strength was higher in supine and lowest in prone. It was matched by discomfort data	Repetitive pronation torques at frequencies (10 vs 20 exertions/min) and intensity (10% vs 20% MVC)
O'Sullivan & Gallwey (2005) Goal: Study the effect of forearm posture and direction of torque on discomfort and torque strength	-0, 30, 45, 60, 75% ROM forearm P/S	-Pronation torque ellicited more discomfort than supination -Increased discomfort with larger forearm deviations from neutral -Larger increase from neutral to supine with supination torque	N/A	-Weaker pronation torque with pronated forearm -Largest decrease in supination torque strength from neutral to supine forearm	1-sec, 20% MVC, repetitive, pronation and supination torques, at a frequency of 10 exertions/min
O'Sullivan & Gallwey (2002) Goal: Study the effect of elbow and forearm posture and torque direction on torque strength and forearm	-0°, 45°, 90°, and 135° of elbow flexion, and - 0%, 75% ROM of forearm P/S - Elbow at 90°flexion	N/A	Various changes in recorded muscles: Biceps, Brachioradialis, ECRB and deltoids	-Overall: supine torque strength is higher than pronation strength -Supine strength more affected by forearm posture - highest at 75% ROM prone, lowest at 75% ROM supine, despite elbow angle -Pronation torque not as affected by forearm posture but pronation torque was lower at 75% prone than in other 2 forearm postures	Maximum pronation and supination torques in the pronation and supination directions
Mogk & Keir (2003) Study the effect of forearm, wrist posture, and grip force on forearm EMG	-0°, 45° of wrist flx/ext -Forearm pronation, neutral, supination	N/A	-Generally higher activity of extensors in pronated forearm (baseline, and	-A trend of lower max force seen in pronation acros all wrist postures *(Similar to other reserachers)* - but only statistically different in wrist flexion	Isometric gripping contractions at 5%, 50%, 70%, 100% of max grip force (normalized in neutral wrist and forearm), and 50N

2.1.3.3 Forearm Posture Effect on Mechanical Loading of the Median Nerve

Nerve compression has been associated with retarded conduction and long-term neuropathy in some cases (Keir & Rempel, 2005). Nerve compression can occur as the result of increased pressure or direct compression on the median nerve (Keir & Rempel, 2005). Controlled application of pressure on the palmar side of the hand over the flexor retinaculum has elicited CTS symptoms immediately after pressure was applied, suggesting that increased CT pressure may be a contributor to CTS (Keir & Rempel, 2005). Changes in CT pressure can be elicited by changes in forearm and wrist postures (Rempel et al., 1998; Werner et al., 1997) (Table 2.2).

Werner et al. (1997) studied the effect of a variety of combined postures of the forearm (pronation, mid-pronation, and supination) and fingers (closed hand, relaxed, straight, and pinched) postures, during flexion/extension as well as radial/ulnar deviation movements, using a fluid-filled catheter (surgically inserted in the wrist) connected to a pressure transducer. The forearm and finger postures were fixed at the beginning of each trial, and active flexion/extension or radial/ulnar deviations were performed. Their results showed consistently higher pressures in supinated postures across all finger and wrist postures, with two exceptions: extreme wrist extension (80°) and radial deviation both elicited higher pressures in pronated postures. The highest pressure (26.8 mmHg) was seen when the wrist was extended 80° with prone forearm; this value is three to nine times the normal resting carpal pressure (Werner et al., 1997).

In a similar study, Rempel et al. (1998) measured changes in CT pressure as a function of changes in posture of the forearm and MP joints (0°, 45°, and 90° of flexion). The MP joint was fixed at the desired posture, while the forearm moved actively from pronation to supination, with

a straight wrist. Data were sampled at 0°, 45°, and full forearm pronation and supination. The highest pressures were found in supinated postures regardless of MP joint posture, with the lowest pressure at 45° of forearm pronation. The CT pressure increased with increased forearm supination for all MP joints, with the highest pressure observed in full supination with 90° of MP joint flexion. These findings suggest that increases in CT pressure may reflect internal changes which can disrupt the mechanical relationship among tissues, thus increasing the risk of developing CTS. These findings suggest that forearm pronation and supination may modify the mechanical loading experienced by the median nerve. Job activities requiring forearm-deviated postures might elicit higher mechanical loading on the median nerve, potentially increasing the risk of developing CTS, and thus should be evaluated.

Summary: Increased pressure surrounding nerves has been associated with delayed conduction and long-term neuropathy. Forearm pronation/supination postures can increase loading on the median nerve, via increased CT pressure or direct compression, suggesting that some forearm postures may contribute to the development of CTS. Jobs requiring forearm deviated postures should be evaluated, as they can affect CT pressure, thus the risk to develop CTS.

Table 2.2. Summary of evidence showing effects of forearm posture on carpal tunnel pressure.

Paper	Posture	Carpal Pressure	Actions
Werner et al. (1997) Study the effect of forearm, wrist, and finger posture on carpal tunnel pressure	-Hand: closed, relaxed, straight, pinch -Forearm: Pronated, neutral, supinated	-Tunnel pressures were higher in supinated than in neutral and pronated postures across all wrist postures -Two exceptions: 1) Extreme wrist flexion (80°) with pronation, 2) Radial deviation and pronation caused higher pressure than supination -Highest pressure in extreme wrist extension with pronation (26.8mmHg)	Active flexion/extension and radial/ulnar deviation of the wrist
Rempel et al. (1998)	MP joints: 0°, 45°, 90° Forearm: 0°, 45°, full P/S	-Highest pressure in supination -Greater increase from neutral to supination -Lowest at 45° prone forearm, but slight increase in full pronation from neutral -Highest pressure in full supination and 90° of MP flexion -Lowest pressure at 45° pronation with 45° MP flexion	-Active forarm pronation and supination in slow motion. - Sampling every 45° of forearm rotation

2.2 Goal 1:

To determine a user-friendly, portable, and reliable method to quantify forearm pronation and supination in the workplace.

2.2.1 Forearm Pronation/Supination Measurement in the Workplace: An Overview

Currently, ergonomists often employ a variety of ergonomic tools to estimate the risk of developing upper limb MSDs, chosen primarily because of their low cost and ease of use. Many of the most common ergonomic methods allow the categorization of wrist postures into degree bins (e.g. Armstrong et al., 1982); however, forearm pronation/supination is often neglected, or taken into account indirectly (e.g. Moore & Garg, 1995 – Strain Index SI) or as a binary variable (e.g. McAtamney & Corlett, 1993 – RULA) (Table 2.3). Given the evidence suggesting the considerable contribution of forearm pronation/supination to MSK loading and injury (Descatha et al. 2003; Domizio & Keir, 2010; Khan et al. 2009a; Kroemer, 1989; Mogk & Keir, 2003; Mukhopadhyay et al. 2007; Rempel et al. 1998; Silverstein et al. 1986; O'Sullivan & Gallwey, 2005; O'Sullivan & Gallwey, 2002; Werner et al., 1997), the inclusion of practical estimation of forearm/wrist posture combinations in observational methods would be of great benefit. The first goal of this thesis is to determine a reliable method to quantify forearm pronation/supination in workplace settings.

Table 2.3. Examples of forearm pronation/supination quantification in the workplace using observational methods. The 'choices available for forearm pronation/supination' are the options on the checklists associated with each of these three methods to achieve a 'risk score'.

Observational Methods		
Authors	***Tools***	****Choices Available for Forearm Rotation***
Armstrong et al. (1982)	-	*Pronation, Neutral, Supination (check mark)
Moore & Garg (1995)	Strain Index	*Forearm rotation not directly quantified. *May be indirectly accounted for as perceived posture
McAtamney & Corlett (1993)	RULA	* Wrist twist: Score of 1 if mid-range, or score of 2 if deviated near end range

Understanding forearm/wrist postural demands of different jobs may allow new insights into the risk of developing specific upper limb disorders for people performing certain jobs. Valid and reliable measurements of external exposure which include both wrist and forearm posture quantification are needed to help us understand the relationships between external exposures and MSD risk.

Summary: The majority of current ergonomic tools attempting to estimate the risk of developing upper limb MSDs associated with work do not account directly for forearm pronation/supination.

2.2.2 Challenges Associated with Forearm Pronation/Supination Measurements

The nature of forearm rotation makes it difficult to accurately measure pronation and supination. The movements involve rotation of the radius over the ulna (the two bones in the forearm). Posture measurements are performed by establishing bi-dimensional or tri-dimensional coordinate systems (CS) of each body segment and measuring the relative angular differences between them. However, because forearm pronation/supination is the relative movement

between two bones within a body segment (the radius and ulna), and are externally inaccessible, proximal and distal CS of the forearm need to be established. Although some optical methods, such as Vicon, may facilitate the development of such CSs (e.g. through the acquisition of marker location data, along with kinematic model development), measuring posture in the workplace with such systems is not feasible, due to challenges such as the lack of safety in the work environment for expensive equipment, inability to control for light sources, lengthy calibration, and people's interference (e.g. worker mobility within the capture space resulting in blockage of participant's movements from camera view). Instead, portable motion capturing systems, such as IMUs, are necessary.

However, measuring forearm pronation/supination may be difficult when using portable motion capturing systems, because acquisition often relies on mounted sensors on moving body segments. Tissue movement of forearms with different anthropometric characteristics could interfere with the accuracy of the measurements. In addition, the need to establish two CS within the forearm is likely to result in the need for more equipment mounted at the forearm, potentially interfering with workers' mobility and comfort.

Finally, forearm pronation and supination is a movement which may be performed at high angular velocities. Marras & Schoenmarklin (1993) measured wrist and forearm motions in industrial jobs with high and low incidence of upper limb disorders. Their findings showed that pronation/supination were a lot faster than flexion/extension of the wrists and radial/ulnar deviation. In the low-risk jobs, they observed velocities of up to 290°/s, 120°/s, and 80°/s of pronation/supination, flexion/extension, and radial/ulnar deviation respectively, illustrating that forearm pronation/supination can be more than double the fastest velocity seen in flexion/extension. Faster movements pose a challenge mainly because higher sampling rates may

be required, and a slight delay could create a large phase-angle deviation between the measuring device and the actual movement. Higher velocities involve higher segmental accelerations, thus potentially more abrupt changes in direction, possibly inducing noise in the signal. In addition, sensor weight should also be considered, as heavier sensors may be difficult to mount; furthermore, due to greater inertia, they are more likely to continue to move at the end of ROMs and record extra movement when subjected to abrupt changes in direction.

Thus, an effective posture quantification device would not only be portable, valid, and reliable, but also small and lightweight in order to minimize both interference with workers' motions during work activities and sensor movement not related to body segment motion due to abrupt directional changes. Ideally, such a system would be able to obtain and transmit posture measurements over a large area to allow free ambulation of participants in large working areas to perform their jobs. In the following sections, the methods currently available for posture quantification will be discussed.

Summary: Forearm rotation is difficult to measure; CSs of the proximal and distal ends of the forearm need to be modeled. The ideal measurement system would be portable, non-intrusive, and reliable.

2.2.3 Current Methodologies Measuring Forearm Pronation/Supination in the Workplace

2.2.3.1 Optical Methods

Historically, basic video has been used to capture movement (Manal & Buchanan, 2004). Armstrong et al. (1982), for example, investigated cumulative trauma disorders in workers at a poultry processing plant using video. They filmed motions of the shoulder, elbow, wrist, and hand at three frames per second and analyzed them using an observational method. Although conventional video can be a very useful tool for analyzing occupational postural requirements, it is often set up to capture only a single plane of movement, which may not necessarily be aligned with the anatomical planes of participants. Additionally, all video is subject to line-of-sight problems, when body parts of interest are outside the field of view of the camera. Thus posture quantification from conventional video is difficult. More recently, multi-camera motion capture systems have been developed which allow movement to be captured tri-dimensionally. However, they still require some form of manual or assisted digitization in order to identify points of interest.

Other motion capture systems involve automatic tracking of markers, thus eliminating the need for manual or semi-automated digitizing. There are currently active and passive systems, both of which track markers mounted on body segments and joints of interest (Manal & Buchanan, 2004). Active systems such as Optotrack (Northern Digital, Waterloo, Ontario, Canada) use light-emitting diodes (LEDs) as markers, whereas passive systems such as Vicon rely on reflective markers, which reflect infra-red light emitted by LEDs on the cameras. Both active and passive systems are able to locate the markers in space, facilitating the creation of anatomical CSs of body segments to measure posture (Manal & Buchanan, 2004). The markers are generally placed over bony landmarks, with the assumption that they closely represent

osseous movement. Although these systems have been widely accepted in biomechanics, they are costly and require lengthy calibration procedures—as well as a motion-capturing space where light sources can be controlled. Given the eventful and unpredictable nature of work environments, the use of optical systems for motion capture in the workplace is often not feasible. As a result, reliable and portable motion capturing systems to measure forearm posture in the workplace are needed.

Summary: Optical motion capturing systems can track markers on bony anatomical landmarks, allowing researchers to create anatomical segments' CSs and estimate 3D postures for a variety of dynamic activities. These systems are not feasible for work settings due to their cost and complexity.

2.2.3.1.1 Vicon

Vicon, a passive optical system, uses multiple two-dimensional cameras to track targets (i.e. markers) in the capture volume (globally), and uses mathematical equations to reconstruct 3D target coordinates (Manal & Buchanan, 2004). The strobe units or LEDs around the camera lens emit light to be reflected by the passive markers at a specific wavelength, allowing the lens to filter out unwanted light of different spectral characteristics. The light passing through the lens projects an image of the targets onto the camera's image sensor, which is a complementary metal-oxide semiconductor (CMOS) composed of a matrix of numerous light sensing elements, which form an internal, two-dimensional coordinate system (image plane) (Vicon Motion Systems Limited, 2006). These light sensing elements transform the light into a voltage modulated by the light intensity, which is important for two-dimensional target tracking (Manal & Buchanan, 2004). Because the projected image is in grayscale, different voltages are

associated with each 2D location on the image plane (Manal & Buchanan, 2004). Image processing occurs in the cameras, where the edges of targets are recognized by scanning the matrix for voltage transitions between elements. Centroid fitting algorithms are used to identify projections which are likely to be markers, and to identify their two-dimensional coordinates in each camera (target centre location) (Vicon Motion Systems Limited, 2006; Manal & Buchanan, 2004). These coordinates are not recorded as the actual target location, but are used instead to generate a ray in the direction of the target in the capture volume. While this is done by each camera in the system, the target locations in 3D space are calculated by the intersections of rays generated by all cameras viewing the same target (Manal & Buchanan, 2004). In order to identify such intersections, cameras must be calibrated first.

Vicon calibration involves proprietary algorithms which are based on direct linear transformation (DLT). DLT is a mathematical procedure which allows determining of various internal (e.g. focal length and image distortion) and external parameters (e.g. camera position and orientation), which are used to establish the relationships between the real and projected object positions and their size ratio (i.e. scaling) (Vicon Motion Systems Limited, 2006, Manal & Buchanan, 2004). In order to establish these relationships, DLT requires at least six static calibration points with known real coordinates. Vicon's calibration procedures however, involve dynamic and static procedures, and do not require static points with known real coordinates. Instead, the dynamic procedure involves an optimization process, where a wand with 5 markers with known distances is waved around the capture volume. The cameras simultaneously modify both, the internal and external parameters, so that measured distances between markers in the image plane match the known inter-marker distances (Park et al. 2013). The static calibration follows the dynamic procedure, where the 3D capture volume axes and origin are defined. At the

end of the calibration procedures, the transformation parameters are defined, which are subsequently used to reconstruct the 3D marker locations in the capture volume from two-dimensional images of multiple cameras (Manal & Buchanan, 2004, Park et al. 2013).

Vicon is widely used in the biomechanics field to quantify body postures, and has often served as a gold standard to evaluate the accuracy of other motion capture systems to measure kinematics of the lower (Picerno et al. 2008; Martin-Schepers et al. 2010), and upper extremities (Martin-Schepers et al. 2010; Roetenberg et al. 2007), possibly due to its lower error compared to other motion capture systems (Richards, 1999). Richards investigated the static and dynamic accuracy of different optical motion capture systems, including passive systems (Ariel system, BTS Elite, Motion Analysis, Peak Motus, Qualisys, and Vicon), and an active system (CODA). He compared the discrepancies between the estimated distance measurements (from motion capture) and the real inter-marker distance, of markers placed on a mobile device. One analysis consisted of estimating the distance between two rotating markers fixed 50 cm from each other, while they remained visible to all cameras during the trial. Vicon had lower error (0.62 mm RMSE) than all but one of the systems (range of discrepancies: 0.59 – 4.87 mm RMSE). A similar analysis was performed using two markers separated by 9 cm, but as markers rotated, they were only visible two or three cameras at the time. This analysis showed that Vicon had lower error (1.29 mm RMSE) than all other systems (range: 1.49 – 4.46 mm RMSE). Finally, this study also evaluated the systems' accuracy to measure the distance between a stationary marker, and a moving marker which varied its distance with respect to the stationary marker, at 1 cm increments, over a 5 cm range. It was found that systems measured location better when inter-marker distance was greatest, with Vicon showing one of the lower errors (0.82 mm RMS), performing better than four systems (1.8 mm – 3.6 mm), and similar to the other two systems

(0.5 – 0.9 mm), as long as the markers were within 2 cm from each other. Markers within 1 cm separation distance were confused by most systems including Vicon.

Even better Vicon accuracy was reported by Windolf et al. (2008), who evaluated the effect of different collection parameters (e.g. camera setup, calibration volume, marker size, and lens filter) on the accuracy and precision of Vicon target location measurements, by comparing them to known marker locations mounted on a high accuracy robot. This was done by systematically moving a marker through predefined grid points, in 30 mm increments. Vicon showed overall discrepancies of 0.06 ($\pm$0.015) mm in their most favourable condition, and although certain parameters affected the accuracy of Vicon measurements, accuracy in other conditions ranged between 0.08 – 0.13 mm. Finally, Eichelberger et al. (2016) also tested the static and dynamic trueness and precision of Vicon measurements, by comparing distance estimates from Vicon marker coordinates to their known spatial distance. For the static measurements, a wand with markers at known distances was positioned at three heights resembling the heights of the ankle, knee, and hip. For dynamic measurements a reference marker plate, also with known inter-marker distances, was positioned on a person at three different locations: the dorsum of the foot, the lateral knee, and the low back. The dynamic Vicon measurements were recorded during a gait. Discrepancies of 0.11 to 2.3 mm mean absolute error (MAE) were reported for the static conditions, while only 0.03 – 0.9 mm were observed during the dynamic conditions. Precision in all static conditions was < 0.07 mm, while dynamic measurements ranged from 0.03 – 3.28 mm. This evidence supports that Vicon displays low error, and it is one of the better systems currently available for motion capture.

Summary: Vicon has been often used as a gold standard because low error in tracking target locations has been reported in the literature.

2.2.3.2 Electrogoniometers

2.2.3.2.1 Potentiometers

Electrogoniometers are probably the most common direct measurement device in the workplace for directly measuring postures of the upper extremities (Manal & Buchanan, 2004). These devices, in the form of rotating potentiometers or strain gauges, give voltage outputs calibrated to joint angles (Manal & Buchanan, 2004). A potentiometer is essentially a voltage divider with three terminals, two of which are connected to a resistive element in the circuit; the third terminal is connected to an adjustable arm, which slides over the resistive element. The arm is in contact with the resistive element, dividing the voltage on either side of it. As a consequence, the resistive element becomes two resistors in series, and the arm determines the resistance ratio between the two and, ultimately, the output voltage of the potentiometer (as seen in Eq. 2.1).

$$V_{out} = \frac{R_2}{R_1+R_2} \cdot V_{in} \qquad \text{(Eq. 2.1)}$$

Where: V_{out} is the output voltage of the potentiometer
R_1 and R_2 the resistances associated with either side of the divider
V_{in} is the input voltage

As one example, Marras et al. (1993) created a device using a potentiometer to measure forearm pronation/supination for a variety of industrial tasks. Their device consisted of a rod attached to a fixed bracket at the proximal end, while it remained parallel to the forearm, and was connected to a rotating potentiometer at the distal end, which was fixed to another bracket. Rotation of the forearm caused rotation of the potentiometer with respect to the fixed rod. Voltages from the potentiometer were calibrated to joint angles. Although this device may have

allowed calibrated forearm pronation/supination measurements, it is proprietary; thus, it is not available for commercial use. However, sources of error were not discussed, and no further research was conducted to validate its output. Wearing a rod across the forearm would have been cumbersome during work activities, possibly affecting workers' movements. Thus, this type of electrogoniometer is not as commonly used as strain gauge goniometers.

Summary: Electrogoniometers are commonly used to measure wrist and forearm postures. They often exist as potentiometers or strain gauge devices. Potentiometers are voltage dividers, and they can be setup so that changes in posture change the voltage ratio on either side of a wiper, and voltage outputs can be calibrated to joint angles. Potentiometer electrogoniometers, although they can produce reliable measurements, are not as easily accessible for commercial use as strain gauge goniometers.

2.2.3.2.2 Strain Gauges

Strain gauge electrogoniometers have been more commonly used in the field of ergonomics, and models have been developed which are relatively small and easy to use, at a relatively low cost. These devices consist of two squared casings or blocks connected by a coil, which contains a strain gauge. Strain gauges are electrical devices whose resistance varies with varying strain experienced (Manal & Buchanan, 2004). In the case of torsiometers (e.g. Biometrics Q series torsiometers), the strain gauge is aligned so that it is sensitive to strain caused by the rotation of one block with respect to the other, giving a voltage output, which is calibrated to relative angle. Forearm pronation/supination is measured with this type of electrogoniometer by placing one block near each end of the forearm.

Several studies have used strain gauge torsiometers (Biometrics LTD) to evaluate the forearm postures of a variety of jobs (Jones & Kumar, 2006; Lowe, 2004; Quemelo & Vieira, 2015; Spielholz, et al., 2001). For example, Jones & Kumar (2006) used torsiometers to evaluate forearm postures on saw filers, professionals within the forest products manufacturing industry. Torsiometers were positioned according to the manufacturer's instructions: on the anterior forearm, with the distal block as close to the wrist as possible and the proximal block towards the medial surface of the olecranon. Although neither calibration procedures were specified in the article, it was reported that errors were measured using uni-planar calibration jigs through anatomical ranges of motion. The maximum error reported for pronation/supination was 3.3° over a ROMs of -41° to 41° of supination/pronation. Although error was acceptable, it is not known whether larger ROM could have had an effect on error.

In another study, Quemelo & Vieira (2013) compared upper limb kinematics of two computer mice (standard vs vertical). The task consisted of moving each mouse across a screen to various targets. Forearm pronation/supination measurements were obtained with a torsiometer (Biometrics LTD), and average postures during the task were compared for the two mice. Torsiometers were placed on the anterior surface of the forearm, with the distal block at the wrist and the proximal block on the radial aspect of the forearm. The average pronation was 28° for the vertical mouse and 42° for the standard mouse. Calibration methods and measurement error were not reported, but the authors assumed that measurements would not be significantly affected by cross-talk because the posture ranges were small, and the postures relatively static.

Two other studies used torsiometers as the gold standard while evaluating the reliability and accuracy of observational methods to estimate forearm posture (Lowe, 2004; Spielholz et al., 2001). Spielholz et al. compared methods which used video analysis and self-report with

electrogoniometer (bi-axial goniometers for radial-ulnar deviation and flexion-extension of the wrist) and torsiometer (for forearm posture) measurements. The torsiometers were placed on the posterior forearm, with the distal block towards the radial styloid, and the proximal block towards the lateral epicondyle of the humerus. Although electrogoniometer and torsiometers were used as a gold standard in this study, the authors recognized common errors associated with electrogoniometers, caused by cross-talk. They developed a series of regression equations based on the relationship between the known and measured postures in each of the three planes (flexion/extension, radial/ulnar deviation, and pronation/supination), using a calibration jig for all planes. Input measurements from the three planes were used in the regression models to correct flexion/extension and radial/ulnar deviation measurements. However, corrections for forearm pronation/supination were not performed. Average standard error reported between direct measurements and the calibration jig was around 4-5° for all axes; however, only $\pm$ 45° of forearm pronation/supination was included (Spielholz et al. 2001).

Lowe (2004) evaluated observational methods with a varying number of posture categories to estimate the risk of developing upper limb disorders in certain jobs. Electrogoniometers (bi-axial for wrist posture measurements) and torsiometers (for forearm pronation/supination measurements) were used as the gold standard in this study, and calibration procedures were similar to those used by Spielholz et al. However, Lowe developed correction algorithms for all planes. The worst discrepancy between corrected torsiometer and jig measurements was 2.6°, which occurred when the forearm was pronated 45°. Both Spielholz et al. and Lowe took into account multi-planar interactions for their corrections. However, like the former, Lowe's calibrated ROM for forearm pronation/supination was only -45° to 45°.

Finally, Shiratsu & Coury (2003) evaluated the accuracy of two Biometrics torsiometers using a calibrated gauging device. Five measurement sequences were performed throughout an unspecified ROM, with 1° increments. Averages of each measurement were performed per degree, and coefficients of variation and mean squared error were used as measures of reliability and accuracy, respectively. Torsiometer error was not symmetrical between directions, with 7° and 5° of error when rotating to the right and left, respectively. The variability of the torsiometers was reported to be around 3-6% of the mean. Interestingly, the authors reported larger errors when measuring smaller amplitudes (0-15°), while the opposite was observed with bi-axial electrogoniometers measuring flexion/extension and radial/ulnar deviations. In this particular study, the torsiometer blocks were mounted on the gauging device rather than on a human forearm, thus error associated with soft tissue or blocks' movement with respect to the forearm was not evaluated.

Summary: Torsiometers can have discrepancies up to 7° when compared to measurements of calibrated devices. However, few studies included calibrated ranges of motion >45° of deviation from neutral. Cross talk in wrist posture measurements elicited by forearm rotation highlights the need of accurate forearm rotation measurements.

2.2.3.3 Electromagnetic Systems

Electromagnetic tracking technology is also used in biomechanics to measure postures of the upper limbs. Essentially, these systems consist of a transmitter and sensors in the form of receiving coils. The transmitter is a stationary base consisting of three coils arranged orthogonally which emit an electromagnetic field composed of three dipole fields (Birkfellner, et

al., 2008). The field is used as a reference to measure the location and orientation of the sensors with respect to the transmitter. Each of the dipoles is activated in sequence in the transmitter. The sensors also have an arrangement of three orthogonal coils, and each coil senses magnetic changes from each of the three dipoles in the transmitter. The voltage generation in the sensors follows Faraday's Law, which describes the spontaneous generation of a voltage or electromotive force (EMF) experienced by electrons in a conductor when it is moved through a magnetic field. The magnitude of the induced force is proportional to the strength of the magnetic field. As the sensors move through space, the magnitude of the magnetic fields experienced by the sensors varies, and the absolute orientation of each sensor in space can be detected (Manal & Buchanan, 2004). Forearm pronation/supination measurements can be estimated by calculating the relative orientation of a sensor placed on the distal forearm with respect to another sensor placed on the proximal forearm or the humerus.

The accuracy and reliability of electromagnetic sensors is very high under optimal conditions (e.g. no magnetic disturbance and transmitter and sensors are in close proximity). However, both large distances between sensors and transmitter and magnetic disturbance can result in considerable measurement errors (Manal & Buchanan, 2004; Polhemus Innovation in Motion, 2012). Furthermore, the volume of the capture area depends on the strength of the magnetic field, which may interfere with effective data capture in jobs requiring ambulation over large areas.

This technology has been used to evaluate upper limb kinematics in a few jobs (Flodgren, et al., 2007; Mohankumar et al., 2014). However little is known about its ability to measure forearm pronation/supination, particularly in a work environment, where presence of metal (which interferes with the magnetic field) is common. Mohankumar et al. (2014) investigated

upper limb kinematics associated with endoscopy maneuvers of the lower GI tract on an endoscopy simulator using an electromagnetic Polhemus FASTRAK system. In this study, pronation and supination of the forearm were measured by means of a sensor on the dorsum of the hand and a transmitter on the lateral humeral epicondyle. Reported values were normalized to the maximum range of motion and binned into four categories: neutral, mid-range, extreme range, and out of range. However, calibration and sources of error were not discussed.

Similarly, Flodgren et al. (2006) also used a FASTRAK system to evaluate upper limb kinematics associated with performing a mouse task. Their neutral posture was defined as the forearm position when the participant's hand rested on the mouse. The average postures ranged from 8.7° for forearm pronation to 19.1° for supination, with respect to neutral. This small range of motion is due to the fact that the task was essentially in sustained pronation. The calibration procedures and sources of error were not discussed. It was not clear where the sensors were placed to measure pronation/supination.

Summary: Electromagnetic tracking systems, consisting of a transmitter and sensors, measure forearm posture from the relative orientation of two adjacent sensors on the distal and proximal forearm. They are greatly affected by magnetic disturbance and increased distance from the transmitter. Little is known about their ability to accurately measure forearm pronation/supination in the workplace.

2.2.3.4 Inertial Motion Units (IMUs)

Inertial motion units are affordable, light, portable sensors, which generally contain tridimensional gyroscopes, accelerometers, and magnetometers (El-Gohary & McNames, 2012). Each of these three devices is capable of providing important information regarding orientation.

Combining these devices greatly improves accuracy, as well as versatility, to facilitate measuring movement in diverse conditions.

Triaxial gyroscopes are able to measure angular velocities in three orthogonal planes, and orientation may be estimated by integrating the angular velocity output from the gyroscope. However, because angular velocity data have to be integrated continuously, errors in position data are likely to arise over time (e.g. drift), which are magnified by small gyroscope offsets in angular velocity. Commercially available gyroscopes alone provide accurate measurements for less than one minute (Luinge, et al., 2007). In addition, gyroscopes are not very sensitive to slow segment orientation changes, but work well when estimating the orientation changes of faster movements.

Tridimensional accelerometers, on the other hand, measure linear acceleration. In cases where there are no external accelerations, linear acceleration outputs can be used in trigonometric calculations to estimate the orientation of a segment with respect to gravity. However, in cases where limbs are accelerating linearly, accelerometer measurements may not be accurate due to noise in the signals (Luinge, et al., 2007). Because accelerometers use the gravity vector as a global reference, rotations about the vertical axis will not lead to changes in accelerometer measurements; thus accelerometers are not capable of giving a complete description of orientation in space. Combining accelerometers with magnetometers can provide a complete estimate of 3D orientation.

Magnetometers are devices capable of measuring the strength and direction of local magnetic fields, which allow them to determine magnetic north (Woodman, 2007). The measurements of magnetometers, along with trigonometric calculations, can provide estimates of rotations of segments in the yaw direction (e.g. heading), using magnetic north as an external

reference. However, magnetometers are greatly susceptible to magnetic disturbance, so they are commonly used in conjunction with other devices (e.g. in IMUs) to improve measurement accuracy (Luinge et al., 2007; Woodman, 2007).

IMUs are capable of combining information from two or more devices to define the state of a system (e.g. orientation). They maintain the advantages of each of these devices while minimizing their flaws through sensor-fusion (Woodman, 2007), a process which uses algorithms to combine measurements from various sources to improve measurements' accuracy.

The Xsens IMU sensors are equipped with three devices: 3D linear accelerometers, 3D magnetometers, and 3D gyroscopes (Xsens motion technologies, 2008), and contain a built-in processor which runs a Kalman filter, a type of sensor-fusion algorithm. A Kalman filter is a set of equations that is used to infer a parameter (e.g. orientation) from inaccurate, uncertain and indirect measurements (e.g. angular velocity, linear accelerations, and magnetic data) (Welch & Bishop, 2006). Although Xsens' Kalman filter is proprietary, it appears that in this context, it was designed to determine the best possible orientation output through the following operations. First by predicting the current state (IMU orientation output) and measurements of each device (gyroscopes, accelerometers, and magnetometers). The prediction of the current state is based on current measurements (e.g. velocity from the gyroscopes), the change in time between the last and current samples, and the past orientation output (from the IMU). The measurements' predictions for each device are based on the next sample's state prediction, and the known relationship between the orientation output or current state (from the IMU) and each of the measurements (e.g. 1) orientation from the integral of gyroscopes' angular velocity output and knowledge of a starting orientation, 2) roll and pitch orientation estimates from accelerometres' measurements – with respect to gravity, and 3) yaw orientation estimates from magnetometer

measurements – with respect to the magnetic north). Measurement residuals are also calculated based on the discrepancies between the measurements' predictions and the actual measurements (e.g. discrepancies between an orientation estimate at time (t) (based on angular velocity from gyroscope data at time (t-1) and an initial orientation (state at t-1)) and the current orientation (from the integral of gyroscopes' angular velocity, a known change in time (t – t-1), and an initial orientation (state at t-1))). At the same time, similar complex procedures are done to estimate the covariance of both, the state and measurement predictions, and their associated noise. The knowledge gained on covariance and noise associated with both, measurements and prediction processes, is used to determine which measurements and predictions are more accurate, as indicated by lower covariance and lower noise levels. At the end, the Xsens' Kalman filter provides an output which includes the best orientation estimate from a series of predictions, measurements, and uncertainty measures. The Xsens' Kalman filter also involves corrections to account for any changing accelerations beside gravity and for magnetic disturbance. Any changing accelerations (besides gravity) will sum to zero, if the participant is not travelling. In the presence of magnetic disturbance the Xsens creates a new local magnetic north and recalibrates. When the magnetic disturbance is not predictable though, (such as when the IMUs and a large metallic object are moving with respect to each other), the Xsens may err in its orientation estimations. An important advantage of this filter, is that it has been optimized to correct for the drift (caused by the continuously integrated angular velocity), noise (from accelerometers), and magnetic disturbance, while weighting inputs of each device when determining the current orientation, depending on probable errors of each device. For example it aims to minimize the weighting of the magnetometers in the presence of ferromagnetic

disturbance, or to emphasize accelerometer and magnetometer measurements in slow movements when magnetic disturbance is not present.

Summary: Xsens units are affordable, light, portable IMUs which contain three devices: tridimensional gyroscopes, accelerometers, and magnetometers. They combine information from all three devices using a Kalman filter, which has the advantage of modifying the weighting of each device to improve measurement accuracy.

2.2.3.4.1 Use of IMUs to Measure Arm Movements

IMUs have commonly been used in biomechanics to estimate posture of various body parts (Luinge et al., 2007), including the upper limb (El-Gohary & McNames, 2012; Zhou, et al., 2008). Some of these studies used IMUs containing gyroscopes and accelerometers (El-Gohary & McNames, 2012; Luinge et al., 2007), while others used IMUs which also included magnetometers (Zhou et al., 2008). The following section describes various studies where the RMSE errors in orientation associated with IMUs ranges from 2°-8° when compared to optical motion capturing systems (Cuesta-Vargas, et al., 2010; El-Gohary & McNames, 2012; Luinge et al., 2007; Zhou et al., 2008).

Cuesta-Vargas et al. (2010) performed a literature review of studies measuring body movements using IMUs. They analyzed 14 articles published between 2000 and 2010 which met their criteria. Studies had to have measured the kinematics of specified body regions and compared the results to those from accepted human movement analysis systems (e.g. optical systems, electrogoniometers, and electromagnetic systems). The studies also had to provide measures of error to denote discrepancies between systems. Of the 14 studies, only four evaluated upper limb movements and compared the IMUs to an optical motion capturing system.

The Xsens IMUs in these studies all included 3D gyroscopes, accelerometers, and magnetometers; however in one study a Kalman filter was not used. The three studies which used the Kalman filter reported errors ranging from 2.3-4.83° RMSE. The one study which did not use a Kalman filter reported larger errors of around 14.6° RMSE. However, the error for specific joints of the upper limb was not reported. The length of the trials, in any of the four studies, were not reported either, which could have an effect on errors seen over time, due to inability of the sensor-fusion algorithm used to compensate for drift errors.

In another study, El-Gohary and McNames (2012) fused signals from 3D accelerometers and gyroscopes using a Kalman filter they created and evaluated its efficacy by comparing their output with Vicon measurements. Postures of the shoulder, elbow, and forearm were measured while participants were doing three different tasks. Forearm postures were measured as the relative orientation of a sensor mounted on the distal forearm with respect to one on the upper arm. The first task involved uniplanar movements of forearm pronation/supination. Trials for this task were 18 seconds long. The second task involved touching the nose with a finger and reaching for and rotating a door knob. These trials were 2 minutes long. The last task involved the same uniplanar movements of task one, but at a faster speed. Uniplanar forearm pronation/supination showed 5.5° RMSE, and a peak error of 7.8° RMSE. The second task exhibited an average error of 6.5° RMSE, and peak error of 8.8° RMSE among both tasks and all joints. The third task showed an average error near 8° RMSE, and peak error of 12° RMSE across tasks and joints. None of their recordings exceeded 2 minutes, thus it is not known whether longer recordings would have had larger RMSEs due to drift.

In a similar study, Luinge and Veltink (2005) also designed a Kalman filter to combine signals from 3D accelerometers and gyroscopes. The filter was designed to estimate (and correct

for) integration drift in all three directions. It was evaluated by determining the agreement between the IMU and Vicon measurements of trunk and arm movements during various tasks. The tasks included lifting crates at different speeds for two minutes, mimicking daily morning activities for ~80 seconds, and eating for 90 seconds. The IMUs were placed on the pelvis, trunk, and forearm. Comparisons involved absolute orientations of IMUs between both systems, and errors were separated into inclination and heading errors. The errors associated with gyroscopes and accelerometers were illustrated separately. They reported that their Kalman filter was able to attenuate the drift of the gyroscopes. Accelerometers' outputs were affected by the speed of movement while lifting crates; faster movements increased noise in the accelerometers' signals, increasing error in orientation estimates. However, they demonstrated that their Kalman filter was also able to attenuate this noise. Good inclination agreement was shown between their IMUs and Vicon, with an error of 3° RMSE. However, heading error continued to drift at a rate of 0.5°/sec, meaning that their filter was unable to accurately estimate yaw movements. Their recordings were never longer than two minutes, so their results may only be applicable to tasks two minutes long or shorter.

Finally, Zhou et al. (2008) compared arm movement measurements from Xsens MT9 sensors (3D gyroscopes, accelerometers, and magnetometers) to measurements using an optical motion capturing system (CODA). In this study, the IMUs were calibrated by re-orienting the IMUs' reference frames to segment orientations. The movements in this study involved movements at single joints, such as forearm pronation/supination alone. The sampling period was 20 seconds. Forearm pronation/supination errors were 4.83° RMSE.

Some studies show that IMUs are promising for posture estimates and that Kalman filters may improve the IMUs' accuracy in work environments. However, the error associated with IMUs during activities in the workplace, particularly with metal nearby, needs to be understood.

2.3 Goal 2:

To study the effect of forearm pronation/supination and wrist posture in the sagittal plane on the orientation and location of the flexor digitorum superficialis and profundus tendons (FDS and FDP, respectively) proximal and distal to the CT.

2.3.1 Wrist and Forearm Anatomy Review

2.3.1.1 Wrist and Carpal Tunnel

The wrist joint is a synovial joint between the distal ends of the radius and ulna of the forearm and the proximal row of carpal bones of the hand. It is enclosed by ligaments, and tough connective tissue (McKinley & O'Loughlin, 2006) The carpal bones form the bony arch of the CT, which contains FDP and FDS tendons, the flexor pollicis longus tendon (FPL), the median nerve, and the nerve's blood supply (Robbins, 2009) (Figure.2.2). The four FDS tendons lie on top of the four FDP tendons, and the FPL runs radial to both, but pushed slightly more dorsal than the FDS tendons. The eight finger flexor tendons passing through the tunnel are pulled together in a protective synovial sheath, also called flexor sheath or ulnar bursa. Similarly, the FPL shares a synovial sheath (the radial bursa) with the tendons of the fifth digit. Synovial sheaths are formed of two layers of connective tissue, a visceral (inner) layer and a parietal (outer) layer. Together they form a sac containing synovial fluid which helps minimize friction between structures. Finally, the bony carpal arch is enclosed at its anterior side by a transverse

band of connective tissue, the flexor retinaculum. Tendons and synovial sheaths in this area are vulnerable to mechanical loading, due to tightly packed structures passing through a narrow tunnel (Armstrong, et al., 1984).

Within the wrist, there are some structures which do not pass through the CT. On the anterior wrist, the ulnar nerve, its artery, and the palmaris longus tendons pass volar to the retinaculum, and the flexor carpi radialis and ulnaris pass on either side of the tunnel (Robbins, 2009). The tendons of the extensor muscles of the wrist and the radial artery pass dorsal to the carpal bones, and are secured with the dorsal transverse ligament (Robbins, 2009).

Summary: There are numerous soft tissue structures passing through the CT, a reduced space at the wrist, which are vulnerable to mechanical loading and may have an increased risk of tissue damage.

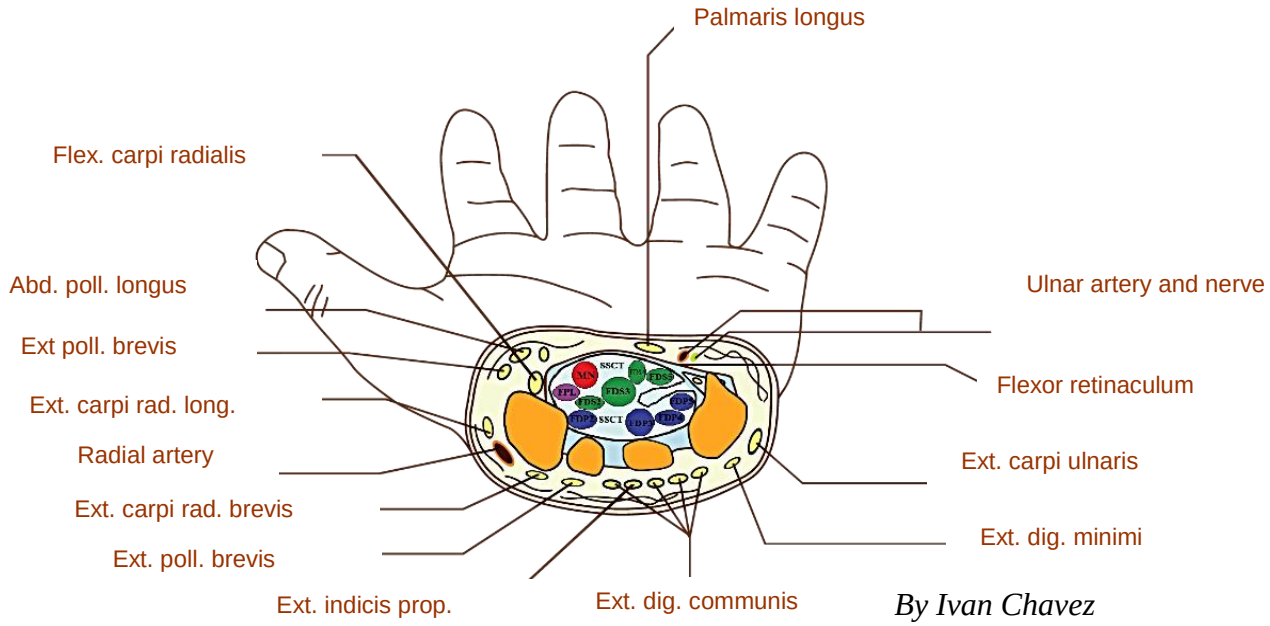

Figure 2.2. Transverse view of the carpal tunnel from the proximal side. Numerous structures pass through the reduced carpal tunnel: 4 flexor digitorum profundus tendons (FDP 1-5), 4 flexor digitorum superficialis tendons (FDS 2-5), flexor pollicis longus tendon (FPL), the median nerve (MN), the sub-synovial connective tissue (SSCT), and the synovial layers, which wrap all tendons and the MN, may be vulnerable to mechanical loading. Adapted from Loudon et al. 2013.

2.3.1.2 Forearm Musculature

There are two main pronators and two main supinators of the forearm. The biceps brachii and the supinator are the two supinator muscles. The supinator passes posteriorly over the elbow from the supinator crest and fossa of the ulna, the lateral epicondyle of the humerus, and elbow ligaments, to the lateral side of the proximal third of the radius (Drake, 2005) (Figure 2.3a). The two pronators, running through the anterior compartment of the forearm, comprise: the pronator teres, which originates from the medial epicondyle and attaches to the lateral mid-shaft of the radius; and the pronator quadratus, which extends between the anterior surfaces of the distal ends of the radius and ulna (Drake, 2005) (Figure. 2.3b).

There are four flexor muscles that cross both the elbow and the wrist: the flexor carpi radialis (FCR) and ulnaris (FCU), the humeral head of the flexor digitorum superficialis (FDS) and the palmaris longus (PL). These four muscles, along with the humeral head of the pronator teres (PT), have a common origin at the medial epicondyle of the humerus (Drake, 2005) (Figure 2.3c). The deeper layers of the finger flexor muscles and flexor pollicis longus do not cross the elbow, but originate along the forearm by the interosseous membrane and cross the wrist (Drake, 2005). On the posterior side of the forearm, there are four extensor muscles with a common origin at the lateral epicondyle: the extensor carpi radialis brevis (ECRB), extensor carpi ulnaris (ECU), the extensor digitorum communis (EDC), and the extensor digiti minimi (EDM) (Figure 2.3d) (Loudon, et al., 2013).

Summary: The complex forearm musculature is described in detail. The wrist flexors and the humeral head of the PT have a common attachment at the humeral medial epicondyle, whereas the wrist extensors and the supinator muscle attach at the lateral epicondyle.

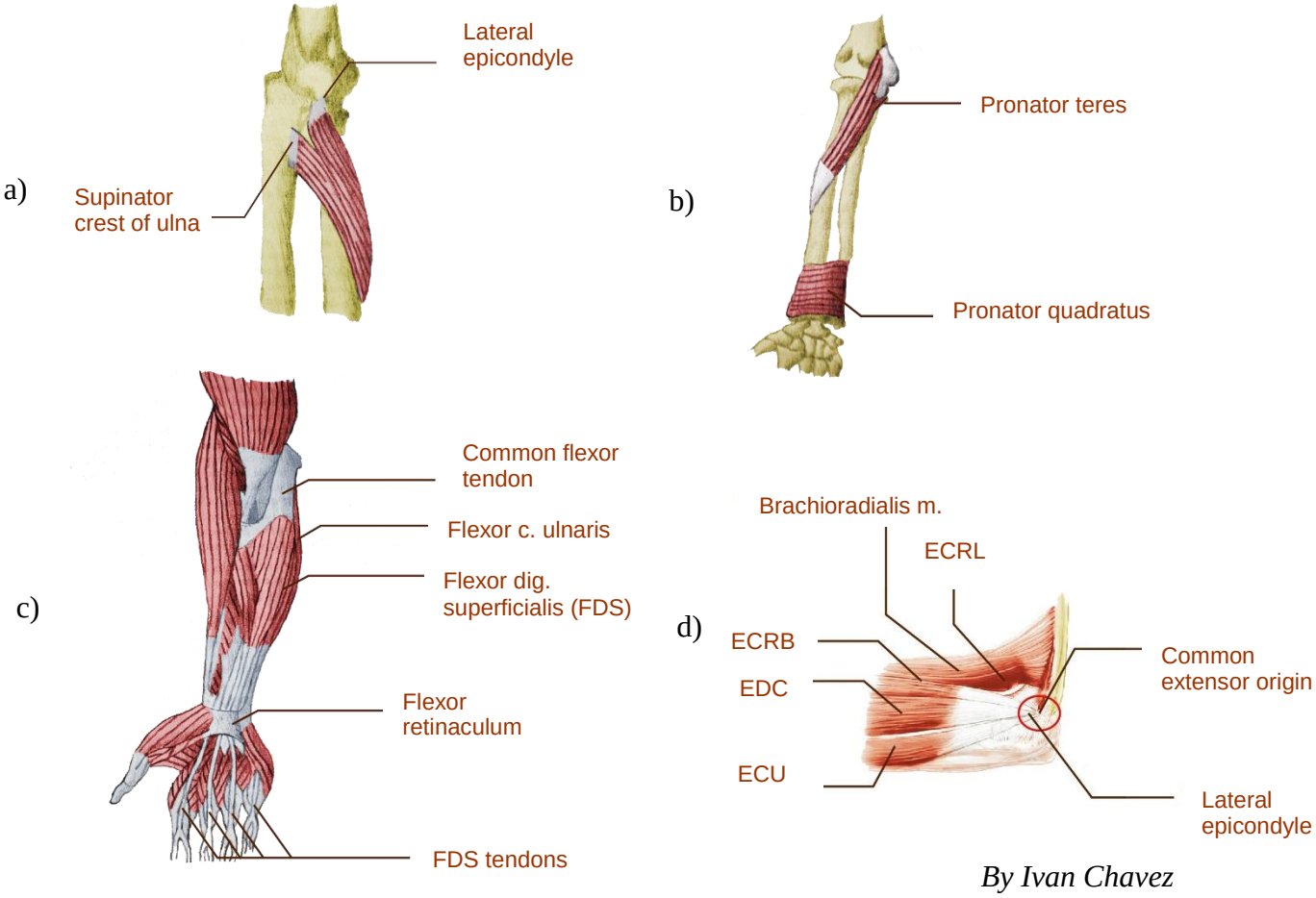

Figure 2.3. Forearm musculature: (a) Supinator muscle, lateral view. (b) Pronator teres and pronator quadratus, anterior view. (c) Flexor muscles which attach to the medial epicondyle and cross the elbow and wrist: FCU, FCR, FDS (ulnar head), and PL. (d) Forearm extensor muscles attaching to the lateral epicondyle through the common extensor tendon: ECRB (not attached through the common extensor tendon), ECU, EDC, and EDM (not shown).

2.3.1.3 Wrist and Forearm Joints

The radius and ulna attach to each other at the proximal and distal ends through the proximal and distal radio-ulnar joints (PRUJ and DRUJ), as well as the interosseous membrane at their central portion, allowing approximately 180° of rotation of the forearm (Loudon, et al., 2013). At the PRUJ, the radius is attached to the ulna via the annular and quadrate ligaments. The DRUJ, where the ulna fits into the ulnar notch of the radius, includes the triangular fibrocartilage complex (TFCC), which provides stability to the joint (Loudon, et al., 2013). Distal to the DRUJ, the concave surface of the radius, along with portions of the TFCC articulates with the carpal bones, which is what we know as the wrist joint. The TFCC articulates with the triquetrum, while the radius meets the scaphoid and lunate. Because the contact area between the radius and the carpals is larger than that between the ulna and the carpals, most of the movement occurring at the radius is transferred to the hand—and forces occurring at the hand are transferred more to the radius than to the ulna (Loudon, et al., 2013).

Summary: There are several joints within the forearm and wrist, together allowing forearm pronation/supination. Hand movements and forces are mostly transferred to the radius than to the ulna due to greater contact area between the carpals and radius.

2.3.1.3.1 Mechanics of Pronation and Supination of the Forearm

In anatomical position, when the forearm is supinated, the radius and ulna are relatively straight with respect to each other and the flexor tendons' pathways into the wrist are relatively straight. During pronation, the circular head of the radius at the proximal end spins within the annular ligament at the radial notch of the ulna. At the distal end, the radius rotates and translates over the relatively stable ulna, rotating the hand with it and forming a cross between the two bones (Drake, 2005).

Summary: When the forearm rotates from supination to pronation, the orientation of the radius and ulna changes from almost parallel to crossed.

2.3.2 Posture Effects on Internal Loading

2.3.2.1 Effect of Posture on Location and Orientation of Internal Structures

Previous researchers have quantified movement of internal structures as a function of wrist and/or finger postural change, and have discussed their implications in terms of MSK loading (Armstrong & Chaffin, 1978; Bower et al., 2006; Keir & Wells, 1999; Loh, et al., 2016; Armstrong & Chaffin, 1979). The following subsections will describe some of the first models, which used cadaver data to understand internal displacements and internal forces as a function of postural change. An overview of studies which have implemented these models to quantify internal loading as a function of postural change in vivo will be presented.

2.3.2.1.1 Initial Models: Cadaveric Studies

Armstrong and Chaffin (1978, 1979) used cadaveric specimens to quantify and model tendon displacements and estimate tendon force on the trochlear surface of the joints. They developed a predictive model to describe axial displacement (excursion) of extrinsic finger flexor tendons as a function of finger and wrist postural change, for a variety of hand sizes. In their study, hand/forearm specimens were dissected, and the finger flexor tendons separated. Each tendon was clamped at the proximal end to a force transducer in line with a displacement micrometer. A constant tensile load was maintained while the tendons were axially displaced in 2.5 mm increments; postures at the desired joints (MP, interphalangeal joints (IP), and wrist) were recorded. Joints were tested one at a time, and those not being tested were splinted in place, so that it was possible to correlate tendon excursion with posture change at each joint.

They developed regression models to predict tendon excursion and the wrist and finger joints, from hand anthropometrics (from Garret, 1970) and joint angle, based on Landsmeer's model I (Appendix A). This model of Landsmeer described tendon excursion as a function of the tendon's moment arm and angle joint, under the assumption that the estimated distance from the center of rotation to the trochlear surface was analogous to the tendon's moment arm, and was represented by:

$$x = r_1\theta \qquad \text{(Eq. 2.2)}$$

Where: x = Tendon excursion or axial displacement over the joint
r_1= Tendon moment arm (Distance from the joint centre to articular surface in this case)
θ = Angular postural change deviated from neutral in radians

Subsequently, Armstrong & Chaffin (1979) proposed another model to quantitatively show how forces inside the wrist are related to wrist size, hand force, and hand position, based

on the representation of the tendon-joint system as a belt-pulley system. According to this model, the force per arch length exerted by the tendon on the pulley (joint; F_L) is a function of the tendon tension (F_T), the radius of the pulley (trochlea; r), the coefficient of friction between the two surfaces (μ), and the angle of contact of the tendon on the pulley (θ). Both the radius of curvature and the angle of contact of the tendon on the pulley are directly affected by posture. However, because the coefficient of friction between synovial surfaces is in the range of 0.01-0.1 (Linn, 1968), the coefficient of friction was neglected, resulting in:

$$F_L = \frac{F_T}{r} \qquad \text{(Eq. 2.3)}$$

Where: F_L is the force/arch length on the pulley
F_T is the tendon tension
r is the radius of the trochlea

Additionally, the effect of posture on the total normal force exerted by the tendon on the pulley was described as:

$$F_R = 2F_T Sin(\theta/_2) \qquad \text{(Eq. 2.4)}$$

Where: F_R is the total normal force of tendon on pulley
F_T is the tendon tension
θ is the wrist angle (in degrees from straight)

These models are very useful for illustrating the effect of posture on the force exerted by the tendon on the entire trochlear surface, as well as on the force experienced at different sections of that surface (force/arc length).

Summary: Armstrong and Chaffin conducted cadaver studies to quantify finger tendon excursions with finger and wrist postural change, and to demonstrate that posture affects contact forces.

2.3.2.1.2 Evidence of Posture Effects on MSK Loading: In-vivo Studies

Keir and Wells (1999) used MRI to evaluate the effect of wrist posture on tendon movement, tendon curvature radii, and taking Armstrong and Chaffin's (1979) contact force model into account, the impact of wrist posture on contact forces within the CT, in living participants. Participants' wrists were imaged in different postures: flexed (20° and 45°), neutral, and extended wrists (20°), while loaded (10N of pinch force) and unloaded (pinch without force). Centroids of the tendon trajectories were digitized in each of the axial slices. They found volar displacements of the finger flexor tendons of the second and third digits in the sagittal plane. Tendons were described as 'closely concentrated against the retinaculum' when the wrist was flexed at 45°, even in the absence of tension. The volar displacements were ~5 mm (FDS2), between neutral and 45° of flexion. Tendon trajectories at the wrist followed a non-constant path, with two straight ends on either side of the joint, similar to that proposed by Lansdmeer's model II (Appendix A). In contrast, tendon trajectories were fairly straight when the wrist postures were extended or neutral. Generally, the tendons' radii of curvature were reduced in postures away from neutral; this reduction was most pronounced when the wrist was flexed 45°. The addition of load reduced the radii of curvature. It was pointed out that the combination of load and posture had a greater effect on the contact force than either one of those factors alone.

Other studies have also evaluated various mechanical changes using imaging techniques (Bower et al., 2006; Loh, et al., 2016). Bower et al. used MRI to investigate the effects of wrist

posture (30° of flexion and extension, neutral, and a fist with neutral wrist) on CT dimensions, as well as on the ratio between the tunnel's dimensions and its contents. Cross-sectional areas were calculated using the perimeter of the CT walls in the axial direction, along the length of the tunnel. By means of signal intensity changes, the outlines of the contents (9 finger flexors and the median nerve) were identified automatically and their respective axial cross-sectional areas were calculated. The addition of the areas of all the flexor tendons and the median nerve, as well as the area of the entire tunnel, were then integrated along the tunnel to calculate the volume of the tunnel and its contents. Ratios of areas and volumes were estimated. Their results showed that CT areas and volumes were smaller in extension, which they suggested may be due to the increased tunnel pressure observed with extension (Werner et al., 1997). In addition, Loh et al. (2016) were able to demonstrate deformation of the median nerve at the CT as a function of finger flexion. The cross-sectional area of the median nerve was quantified using ultrasound, in three finger postures (relaxed fingers, full finger flexion without force, full fist with grip), while the wrist was held neutrally. They reported that the median nerve cross-sectional area when the fingers were relaxed was significantly larger than that seen in the other two conditions. The smallest area was seen when the fingers formed a fist with a grip.

Summary: Findings indicate that postural change can be a significant contributor to MSK loading, particularly under loading conditions. Compiling results from a variety of studies could help researchers model the transfer of external exposures to internal loading in-vivo.

2.3.3 Association of External Exposures to Internal Loading

The goal of research such as the study described above is to estimate internal MSK loading for a variety of work tasks. Unfortunately, estimating the risk of developing MSDs for particular work tasks is very difficult, due to the complex interrelationships of contributing factors. One study in particular took this complexity into account when trying to create a link between external exposures and internal MSK loading; Moore et al. (1991) combined previous biomechanical models to develop their own. The model is able to highlight the contribution of each factor alone on internal loading—while taking into account the effects of external exposures (posture, repetition, and force), the cumulative effects of tasks, individual variability (e.g., anthropometrics), and worker tendencies (e.g., over-gripping). Input measurements included forearm EMG, as well as wrist and finger posture measurements, for a variety of manual tasks. These measurements helped to estimate various variables to describe internal loads. This model was a significant step towards being able to estimate the risk of developing specific MSDs for a variety of jobs, and understanding the role of each external exposure factor in the mechanism of injury. However, this work did not take into consideration the loading effect of forearm pronation/supination posture. The inclusion of forearm posture may be a valuable addition to this model, potentially improving internal loading estimates from external exposures associated with manual activities.

Summary: A previous model took a number of occupational exposures into account when correlating external exposures with internal MSK loading. The addition of forearm posture to this model may be able to improve internal loading estimates.

2.3.4 Evidence of Histological Changes due to Mechanical Change

Several researchers have demonstrated histological changes in the structures within the CT as a function of mechanical loading, including synovial hyperplasia, increased density of synovial and adjacent connective tissue, muscular hypertrophy of the arterioles that supply the median nerve (Armstrong et al., 1984), and increased density of the median nerve's epineurium (Armstrong et al., 1984; Keir & Rempel, 2005).

Armstrong et al. (1984) compared the histological characteristics of various tissues (i.e. synovial layers, connective tissue, median nerve, and vascular tissue) in areas of high and low stress within the wrist. Assuming that every wrist had been subjected to mechanical loading, healthy wrists from cadavers (60-81 years) were transversely cut into serial sections beginning at the wrist crease. The cuts were performed at 5 mm intervals proximal and distal to the crease over a 9 cm range. Samples of tissues from synovial layers, median nerve layers, and vasculature were obtained from each section. Histological properties were compared at cut locations for each tissue. Higher synovial, sub-synovial, and adjacent connective tissue densities were seen near the crease, along with gradual decreases in density with greater distances both proximally and distally. Greater muscular hypertrophy of arteriole walls was also seen near the wrist crease, along with an increase in epineurium density. These findings were recognized by the authors as histological deterioration that occurs with mechanical loading in the absence of CTS. Notably, similar findings were reported in CTS patients in a literature review by Keir & Rempel (2005). Wrists with CTS also exhibited thickening of vessel walls, the median nerve's endoneurium, and the perineurium, in addition to perineurial edema. Cumulatively, these changes may result in a more crowded environment within the CT, which can lead to further MSK loading increases.

Summary: The evidence suggests that all MSK loading causes chronic changes in tissues, even in the absence of pathology, further supporting the need to quantify postural demands of work tasks, and their relationship to internal loading

2.4 Objective:

In light of epidemiological evidence linking forearm pronation/supination to injury, as well as biomechanical evidence demonstrating that features of forearm pronation/supination can magnify discomfort and exertional demands, the general objective of this study was twofold. First, to develop a feasible method for measuring forearm pronation/supination in the workplace; and second, to examine the effects of wrist and forearm postural changes on tendon trajectories at the wrist, to better understand their potential implications for MSK loading.

3 CHAPTER 3. Study I

Assessing Forearm Pronation/Supination in the Workplace: A Comparison between Xsens and Vicon Measurements during a Handle Turning Task.

3.1 Introduction

Distal upper limb injuries are prevalent and costly, with a relatively lengthy recovery period. There were nearly 1,200,000 musculoskeletal disorders (MSDs) reported in 2014 in the United States in all sectors—and approximately 30% of them affected the upper limb (arm, wrist, and hand), making upper extremities the leading injured body part (BLS, 2015). Upper limb injuries required approximately 15 days away from work (BLS, 2015). Both their cost and their impact on quality of life demonstrate the need to minimize their occurrence.

The Bureau of Labor Statistics reported worker motions and postures as the second-most common source of injury in the workplace (BLS, 2008). Thus the quantification of hand and forearm motions is important, because it can help identify potentially injurious hand/wrist and forearm motions. Knowing what high risk motions can be useful when developing jobs, creating work stations, and designing hand tools. Forearm pronation/supination, although it has not been extensively studied, has been associated with injuries of the upper limb. The number of years spent performing tasks involving repetitive forearm pronation/supination (forearm twisting), such as tying with pliers or using a manual screwdriver, has been associated with hand/wrist and elbow/forearm disorders (Hughes et al., 1997). Forestry machine operators who used controls requiring a pronated forearm have been on sick leave more often due to elbow and shoulder injuries than those using controls requiring semi-pronated postures (Grevsten & Sjögren, 1996). Additionally, full forearm supination in combination with 90° flexion of the metacarpophalangeal joint (a common posture when lifting and carrying) has been reported to

produce the highest CT pressure, which is correlated with the development of CTS (Rempel et al., 1998).

In spite of evidence demonstrating a link between certain forearm pronation/supination actions and upper limb disorders, there is little information on quantified forearm kinematics associated with work tasks. A better understanding of the forearm/wrist postural combinations which are capable of dangerously loading the MSK system is needed for the development of safety guidelines. A key aspect of this goal is the ability to reliably quantify the ranges of motion, numbers of repetitions, and time durations required for various work tasks.

In ergonomics studies, it is often preferable to analyze tasks at the workplace in order to capture realistic exposure measures. However, because workplace conditions cannot usually be controlled, particularly with respect to light sources and space, the use of motion capturing systems, such as Vicon (Vicon motion system LTD., Oxford, UK), to measure body postures is not feasible. Instead, portable systems, such as the Xsens inertial motion units (IMUs) (Xsens Technologies B.V., Enschede, Netherlands, 2008), are often used to quantify postures outside of a laboratory setting. These portable systems, which (unlike Vicon) do not require lengthy calibration procedures, allow workers to ambulate freely and perform all tasks.

Portable motion capturing systems other than IMUs have also been used to measure forearm pronation/supination, including electromagnetic sensors, torsiometers, and customized potentiometers (Jones & Kumar, 2006; Marklin & Monroe, 1998; Mohankumar et al., 2014; Schoenmarklin et al., 1994). However, there are some challenges associated with their use. For instance, Schoenmarklin et al. (1994) used a proprietary potentiometer, which is not available on the market. Magnetic motion trackers can be subject to large errors induced by magnetic disturbances because (unlike IMUs) they rely solely on magnetism. Also, magnetic receivers and

transmitters must be in close proximity in order to maintain measurement accuracy, but certain work activities may require to extend beyond the useful range. Some uni-axial measurement sensors, such as torsiometers, can be prone to underestimating forearm pronation/supination if not perfectly aligned with the forearm long axis—and obtaining perfect alignment is difficult. In addition, torsiometers are subject to translation when measuring forearm pronation/supination, suggesting complex calibration may be required, particularly as the distance from the axis of rotation increases.

Xsens IMUs, equipped with gyroscopes, accelerometers, and magnetometers, have been successfully used in previous studies to measure body posture of the upper limb, back, and lower extremities in work and sports environments (Browning,et al., 2012; Denbeigh, et al., 2013). Combining all three devices has the advantage of overcoming challenges presented by any of these devices alone, such as the integration drift over time associated with gyroscopes, the noise induced by the presence of accelerations not associated with the movement of interest, or magnetic disturbance caused by metal nearby. Moreover, the IMUs are easily mounted on participants; they do not need to be perfectly aligned with segment axes, given their ability to measure 3D orientations. However, the IMU's validity and reliability when measuring forearm pronation/supination have not been extensively studied, and the effect of nearby metal on its measurements is unknown.

A preliminary study at the York University biomechanics laboratory compared forearm pronation/supination measurements obtained from Xsens and Vicon, and evaluated the effect of metal on the agreement (Lagree et al., 2016). The study compared summary statistical data between motion capture systems, including percentiles (10^{th}, 50^{th}, and 90^{th}), maximum and minimum values, and the number of turns. These are common variables of interest in ergonomics

research to evaluate physical exposures of continuous tasks. Relatively good agreement was found (3.9° was the largest average difference). Another study (Shublaq, et al., 2009) evaluated the instantaneous agreement of forearm pronation/supination measurements obtained with Xsens and Vicon. The study, published as a conference proceeding, found moderately high correlations ($r=0.87$) during rehabilitation tasks without metal. However, applying these results to measurements in the workplace may not be appropriate, because ferromagnetic environments and the use of metallic tools are common in the workplace.

The objective of the current study was to assess the extent of the instantaneous agreement between Vicon and Xsens IMUs when measuring the forearm pronation/supination of participants turning metallic and non-metallic handles. It was hypothesized that the Vicon and Xsens measurements would have good agreement, and agreement would vary in the presence of metal.

3.2 Methods

3.2.1 Participants

Data were collected from a convenience sample of twenty males, who were recruited by word of mouth from the university community. This sample size afforded sufficient statistical power β (0.8) to detect differences in measure errors (RMSE) among all conditions (see statistics section for information on the power analysis), given that only 11 participants would have been needed for this study. Participants' age ranged from 18-55 years, and BMI ranged between 21-32 (Table 3.1). Exclusion criteria included MSK injury within the last year, receiving MSK rehabilitation during the time of the study, or the presence of any disease that may influence movement or produce MSK discomfort.

Table 3.1. Participant anthropometrics.

	Height (m)	Weight (Kg)	BMI
n		20	20
$\bar{x}$	1.77	81.87	26.01
SD	0.08	9.26	2.40

3.2.2 Experimental Setup

An iron vertical wall containing nine iron handles was built (see Figure. 3.1). The locations of all handles were normalized to handle 5, which was placed roughly in front of the elbow, and was defined as the neutral position. The goal of the arrangement was to orient IMUs within a functional range of working postures, defined with respect to the elbow: top right, top left, bottom right, bottom left, top, bottom, right and left. The handles, designed so that participants could grasp them comfortably in the palm of the hand, could be moved to normalize their

locations to each participants' anthropometrics. A plastic/acrylic wall of similar design was also built, fully free of metal. Handles were numbered for easy identification. A tenth iron handle, identical to the other metallic handles, was placed on the floor to test whether the instantaneous agreement between Xsens and Vicon was affected when the x axes of the arm IMUs (pointed proximally) came into close alignment with the global vertical, when metal was near the IMUs.

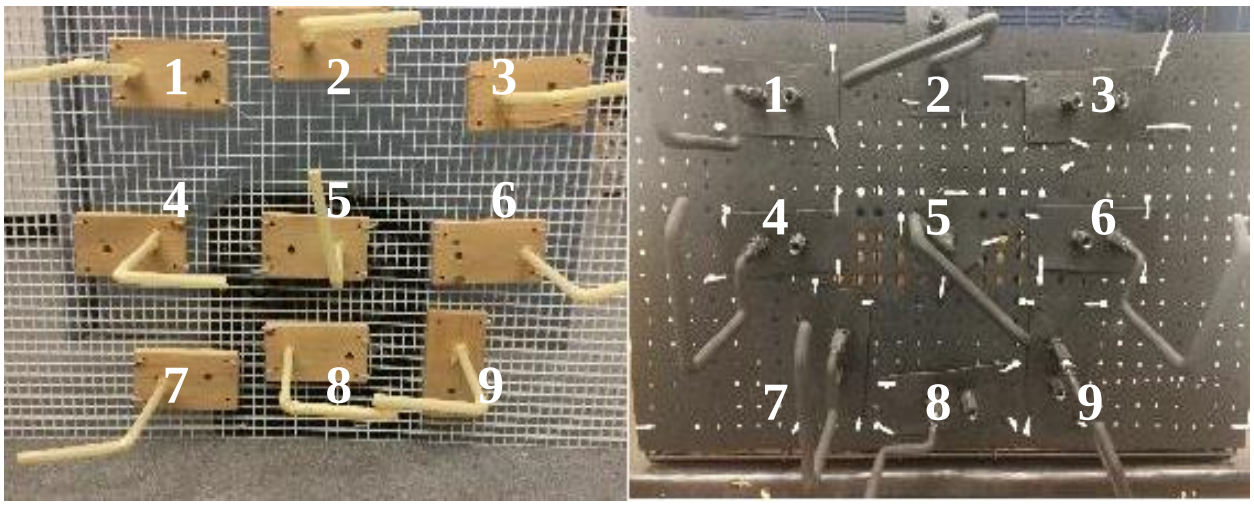

Figure 3.1. Illustration of the plastic (left) and metallic (right) handles used in the study.

Prior to normalizing the locations of the nine handles, the standing location was determined by instructing participants to stand at a comfortable distance from the vertical handle wall in front of them, so that they were able to easily grasp handle 5, while the shoulder remained in approximately 45° of flexion, and the forearm parallel to the ground (Figure. 3.2). The standing location was marked and remained constant during the testing period. The rest of the handles were placed so that participants could easily grasp them by performing humeral rotation and/or elbow flexion or extension. Handles 4 and 6 were placed to elicit approximately

45° of internal and external rotation of the humerus, respectively. Handles 2 and 8 were placed to elicit approximately 45° of elbow flexion or extension, respectively. Handles 1, 3, 7, and 9 were placed at locations that required combinations of elbow flexion/extension and humeral external/internal rotation. Reaching for the tenth handle on the floor (not shown) elicited a relaxed posture of the arm, as it was positioned in front of the participant's shoulder, requiring trunk flexion to reach the handle.

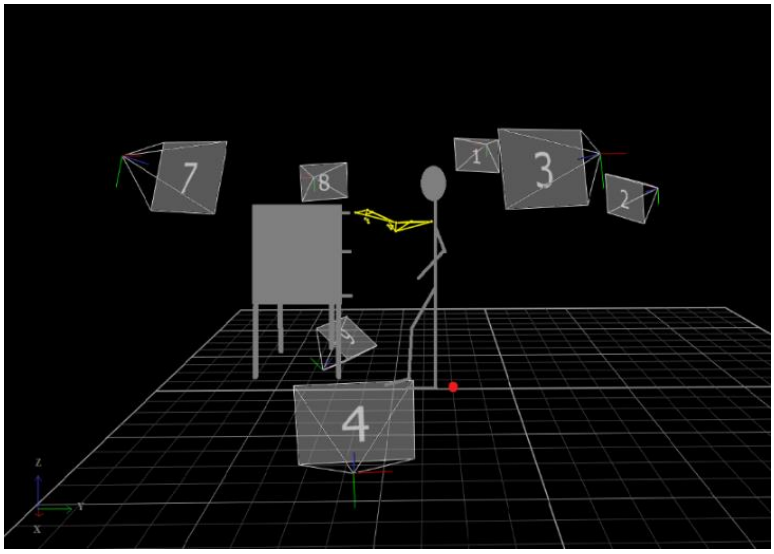

Figure 3.2. General body posture of a participant turning the top handles, in a motion capture area in front of seven Vicon cameras. Origin is marked in red, and the global coordinate system is illustrated at the bottom left.

3.2.3 Protocol

This study was approved by the Office of Research Ethics at York University in accordance with the policy of the Human Participants Review Committee. The Vicon system was calibrated prior to the arrival of participants. An initial questionnaire was administered to participants to obtain general demographic information, handedness, anthropometrics, and musculoskeletal health. Participants were equipped with Xsens IMUs and Vicon reflective markers (Figure 3.3a). Once participants were fully equipped, the Xsens was calibrated.

During data collection, participants were required to turn the nine handles of one vertical wall (metal or plastic) in random order. The order of presentation of the two vertical wall structures was also random, although all nine handles of the first wall were turned before those of the second one. The order of presentation was randomized by drawing a number. A new marker configuration was created with the goal of defining proximal and distal forearm segments. Participants started each trial in a position that facilitated marker identification in the Vicon system, standing with their right arm flexed in front of them, with an extended elbow and the thumb pointing up (Figure. 3.3b). There were 19 trials in total, one for each of the nine handles of each vertical wall and one for the metallic handle on the floor. Each trial consisted of three consecutive turns in each direction: pronated to supinated forearm, and supinated to pronated forearm. Participants were required to position their arm in the initial posture in the middle of each trial, once they had completed the first three consecutive turns in one direction before turning the handles in the opposite direction. The order of the direction of the turns, instructed to them in each trial, was randomized. Participants were required to ensure that the handles remained horizontal at the start and end of each turn. An assistant supervised the participants to ensure they followed the researcher's instructions. Trials were repeated when the

movement was not continuous, or the instructions were not thoroughly followed. Kinematics of their arm were recorded during the turning tasks using Vicon and Xsens simultaneously.

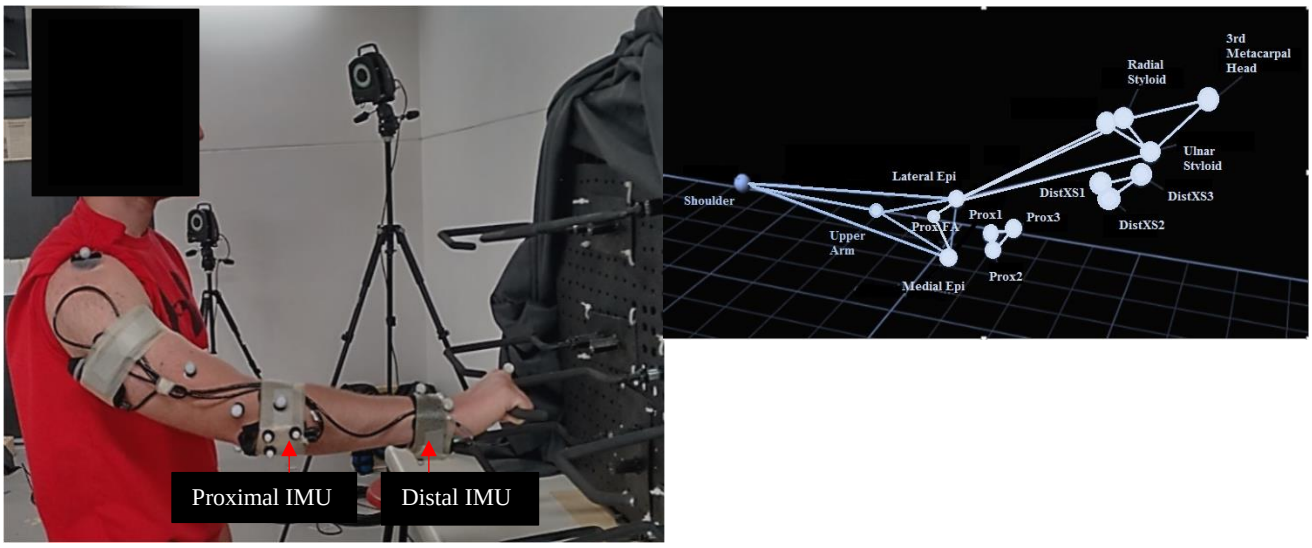

Figure 3.3. (a) Participant setup with Xsens sensors and Vicon reflective markers, while turning a metallic handle. (b) Vicon marker configuration while participant stood in the calibrating position (handle 5): dominant arm flexed in front, with an extended elbow and the thumb pointing upwards.

3.2.3.1 Vicon Motion Capturing System

The Vicon system was used as the gold standard for motion capturing. Seven Vicon MX40 cameras were placed around the capturing area at varying heights, approximately 1-2m away, including one near the floor on the right side of the participant to capture the bottom of the forearm during rotation (Figure. 3.2).

The x axis of the global frame of reference pointed to the left of the participant, the y axis pointed dorsally, and the z axis pointing superiorly. (Figure. 3.2). The origin of the capturing volume, constant across trials, was situated at a point on the floor behind the participant.

Participants were set up with 15 reflective markers on the dominant arm. Nine were placed directly on anatomical landmarks of the arm (9.5 mm). The anatomical landmarks comprised: 1) acromion, 2) upper arm (laterally), 3) lateral humeral epicondyle, 4) medial humeral epicondyle, 5) proximal forearm (dorsally on the radial side, approximately an inch distal to the humeral condyles), 6) radial styloid, 7) ulnar styloid, 8) distal forearm (dorsally on the radial side, approximately an inch proximal to the styloid), and 9) head of third metacarpal. The remaining six sensors were placed on the two lower arm Xsens sensors: two on the proximal corners, and one on the distal, radial corner of each sensor (Figure. 3.3a).

3.2.3.2 Inertial Measurement Unit Sensors (IMUs)

The Xsens sensors are inertial measurement units that rely on a combination of triaxial gyroscopes, triaxial linear accelerometers, and triaxial magnetometers to measure the orientation of each sensor in space. In addition to its capability of providing individual outputs of acceleration, angular velocity, and magnetization, Xsens also provides the orientation of each sensor in space, combining data from the three devices with the use of a Kalman filter. The filter reduces both the high frequency noise from the accelerometers and the drift associated with the continuous integration of angular velocity into position (Xsens, 2008).

The orientation calculated by the Xsens is a weighted average of the outputs from the 3D accelerometers, gyroscopes, and magnetometers (Xsens, 2008). Any changing accelerations (besides gravity) will sum to zero, if the participant is not travelling. The accelerometer measurements are used to stabilize attitude (roll and pitch combined), while the magnetometer measurements are used to stabilize yaw; in the presence of magnetic disturbance the Xsens creates a new local magnetic north and recalibrates. However, when the magnetic disturbance is

not predictable (such as when the IMIs and a large metallic object are moving with respect to each other), the Xsens may err in its orientation estimations.

3.2.3.2.1 Global/Local Coordinate Systems

The Xsens sensors calculate the orientation of the sensor-fixed local system with respect to a global, earth-fixed system. The global coordinate system follows the right-hand rule (Figure 3.4). The sensors use the acceleration of gravity and the local magnetic north to create two of the axes of the global system, and an orthogonal third axis is calculated as the cross product of the first two (Xsens motion technologies, 2008).

- 'x' pointing to local magnetic north
- 'y' pointing west
- 'z' pointing upwards

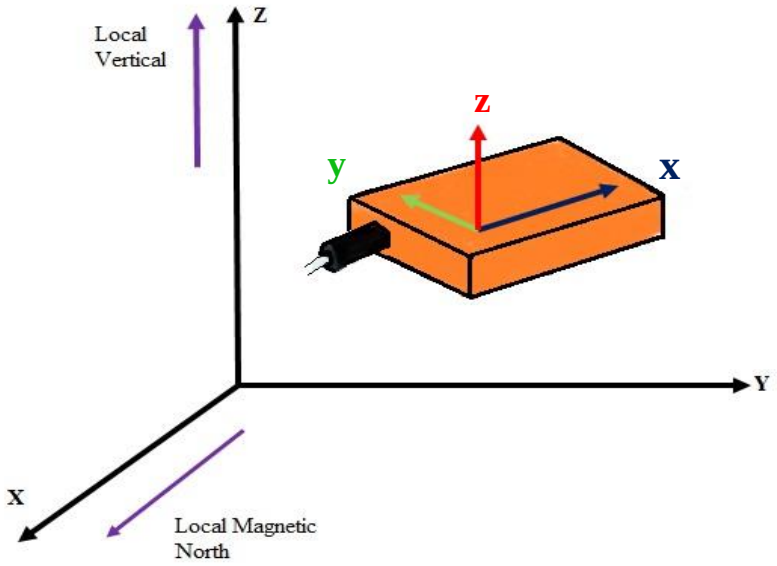

Figure 3.4. Depiction of the Xsens sensor-fixed coordinate system (local system), in a global frame of reference (black arrows) created by the gravity vector (z), the magnetic north (x), and the cross product of the two (y).

The sensor-fixed system consists of three orthogonal axes that follow the right-hand rule (Figure. 3.4). All sensors were mounted on participants so that their CSs were aligned in anatomical position. The directions of the local vectors with respect to the participant, while standing in anatomical position, were as follows:

- 'x' pointing proximally on the participant's forearm (pronation/supination axis)
- 'y' pointing to the left of the participant
- 'z' pointing posteriorly

Four Xsens IMUs were placed on participants, with the cords towards the distal forearm, while standing in anatomical position (Figure.3.3a). Participants wore one IMU on the back, at the T7 level, adjacent to the inferior border of the scapula, and three other IMUs on the dominant arm at the following locations: 1) immediately below the axilla at the posterior midline of the humerus, approximately at the level of the fourth thoracic vertebrae; 2) just below the olecranon at the posterior midline of the dominant forearm; and 3) directly proximal to the wrist, at the distal midline on the anterior surface of the forearm. The distal forearm IMU was positioned bottom plate up, in order to align its CS with the CSs of the other three sensors (which were positioned posteriorly). Care was taken to reduce movements of the IMUs with respect to the body segments as much as possible, by securing them with pro-wrap and medical tape. The positions of the IMUs were selected to avoid interfering with other collection equipment, permit mobility, and allow the researcher to place IMUs consistently over easily palpated landmarks. Initial 30-second measurements were taken in order to allow IMUs to find a local magnetic north for external reference. Initial measurements were obtained while participants stood relaxed with arms by their sides. (According to Xsens instructions, Xsens IMUs need at least 10 seconds to recognize a local magnetic north.)

3.2.3.2.2 Anthropometrics

Height and weight were measured, and used to calculate the body mass index (BMI). BMI was of interest because it has been previously shown to be closely related to forearm thickness (Günther, et al., 2008), and it is unclear whether forearm thickness could affect Xsens-Vicon agreement when measuring forearm pronation/supination.

3.2.4 Data Collection

3.2.4.1 Vicon

The three-dimensional location of each Vicon marker was continuously tracked over the duration of the tasks at 100 Hz. When gaps were found in the marker trajectories, they were corrected in Vicon Nexus 1.6.1 (Vicon, Oxford, UK), using the pattern fill function. After eliminating all gaps in the kinematic data, marker coordinates were further processed using Visual 3D biomechanical analysis software (C-Motion, Inc., Germantown, MD, USA).

3.2.4.2 Xsens

Postures of the dominant arm were recorded with Xsens sensors in three planes at a sampling frequency of 30 Hz, using the X-Analyzer software (NexGen Ergonomics Inc., Quebec, Canada). The X-Analyzer provided continuous relative Euler angles of the distal forearm IMU with respect to the proximal forearm IMU, using an X-Y-Z sequence. The configuration provided relative angles of the shoulder, elbow, and forearm pronation/supination, however only forearm rotation measurements are discussed.

The Xsens output used for comparison with Vicon measurements comprised the transverse plane rotations of the forearm distal sensor with respect to the proximal forearm

sensor, which represented the rotation of the local y-z plane about the local x axis between sensors, because it was assumed that the x axes of both forearm sensors were perfectly aligned with each other, and with the forearm's long axis.

3.2.5 Signal Processing

Marker data were transferred from Vicon to Visual 3D. The continuous x-y-z coordinates of each marker were low-pass filtered using a dual pass 6 Hz Butterworth filter. The forearm pronation/supination angles were calculated using a custom-made model in Visual 3D, and low-pass filtered with a dual pass 6 Hz Butterworth filter.

3.2.5.1 Kinematic Model – Visual3D

The kinematic model used to measure rotation of the forearm consisted of two triangular planes, which shared the longitudinal axis of the forearm. The proximal forearm segment was created using the two markers on the medial and lateral humeral epicondyles, and a third point was calculated as the midpoint between the ulnar and radial styloids. The distal forearm segment was created using the two markers on the radial and ulnar styloids, and a third point was calculated as the midpoint between the medial and lateral humeral epicondyles (Figure.3.3.b.). The shared longitudinal axis was helpful for isolating forearm pronation/supination and eliminating cross-contamination from movement in other planes. Vicon forearm pronation/supination angle measurements for comparison with Xsens was estimated as the relative angle created by the rotating transverse plane of the distal forearm segment with respect to the proximal forearm segment, about a shared longitudinal axis.

Forearm pronation/supination can cover a range of 180 degrees, so the Xsens signals were checked for evidence of gimbal error. In a most cases (300/361 trials), Xsens signals approaching -90° had a polarity change from one frame to the next, creating peaks within some of the signal's valleys. A custom-made Matlab program (Matlab 8.10.604 (R2013a), The MathWorks, Inc., US) was coded to identify these errors. The criterion used to identify them was an abrupt change in direction occurring within valleys that dropped below -82°.

3.2.5.2 Xsens-Vicon Comparisons

Another program was coded in Matlab to do a series of operations on the forearm position time-series from Xsens and Vicon, to correlate and analyze the agreement between them. First, due to the difference in sampling frequency, the Vicon signals had to be resampled to 30 Hz using linear interpolation. A cross-correlation of each Xsens-Vicon pair for the same trial was performed in order to synch them in time. The researcher then isolated six turns of interest within the signals of each trial.

In order to compare Xsens and Vicon signals, biases were removed for each single Xsens-Vicon pair. The mean of each signal was calculated and used as the respective bias. A calibration factor was calculated using the signals of the handle 5 trial, which was the trial with the most neutral posture in terms of forearm pronation. The factor (*c1*) was calculated by first dividing the Vicon range by the Xsens range over the trial; then a sequence of calibration factors that ranged from *c1*-1 to *c1*+1 in 0.01 increments was tested in a loop to repeatedly measure the squared error difference associated with each one. The factor resulting in the smallest error (*cf*) was selected as the calibration factor for all of the Xsens trials of that participant.

3.2.6 Statistical Analyses

The root mean square error (RMSE) and ICC (Intra-class correlation coefficient) were calculated for each pair of Xsens and Vicon forearm pronation/supination posture time series to analyze the discrepancies between them. The effect of forearm anthropometrics was tested, to investigate the possibility of a confounding effect, by evaluating the correlation between BMI and error measures (ICC and RMSE) with a Pearson's correlation test. Three-way repeated measure ANOVAs were performed to test the effect of material, vertical (top, middle, and bottom rows), and horizontal (left, middle, right) handle locations on the error measures (2x3x3). Post-hoc Bonferroni comparisons were used to identify specific differences among variable levels of each significant main effect, differences between locations for each material, and differences between materials within each location. The Greenhouse-Geisser correction was used when sphericity was violated. A sample size calculation was performed based on the results, using the most stringent effect size observed among all within subject comparisons ($d = .24$) (corresponding to the three-way interaction effect), power β of 0.8, and alpha level of 0.05.

The effect of vertical location among metal handles was tested using a one-way repeated measures ANOVA, which included the three handles located within the centre column and the floor handle. Post-hoc Bonferroni comparisons were used to identify specific differences among the four locations.

3.3 Results

Data from 19 participants were included in the analyses due to missing data of one participant. The range of calibration factors across subjects was small (1.05-1.26). Pearson correlations showed that BMI was not significantly correlated with error measures (BMI-ICC r=-0.054, p>0.05 and BMI-RMSE r= -0.008, p>0.05). Overall, Xsens and Vicon differed on average by 12.6° and 8.6° RMSE on metal and plastic, respectively (Table. 3.2). As a measure of absolute agreement, ICCs were on average 0.947 and 0.977 for metal and plastic, respectively (Table 3.2).

Table 3.2. Means and standard deviations of forearm pronation/supination Vicon-Xsens root mean square error (RMSE) (left) and absolute agreement (right), during a handle turning task at 9 different locations, with and without metal. Darker shades of red represent larger Xsens-Vicon discrepancies. Repeated measures ANOVA results are presented below.

RMSE

Metal	**Right**		**Centre**		**Left**	
	Mean	*SD*	*Mean*	*SD*	*Mean*	*SD*
High	9.4	2.9	9.4	2.8	10.4	3.4
Middle	12.4	3.8	12.4	3.6	15.1	8.6
Low	14.4	5.9	15.4	5.3	14.8	5.0
Plastic	**Right**		**Centre**		**Left**	
	Mean	*SD*	*Mean*	*SD*	*Mean*	*SD*
High	7.6	1.8	8.8	3.2	8.0	2.1
Middle	8.4	2.1	8.4	2.3	8.2	1.8
Low	8.9	2.2	9.5	2.5	9.3	2.4

ANOVA results	*F*	*df*	*p*
Material	72.132	(1, 18)	<0.05*
Vertical	31.073	(2, 36)	<0.05*
Horizontal	2.529	(2, 36)	>0.05
Material * Vertical	14.000	(1.497, 26.948)[a]	<0.05*
Material * Horizontal	1.616	(2, 36)	>0.05
3-way Interaction	1.074	(2.234, 40.221)	>0.05

ICC

Metal	**Right**		**Centre**		**Left**	
	Mean	*SD*	*Mean*	*SD*	*Mean*	*SD*
High	0.97	0.02	0.96	0.02	0.97	0.02
Middle	0.95	0.04	0.95	0.03	0.95	0.03
Low	0.94	0.04	0.92	0.08	0.92	0.05
Plastic	**Right**		**Centre**		**Left**	
	Mean	*SD*	*Mean*	*SD*	*Mean*	*SD*
High	0.98	0.01	0.98	0.02	0.98	0.01
Middle	0.98	0.01	0.98	0.01	0.98	0.01
Low	0.98	0.01	0.97	0.02	0.97	0.02

ANOVA results	*F*	*df*	*p*
Material	37.541	(1, 18)	<0.05*
Vertical	16.284	(2, 36)	<0.05*
Horizontal	2.104	(2, 36)	>0.05
Material * Vertical	10.994	(2, 36)	<0.05*
Material * Horizontal	0.548	(2, 36)	>0.05
3-way Interaction	0.871	(1.884, 33.904)[a]	>0.05

Two examples of Xsens-Vicon discrepancies when measuring forearm pronation/supination are shown in Figure 3.5, one with the lowest RMSE (upper graph) and one with the highest (lower graph).

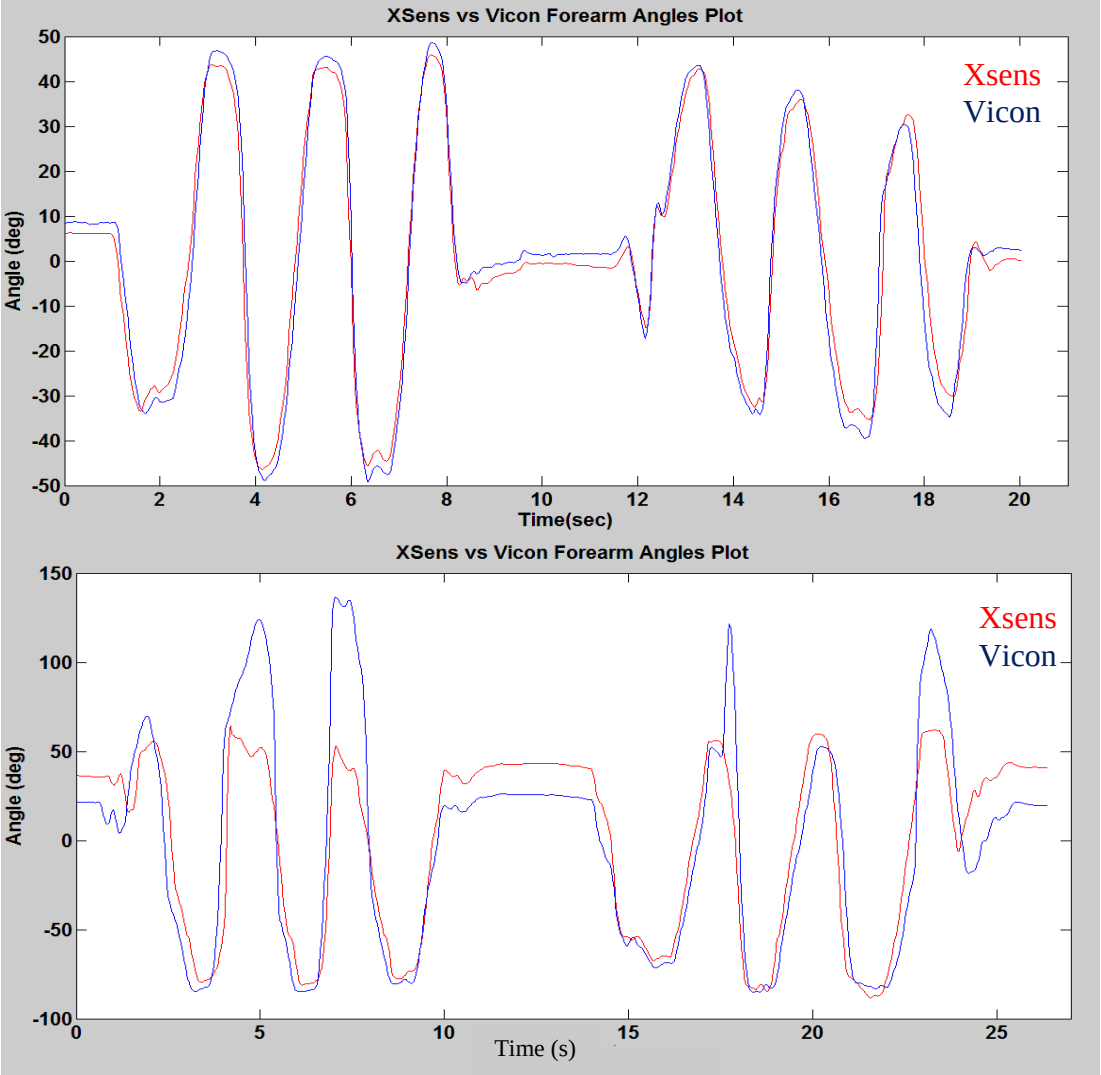

Figure 3.5. Samples of simultaneous time-histories of Xsens-Vicon forearm pronation/supination measurements of two trials of separate participants. Top plot: a plastic trial of handle 1 with low RMSE. Bottom plot: a metallic trial of handle 8 with high RMSE. Supination is positive, and pronation negative. Note that this plot includes the highest error observed, and there were only a few trials with such large error.

High correlation coefficients were seen after testing for absolute agreement. Approximately 95% of all trials of all participants showed ICCs of 0.90 or above (Figure 3.6).

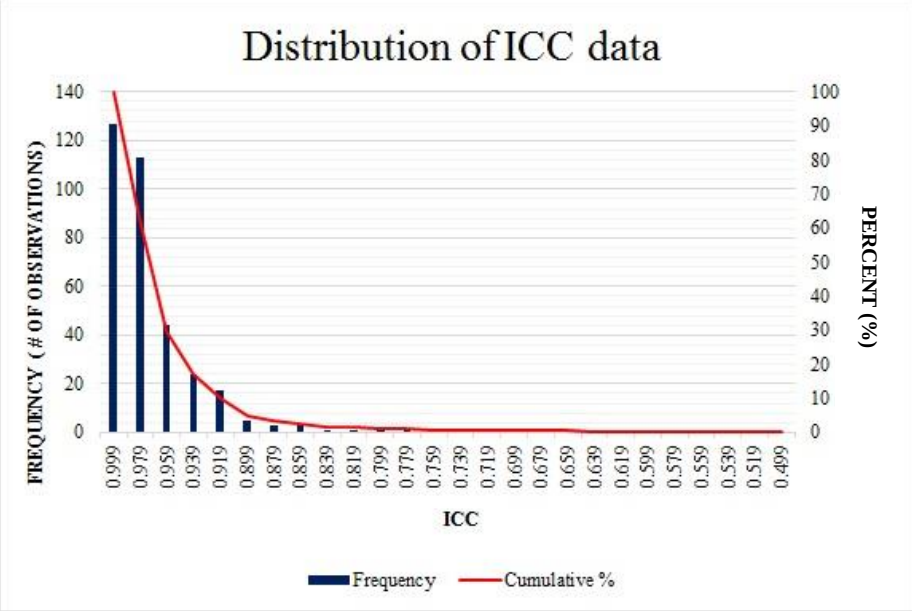

Figure 3.6. Distribution of ICC values (0.499-0.999) of all trials and all participants. More than 95% of all trials showed ICC >0.90.

A Mauchly's Sphericity test revealed that sphericity could be safely assumed for all variables in the ICC and RMSE analyses. The 2x3x3 ICC ANOVA showed an interaction between material and vertical location on Xsens-Vicon agreement ($F(2, 36) = 10.994$, $p = 0.000$), and main effects of both material ($F(1, 18) = 37.541$, $p = 0.000$) and vertical location ($F(2, 36) = 16.284$, $p = 0.000$). The RMSE analyses were similar, showing an interactive effect of material and vertical location on Xsens-Vicon RMSE ($F(2, 36) = 14.000$, $p = 0.000$), along with a main effect of both material ($F(1, 18) = 72.132$, $p = 0.000$) and vertical location ($F(2, 36) = 31.073$, $p = 0.000$). Post-hoc Bonferroni comparisons revealed that measurements from plastic trials had overall better agreement (higher ICC, and lower RMSE) than those from metallic trials, for all

handle locations (Figure 3.7). This material effect was more pronounced for the two bottom rows (handles 4-9) (Appendix B).

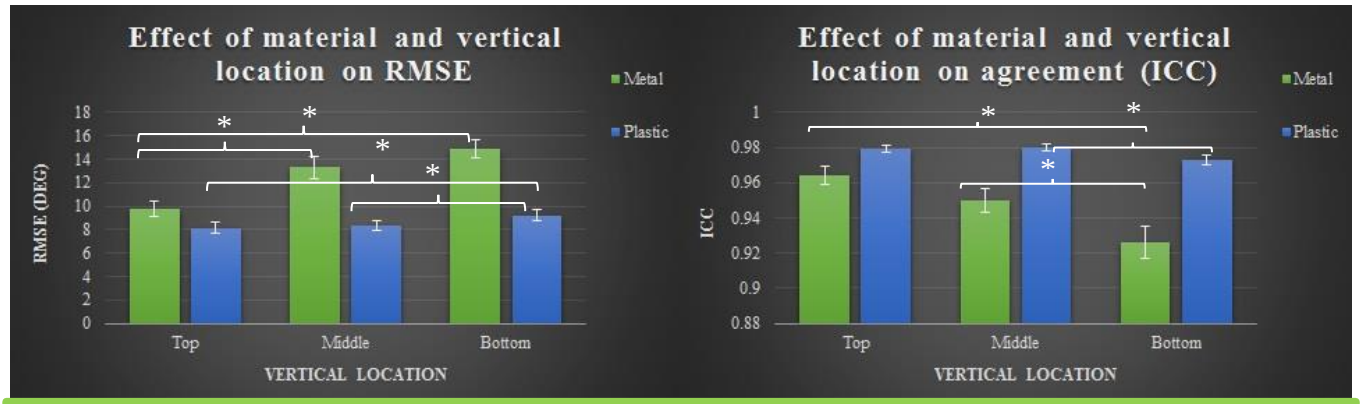

	Top	Middle	Bottom
Metal	9.747	13.29	14.872
Plastic	8.126	8.366	9.227

	Top	Middle	Bottom
Metal	0.964	0.95	0.926
Plastic	0.979	0.98	0.973

Figure 3.7. Significant effects of vertical location, within each material, on RMSE (left), and agreement (right) between Xsens and Vicon time-histories. The effect of horizontal location was not illustrated because it was found not to have significant effects on either measure. Bars represent standard error, and asterisk denotes significance at $p<0.05$ Bonferroni corrected for multiple comparisons.

Better agreement between the two systems was seen at the top row handles, than when turning the handles of the middle and lower rows. This effect was more pronounced in the metal than in the plastic trials (Appendix B). A similar trend (decreased agreement in lower locations) was observed in the analyses including only the metallic handles of the middle column and the tenth handle on the floor; Bonferroni comparisons found the RMSE of the tenth handle only differed statistically from the top handle (Appendix C).

Although RMSE and ICC analyses were similar, the RMSE reached significance in more comparisons than the ICC did, suggesting that the RMSE was more sensitive to changes. Horizontal location (i.e. left and right handle locations) did not have an effect on Vicon-Xsens agreement.

3.4 Discussion

3.4.1 Agreement of Current Study in Comparison to Previous Research

The ICC results showed that absolute agreement between Vicon and Xsens was generally high, thus not only were signals correlated, but also their values were relatively close to each other. The estimate of measurement errors approximated 9° RMSE when using Xsens around plastic and 15° around metal. These results appear to show larger errors than those reported in Shublaq et al.'s previous study (2009), which reported an RMSE of 2.5° between Xsens and Vicon measurements of pronation/supination of the forearm during rehabilitative tasks; they are also larger than the dynamic accuracy indicated in the Xsens specification documentation (2° RMSE) (Xsens motion technologies, 2008).

Differences between the errors observed could be the result of magnetic disturbance in my study and/or anatomical constraints in Shublaq et al.'s study (i.e., a smaller range of motion). The latter possibility makes sense only if the error increases of the current study occurred at the ends of the range of motion.

Although an iterative process was used to select an optimal calibration factor, and measurement ranges of both systems were taken into account, Xsens-Vicon plots (Figure 3.5) suggest that Xsens measurements in some of the trials with the highest error (mostly metallic trials) underestimated pronation—and to a lesser extent, supination. A possible explanation is a time lag in the Kalman filter's processing as the Xsens attempted to compensate for changes in magnetic disturbance and/or movement's angular velocities and accelerations, making it difficult to capture short-lived peak values.

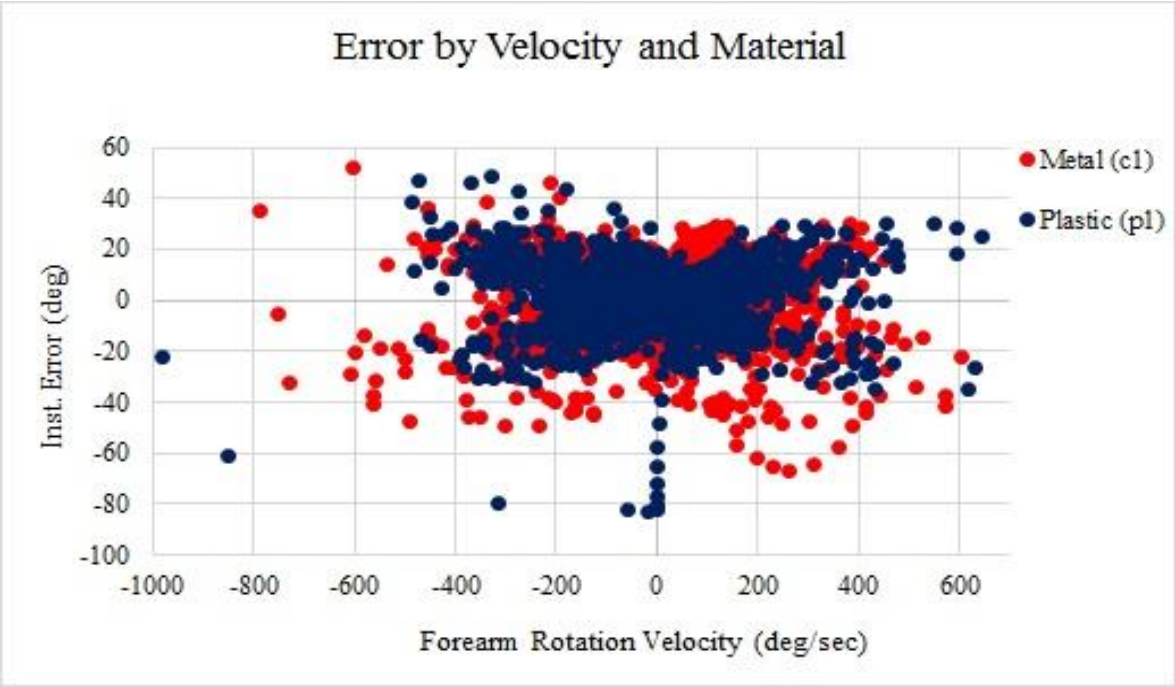

Figure 3.8. Scatterplot of the relationship between forearm rotation velocity and instantaneous error (RMSE) of nine participants, when turning the top left handle (red represents metal and blue plastic). Larger differences appear associated with faster movements, particularly when moving in the pronation direction (negative).

Additionally, some of the error seems to be associated with fast orientation changes, particularly when pronating (Figure 3.5, Figure 3.8). The angular velocity associated with the tasks in the current study was not controlled; participants used their preferred speed to turn the handles (a common, functional task). Although the speed at which Shublaq et al.'s participants performed the exercises was not discussed, it is possible that given the rehabilitative nature of their tasks, their movement speed could have been considerably slower than in the current study. Thus, differences in speed along with reduced ranges of motion could help explain Shublaq et al.'s lower observed error. Consequently, although its observed error is larger than previously reported, the current study was able to quantify some errors that are endemic to workplace environments, such as magnetic disturbance, fast rotations, and large ranges of motion.

3.4.2 Additional Potential Sources of Error

In the plots illustrating Vicon and Xsens signals (Figure 3.5), show that despite having taken steps to synchronize Vicon and Xsens signals, poor synchronization seems to still be a problem. The error seemed to be largest while the forearm was moving at high velocity, particularly in the pronation direction (Figure 3.8). Although the leads and lags were removed through the cross-correlation process, observations of the signal showed that the largest errors between the two signals occurred during the movement phase, with the each signal switching between leading and lagging at times within the same trial. It was speculated that this irregularity, too, could be due to the time required by the Kalman filter to process sensor orientation, because the Xsens may need to re-assess the weighting associated with each of its triaxial devices (the gyroscopes, accelerometers, and magnetometers). The relative weighting is continuously updated according to changes in acceleration and angular velocity, as well as magnetic disturbances of the environment. This contribution to measurement error may be relevant primarily in situations where timing is important. It would have less of an effect on most measurements required for typical ergonomic analyses, such as estimating how much time is spent at particular postures (e.g., percentiles) during a work task, or estimating how much repetition is associated with a task (e.g., turns analysis).

Recall that, within the metallic trials, vertical location had an effect, observing reduced agreement from top to bottom rows of handles, due perhaps to the resetting of the sensors at the start of a trial (i.e. initial magnetic north recognition). The posture adopted was typically slightly above horizontal and the sensors did not appear to be able to adjust the attitude (i.e. pitch and roll or orientation changes required to reach top, middle, and bottom rows) within a trial's timeframe. In contrast, the headings (i.e yaw or orientation changes required to reach right and left handles)

were in agreement; no difference was found. Although vertical location continued to have an effect on the RMSE in the analysis of only metallic handles, including the 10th handle, Bonferroni pairwise comparisons found that the 10th handle's RMSE differed statistically only from that of the handles on the top row (Appendix C). This finding suggests that it was not the specific orientation of the sensor's x axis that was problematic, but the fact that the x axis differed from the start. Further study is needed to assess the time required for successful realignment.

Additionally, the handles were fabricated as similar as possible, however the resulting two vertical surfaces and their handles had some differences, which could have affected the results. First, the force requirements of plastic and metallic handles differed, with metallic handles requiring more force to turn. This kinetic difference could have resulted in different velocities elicited by each of the handle type (e.g. metallic handles associated with slower turns), potentially resulting in an increased error in the plastic handles compared to the metallic handles. However, this did not seem to be the case, as angular velocities in plastic and metallic handles were similar and a few metallic trials exhibited faster movements when moving intro pronation (Figure 3.8). Furthermore, differences in the shape of the handles could have also affected findings, because the centre of rotation for metallic handles was more in line with the long axis of the forearm (movement axis), whereas the axis of rotation of plastic handles was slightly to the side. Such differences could have affected ROM at the forearm, as it is possible that plastic handles may have required some shoulder involvement, which may not have been needed during metallic handle rotation. However, Lagree et al. (2016) who tested differences in the ROM of the same data did not find significant differences between materials. Lastly, the differences in the handle rotation axes could have affected the moment of inertia associated with each of the handle

types. A shorter radius of gyration (associated with metallic handles) could have resulted in lower moment of inertia leading to higher angular velocities, thus higher error, as higher velocities seemed correlated with larger errors (Figure 3.8). However, the increased mass of the metallic handles would have a compensating effect. As reported above, the similar angular velocities between the trials would suggest the different handle shapes helped in minimizing the effect of the mass differences.

In terms of kinematics, ergonomics studies are often interested in evaluating movement features that describe exposure to dangerous postures by estimating time spent in postures away from neutral and average postures, as well as repetitive motions during continuous working tasks. These features can be evaluated by pooling data and calculating variables such as the minimum and maximum, and 10^{th}, 50^{th}, and 90^{th} percentiles (Jonsson, 1978), as well as the number of turns (the number of times a movement changes direction). Lagree, et al. (2016) reported that the largest average difference between Vicon and Xsens was 3.9°, suggesting that the two systems are in good agreement when comparing percentile data using an amplitude probability distribution function (Jonsson, 1978). The good agreement between the systems suggests that Xsens has great potential for measuring forearm posture in the workplace using this type of analysis; there were no differences between the ranges of motion measured. However, the current study, although it used the same data as Lagree et al., showed larger differences between the systems' measurements. These differences may indicate that large part of the error may be due to inconsistencies in the synchronization of Xsens signals. Thus, using Jonsson's method (Jonsson, 1978) appears promising for future investigation for forearm postures, until further investigation is able to resolve the issue with Xsens synchronization.

3.5 Limitations

A limitation of the current study is that the kinematics of turning the two types of handles (plastic or metal) may have been different, potentially affecting signal characteristics (e.g., velocity, ranges of motion) and introducing potential confounding effects. Additionally, although every attempt was made to control for magnetic disturbance in the collection area, there may have been sources of magnetic disturbance beyond the researcher's control, such as that emitted by alternating current (AC) or the electromagnet of the magnetic resonance imaging facility within the building. No measurements were taken.

3.6 Recommendations

The gimbal lock errors when forearm pronation/supination angle approached -90° could be easily eliminated in the future; mounting one of the sensors on a firm wedge during participant setup would make rotation measurements more positive. Additionally, because sensors had better agreement with Vicon when turning handles in locations which elicited a sensor orientation similar to that of the initial static recording, it may be useful to make the initial static recording, during which sensors locate local magnetic north, more similar in orientation to the tasks.

3.7 Conclusion

Xsens can be used reliably in the ergonomics field for evaluating repetition and task time spent in different forearm postures, although care must be taken when choosing variables to identify risks. Outputs classified into degree bins, providing static (10^{th} percentile), median (50^{th} percentile), and peak (90^{th} percentile) values to quantify the percent time spent at particular postures, can be most useful (Jonsson, 1978). Absolute values may be used to compare tasks within subjects, and normalization can facilitate between-subject comparisons. Given the Xsens limitations, there is a concern when degree accuracy at a specific instant in time is needed, particularly with high velocity movements. However, considering the similarities between Xsens and Vicon measurements, Xsens sensors are very promising for the quantification of forearm pronation/supination in the workplace. Compared to Vicon systems, Xsens systems have the advantages of smaller size, greater portability, and simpler calibration.

4 CHAPTER 4. STUDIES II AND III: INTRODUCTION AND METHODS

Evaluation of Finger Flexor Tendon Trajectories at the Wrist as a Function of Forearm and Wrist Postural Change, Using MRI.

4.1 Introduction

Musculoskeletal (MSK) injuries or disorders are common in the workplace and quite costly. These injuries can cause sufficient impairment to compromise productivity and decrease the quality of life of workers. The upper extremities are among the most commonly injured body parts, making up approximately 30% of all musculoskeletal disorders (MSDs) in 2014, in all work sectors, in the United States. Workers' postures and motions were the second-most common source of exposure.

Previous epidemiological research has shown that forearm pronation/supination postures and motions are associated with distal upper limb injury. Hughes et al. (1997) found years of 'forearm twist' significant predicted hand/wrist disorders (OR=17, 95% CI=2.9-106) and elbow/forearm disorders (OR=37, 95% CI=3.-470). Sustained pronated postures have also been associated with increased sick leave due to injury in machine operators in the forestry industry (Grevsten & Sjögren, 1996). Forearm postures/actions have been recognized as contributing to common upper limb disorders, such as lateral (Kroemer, 1989; Silverstein et al. 2014) and medial epicondylitis (Descatha et al., 2003; Kroemer, 1989), CTS (Kroemer, 1989), wrist tenosynovitis, DeQuervain's disease, ganglions cysts, and radial tunnel and pronator teres syndromes (Kroemer, 1989). Although epidemiological evidence shows that forearm pronation/supination may somehow be contributing to the development of MSDs, it is unclear what features of forearm pronation/supination may be injurious.

Previous biomechanical evidence has suggested that forearm postures away from neutral increase MSK loading, reflected by increases in discomfort, forearm EMG, and CT pressure, and decreases in strength (Domizio & Keir, 2010; Khan et al., 2009b; Mogk & Keir, 2003; Mukhopadhyay et al., 2007; Rempel et al., 1998; O'Sullivan & Gallwey, 2005; O'Sullivan & Gallwey, 2002; Werner et al., 1997). Khan et al. (2009) demonstrated increases in discomfort ratings when deviating in only one plane (forearm or wrist). However, discomfort ratings more than doubled when deviating in two planes (e.g., 30° forearm supination with about 20° of ulnar deviation), suggesting an additive loading effect.

Pronated postures have been shown to increase the EMG of forearm extensors when performing various tasks, such as gripping, pushing, pulling, and pronating the forearm (Domizio & Keir, 2010; Mogk & Keir, 2003; Mukhopadhyay et al., 2007). Furthermore, pronation torque strength decreases have been seen in pronated forearm postures, and supination torque strength decreases in supinated forearm postures (Mukhopadhyay et al., 2007; O'Sullivan & Gallwey, 2005; O'Sullivan & Gallwey, 2002), while grip strength has shown a trend to decrease with increasing pronation of the forearm (Mogk & Keir, 2003).

Additionally, higher CT pressures have been documented in full supination when compared to neutral (Werner et al., 1997), particularly in combination with flexion of the metacarpophalangeal joint (Rempel et al., 1998). Although pronation has been associated with lower CT pressures, higher pressures have been documented when forearm pronation is combined with wrist radial deviation or wrist extension (Werner et al., 1997).

Although this evidence demonstrates a relationship between increased MSK demands features and forearm posture, more research is needed to understand how forearm postures load internal tissues.

Previous researchers have quantified features to describe movement of internal structures, as a function of wrist and/or finger postural change, and have discussed the implications of these features on MSK loading (Armstrong & Chaffin, 1978; Keir & Wells, 1999; Loh, et al., 2016). However, none of these studies has evaluated internal MSK loading associated with forearm pronation/supination.

Armstrong & Chaffin (1978, 1979) used cadaver data to develop models to help understand the impact of wrist/finger postural change on internal loading. In their later study, the models demonstrated the effect of several factors on the tendon-joint contact force, including posture of the wrist and fingers. They showed that tendon-joint normal forces increased with greater wrist posture deviations from neutral in the sagittal plane. It was noted that posture influences the radius of curvature of the trochlear surface as well as the angle at which the tendon wraps the trochlear surface, thus affecting intra-wrist contact forces (Armstrong, & Chaffin, 1979). The authors suggested that the median nerve could potentially be compressed between extrinsic finger flexors and the flexor retinaculum during hand exertions, particularly with a flexed wrist. Thus certain hand actions may aggravate or precipitate CTS. Although these findings have been useful in modeling the transferability of external exposures to internal loading, in-vivo studies are needed to understand in-vivo loading situations.

Other studies have demonstrated changes in MSK loading in-vivo, as a function of postural change of the upper limb. Keir and Wells (1999) evaluated finger flexor trajectories within the CT, as a function of wrist flexion/extension, using MRI. Volar displacements of finger flexors of about 5 mm towards the flexor retinaculum (in the sagittal plane) were seen with 45° of wrist flexion. However, relatively straight trajectories were seen in wrist extension (20°) and neutral postures. The tendons' radii of curvature were smaller in a flexed wrist compared to

extension and neutral, and were further reduced when tendons were under tension. These findings used Armstrong & Chaffin's model to estimate the contact forces per unit arch. It was suggested that both the volar displacements of the flexor tendons in wrist flexion and the decreased radii of curvature could result in increased contact force around the median nerve. These observations were similar to those pointed out by Armstrong & Chaffin, highlighting their relevance to an increased risk for CTS development. Furthermore, these findings have been supported by recent research by Loh et al. (2016), who demonstrated deformations of the median nerve as a function of changes in finger posture. Smaller cross-sectional areas of the median nerve were reported when the fingers formed a full fist, compared to postures with relaxed fingers or with full finger flexion (without force). Studies such as these have provided new insights into the role of wrist and finger postures in injury development. However, the role of forearm pronation/supination on MSK loading has not been evaluated.

Given that epidemiological evidence has linked forearm pronation/supination to injury, and that biomechanical evidence has shown forearm pronation/supination effects on discomfort and MSK demand, further work is needed to understand the role of forearm posture on anatomical relationships within the wrist.

Knowledge of the effects of forearm pronation/supination on tendon kinematics may allow further understanding MSK loading at the wrist. This knowledge may help gain a better understanding of injury mechanisms, which are needed to reduce injury incidence in the workplace. Thus, this study is meant to be the first of a series of studies to evaluate the role of the combined effect of forearm pronation/supination and wrist posture on tendon movement.

The purpose of this particular study was to evaluate the effect of forearm pronation/supination, combined with wrist flexion/extension, on the location and orientation of

finger flexor tendons, proximal and distal to the CT. It was hypothesized that, with increased forearm pronation or supination, finger flexor tendons would exhibit angular trajectory changes and displacements proximal and distal to the CT when compared to a mid-pronated/supinated position. A primary goal of this study is to document the amount of tendon displacement and tendon “sweep” (angular movement of the tendon) as a function of forearm pronation and supination, and wrist flexion/extension.

4.2 Methods

4.2.1 Participants

Four participants of university age (1 female, 3 males) were recruited for this study by word of mouth. Participants gave informed consent in accordance with the Human Participants Review Committee at York University (Appendix D) prior to the start of the study. Consequently, they were administered a questionnaire regarding demographic information and MSK health. All participants were screened for MRI and upper limb MSK contraindications (Appendix E, F). Exclusion criteria included neurological conditions or MSK injuries affecting the upper limb within the past year, as well as permanent deformations or damage near the wrist, current pregnancy, current pain or discomfort, as well metal or implanted devices that were not MRI-safe. This study was reviewed and approved by the Human Participants Review Committee at York University.

4.2.2 Image Acquisition

High resolution 3D VIBE images of the wrist were acquired with a 3T Siemens TIM Trio MRI scanner (MAGNETOM Trio, A Tim System, Siemens Healthcare, Erlangen, Germany) at the MRI facility at York University. MRI parameters included TR=12.8 ms, TE= 5.29 ms, FOV=100 mm, voxel size = 0.3x0.3x0.8, and flip angle=10°. A total of 112 axial images were acquired per scan. Scanning time was approximately 6-7 minutes for each of the nine. Images captured the wrist from approximately 2cm proximal to the wrist crease, to mid-shaft of the metacarpal bones (Figure 4.1).

Figure 4.1. MRI scan of the wrist in the frontal plane of one participant. Scans imaged the wrist from approximately 2cm proximal to the wrist crease to mid-shaft of the metacarpals.

4.2.3 Participant Setup

Plastic splints secured with Velcro and tape were used to fix the desired wrist postures (Figure 4.2a). An MRI-safe device was customized to fix the forearm at the proximal and distal ends (Figure 4.2b). The forearm was fixed at the proximal end by resting the humeral condyles on a fixed, V-shape mould and rotating the distal end so that the hand rested comfortably on an MRI-safe hand dynamometer (Biopac Systems Inc, Canada) at the desired forearm pronation/supination posture (Figure 4.2a). A small flex coil was secured with Velcro on the wrist area, while ensuring postures of the forearm and wrist remained fixed.

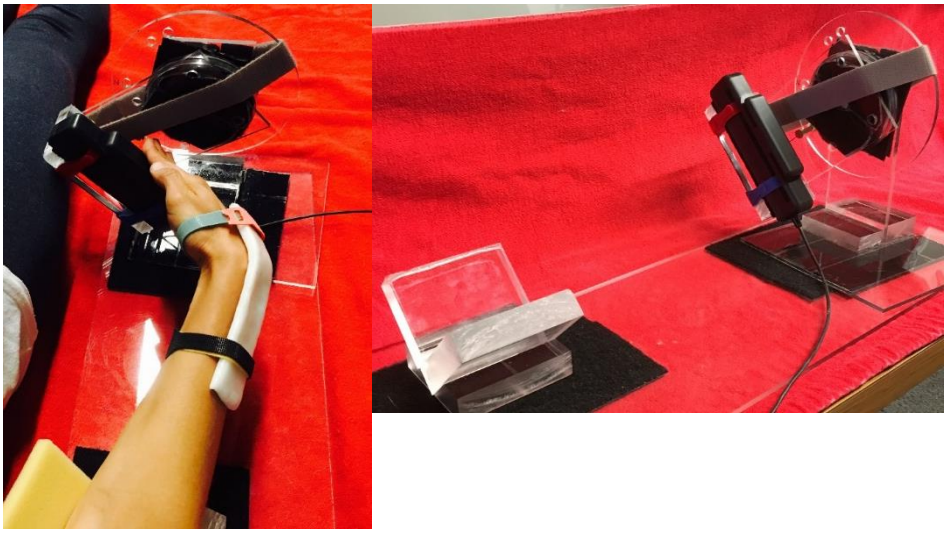

Figure 4.2. MRI-safe customized device used during scan acquisition (right). Left figure shows the setup prior to scanning; participant wears a plastic splint to fix wrist posture; while the elbow remains fixed, the forearm is rotated at the distal end to press on hand dynamometer.

4.2.4 Experimental Protocol

Participants were supine with their body towards the left side of the bed, so that their right arm could be positioned beside their body, close to the center of the table. Padding was placed between their body and the scanner to prevent injury from contact with the coil. Participants' wrists were imaged in nine different postures, combining three forearm (40° pronation, mid-pronation, and 60° supination) and three wrist postures in the sagittal plane (30° flexion, neutral, and 30° extension). The forearm postures were easily changed by rotating the fixture, whereas the wrist posture setup required re-splinting of the hand, as well as movement of the handgrip dynamometer. Thus, wrist postures were chosen randomly (from a hat) first, then the three forearm postures were chosen in random order within each wrist posture (Figure 4.2a).

Scans for each participant were performed over two or three sessions, depending on scan quality as well as forearm/wrist fatigue. Only one participant did not report fatigue and was able to finish all nine conditions in one day. Within each day, participants rested between conditions to minimize fatigue, while researchers were setting up for the next condition. Given that McGill et al. (1996) demonstrated the need to image structures while loaded in functional ways, participants were asked to keep their fingers straight on the hand dynamometer, and push to maintain a constant force of 10N for the duration of the scan. The researcher provided verbal feedback to participants if their exerted force diverted from the 10 N line on a visual feedback monitor in the control room.

4.2.5 Image Analysis

4.2.5.1 Segmentation

MRI images were imported into Mimics image processing software (Materialise, Belgium) for the segmentation of various structures (Table 4.1). Segmentation is the process which creates 3D models of anatomical structures in order to define their boundaries within each scan to allow 3D quantitative analyses.

Table 4.1. Segmented structures and points of interest for creating coordinate systems.

Segmented Structure	**Site of Interest**	**Points of Interest**
Radius	*Distal end*	•Dorsal edge of ulnar notch •Radial Styloid •Palmar edge of ulnar notch (Digitized)
Ulna	*Distal end*	•Styloid Process •Radio-distal prominence ulna across from styloid (Digitized)
3rd Metacarpal	*Base to mid-shaft*	•Styloid Process •Dorso-ulnar corner on base •Proximal and distal centroids (Digitized)
Forearm	*Radial styloid (RS) to 2cm proximal to RS*	•Proximal and distal centroids (Calculated and digitized)
Flexor Digitorum Superficialis (FDS) Flexor Digitorum Profundus (FDP) Flexor Pollicis Longus (FPL)	*2nd-4th digits - Along scan* *2nd-5th digits - Along scan* *Along scan*	Centerlines (Calculated)

Structures were segmented manually (Appendix G, Table a). Four research assistants created masks for each structure of interest, by using the Livewire tool to draw contours around the structure of interest in the transverse plane, capturing a series of 2D perimeters of the structure along the longitudinal axis of the forearm (Figure 4.3). A similar procedure was followed in either the sagittal or frontal plane, whichever plane allowed a clearer view of the structure of interest. Once contours were completed in two planes, Mimics calculated the contours along the third plane. A Mimics proprietary algorithm generated a 3D mask of the structure. However, due to mask imperfections (e.g., holes and leakage to other structures), several tools were used for subsequent manual editing, such as mask erosion, dilation, expansion, smoothing, and a manual pen. Careful revision in all planes ensured that the mask was of good quality, meaning that it fully covered the structure of interest and only the structure of interest. The 3D surface of the anatomical structure was calculated with a Mimics proprietary algorithm. The raw 3D models were further smoothed using proprietary Mimics functions (Appendix G, Table a).

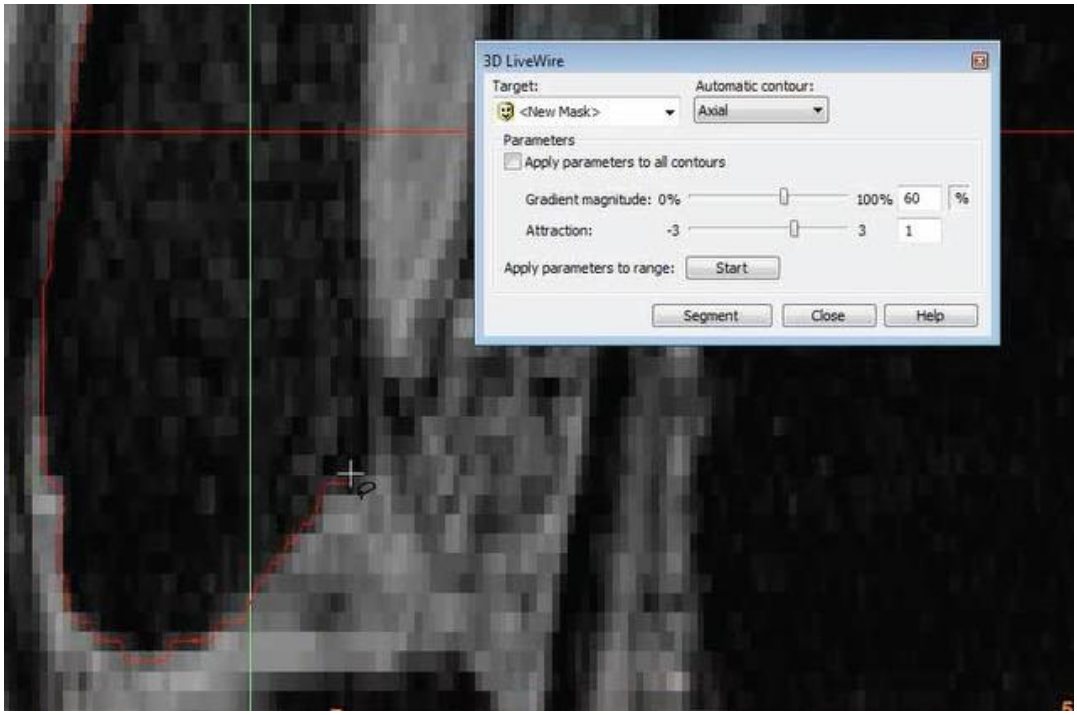

Figure 4.3. Screenshot of the use of the Mimics Livewire tool (red line) drawing a contour around the ulna.

4.2.5.2 Digitization & Registration

After bone segmentation, segmented models were imported into 3-Matics software (Materialise, Belgium). Seven landmarks were identified on the scans of the NM trial (neutral wrist in mid-pronation; see Table 4.1). All points of interest listed on table 4.1 for the radius, ulna, and metacarpal were digitized using this software, except for the metacarpal centroids. The landmarks of all participants were digitized by the same researcher, whose average error difference in repeatedly identifying the same bony landmark was 1.14 $\pm$0.35 mm (Dang A., et al., 2016).

Subsequently, each of the three bones in condition NM and all their digitized points were registered (i.e. superimposed) onto the other eight scans of the same subject. Maintaining the

same relationship between landmarks on the same bone in all scans for each participant was important for accurately calculating the local or anatomical coordinate systems (CS). The registration process involved two methods. First, the n-point registration rotated and translated the NM bones (e.g., a radius and the three previously digitized points on it) onto another scan of the same participant. This type of registration was used for gross alignment between registered structures. A second type of registration, called global registration, was then performed to provide a finer alignment between registered structures. The global registration was iteratively performed until the error between both segmented surfaces was minimized, in terms of both location and orientation (Figure 4.4). The original coordinates of the NM scan-digitized points or landmarks, as well as the coordinates of the same landmarks registered onto the other eight scans of each subject, were exported as text files, to be used in the calculation of anatomical coordinate systems (CSs) with respect to the radius of each scan (See Section 4.2.6.1).

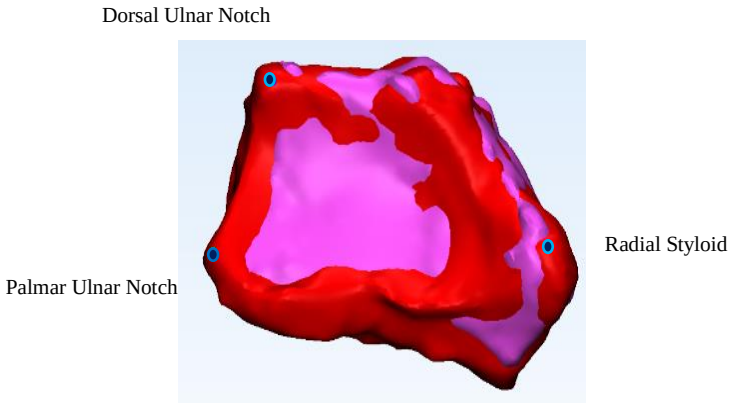

Figure 4.4. . Example of two superimposed radii from two scans of the same participant, along with the digitized points (blue dots).

4.2.5.3 Centerline and Centroid Calculations

Numerous functions in Mimics were used to obtain forearm centroids, and entire centerlines of the FDS (flexor digitorum superficialis) tendons (second-fourth digits), and FDP (flexor digitorum profundus) tendons, and the third metacarpals. Conceptually, the centerline is a continuous centroid of a tubular structure along its length, which in essence tracks the instantaneous location of the geometric center of each slice throughout its length. Note that parts of centerlines that were generated using partly imaged structures, or non-tubular bony shapes, were eliminated from analyses. The xyz coordinates of the FDS and FDP tendons' centerlines were saved as text files and used to calculate tendon locations and orientations (to be explained).

For the metacarpal, the centerline's xyz coordinates, and the instantaneous curvature (used to determine proximal and distal metacarpal centroids) were saved. The instantaneous curvature was important in this context because it helped the researcher identify the tubular portions of the metacarpal. The metacarpal is relatively straight at the shaft in the frontal plane and has a slight posterior curve in the sagittal plane. Observed instantaneous curvature values within the shaft portion were <0.05, whereas portions near the base or the distal end had higher values. The proximal centroid of the metacarpal was determined by selecting a point which coincided with the first point of curvature < 0.05 and distal to the base of the metacarpal. The most distal point along the metacarpal centerline with curvature <0.05 was selected as the distal metacarpal centroid. The researcher visually inspected the centerline to ensure that the proximal and distal centroid points were well outside both the partially scanned areas at the distal end and the base of the metacarpal at the proximal end (of the metacarpal shaft).

Segmented forearm structures were exported from Mimics into 3-Matics, where distal and proximal forearm centroids were calculated. First, a transverse contour was generated to cover

the perimeter of the proximal surface of the 3D forearm model, and a circle was fitted through it (Figure 4.5); the center of the circle was considered the proximal forearm centroid. A similar approach was used to calculate the distal forearm centroid. The proximal and distal forearm centroids in turn were used to create the longitudinal axis of the forearm, which was used to calculate the local CS for each scan.

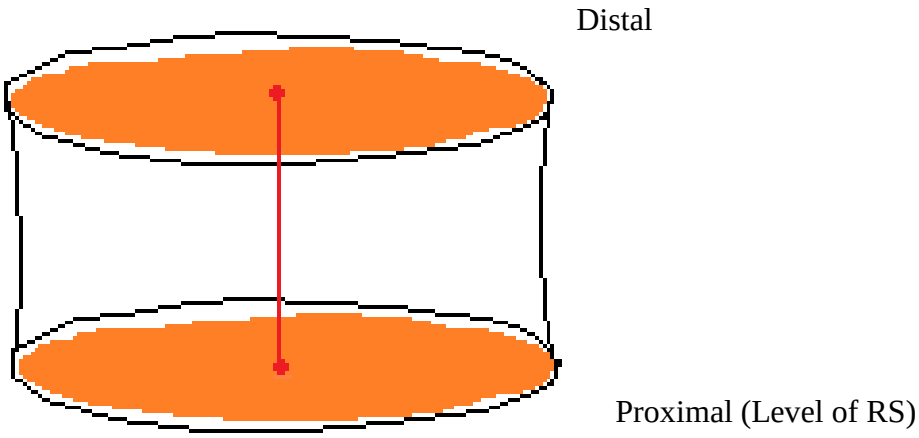

Figure 4.5. Sample of forearm centroid calculations. The proximal and distal cross-sectional areas of the forearm were selected (orange), and circles fit through them. The centers of the circles (red) were selected as the centroids. Red line represents the longitudinal axis.

4.2.6 Mathematical Analyses

4.2.6.1 Coordinate Systems

The CSs of the radius, ulna, and metacarpal were created. All calculations used the global coordinates of the seven digitized landmarks on the NM scan, the superimposed landmarks on the other eight scans of each participant, and the metacarpal and forearm centroids. The anatomical CSs were calculated with custom programs created in Matlab (Matlab 8.10.604 (R2013a), The MathWorks, Inc., USA). All postures and tendon locations and orientations were expressed with respect to the radial CS with its origin at the radial styloid (Figure 4.6).

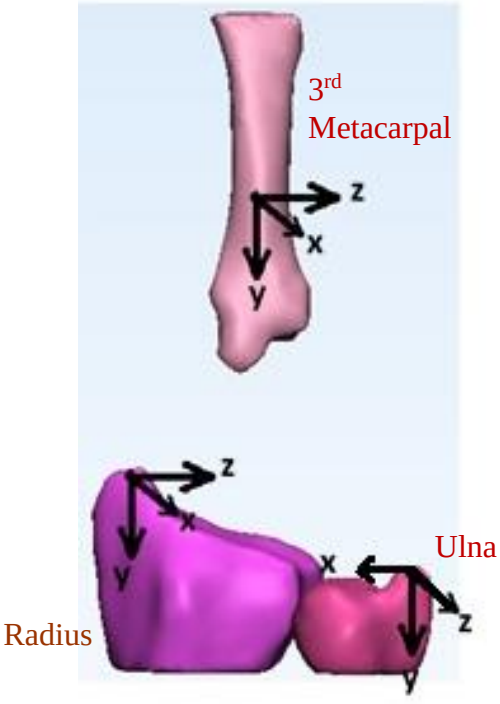

Figure 4.6. Coordinate systems of the radius, ulna, and 3rd metacarpal. Radius and metacarpal: x dorsal, y proximal, z ulnar. Ulna: x radial, y proximal, z dorsal.

The radial CS was created in the following manner. First, the two points on either side of the ulnar notch of the radius (dorsal and palmar), were used to determine the ulnar notch (UN) location. The interim vector of the mediolateral axis of the radius z'_r was calculated by subtracting the global xyz coordinates of the UN from those of the radial styloid of the radius (RS), and then the axis was normalized. The longitudinal axis of the radius y_r was calculated by subtracting the coordinates of the distal forearm centroid from those of the proximal forearm centroid, and was subsequently normalized. These points were used to create the long forearm axis because an axis aligned with the forearm, rather than the radial base, would be more anatomically relevant. The anteroposterior axis x_r was calculated as the cross product of the mediolateral and long axes and subsequently normalized. Because the z'_r and the y_r axes were not necessarily orthogonal to each other, a correction was made by crossing the two normalized vectors x_{rNorm} and y_{rNorm}. An orthogonal radial CS with unit vectors was obtained, where x_{rNorm} pointed dorsally, y_{rNorm} pointed proximally, and z_{rNorm} pointed ulnarly. A 3x3 rotation matrix to rotate from the global CS (i.e., the CS of the scanner) to the radial CS R_r was created (Appendix H, Section 1).

The ulnar CS was determined using a similar approach. Both the radius and ulna shared the same long axis y_{rNorm}. The interim mediolateral axis x'_u of the ulna was created by subtracting the global xyz coordinates of the ulnar styloid from the coordinates of the radio-distal prominence across from it, and was subsequently normalized. The anteroposterior axis z_u was calculated as the cross product between x'_{uNorm} and y_{rNorm}. Finally, the corrected mediolateral axis x_u was calculated as the cross product of y_{rNorm} and z_{uNorm}. The ulnar CS was an orthogonal CS, where x_{uNorm} pointed radially, y_{rNorm} pointed proximally, and the z_{uNorm} pointed dorsally. This CS was expressed as a 3x3 rotation matrix (Appendix H, section 2).

Finally, the third metacarpal CS was determined similarly. The interim mediolateral axis z'_m was created by subtracting the global xyz coordinates dorso-ulnar corner of the metacarpal head from the metacarpal styloid coordinates, which was then normalized. The metacarpal's long axis y_m was created using the distal and proximal metacarpal centroids, and was normalized. The anteroposterior axis x_m was calculated as the cross product between z'_{mNorm} and y_{mNorm}, and was subsequently normalized. A final correction of the mediolateral axis z_m was done by taking the cross product between x_{mNorm} and y_{mNorm}. The metacarpal CS was an orthogonal CS, where the x_{mNorm}pointed dorsally, the y_{mNorm} pointed proximally, and the z_{mNorm} pointed ulnarly. The metacarpal CS was also expressed as a 3x3 rotation matrix (Appendix H, section 3).

4.2.6.2 Posture Calculations

The posture of the wrist was calculated as the orientation of the third metacarpal with respect to the radial CS. A rotation matrix was first calculated to rotate and align the metacarpal to the radial CS, and Euler angles were calculated using an xyz sequence, according to Winter (2005) (Appendix I, section 1). Wrist radial/ulnar deviation was defined as θ1 and wrist flexion/extension as θ3.

Similarly, forearm pronation and supination angles were calculated by determining the orientation of the ulnar CS with respect to the radial CS. This was accomplished by calculating the product of their respective matrices (Appendix I, section 2). Euler angles were obtained using the xyz sequence (as mentioned above). In this case, however, only the rotation of the ulna with respect to the radius (i.e., forearm pronation/supination), defined as θ2, was of interest. The x and z axes of the ulnar CS were not aligned with the radial CS, thus pronation/supination angles had to be normalized to the NM trial of each participant (Appendix I, Section 3).

4.2.6.3 Tendon Locations and Orientations

4.2.6.3.1 Centerline Transformation from Global to Radial CS

The tendon centerlines of the FDS and FDP, from section 4.2.5.3, were further processed in a custom made Matlab program. The centerline coordinates were initially saved as $x_0y_0z_{0\_ct}$ coordinates with respect to the MRI scanner (global CS). Each tendon centerline was translated and rotated, so that each sample point on every centerline was expressed with respect to its radial CS. This was accomplished by subtracting the RS global coordinates from each of the centerline points, and then multiplying each translated point by the radial rotation matrix R_r (Appendix J).

4.2.6.3.2 Line Fitting through Tendon Centerlines

In order to estimate angular trajectories, each transformed tendon had to be defined as a line. At the proximal end, a 3D line of best fit was calculated to pass from the tendon location at the RS to the tendon location at y=15 mm, proximal to the RS (Appendix K). This iterative process systematically translated and rotated the line, joining all possible connections between two grids of $\pm$5 mm along the antero-posterior x and medio-lateral z axes around each of the identified tendon centerline points at y=0 and y=15, in 1 mm increments. The fit was tested by averaging the perpendicular deviations of all original centerline points from the line. The line of best fit then yielded two new proximal and distal points, and another series of finer iterations was performed, using $\pm$0.5 mm grids around the new points and 0.1 mm increments (Appendix K).

A similar procedure was performed to fit a line at the distal end from the CT. This line started at the y coordinate corresponding to the y value of the metacarpal styloid (MS), and ended 15 mm distal to its start, along the longitudinal y axis. Analyses associated with measures

to describe tendon movement in regions proximal and distal to the CT will be addressed separately in the last few sections.

4.2.6.3.3 Tendon Displacements and Rotational Movement

4.2.6.3.3.1 Tendon Displacements

Changes in all tendon positions at the level of the RS (indicated by coordinates at y=0) were used to estimate displacements of the tendons proximal to the CT as a function of forearm and wrist postural change. Frontal displacements indicate changes in the z coordinate of the tendon centerlines at the level of the RS (with posture change), and sagittal plane displacements indicate changes in the x coordinate.

Tendon displacements distal to the CT as a function of forearm and wrist postures were estimated by measuring the tendon's positional change at the level of the MS, along the long forearm's axis. As mentioned above, sagittal and frontal displacements were estimated similarly, from changes in x and z coordinates, respectively.

4.2.6.3.3.2 Tendon Angles

The proximal angles of each of the estimated tendon centerlines were measured with respect to the longitudinal y axis in the frontal (Eq. 4.1a, and Figure 4.7.) and sagittal (Eq. 4.1b) planes, as follows:

$$\theta_{yz} = Tan^{-1}\left(\frac{prx_z - dit_z}{prx_y - dit_y}\right) = Tan^{-1}\left(\frac{prx_z - dit_z}{15}\right) \qquad \text{(Eq. 4.1a)}$$

$$\theta_{yx} = Tan^{-1}\left(\frac{prx_x - dit_x}{prx_y - dit_y}\right) = Tan^{-1}\left(\frac{prx_x - dit_x}{15}\right) \qquad \text{(Eq. 4.1b)}$$

Where:
θ_{yz} represents the angle between the tendon centerline and the long axis of the forearm in the frontal plane (subscripts denote the plane in which the angle was measured)
θ_{yx} represents the angle between the tendon centerline and the long axis of the forearm in the sagittal plane (subscripts denote the plane in which the angle was measured)
prx_z and dit_z represents the z coordinate of the proximal and distal points of the tendon centerline (at y=15 mm and 0 mm respectively)
prx_x and dit_x represents the x coordinate of the proximal and distal points of the tendon centerline (at y=15 mm and 0 mm respectively)

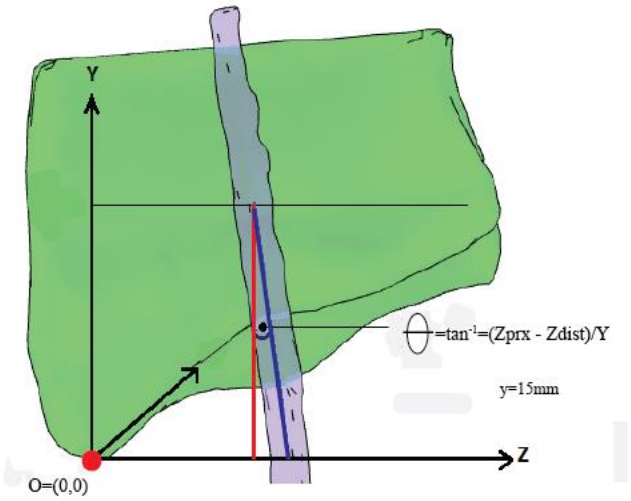

Figure 4.7. Anterior view of the radius and a sample tendon, depicting the calculation of frontal tendon angles with respect to the forearm's long axis, proximal to the CT. Positive angles open ulnarly at the proximal end.

The angle of the distal fitted line with respect to the forearm's long axis was calculated using the same convention described in Eq. 1a and 1b. Subsequently, the planar angles (sagittal

and frontal) of each tendon were calculated using their respective fitted lines at their proximal and distal tendon portions (see Figure 4.8).

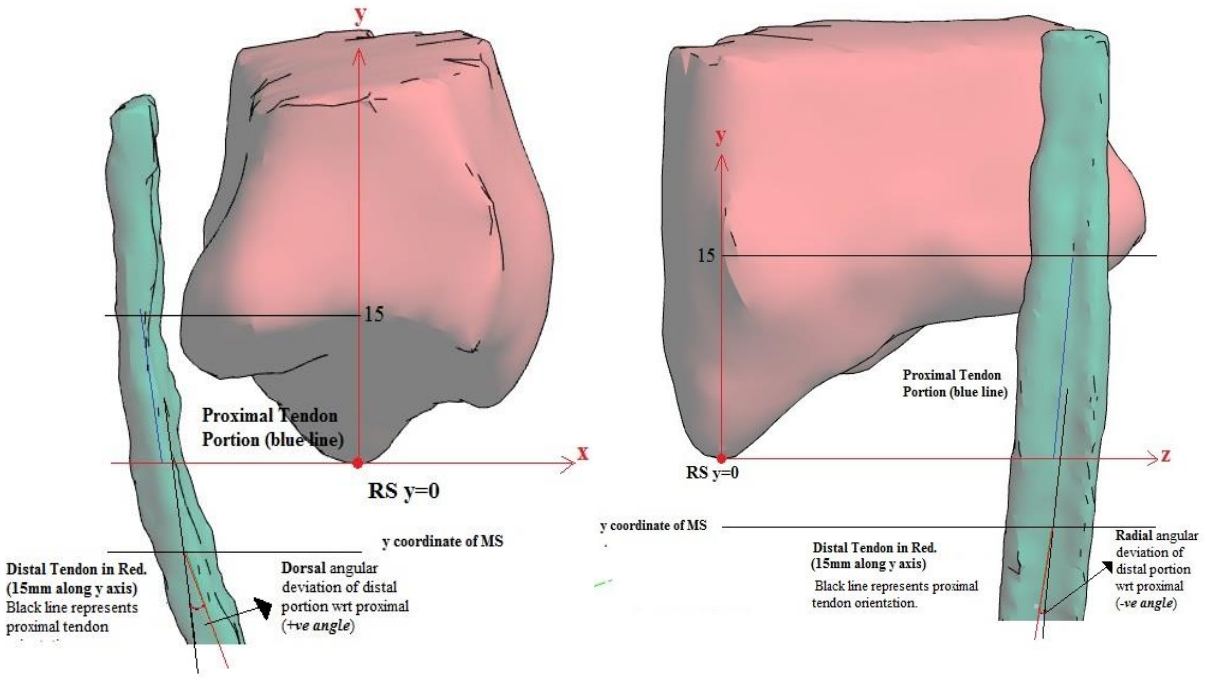

Figure 4.8. Tendon angles represented by the angle between the proximal and distal tendon portions (labelled), in the sagittal (left) and frontal (right) planes.

4.2.7 Statistical Analyses

To validate postural change and detect potential interactions of postures across different planes, two-way (3x3) repeated measures ANOVAS were performed on posture data measured from the MRI. The combined effect of forearm and wrist posture on frontal and sagittal tendon displacement angles proximal to the CT (θ_{yx} and θ_{yz} respectively), was evaluated using two-way (3x3) repeated measures ANOVAS. Significant differences were further evaluated with Bonferroni-corrected, multiple comparisons, adjusting the critical p value according to the

number of individual comparisons (e.g., 0.05/3 comparisons = 0 .017, to avoid inflating the chance of a false positive (type I error)).

The effects of wrist and forearm posture on distal tendon displacements at the level of the MS, and on tendon angles between the proximal and distal portions of the tendons just outside the CT, were also analyzed with two-way (3x3) repeated measures ANOVAs. Bonferroni-corrected multiple comparisons were used for further evaluation of significant findings. Summary statistics were used to document the amount of tendon movement occurring in the forearm (proximal analyses) and at the CT and distal to it (distal analyses).

The results of the current study are presented in two chapters; their results and discussions are addressed separately based on measurement site. Chapter 5 presents and discusses tendon movement measured proximal to the CT. Chapter 6 elaborates on tendon movement measured distal to the CT and modeled tendon angular trajectories within the CT based on measurements at the proximal and distal ends of the tunnel.

5 CHAPTER 5: STUDY II: PROXIMAL RESULTS AND DISCUSSION

Finger Flexor Tendon Trajectories Proximal to the Carpal Tunnel as a Function of Forearm and Wrist Posture: Results and Discussion.

5.1 Results

This chapter presents the postures achieved during data acquisition, and results of the tendon displacements and angular sweep as a function of forearm and wrist postural change, proximal to the CT. FPL tendon displacements and angular sweep were presented in this chapter, however, changes seen in this tendon may not accurately represent changes as a function of wrist or forearm posture, because we did not control thumb posture, which may affect FPL displacement. Data from four participants were analyzed (Table 5.1).

Table 5.1. Participant demographic information.

Sex	*n*	*Age (Years)*	*Height (m)*	*Weight (Kg)*	*Handedness*	
					Left	Right
F	1	34	1.83	66	1	0
M	3	23.5 (+2.1)	1.76 (+0.06)	72.7 (± 9.9)	1	2

5.1.1 Posture

The researcher originally intended to acquire data from postural combinations of 30° of extension, straight (0°), and 30° of flexion of the wrist, along with 40° of pronation, neutral mid (0°), and 60° of supination of the forearm. However, the average ranges of motion observed were 24.9° at the wrist and 68.7° at the forearm, both of which were lower than expected (60° and 100°, respectively) (Table 5.2).

Table 5.2. Means and standard deviations of each wrist and forearm postures, achieved during scan acquisition, of all scans for all participants. Forearm pronation/supination values presented were normalized to the NM condition of each

Wrist Posture			
	Mean (deg)	*SD (deg)*	*n*
R/U	-1.7	5.6	36
Extension	17.3	6.3	12
Neutral	6.8	6.7	12
Flexion	-7.6	6.8	12
Normalized Forearm Posture			
	Mean (deg)	*SD (deg)*	*N*
Pronation	16.8	7.8	12
Neutral	-4.3	7.7	12
Supination	-51.9	8.1	12

Although radial and ulnar deviations were not controlled during acquisition, movement in the frontal plane was minimal. The average range of motion at the wrist in this plane was 4.3° as a function of wrist flexion/extension and 4.4° as a function of forearm pronation/supination. The average ulnar deviation was 1.7° across all conditions (Table 5.2).

The ANOVAs tested for interactions between movements in one plane and measurements in another. The relative angle in the radial/ulnar direction of the metacarpal with respect to the radius was not significantly affected either by wrist flexion/extension or by forearm pronation/supination. Similarly, the relative angle of the metacarpal with respect to the radius in the sagittal plane was only affected by wrist flexion/extension and not by forearm pronation/supination. The relative angle of the ulna with respect to the radius was only affected by wrist flexion/extension, but not affected by wrist flexion/extension. These results suggest that these postures were independently controlled by the researcher.

5.1.2 Tendon Displacements

5.1.2.1 Sagittal Displacements

Sagittal displacements were changes in tendon locations along the x axis at the level of the RS. (Recall that positive x points towards the dorsum of the hand.) Only wrist flexion/extension had an effect on the sagittal location of all finger flexor tendons except FPL and FDP2, whereas forearm pronation/supination did not have an effect on the sagittal location of any tendon (Table 5.3). Average locations along the antero-posterior x axis of all tendons (except FPL) across forearm postures, within each wrist posture, showed that tendons were located more volarly in wrist flexion (-16.8 $\pm$ 2.1 mm), and more dorsally in wrist extension (-13.0 $\pm$ 2.2 mm), compared to neutral wrist (-13.9 $\pm$ 2.2 mm) (Table 5.4, Figure 5.1). There was more change in location between flexed and neutral postures (2.9 mm) than between neutral and extended postures (0.9 mm) (Table 5.5). See Appendix L for pairwise comparisons.

Table 5.3. Results of the effect of forearm and wrist postures on the antero-posterior tendon location (along the x axis) and on the medio-lateral location (along the z axis), at the level of the RS. P values are shown for Bonferroni-adjusted pairwise comparisons, unless denoted with the superscript c.

	Wrist				Forearm			
x at y=0								
	F	**dof**	**p[a]**	**Post Hoc Comparisons**	**F**	**dof**	**p[a]**	**Post Hoc Comparisons**
FPL	1.331	(2,6)	0.332[c]	*ns*	1.536	(2,6)	0.289[c]	*ns*
FDS2	25.100	(1.005,3.014)[b]	0.048* 0.009* 0.309	*ext vs flx* *neut vs flx* *ext vs neut*	6.728	(2,6)	0.280 0.175 0.507	*pro vs sup* *mid vs sup* *pro vs mid*
FDS3	15.235	(2,6)	0.066 0.002* 0.656	*ext vs flx* *neut vs flx* *ext vs neut*	0.652	(2,6)	0.555[c]	*ns*
FDS4	17.908	(2,6)	0.070 0.013* 0.445	*ext vs flx* *neut vs flx* *ext vs neut*	4.941	(2,6)	0.054[c]	*ns*
FDP2	5.950	(2,6)	0.368 0.113 1.000	*ext vs flx* *neut vs flx* *ext vs neut*	2.152	(2,6)	0.197[c]	*ns*
FDP3	5.347	(2,6)	1.000 0.033* 0.394	*ext vs flx* *neut vs flx* *ext vs neut*	0.614	(2,6)	0.572[c]	*ns*
FDP4	15.888	(2,6)	0.047* 0.022* 1.000	*ext vs flx* *neut vs flx* *ext vs neut*	5.711	(2,6)	0.098 0.664 0.576	*pro vs sup* *mid vs sup* *pro vs mid*
FDP5	18.195	(2,6)	0.065 0.014* 0.517	*ext vs flx* *neut vs flx* *ext vs neut*	3.844	(2,6)	0.084[c]	*ns*
z at y=0								
	Wrist				**Forearm**			
FPL	5.472	(2,6)	0.233 0.073 1.000	*ext vs flx* *neut vs flx* *ext vs neut*	0.285	(2,6)	0.761[c]	*ns*
FDS2	0.669	(2,6)	0.547[c]	*ns*	15.293	(2,6)	0.111 0.070 0.231	*pro vs sup* *mid vs sup* *pro vs mid*
FDS3	2.286	(2,6)	0.183[c]	*ns*	29.443	(2,6)	0.065 0.016* 0.222	*pro vs sup* *mid vs sup* *pro vs mid*
FDS4	7.059	(2,6)	0.295 1.000 0.063	*ext vs flx* *neut vs flx* *ext vs neut*	37.472	(2,6)	0.16 0.032* 1.000	*pro vs sup* *mid vs sup* *pro vs mid*
FDP2	0.686	(2,6)	0.539[c]	*ns*	2.326	(2,6)	0.179[c]	*ns*
FDP3	2.974	(2,6)	0.127[c]	*ns*	4.524	(2,6)	0.063[c]	*ns*
FDP4	4.571	(2,6)	0.062[c]	*ns*	4.562	(2,6)	0.062[c]	*ns*
FDP5	6.587	(2,6)	0.233 0.226 0.312	*ext vs flx* *neut vs flx* *ext vs neut*	6.307	(2,6)	0.223 0.264 0.621	*pro vs sup* *mid vs sup* *pro vs mid*

[a]Bonferroni corrected p value, unless specified with the d superscript

[b]Sphericity violated, Greenhouse-Geisser Corrected

[c]ANOVA priori tests p value

*Denotes significance

Table 5.4. Means and standard deviations of tendon locations in the sagittal and frontal planes at the level of the radial styloid. Positive values in the sagittal and frontal planes correspond to dorsal and ulnar displacements, respectively. Different letters denote significance in tendon location as a function of wrist posture (sagittal location), and forearm posture (frontal location), at $p<0.05$ Bonferroni corrected for multiple comparisons.

	Means and Standard Deviations of Location in the Sagittal and Frontal Planes (Proximal to Tunnel)											
	Sagittal Location (x at y=0) n=12						*Frontal Location (z at y=0) n=12*					
Tendon	*Flx*		*Neutral*		*Ext*		*Prone*		*Neutral*		*Sup*	
	Mean	*SD*	*Mean*	*SD*	*Mean*	*SD*	*Mean*	*SD*	*Mean*	*SD*	*Mean*	*SD*
FPL	-15.8[a]	1.5	-16.6[a]	2.0	-15.5[a]	1.7	12.0[a]	2.4	11.8[a]	1.5	12.4[a]	0.8
FDS2	-19.2[a]	1.8	-15.9[b]	1.9	-14.5[b]	2.7	14.9[a]	2.1	14.2[a]	2.2	17.5[a]	3.0
FDS3	-20.5[a]	2.1	-17.2[b]	2.4	-15.4[a,b]	2.5	17.3[a,b]	2.4	16.7[a]	2.2	20.1[b]	2.5
FDS4	-18.9[a]	2.1	-16.2[b]	2.4	-15.0[a,b]	2.7	22.3[a,b]	2.2	22.5[a]	2.0	25.6[b]	1.6
FDP2	-16.6[a]	3.2	-12.9[a]	2.3	-13.0[a]	2.0	16.9[a]	1.8	16.4[a]	1.4	17.4[a]	1.4
FDP3	-14.5[a]	2.4	-12.7[b]	2.1	-12.8[a,b]	1.7	22.0[a]	1.7	22.0[a]	1.5	23.3[a]	1.4
FDP4	-13.4[a]	1.7	-11.2[b]	2.3	-10.7[b]	1.8	26.6[a]	2.6	26.4[a]	2.0	27.8[a]	1.6
FDP5	-14.7[a]	1.5	-11.4[b]	1.7	-10.0[a,b]	2.0	28.5[a]	2.8	28.1[a]	2.3	29.8[a]	1.7

Table 5.5. Average linear displacements at the level of the RS and angular sweep of all FDS and FDP tendons (top) and FPL tendon (below).

Average Linear and Angular Tendon Displacements Proximal to Tunnel				
ALL TENDONS OF DIGITS 2-4				
		A-P Displacements (mm)	**M-L Displacements (mm)**	**Frontal Angle Sweep (deg)**
Forearm	*Pro-Neutral*		0.3	0.4
	Sup-Neutral		2.2	6.5
	Pro-Sup		2.5	6.04
Wrist	*Ext-Neutral*	0.9		
	Flx-Neutral	2.9		
	Ext-Flx	3.8		
FLEXOR POLICIS LONGUS				
		A-P Displacements (mm)	**M-L Displacements (mm)**	**Frontal Angle Sweep (deg)**
Forearm	*Pro-Neutral*		0.3	0.3
	Sup-Neutral		0.7	6
	Pro-Sup		0.4	6.3
Wrist	*Ext-Neutral*	1.1		
	Flx-Neutral	0.8		
	Ext-Flx	0.3		

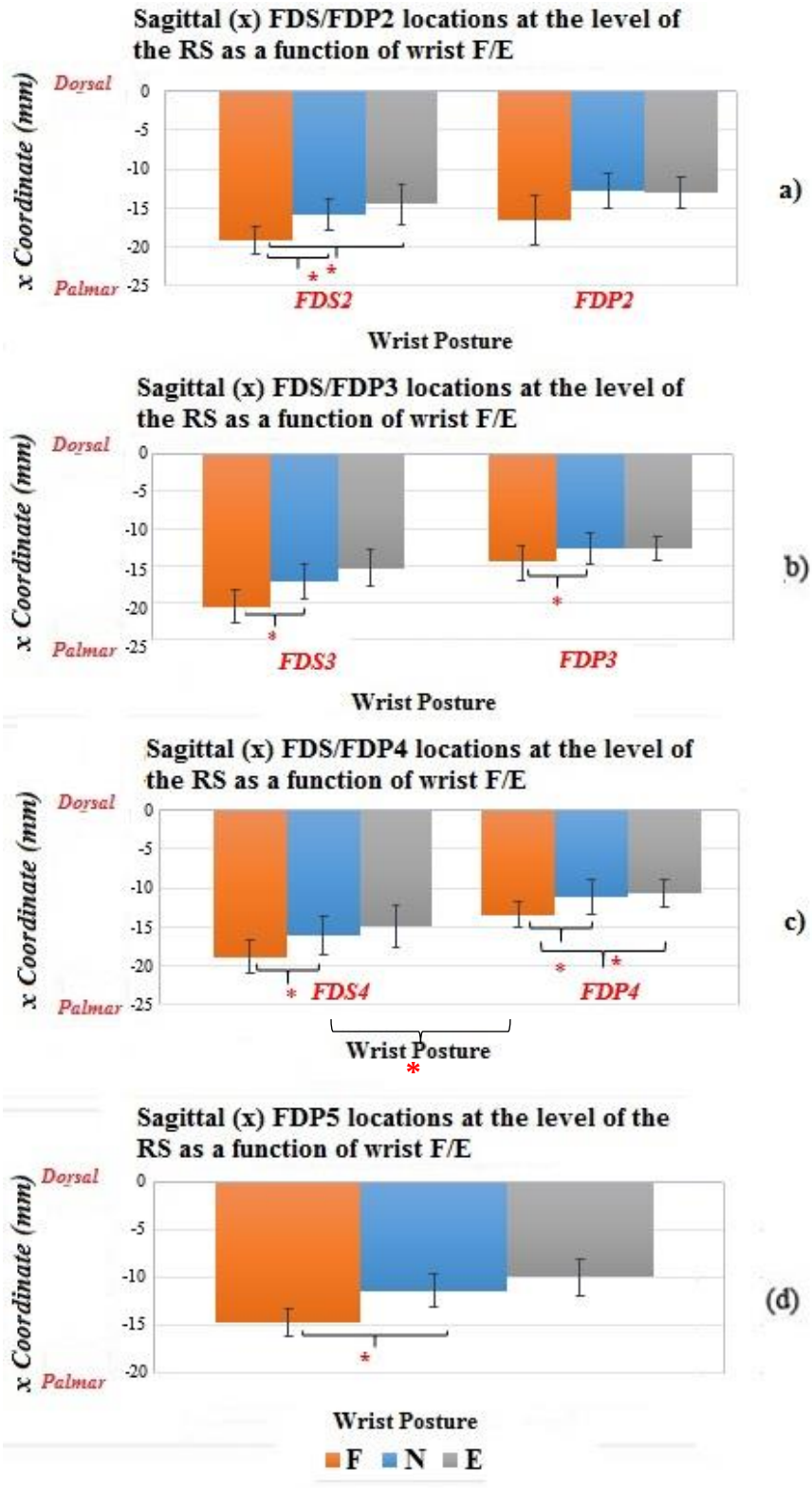

Figure 5.1. Significant effects of wrist posture on tendon sagittal locations at the level of the RS for all FDS and FDP tendons of the 2nd (a), 3rd (b), 4th (c), and 5th (d) digits. Asterisk denotes significance at $p<0.05$ Bonferroni corrected for multiple comparisons. Error bars represent SD.

5.1.2.2 Frontal Displacements

Frontal displacements were changes of tendon locations along the medio-lateral z axis at the level of the RS. (Recall that positive z points towards the ulna.) Wrist posture did not change the frontal locations of any tendons, but forearm pronation/supination had an effect on FDS3 and FDS4 (Tables 5.3, 5.4). Average locations along the medio-lateral axis of these two tendons across wrist postures, within each forearm posture, showed that tendons were located more ulnarly in supination (22.9 $\pm$ 2.0 mm) than in pronation (19.8 + 2.3 mm), and neutral forearm (19.6 $\pm$ 2.1 mm) (Table 5.4, Figure 5.2). The average location changes of these two tendons were larger for supinated and neutral postures (3.3 mm) than for pronated and neutral postures (0.2 mm) (Figure 5.2). See Appendix L for pairwise comparisons. However, even though other tendon displacement values did not reach significance, they also exhibited a similar pattern. The average location differences of all tendons showed that forearm supination tended to shift tendons more ulnarly (2.2 mm) than radially with pronation (0.3 mm) from the neutral forearm position (Table 5.5).

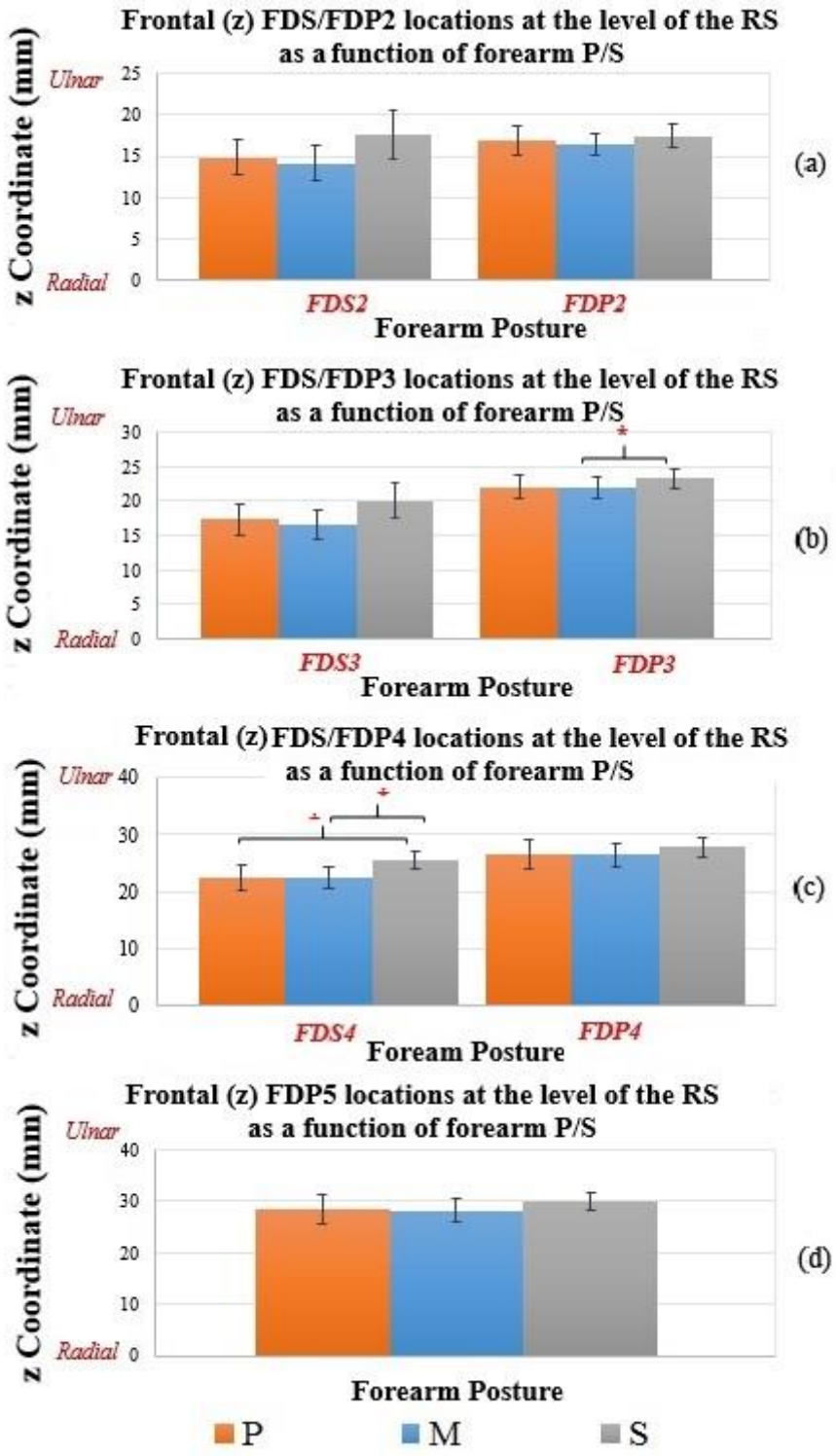

Figure 5.2. Significant effects of forearm posture on frontal locations at the level of the RS for all FDS and FDP tendons of the 2nd (a), 3rd (b), 4th (c), and 5th (d) digits. Asterisk denotes significance at $p<0.05$ Bonferroni corrected for multiple comparisons. Error bars represent SD.

5.1.3 Orientations

The findings revealed that significant angular changes only occurred in the frontal plane. Neither forearm pronation/supination nor wrist flexion/extension had a significant effect on the sagittal angle of any tendon. Sagittal angles did not change much between postures, with an average angle of -8.2° (a proximal angle opening palmarly) for all tendons (except FPL), across postures (Table 5.7).

5.1.3.1 Frontal Angles (zy)

Recall that tendon angles were measured with respect to the forearm's long axis, proximal to the RS, and positive angles open to the ulnar side (Figure 5.3). Forearm pronation/supination had an effect on the frontal plane angles of all tendons, whereas wrist posture did not have an effect on any frontal angle (Table 5.6). Forearm supination consistently shifted the angle of all tendons towards the ulna (Figure 5.4, Table 5.7). Frontal angle averages of all tendons (except FPL) across wrist postures, within each forearm posture, showed that supination tended to elicit ulnar angles ($4 \pm 4.2°$), whereas neutral ($-2.5 \pm 3.7°$) and pronation ($-3 \pm 3.3°$) tended to elicit radial angles of tendons with respect to the forearm's long axis (Table 5.7).

A relatively large tendon sweep (i.e., the angular difference between postures) was observed between neutral and supinated postures (6.5°) when comparing average angles of all tendons (except the FPL). The average tendon sweep of superficialis and profundus tendons separately highlighted that tendon movement was more pronounced in superficialis tendons (8.6°), than in deep tendons (5.7°) (Table 5.7). Compared with all other tendons in all postures, the FDS3 had the most radial angle, and the FDP5 had the most ulnar angle (Table 5.7). The

FDS3, FDS4, and, to a lesser extent the FDS2, exhibited greater radial angles in pronated and mid-pronated postures than did other tendons. The FDS3 however, came in close alignment with the forearm's long axis in supination, and the FDS4 and FDS2 changed orientation angles to the ulnar side by a few degrees (Table 5.7). The FDP5, FDP4, and, to a lesser extent the FDP3, on the other hand, exhibited larger ulnar angles in supination than other tendons. The FDP4 and FDP3 nearly aligned with the forearm's longitudinal axis in pronated and mid-pronated postures, whereas the FDP5 maintained a small ulnar angle even in full pronation (Table 5.7).

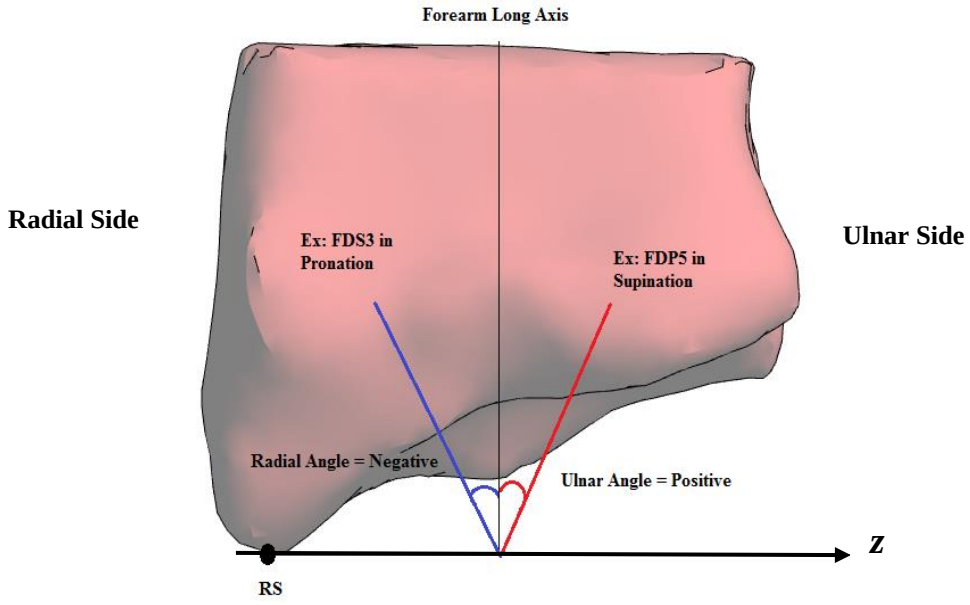

Figure 5.3. Frontal angle polarity: angles opening to the ulnar side were positive, and angles to the radial side negative. Examples of tendons with the most radial angle in pronation (FDS3), and the most ulnar angle in supination (FDP5), are illustrated.

Table 5.6. Results summary of the effect of forearm and wrist posture, on the frontal tendon angle, proximal to the carpal tunnel. P values are shown for Bonferroni-adjusted pairwise comparisons unless denoted with the superscript c.

yz frontal angle								
	Wrist				Forearm			
	F	dof	p[a]	Post Hoc Comparisons	F	dof	p[a]	Post Hoc Comparisons
FPL	0.003	(1.105,3.046)[b]	0.997[c]	*ns*	8.654	(2,6)	0.129 0.008* 1.000	*pro vs sup* *mid vs sup* *pro vs mid*
FDS2	0.567	(2,6)	0.595[c]	*ns*	17.349	(2,6)	0.069 0.004* 1.000	*pro vs sup* *mid vs sup* *pro vs mid*
FDS3	0.783	(2,6)	0.499[c]	*ns*	16.21	(2,6)	0.067 0.002* 1.000	*pro vs sup* *mid vs sup* *pro vs mid*
FDS4	2.236	(2,6)	0.188[c]	*ns*	31.285	(2,6)	0.043* 0.002* 1.000	*pro vs sup* *mid vs sup* *pro vs mid*
FDP2	0.736	(2,6)	0.518[c]	*ns*	6.332	(2,6)	0.244 0.017* 1.000	*pro vs sup* *mid vs sup* *pro vs mid*
FDP3	0.643	(2,6)	0.599[c]	*ns*	6.882	(1.019,3.057)	0.311 0.003* 1.000	*pro vs sup* *mid vs sup* *pro vs mid*
FDP4	1.425	(1.008,3.025)[b]	0.312[c]	*ns*	24.117	(2,6)	0.071 0.003* 1.000	*pro vs sup* *mid vs sup* *pro vs mid*
FDP5	1.948	(2,6)	0.223[c]	*ns*	17.795	(2,6)	0.022* 0.54 1.00	*pro vs sup* *mid vs sup* *pro vs mid*

[a]Bonferroni corrected p value, unless specified with the d superscript

[b]Sphericity violated, Greenhouse-Geisser Corrected

[c]ANOVA priori tests p value

*Denotes significance

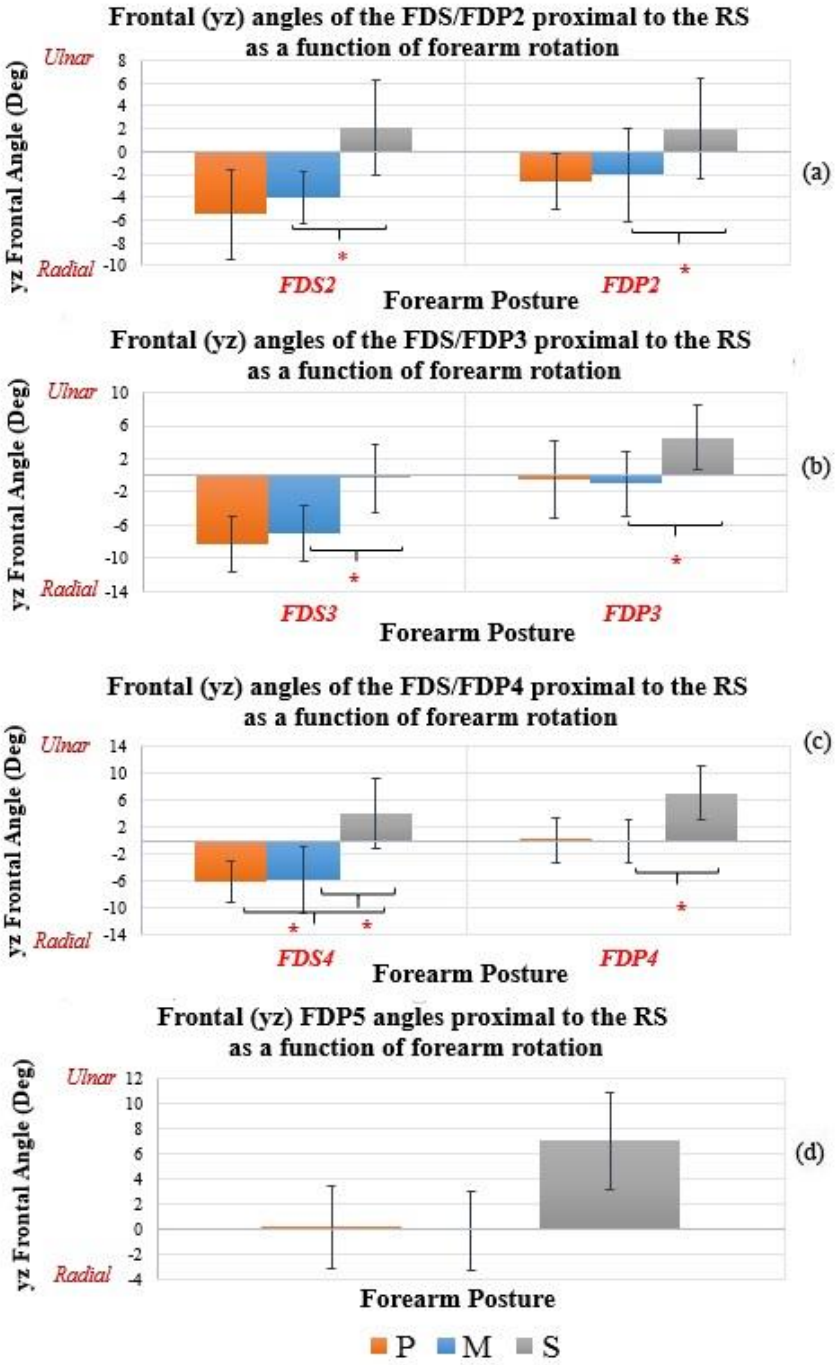

Figure 5.4.Significant effects of forearm posture on frontal tendon angle, proximal from the carpal tunnel, of all FDS and FDP tendons of the 2nd (a), 3rd (b), 4th (c), and 5th (d) digits. Asterisk denotes significance at $p<0.05$ Bonferroni corrected for multiple comparisons. Error bars represent SD.

Table 5.7. Means and standard deviations of sagittal and frontal tendon angles proximal to the carpal tunnel.

	Tendon Angle Means and Standard Deviations with Respect to the Longitudinal Axis of the Forearm (Proximal to RS)											
	Sagittal (yx) Angle (deg) n=12						*Frontal (yz) Angle (deg) n=12*					
Tendon	*Flx*		*Neutral*		*Ext*		*Prone*		*Neutral*		*Sup*	
	Mean	*SD*	*Mean*	*SD*	*Mean*	*SD*	*Mean*	*SD*	*Mean*	*SD*	*Mean*	*SD*
FPL	-6.7[a]	2.1	-6.8[a]	4.1	-6.6[a]	4.4	-8.9[ab]	4.2	-8.6[b]	2.9	-2.6[a]	3.5
FDS2	-5.0[a]	2.8	-6.0[a]	2.5	-4.6[a]	3.9	-5.5[ab]	3.9	-4.1[b]	2.3	2.2[a]	4.2
FDS3	-8.2[a]	3.8	-8.8[a]	3.0	-8.5[a]	4.3	-8.4[ab]	3.4	-6.9[b]	3.4	-0.4[a]	4.2
FDS4	-11.8[a]	3.3	-12.0[a]	2.2	-10.4[a]	3.8	-6.1[a]	3.1	-5.8[a]	4.8	4.0[b]	5.1
FDP2	-5.9[a]	2.9	-7.1[a]	2.2	-5.6[a]	3.4	-2.6[ab]	2.5	-2.1[b]	4.1	2.0[a]	4.4
FDP3	-9.7[a]	3.0	-9.9[a]	1.5	-7.9[a]	4.3	-0.4[ab]	4.7	-1.0[b]	3.9	4.6[a]	3.9
FDP4	-9.9[a]	2.9	-10.9[a]	2.5	-8.8[a]	2.8	0.1[ab]	3.4	-0.2[b]	3.2	7.1[a]	3.9
FDP5	-6.6[a]	3.2	-6.5[a]	2.9	-7.3[a]	2.9	2.1[a]	2.2	2.4[ab]	4.0	8.2[b]	3.9

5.2 Discussion

Understanding the anatomical impact of forearm pronation/supination on tendons crossing the wrist is important; and yet, it has not been studied. The wrist, particularly the CT, is a vulnerable area because it contains a large number of structures in a small space. Changes of posture may displace internal structures in ways which increase internal loading. This study is novel because, for the first time, the impact of forearm pronation/supination on tendon kinematics is evaluated. This study is a step towards understanding the role of forearm pronation/supination on injury, so that internal exposures can be modeled based on external posture measurements. The purpose of this study was to investigate the effect of forearm pronation/supination and wrist flexion/extension on the displacements and tendon "sweep" (angular movement of the tendon) of finger flexor tendons. It was hypothesized that finger flexor tendons would exhibit angular changes and displacements just proximal to the CT, with greater changes with increased forearm pronation or supination compared to a mid-pronated position. Findings showed that generally, forearm rotation affected frontal plane tendon movement, whereas wrist flexion/extension affected sagittal plane. Tendon movement implications is discussed in the following sections.

5.2.1 Sagittal Displacements

Forearm pronation/supination did not have an effect on sagittal displacement. However, wrist flexion/extension had a consistent effect on the sagittal displacement of all tendons. Tendons were located more volarly in flexed wrist postures, and more dorsally in extended wrist postures, when compared to neutral. The average tendon displacement from extension to flexion was 3.8 mm (Table 5.5), slightly lower than that seen by Keir & Wells (1999). They found volar

displacements from extension to flexion of 5 mm. However, in the current study, the observed range of wrist motion was only 24.9° (Table 5.2) compared to their larger range achieved at the wrist of approximately 57°.

Recall that generally, larger displacements were seen between neutral and flexed postures than between neutral and extension (Table 5.3), consistent with Keir and Wells' findings. These observations indicate that tendons move towards the flexor retinaculum, which—although it may allow some movement—primarily functions by constraining tendons to prevent bowing (Loudon, J. et al., 2013). This suggests that increased volar contact may occur, which may also affect contact forces around the median nerve, further supporting their conclusion that flexion may increase the risk of developing CTS.

5.2.2 Frontal Displacements

Although forearm pronation/supination had a significant effect only on the frontal displacements of the FDS3 and FDS4 tendons, other tendons showed a similar pattern. Tendon movement was larger in superficial tendons than in the FPL and FDP tendons (Figure 5.2, Table 5.4). The location change of the FDS2 between neutral forearm and supine approached significance. However, it is possible that the FDS2 tendons exhibited the least movement of all FDS tendons, because the FDS2 is the only bundle of this muscle originating on the anterior radius.

Additionally, recall that displacements between neutral and supinated forearm were greater than those seen between neutral and pronated forearm. However, this difference could be due to the different range of motion achieved in either direction; participants achieved approximately

20° of pronation and 52° of supination. The forearm pronation/supination postures in the methodology of this study were selected because they were within a comfortable anatomical range of motion, and may be replicated in manual work activities.

The larger displacements seen in supination may suggest that the FDS musculature is located on the ulnar side of the forearm in this posture, rather than directly on the anterior surface. This change in musculature location with respect to the CT could increase tendon tension, as muscle bundles elongate to reach the tunnel, resulting in a pull on the ulnar tendon. These findings could have potential clinical relevance, because when tendons are under tension and are located more ulnarly, compression of nearby structures against the tunnel walls might increase in the direction of the movement. Thus, structures such as the common tendon sheath and sub-synovial tissue on the ulnar side, near the proximal end of the CT, may be at risk of increased MSK loading. Activities requiring supinated postures, particularly with intermittent finger actions (such as guitar playing at the fingerboard), may increase the risk of developing ulnar pain or discomfort, or even tenosynovitis (on the ulnar side).

5.2.3 Frontal Angular Deviations

Angular changes in the frontal plane of all tendons were affected only by changes in forearm posture. The larger angular deviations of the FDS compared to FDP tendons may have occurred because the FDP tendons originate more distally than the FDS tendons. Generally, angles tended to shift more ulnarly with supination than with mid-pronated or pronated postures. (Recall that the FDS3 had the most radial angles in all postures, and the FDP5 the most ulnar). Given that the third digit is not the most radial digit, it seems reasonable to suggest that digit location along the radio-ulnar axis probably does not have an effect on the frontal angular orientation proximal to

the CT. Instead, it seems that tendons have different angle orientations, depending on their respective radio-ulnar location proximally into the forearm.

Each of the FDS and FDP muscles are normally considered single muscles; however, each one is a bundle of four muscle bellies (for the second-fifth digits). Thus, recognizing the magnitude of the angular shifts associated with each particular digit in various forearm postures may be important for identifying favorable/unfavorable postures for each finger.

On one hand, increased angular bends in the radial or ulnar direction may increase contact against nearby structures in the direction of the bend. Because the FDS3 and FDP5 had the largest angular deviations in pronation and supination, respectively, they probably experienced higher contact forces against the adjacent carpal walls on their respective sides. The increase in normal forces may in turn contribute to higher frictional work performed by tendons against nearby structures, in activities with repetitive finger motion of those digits.

On the other hand, friction experienced by a tendon bent over a trochlear surface could elicit some loss of muscle force distal to the trochlea, causing a slight increase in exertional demand on the muscle bundle, because more force will have to be produced to create a given torque at the respective joints. Further increases in normal force between the two surfaces, via displacement in the direction of the bend or added tension, would further increase frictional work, aggravating the loss of force distal to the trochlea and resulting in added muscular demand.

In addition, larger angle deviations could mean that individual muscle bundles are lengthening, which may result in a reduced capability to produce force via fewer available cross-bridges, and thus an increased exertional demand on the bundle. In light of this possibility, activities requiring continuous/sustained exertions of finger tendons angularly deviated in particular forearm postures may be at risk of muscular fatigue. For instance, use of the third digit

in sustained pronation could increase the exertion of the FDS3 bundle; use of the fifth digit in supination, on the other hand, could increase exertional demand of the FPD5 (Table 5.7). Because the orientation of these two tendons mirror each other, pronation may be favorable for the FDP5 and supination for the FDS3. Thus, knowledge about individual angle deviations for each of the FDS and FDP tendons in sustained forearm postures away from neutral may help identify posture/action combinations likely to induce higher MSK loading.

Lastly, the individual angle sweep of each tendon may be relevant for identifying tendons vulnerable to frictional work in actions requiring repetitive forearm pronation/supination (Table 5.8). Recall that the average sweep among tendons was 6.5°. Some tendons, such as the FDS4 (10°), traveled larger angles when the forearm rotated from one end to the other, while others travelled less than half that distance (e.g., FDP2). Tendons with larger angle sweep may be at increased risk of abrasive wear when performing manual activities requiring repetitive forearm pronation/supination in combination with sustained wrist flexion or extension, due to combined medio-lateral translations with forearm pronation/supination, and volar or dorsal contact forces with wrist flexion/extension deviations. For instance, continuous pinch grips of the second, third, and fourth digits (which are tendons with the largest sweep angles), along with repetitive forearm pronation/supination and sustained wrist flexion, may increase frictional work against the flexor retinaculum in the medio-lateral direction of such tendons. Thus, knowledge about the angular sweep with forearm pronation/supination, for individual FDS and FDP tendons, combined with an awareness of the implications of the combined effects of wrist posture, may help identify tendons vulnerable to MSK loading in certain manual activities.

.

Table 5.8. Frontal tendon sweep of individual finger flexor tendons, between forearm postures in degrees.

Average Angular Sweep per Individual Digit (deg)			
	Pro-Mid	*Mid-Sup*	*Pro-Sup*
FDS4	0.3	9.8	10.1
FDS3	1.5	6.5	8.0
FDS2	1.4	6.3	7.7
FDP4	0.3	7.3	7.0
FDP5	0.3	5.8	6.1
FDP3	0.6	5.6	5.0
FDP2	0.5	4.1	4.6

5.2.4 Sagittal Angular Deviations

Sagittal tendon trajectories showed that tendons were more palmar more proximal to the RS (in the forearm), but deviated dorsally as they approached the CT; these changes may reflect some volar movement constraint at the proximal end of the tunnel. However, neither forearm nor wrist posture had an effect on sagittal angles. Bulking of the flexor muscles due to contraction during wrist flexion, along with volar tendon movement at the level of the RS in flexion, may explain the lack of angular sweep in the sagittal plane as a function of wrist posture.

5.3 Limitations

Although the amount of force was theoretically controlled during image acquisition, it was difficult for some participants to maintain the force towards the end of the scan. It is unclear if these small fluctuations in force added noise in some of the scans. It is also unclear whether this noise, along with segmentation and centerline calculations, affected tendon trajectories. However, even if the tendon trajectories had been affected, it is possible that the changes were very small; the findings may be as accurate as the image resolution (0.3mm x 0.03mm x 0.8 mm).

Furthermore, between-subject variability should be acknowledged. While the within-subject variability (in terms of identifying bony landmarks, which were used to create the anatomical frames of reference) was reduced through the registration process, between-subject variability identifying landmarks, particularly for the radio-distal prominence of the ulna across the ulnar styloid, may have introduced significant variability into the results. Even though comparisons between conditions for each participant were plausible, the magnitude of the differences in orientations and locations between participants was not quantified.

The centroids used to define the forearm's long axis were calculated as the centers of two circles fitted through the proximal and distal forearm surfaces, which were perpendicular to the global long axis (along the scanner). The forearm's axis was not the same for every scan, because forearm orientations varied. It is unclear, however, whether changes in the proximal and distal surface orientation could have affected the location of the calculated centers, possibly resulting in increased variability between the alignment of the calculated long axis and the respective forearm's long axis.

5.4 Conclusions and Future Directions

This study represents an important milestone in understanding the effect of forearm posture on tendon movement, relevant to understanding the contribution of forearm pronation/supination to MSK loading of the upper limb; for the first time, tendon movement as a function of forearm posture was documented at the proximal end of the forearm. In summary, wrist flexion/extension posture only affected tendon location changes in the sagittal plane, whereas forearm pronation/supination only affected tendon movement in the frontal plane. Small dorsal movement was seen with wrist extension. These findings support previous reports of volar displacements with increased wrist flexion, which may increase anterior contact forces, potentially affecting the median nerve. The relatively constant palmar angle across postures may reflect a movement constraint at the CT, potentially having implications for the volar contact forces at the proximal CT. Actions requiring constant wrist flexion, particularly under loading conditions, may increase the risk of developing CTS. Wrist flexion combined with repetitive finger or forearm motions may elicit axial or medio-lateral frictional work against surrounding tissues.

Forearm pronation elicited minimal radial displacements, whereas supination elicited larger ulnar displacements, in FDS tendons. Greater angular displacements of the FDS tendons were seen when compared to the FDP tendons, in the frontal plane. Pronation increased the radial angle of the most radial tendons, whereas supination increased the ulnar angle of the most ulnar tendons. Smaller radial tendon displacements with pronation from neutral forearm may reflect radial constraints, which along with increased radial angles of radial tendons, may result in further radial contact increases at the proximal end of the CT.

Large frontal angle deviations suggest increased contact with lateral carpal walls in the direction of the bend in the proximal CT. Increased contact forces in any direction with repetitive

motions (of finger and/or wrist) may contribute to MSK loading via frictional work of tendons on nearby structures. Lastly, forearm deviated postures seemed to affect muscular demands of flexor muscles, via force reductions distal to the trochlear surface (due to frictional work and muscle length changes).

Thus, forearm deviations from neutral posture could increase MSK loading. Frictional work depends on the contact (normal) force of the tendons against other structures, and can induce histological changes to eventually lead to pathologies (e.g., tendonitis/tenosynovitis).

In conclusion, wrist flexion together with forearm postures away from neutral change the tendon locations and orientations proximal to the CT, which has the potential to alter the relationship of tendons to nearby structures, and potentially increase MSK loading. Further investigation into tendon trajectories within the tunnel and the tendons' relationships with other structures is necessary, as is an evaluation of the tendons on the extensor side of the wrist.

6 CHAPTER 6. STUDY III: DISTAL RESULTS AND DISCUSSION

Finger Flexor Tendon Trajectories Distal to the Carpal Tunnel as a Function of Forearm and Wrist Posture: Results and Discussion.

6.1 Results

This chapter presents findings regarding changes in tendon locations distal to the CT, and angular deviations within the CT, in the frontal and sagittal planes, from data acquired in the study described in chapter 4. Tendon location and orientation data from the proximal and distal ends of the tunnel are presented separately because they seem to have potential implications on different regions. Findings at the proximal end of the CT may be found to be more relevant to loading of the forearm, whereas findings on chapter 6, which include tendon locations distal to the CT, and estimated angle trajectories through the wrist, may be more relevant to the wrist. Information on those who participated in the MRI study is presented again for reference (Table 6.1).

Table 6.1. Participant demographic information.

n		4	
Age (years)		27 (± 6.24)	
Height (m)		1.78 (±0.06)	
Weight (Kg)		71.0 (± 8.72)	
Sex	F	1	0 Right 1 Left
	M	3	1 Right 2 Left

6.1.1 Posture

Posture information is reported in this chapter for easier reference. Conditions included a combination of three wrist postures (30° extension, straight (0°), and 30° flexion) and three forearm postures (40° pronation, mid-pronation (0°), and 60° supination). However, the observed ranges of motion (based on relative bone motion) were only 24.9° at the wrist (radius with respect to third metacarpal), and 68.7° at the forearm (radius with respect to ulna). Average postures are shown in table 6.2. Although not controlled, radial/ulnar deviation motion was minimal, with an average range of motion of 4.3° and 4.4° as a function of wrist flexion/extension and forearm pronation/supination, respectively. Findings showed no effect of wrist posture on forearm pronation/supination, or vice versa, suggesting that these postures were independent from each other.

Table 6.2. Means and standard deviations of each wrist and forearm posture, achieved during scan acquisition, of all scans for all participants. Forearm pronation/supination values were normalized to the NM condition of each participant.

Wrist Posture			**Normalized Forearm Posture**		
	x(SD)	*n*		*x(SD)*	*n*
Extension	17.3 (±6.3)	12	Pronation	16.8 (±7.8)	12
Neutral	6.8 (±6.7)	12	Neutral	-4.3 (±7.7)	12
Flexion	-7.6 (±6.8)	12	Supination	-51.9 (±8.1)	12
R/U	-1.7 (±5.6)	36			

6.1.2 Displacements

6.1.2.1 Frontal Displacements

Frontal displacements were changes in tendon locations along the mediolateral radius' axis z, at the level of the y coordinate of the metacarpal styloid of the third metacarpal (MS). The tendon remained expressed with respect to the radial CS, and the MS location was rotated and translated to be in the same radial CS to obtain the y coordinate. (Recall that positive z pointed towards the ulna.) ANOVA analyses revealed that forearm pronation/supination had an effect on all FDS tendons, whereas wrist posture did not have an effect on the frontal locations of any tendon (Table 6.3). However, after performing a Bonferroni-adjusted, multiple comparisons test, differences between supination and neutral were significant for the FDS3 only (Table 6.3, Figure 6.1). The average locations of the FDS3 tendons across wrist postures within each forearm posture showed that tendons were located more ulnarly in supination (20.3 $\pm$ 2.7 mm) than in neutral posture (17.4 $\pm$ 2.8 mm) (Table 6.4). The average locations of all tendons across wrist postures, within each forearm posture, showed that although most displacements did not reach significance, a movement pattern similar to that of the FDS3 tendons was observed. Tendons were generally located more ulnarly in supination (22.0 $\pm$ 2.0 mm) than in neutral (20.6 $\pm$ 2.4 mm) or pronation (20.9 $\pm$ 2.8 mm) (Figure 6.1, Table 6.4). A range of movement of 0.03-2.49 mm was observed across all tendons, with the FDS3 exhibiting the maximum frontal displacement (Table 6.4). Average frontal displacements of all tendons showed a small, but consistent, shift between neutral and supination of 1.4 mm, and an even smaller shift between prone and neutral postures of 0.03 mm (Table 6.8). See Appendix N for pairwise comparisons.

Table 6.3. Results summary of the effect of forearm and wrist posture on the antero-posterior tendon location (along the x axis), and on the medio-lateral location (along the z axis), at the level of the MS. P values are shown for Bonferroni-adjusted pairwise comparisons unless denoted with the superscript c.

x at y of MS								
	Wrist				**Forearm**			
	F	**dof**	**p[a]**	**Post Hoc Comparisons**	**F**	**dof**	**p[a]**	**Post Hoc Comparisons**
FDS2	31.532	(2,6)	0.029* 0.009* 0.225	*ext vs flx* *neut vs flx* *ext vs neut*	13.281	(2,6)	0.031* 0.148 1.000	*pro vs sup* *mid vs sup* *pro vs mid*
FDS3	22.729	(2,6)	0.033* 0.003* 0.603	*ext vs flx* *neut vs flx* *ext vs neut*	4.410	(2,6)	0.066[c]	*ns*
FDS4	30.890	(2,6)	0.026* 0.007* 0.374	*ext vs flx* *neut vs flx* *ext vs neut*	3.390	(2,6)	0.082[c]	*ns*
FDP2	22.158	(2,6)	0.050 0.020* 0.460	*ext vs flx* *neut vs flx* *ext vs neut*	0.329	(2,6)	0.732[c]	*ns*
FDP3	28.578	(2,6)	0.026* 0.001* 0.629	*ext vs flx* *neut vs flx* *ext vs neut*	3.257	(2,6)	0.110[c]	*ns*
FDP4	30.098	(2,6)	0.021* 0.006* 0.351	*ext vs flx* *neut vs flx* *ext vs neut*	5.147	(2,6)	0.05[c]	*ns*
FDP5	27.025	(2,6)	0.029* 0.010* 0.287	*ext vs flx* *neut vs flx* *ext vs neut*	4.812	(2,6)	0.057[c]	*ns*
z at y of MS								
	Wrist				**Forearm**			
FDS2	2.002	(2,6)	0.216[c]	*ns*	17.197	(2,6)	0.077 0.074 0.131	*pro vs sup* *mid vs sup* *pro vs mid*
FDS3	3.900	(2,6)	0.082[c]	*ns*	20.558	(2,6)	0.080 0.032* 0.732	*pro vs sup* *mid vs sup* *pro vs mid*
FDS4	3.105	(1.004,3.011)[b]	0.119[c]	*ns*	6.534	(2,6)	0.242 0.184 1.000	*pro vs sup* *mid vs sup* *pro vs mid*
FDP2	2.455	(2,6)	0.166[c]	*ns*	3.204	(2,6)	0.113[c]	*ns*
FDP3	3.527	(2,6)	0.097[c]	*ns*	1.643	(1.006,3.019)[b]	0.290[c]	*ns*
FDP4	1.072	(2,6)	0.400[c]	*ns*	0.52	(2,6)	0.619[c]	*ns*
FDP5	1.229	(2,6)	0.357[c]	*ns*	0.697	(2,6)	0.534[c]	*ns*

[a]Bonferroni corrected p value, unless specified with the d superscript

[b]Sphericity violated, Greenhouse-Geisser Corrected

[c]ANOVA priori tests p value

*Denotes significance

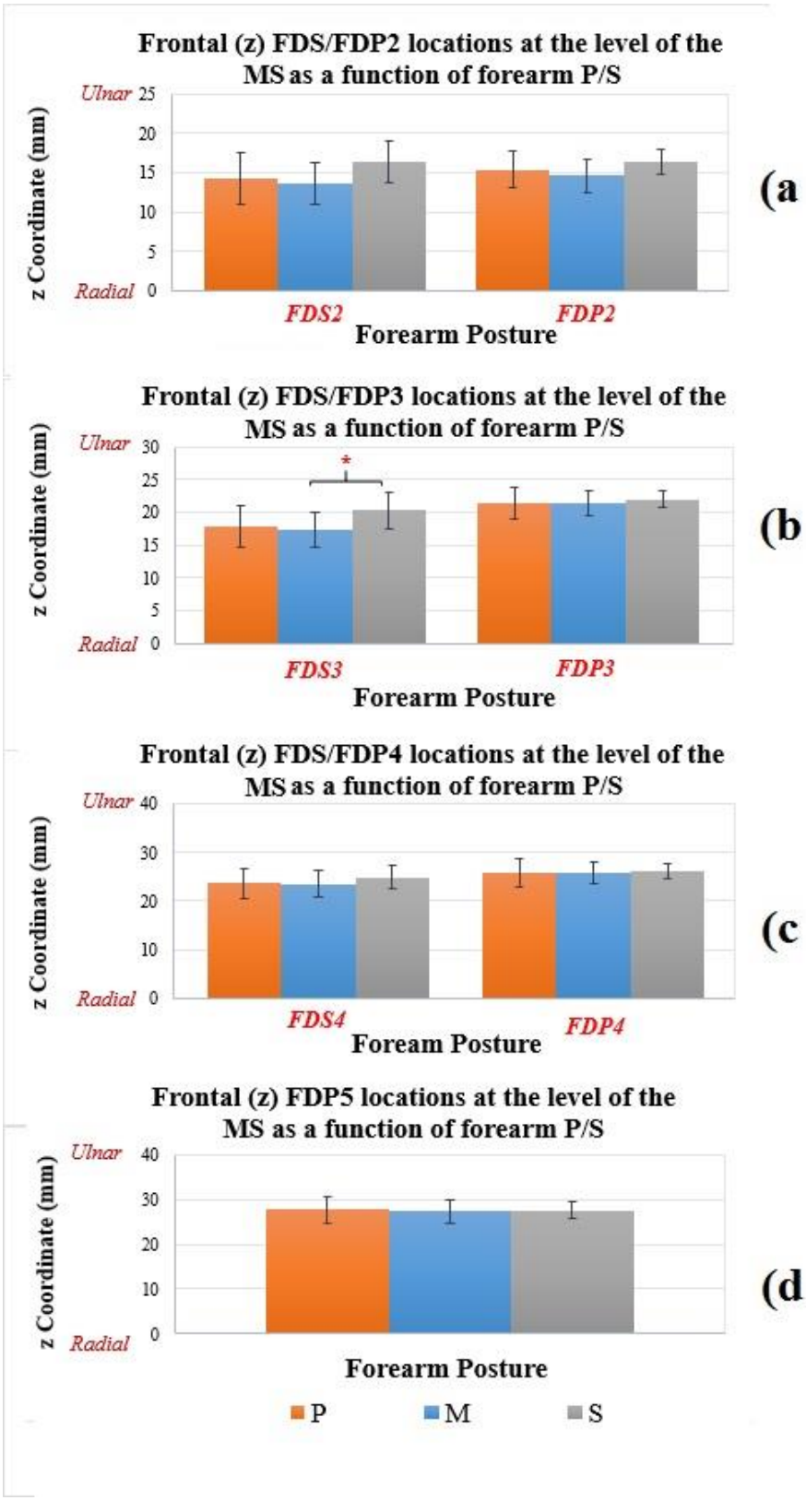

Figure 6.1. Significant effects of forearm posture on frontal locations, at the level of the MS, of all FDS and FDP tendons of the 2nd (a), 3rd (b), 4th (c), and 5th (d) digits. Asterisk denotes significance at $p<0.05$ Bonferroni corrected for multiple comparisons. Error bars represent SD.

Table 6.4. Means and standard deviations of tendon locations in the sagittal (across forearm postures) and frontal (across wrist postures) planes, at the level of the metacarpal styloid. Positive values in the sagittal and frontal planes correspond to dorsal and ulnar displacements respectively.

	Means and Standard Deviations of Location in the Sagittal and Frontal Planes (Distal to Tunnel)											
	Sagittal Distal Location (x at y=MS) n=12						*Frontal Distal Location (z at y=MS) n=12*					
Tendon	*Flx*		*Neutral*		*Ext*		*Prone*		*Neutral*		*Sup*	
	Mean	*SD*	*Mean*	*SD*	*Mean*	*SD*	*Mean*	*SD*	*Mean*	*SD*	*Mean*	*SD*
FDS2	-19.4[a]	2.7	-14.2[b]	2.5	-11.6[b]	2.4	14.3[a]	3.3	13.[7a]	2.7	16.4[a]	2.7
FDS3	-19.5[a]	2.3	-13.9[b]	2.7	-11.5[b]	2.5	17.8[ab]	3.1	17.4[a]	2.8	20.3[b]	2.7
FDS4	-18.0[a]	2.3	-13.0[b]	2.6	-10.9[b]	2.4	23.7[a]	3.1	23.6[a]	2.7	25.0[a]	2.4
FDP2	-16.7[a]	3.1	-11.2[b]	3.1	-9.2[ab]	2.3	15.4[a]	2.3	14.6[a]	2.2	16.3[a]	1.6
FDP3	-14.4[a]	2.5	-9.6[b]	2.5	-7.8[b]	1.8	21.4[a]	2.4	21.5[a]	1.9	22.0[a]	1.3
FDP4	-13.4[a]	2.1	-8.3[b]	2.3	-5.7[b]	2.3	25.9[a]	2.8	25.9[a]	2.2	26.2[a]	1.6
FDP5	-14.9[a]	1.9	-9.7[b]	2.0	-6.8[b]	2.3	27.7[a]	2.9	27.4[a]	2.7	27.7[a]	1.9

6.1.2.2 Sagittal Displacements

Distal sagittal displacements were changes in tendon locations along the radial antero-posterior x axis at the level of the MS, as defined by the y coordinate of the MS. The tendon remained expressed with respect to the radial reference frame, and the MS location was rotated and translated to be in the same reference frame to obtain the y coordinate. (Recall that positive x pointed towards the dorsum of the hand.) ANOVA analyses revealed that all tendons were displaced in the sagittal plane as a function of wrist flexion/extension, whereas only the FDS2 was displaced sagittal with changes in forearm posture (Table 6.3). The average sagittal locations of all tendons across forearm postures, within each wrist posture, showed that they were generally more volarly located with wrist flexion (-16.6 $\pm$ 2.4 mm), and to a lesser extent more dorsal with extension (-9.1 $\pm$ 2.3 mm), compared to neutral (-11.4 $\pm$ 2.5 mm) (Table 6.4, Figure 6.2). Bonferroni-adjusted, multiple comparisons showed that only displacements between neutral and flexion (5.2 mm) and between extension and flexion (7.5 mm) were significant, whereas displacements between neutral and extension (2.3 mm) were not (Table 6.3, 6.8).

The antero-posterior movement of the FDS2 as a function of forearm pronation/supination was considerably smaller than the movement observed as a function of wrist posture. On average, the FDS2 tendons were more dorsal in supination (-13.8 $\pm$ 2.4 mm) when compared to pronation (-15.7 mm $\pm$ 2.6 mm) or neutral (-15.6 $\pm$ 2.5 mm) (Appendix M). Multiple comparisons showed that only FDS2 displacements from pronation to supination (1.9 mm) were significant. More of this displacement occurred between supination and neutral (1.8 mm), than between pronation and neutral (0.13 mm) (Table 6.3). See appendix N for pairwise comparisons.

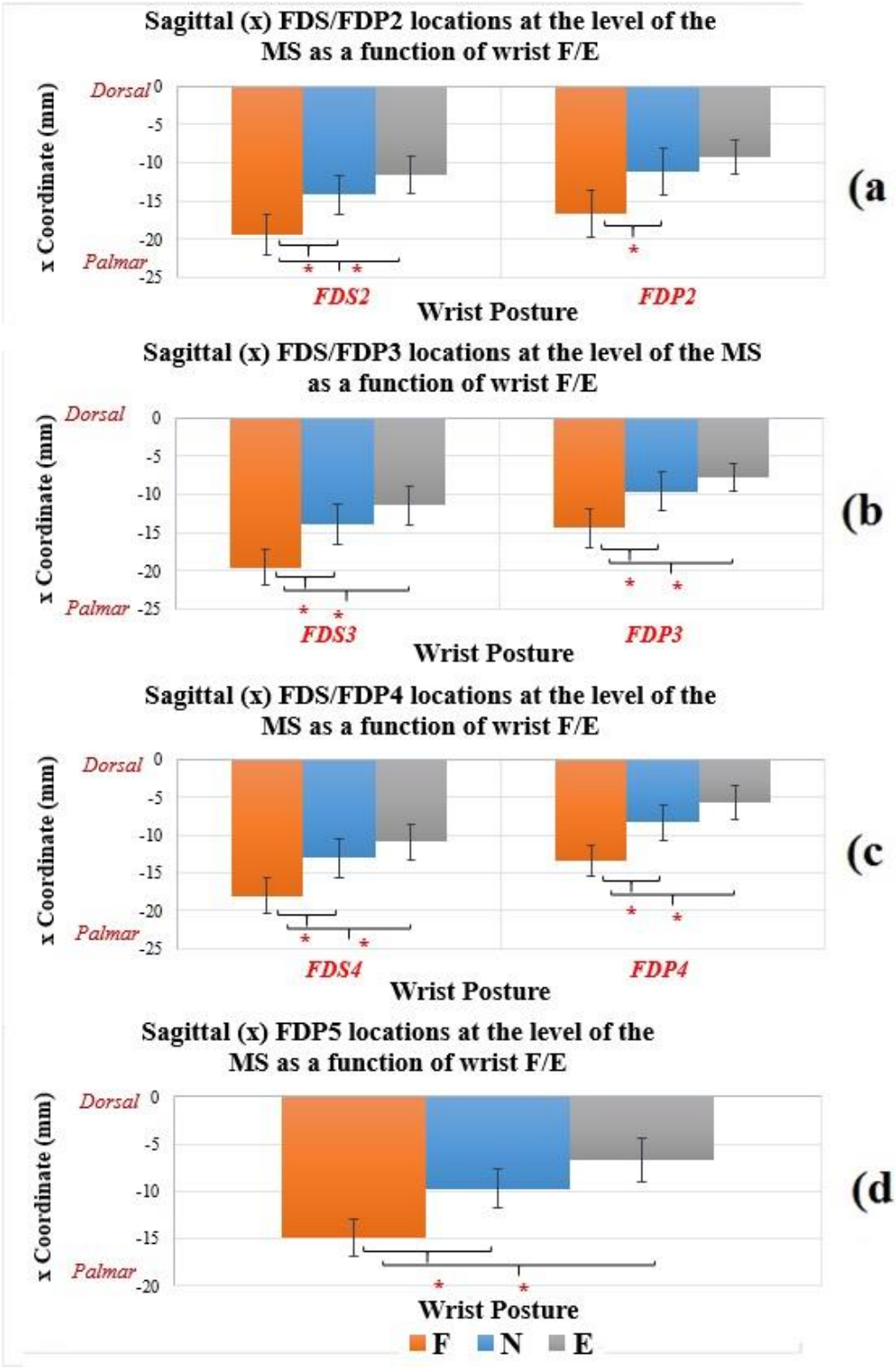

Figure 6.2. Significant effects of wrist posture on sagittal locations, at the level of the MS, of all FDS and FDP tendons of the 2nd (a), 3rd (b), 4th (c), and 5th (d) digits. Asterisk denotes significance at $p<0.05$ Bonferroni corrected for multiple comparisons. Error bars represent SD.

6.1.3 Orientations

All sagittal and frontal tendon angles used for comparisons were defined by the angular deviations of the distal portion of the tendon with respect to the proximal portion. These two portions were represented by two straight lines that best fit the tendon centerline coordinates in their respective tendon sections.

6.1.3.1 Frontal Tendon Angles

Frontal angles describe the angular deviation of the distal end of each tendon with respect to the proximal portion in the zy plane, as illustrated in Figure 6.3. Positive angles deviated ulnarly. ANOVA analyses revealed a main effect of forearm posture on the frontal angles of all tendons, and an effect of wrist posture on the FDS2, FDS4, and FDP3 tendons, without interactive effects (Table 6.5).

Multiple comparisons among forearm postures showed significant angle sweep differences in frontal angles, between supination and mid-pronation in nearly all tendons (except FDP2, 5). Differences between pronated and supinated postures were only significant for the FDS4 and the FDP3, 4, 5 tendons (Table 6.5, Appendix N). Generally, tendon angles shifted ulnarly from pronation to supination (Figure 6.4, Table 6.6). When averaging the frontal angular displacement of all tendons, shifts of 9.8° were seen between supination and pronation (8.1° of which occurred between supination and neutral, and 1.7° between pronation and neutral (Table 6.8).

Tendons of the most radial digits (second and third) tended to exhibit larger radial deviations in pronation (-10.2° average for both tendons) and mid-pronation (-7.8°), and became almost straight in supination (-0.2°) (Table 6.6, Figure 6.4). Angles of both tendons of the second

digit remained slightly deviated radially in supination (-3.3°), whereas those of the third digit shifted into a slight ulnar angle (2.9°). Conversely, the more ulnar tendons (of the fourth and fifth digits), exhibited ulnar deviations in all three postures. Greater deviations were seen in supination (13.1°), than in neutral (4.4°) and pronation (3.6°). The tendons of the fourth digit became nearly straight in pronation and mid-pronation (0.9° and 1.5° respectively), whereas the FDP5 remained with a relatively large ulnar angle in pronation and neutral (9° and 10.3° respectively).

Multiple comparisons among wrist postures showed significant differences in frontal angles between extension and neutral in the FDS2 and FDP3 (7.1° and 5.3° respectively), and between neutral and flexion in the FDS4 (4.7°) (Appendix N). In this case, angles of the FDS2 and FDP3 tendons angled more radially, and the FDS4 more ulnarly, with both wrist flexion and extension (when compared to neutral).

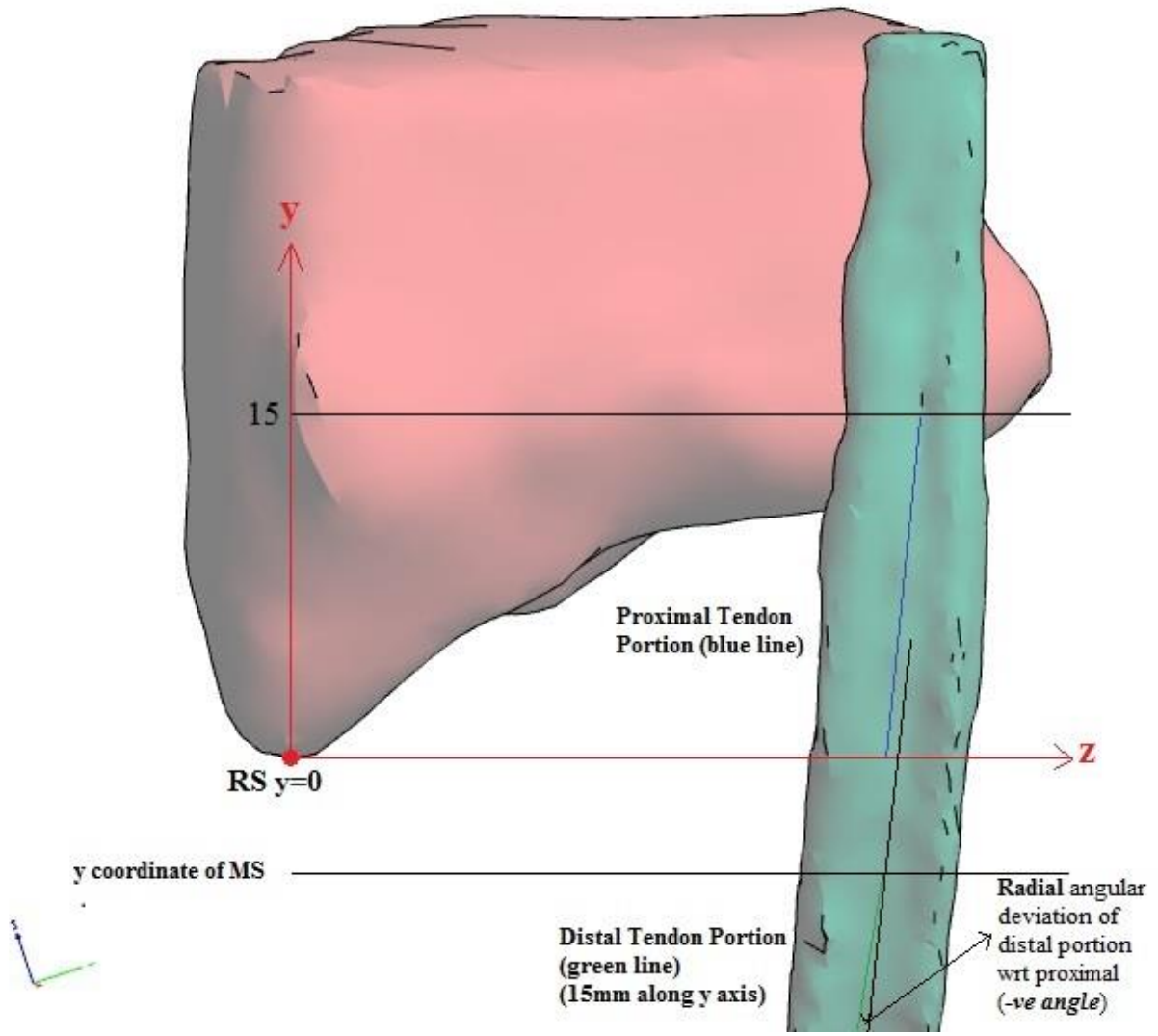

Figure 6.3. Illustration of whole tendon frontal angles, corresponding to the angular deviation of the distal portion (green line) of each tendon with respect to the proximal portion (blue line), in the zy plane. Positive angles in the frontal plane were deviated ulnarly.

Table 6.5. Results summary of the effect of forearm and wrist posture, on angular deviations of distal tendon portions with respect to their proximal end, in the frontal plane. P values are shown for Bonferroni-adjusted pairwise comparisons unless denoted.

Frontal Angle between Tendons' Proximal and Distal Portions								
	Wrist				Forearm			
	F	dof	p[a]	Post Hoc Comparisons	F	dof	p[a]	Post Hoc Comparisons
FDS2	16.232	(1.008,3.025)[b]	0.238 0.401 0.001*	*ext vs flx* *neut vs flx* *ext vs neut*	16.362	(2,6)	0.074 0.025* 0.310	*pro vs sup* *mid vs sup* *pro vs mid*
FDS3	9.439	(2,6)	0.854 0.221 0.062	*ext vs flx* *neut vs flx* *ext vs neut*	15.470	(2,6)	0.073 0.040* 0.415	*pro vs sup* *mid vs sup* *pro vs mid*
FDS4	5.726	(2,6)	1.000 0.037* 0.371	*ext vs flx* *neut vs flx* *ext vs neut*	29.029	(2,6)	0.033* 0.010* 1.000	*pro vs sup* *mid vs sup* *pro vs mid*
FDP2	4.994	(2,6)	0.053[c]	*ns*	12.204	(2,6)	0.095 0.062 0.930	*pro vs sup* *mid vs sup* *pro vs mid*
FDP3	10.661	(2,6)	1.000 0.066 0.031*	*ext vs flx* *neut vs flx* *ext vs neut*	29.432	(2,6)	0.045* 0.010* 1.000	*pro vs sup* *mid vs sup* *pro vs mid*
FDP4	3.769	(2,6)	0.087	*ns*	74.828	(2,6)	0.004* 0.001* 1.000	*pro vs sup* *mid vs sup* *pro vs mid*
FDP5	2.328	(2,6)	0.179[c]	*ns*	12.754	(2,6)	0.003* 0.158 1.00	*pro vs sup* *mid vs sup* *pro vs mid*

[a]Bonferroni corrected p value, unless specified with the d superscript

[b]Sphericity violated, Greenhouse-Geisser Corrected

[c]ANOVA priori tests p value

*Denotes significance

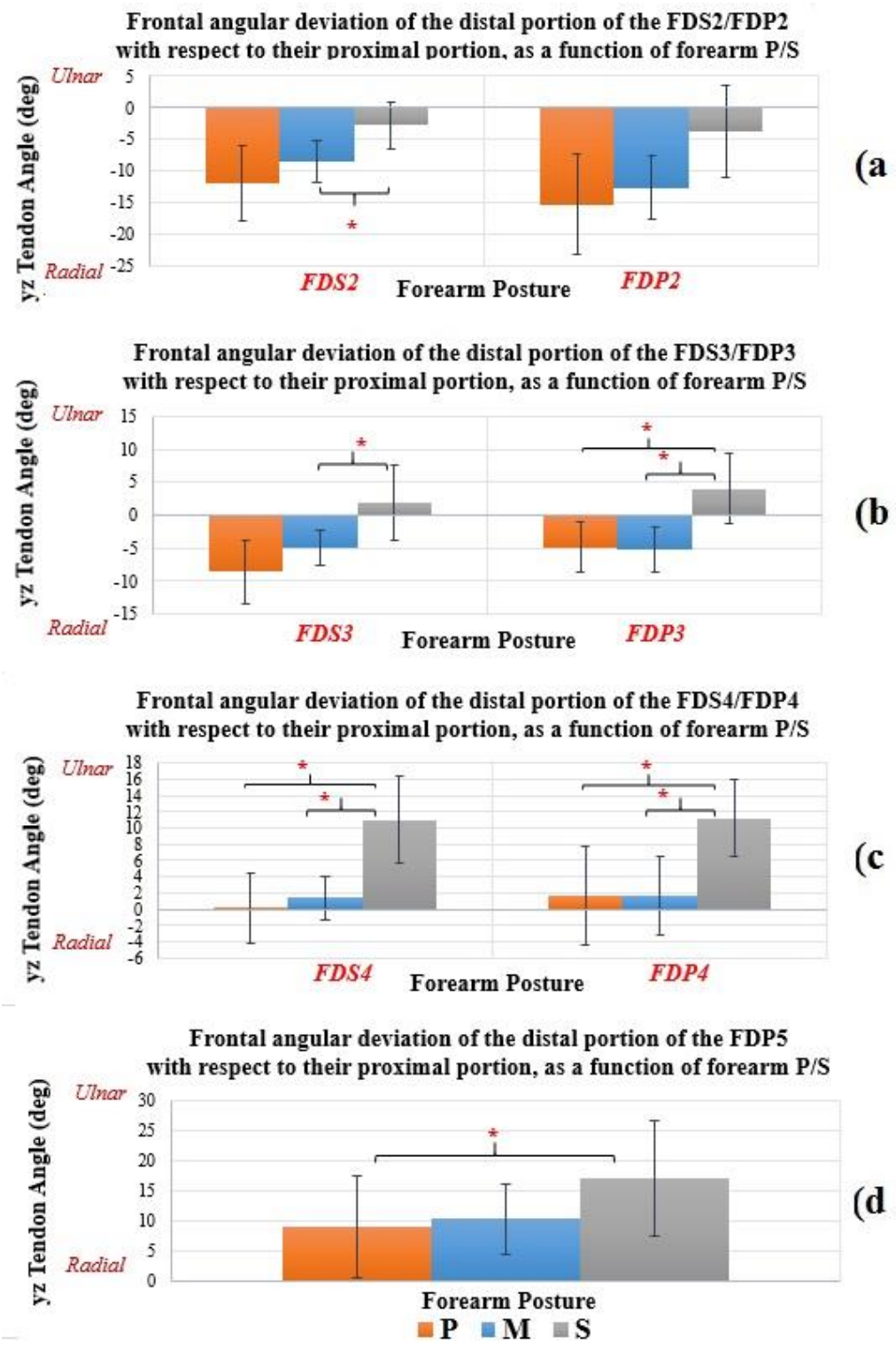

Figure 6.4. Significant effects of forearm posture on frontal angular deviations of the distal tendon portions with respect to their proximal portions, of all FDS and FDP tendons of the 2nd (a), 3rd (b), 4th (c), and 5th (d) digits. Asterisk denotes significance at $p<0.05$ Bonferroni corrected for multiple comparisons. Error bars represent SD.

Table 6.6. Means and standard deviations of sagittal (across forearm postures) and frontal (across wrist postures) angular deviations of distal tendon portions with respect to their proximal end. Positive values in the sagittal and frontal planes correspond to distal deviations in the dorsal and ulnar directions, respectively.

Means and Standard Deviations of Sagittal and Frontal Tendon Angles, Across the Carpal Tunnel, as a Function of Wrist and Forearm Posture.

	Tendon Sagittal Angles n=12						*Tendon Frontal Angles n=12*					
	Flx		*Neutral*		*Ext*		*Prone*		*Neutral*		*Sup*	
	Mean	*SD*	*Mean*	*SD*	*Mean*	*SD*	*Mean*	*SD*	*Mean*	*SD*	*Mean*	*SD*
FDS2	-9.3^{a}	5.9	3.5^{b}	7.3	12.4^{b}	6.6	-12.0^{ab}	5.9	-8.5^{b}	3.3	-2.8^{a}	3.7
FDS3	-11.4^{a}	3.9	2.9^{b}	3.8	9.8^{b}	5.8	-8.6^{ab}	4.8	-5.1^{b}	2.6	1.8^{a}	5.7
FDS4	-19.8^{a}	5.5	-3.8^{b}	4.5	5.3^{b}	4.2	0.2^{a}	4.4	1.4^{a}	2.7	11.0^{b}	5.3
FDP2	-13.3^{a}	4.0	-0.9^{b}	5.9	10.3^{c}	6.0	-15.3^{a}	7.9	-12.6^{a}	5.0	-3.8^{a}	7.2
FDP3	-17.7^{a}	3.9	-1.3^{b}	4.4	9.8^{b}	7.9	-4.9^{a}	3.9	-5.2^{a}	3.3	4.0^{b}	5.4
FDP4	-21.4^{a}	5.9	-6.0^{b}	5.0	3.3^{b}	5.4	1.6^{a}	6.0	1.6^{a}	4.9	11.2^{b}	4.8
FDP5	-19.4^{a}	9.4	-2.6^{a}	4.4	3.8^{a}	3.4	9.0^{a}	8.6	10.3^{ab}	5.8	17.0^{b}	9.5

6.1.3.2 Sagittal Tendon Angles

Sagittal angle displacements refer to the angular deviations of the distal end of each tendon with respect to the proximal end, on the xy plane, as illustrated in Figure 6.5. Positive angles deviated dorsally. ANOVAs revealed an effect of wrist posture on the sagittal angle of all tendons, whereas forearm posture did not have an effect (Table 6.7). The average sagittal angles of all tendons across forearm postures, within each wrist posture, showed larger palmar deviations in flexion (-16° $\pm$ 5.5°) than in neutral (-1.2° $\pm$ 5.0°) as well as dorsal deviations with extension (7.8° $\pm$5.6°) (Table 6.6, Figure 6.6). Post-hoc analyses showed that the FDP5 was not affected by wrist posture, although significant angle differences for the other tendons were found between wrist flexion and neutral (14.6° average angular difference) and between flexion and extension (24° average angular difference) (Table 6.6, 6.7). However, angle changes between extended and neutral were only statistically different for the FDP2 tendons (11.3°) (Table 6.7). Pairwise comparisons are available in Appendix N.

Although the FDP5 displacement did not reach significance after the Bonferroni-corrected multiple comparisons test, it exhibited a pattern similar to other tendons. Average angular deviations of the FDP5 across participants showed larger palmar angles in flexion (-19.41° $\pm$ 9.37°) when compared to neutral (-2.61° $\pm$ 4.41°), and dorsal angles in extension (3.76° $\pm$ 3.44°). Average displacements across all tendons are shown in Table 6.8.

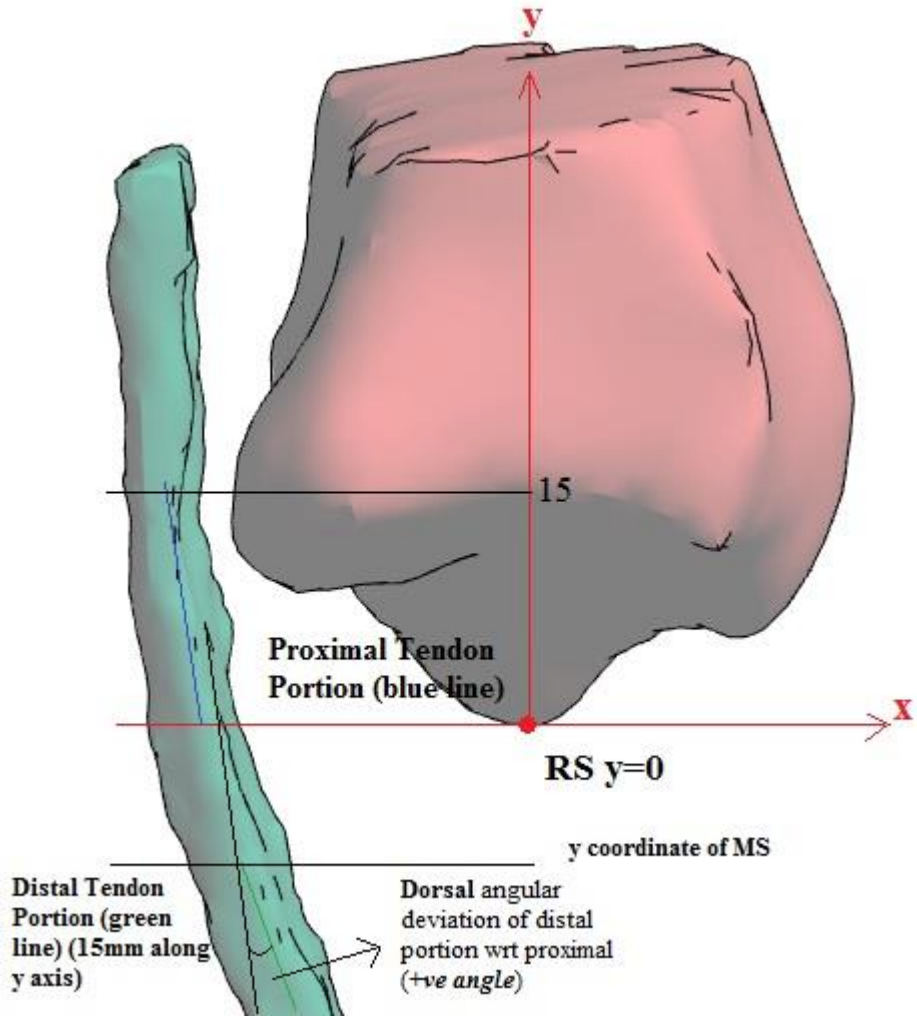

Figure 6.5. Illustration of whole tendon sagittal angles, corresponding to the angular deviation of the distal portion (green line) of each tendon with respect to their proximal portion (blue line), in the xy plane. Positive angles in the sagittal plane were deviated dorsally.

Table 6.7. Results summary of the effect of forearm and wrist posture, on angular deviations of distal tendon portions with respect to their proximal end, in the sagittal plane. P values are shown for Bonferroni-adjusted pairwise comparisons unless denoted by the superscript c.

Sagittal Angle between Tendons' Proximal and Distal Portions								
	Wrist				Forearm			
	F	dof	p[a]	Post Hoc Comparisons	F	dof	p[a]	Post Hoc Comparisons
FDS2	55.444	(2,6)	0.010* 0.011* 0.061	*ext vs flx* *neut vs flx* *ext vs neut*	1.286	(2,6)	0.343	*ns*
FDS3	48.424	(1.021,3.064)	0.018* 0.003* 0.121	*ext vs flx* *neut vs flx* *ext vs neut*	0.198	(2,6)	0.826	*ns*
FDS4	50.623	(2,6)	0.014* 0.002* 0.126	*ext vs flx* *neut vs flx* *ext vs neut*	2.086	(2,6)	0.205[c]	*ns*
FDP2	75.681	(2,6)	0.005* 0.018* 0.025*	*ext vs flx* *neut vs flx* *ext vs neut*	1.604	(2,6)	0.277	*ns*
FDP3	30.468	(2,6)	0.031* 0.004* 0.161	*ext vs flx* *neut vs flx* *ext vs neut*	0.774	(2,6)	0.502[c]	*ns*
FDP4	31.086	(2,6)	0.031* 0.006* 0.171	*ext vs flx* *neut vs flx* *ext vs neut*	1.424	(2,6)	0.312	*ns*
FDP5	17.739	(2,6)	0.055 0.088 0.235	*ext vs flx* *neut vs flx* *ext vs neut*	3.849	(2,6)	0.084[c]	*ns*

[a]Bonferroni corrected p value, unless specified with the d superscript

[b]Sphericity violated, Greenhouse-Geisser Corrected

[c]ANOVA priori tests p value

*Denotes significance

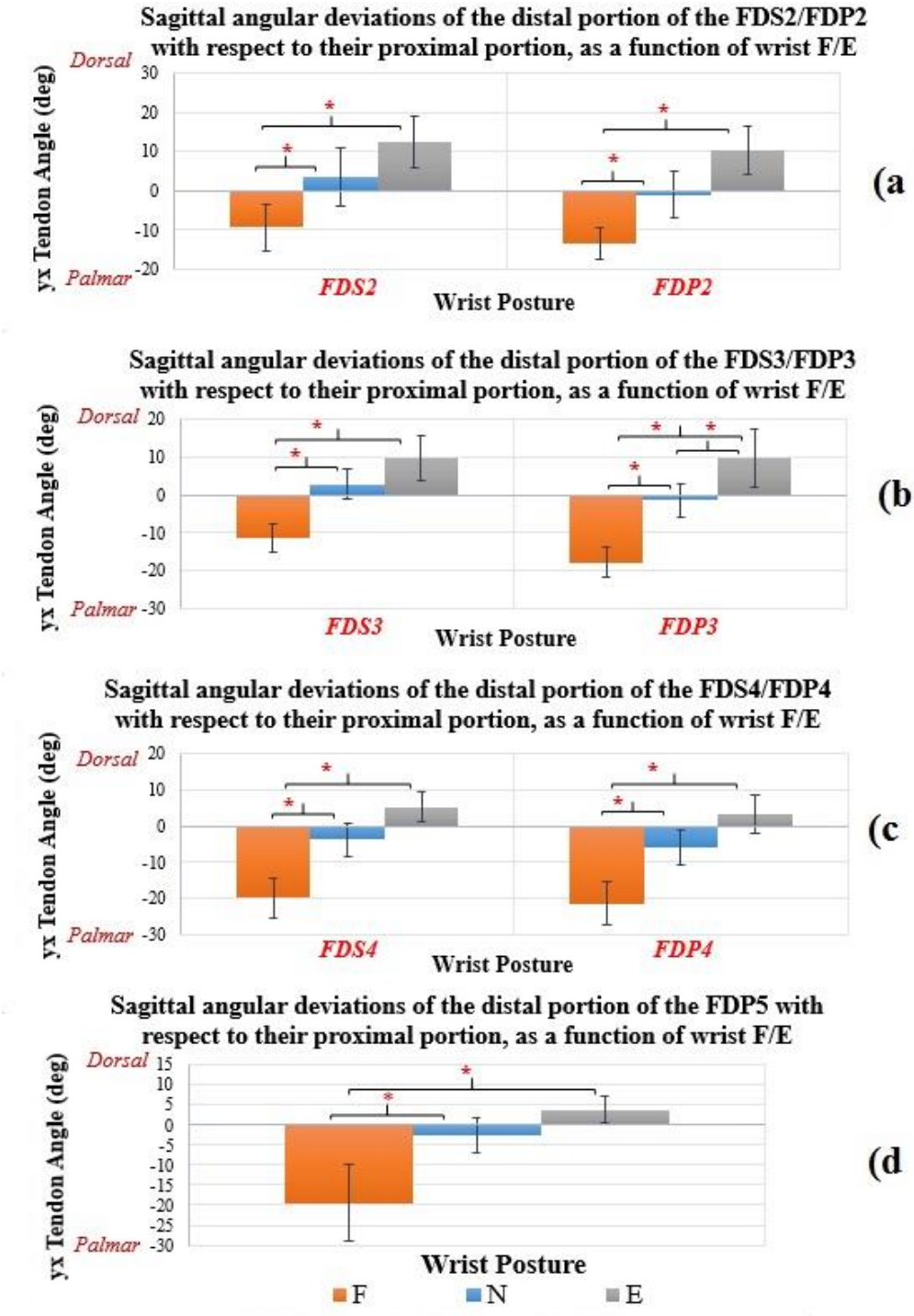

Figure 6.6. Significant effects of wrist posture on sagittal angular deviations of the distal tendon portions with respect to their proximal portions, of all FDS and FDP tendons of the 2nd (a), 3rd (b), 4th (c), and 5th (d) digits. Asterisk denotes significance at $p<0.05$ Bonferroni corrected for multiple comparisons. Error bars represent SD.

Table 6.8. Average frontal and sagittal tendon displacements at the level of the MS (top), and angular sweep (bottom), of all FDS and FDP tendons.

Average Linear Tendon Displacements at the Level of the MS			
ALL TENDONS OF DIGITS 2-5			
		A-P Displacements (mm)	**M-L Displacements (mm)**
Forearm	*Pro-Neutral*		0.3
	Sup-Neutral		1.4
	Pro-Sup		1.1
Wrist	*Ext-Neutral*	2.3	
	Flx-Neutral	5.2	
	Ext-Flx	7.5	
Average Angular Tendon Displacements at the Level of the MS			
Forearm	*Pro-Neutral*		1.7
	Sup-Neutral		8.1
	Pro-Sup		9.8
Wrist	*Ext-Neutral*	9.0	
	Flx-Neutral	10.2	
	Ext-Flx	19.2	

Figures 6.7 and 6.8 are a representation of the tendon trajectories, across participants, as they pass through the wrist in the frontal and sagittal planes. Frontal angles are shown in three forearm postures, and sagittal angles are shown in three wrist postures.

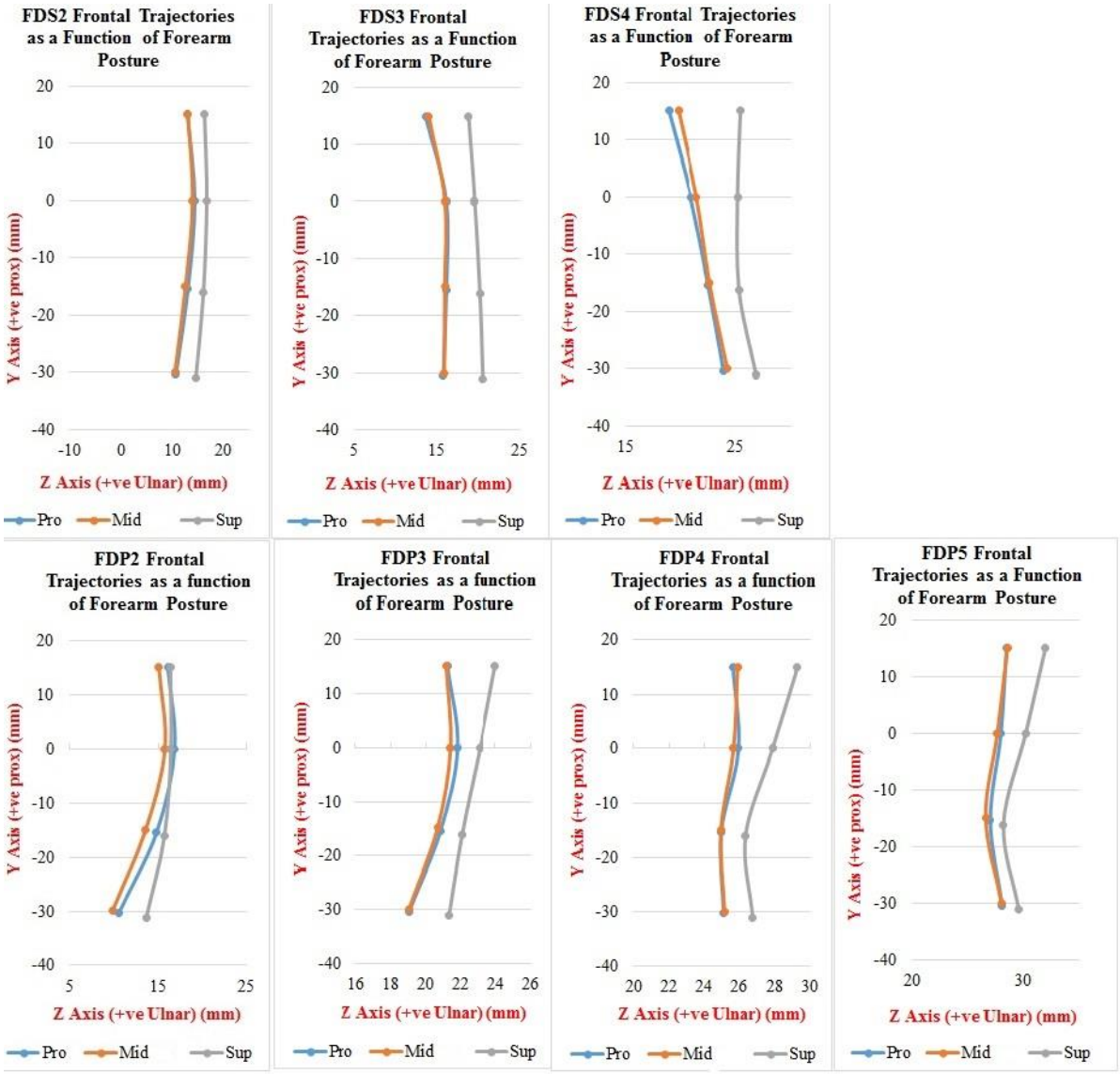

Figure 6.7. Plots of individual whole FDS and FDP tendon frontal trajectories, based on average locations of the start and end points of the proximal and distal portions, across wrist postures.

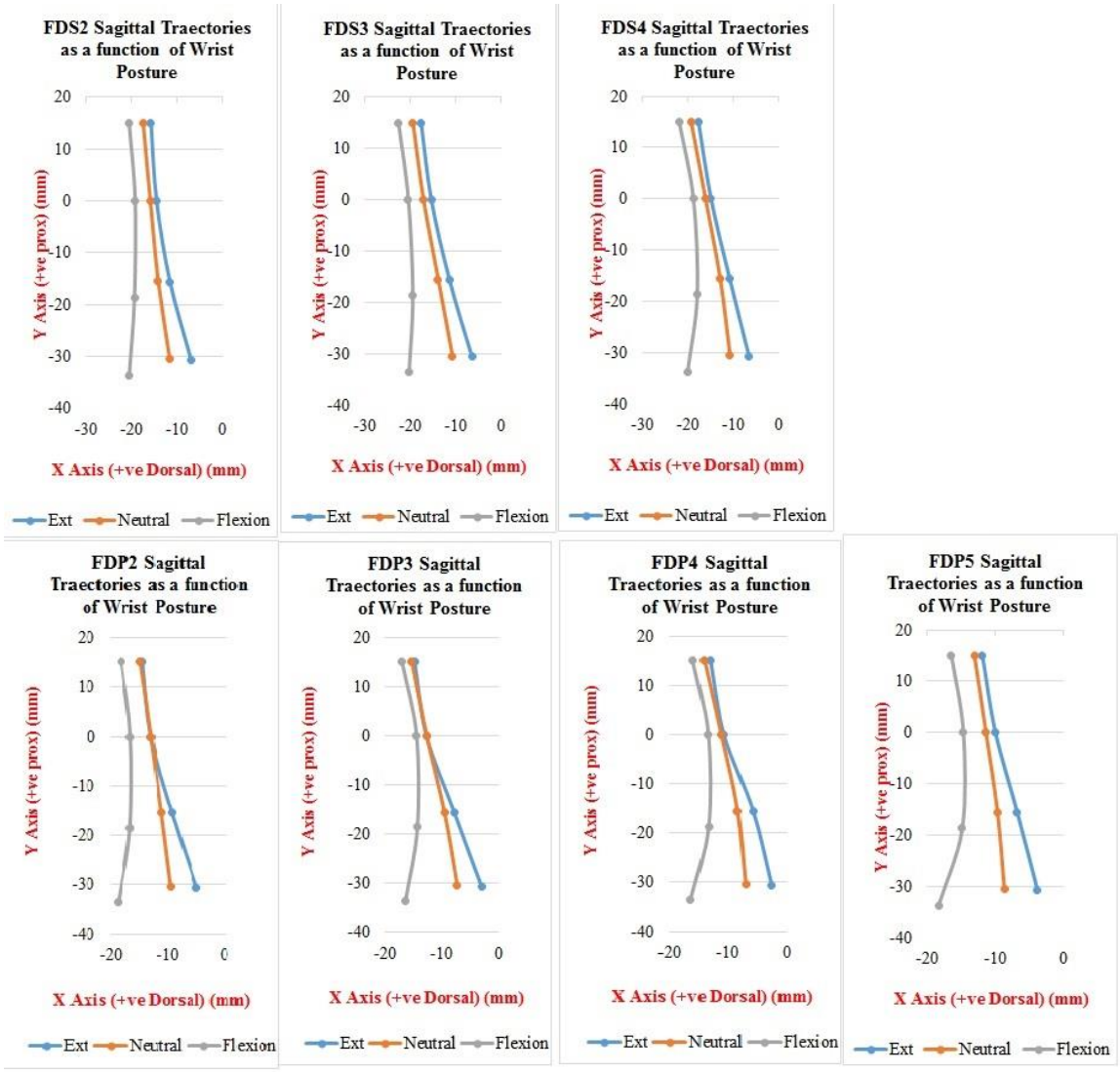

Figure 6.8. Plots of individual whole tendon sagittal trajectories, based on average locations of the start and end points of the proximal and distal tendon portions, across wrist postures, for individual FDS and FDP tendons.

6.2 Discussion

This study evaluated the effect of forearm pronation/supination and wrist flexion/extension postures on tendon displacements distal to the CT and on tendon angles as they entered and exited the tunnel. Understanding and quantifying tendon displacement is important, because changes in the anatomical relationships of tissues can modify the contact forces among structures, and these contact forces could lead to tissue damage and injury. When modelling tendons as a pulley/belt system, tendon angular displacement from neutral means that adjacent structures may be loaded (i.e. increased contact force) in the presence of axial tendon tension. The novelty of this study is that, for the first time, the contribution of forearm pronation/supination to tendon movement at the wrist was taken into consideration, and its potential effect on MSK loading was explored. Although previous research has evaluated the effects of wrist flexion/extension on MSK loading, the loads may not have been appropriately estimated because the effect of forearm posture was not considered. In fact, forearm movement is essential for hand activities, and potentially intensifies the loading elicited by wrist postures. Because it includes the effects of forearm pronation/supination on MSK loading, this study is a step towards developing internal exposure measures from external exposures, in order to estimate the risk of developing upper limb injury associated with particular work tasks. In the following sections, a discussion of the changes in tendon locations and angles, as a function of posture, will be presented, and the implications of these changes will be addressed.

6.2.1 Frontal Displacements

All FDP and FDS tendons showed small displacements in the frontal plane, with significant ulnar displacements exhibited only by the FDS3 tendons when supination was compared to mid-

pronation. Although the FDS2 tendons were not significantly affected by forearm posture, frontal locations between mid-pronation and supination, and between supination and pronation approached significance. A similar pattern was observed in the FDS2/3 tendons—and to a lesser extent in all other tendons, as they were located more ulnarly in supination when compared to pronation and mid-pronation. Frontal locations were essentially the same for mid-pronation and pronation, with an average displacement of 0.03 mm of all tendons. Even small ulnar displacements with supination have the potential to increase contact of tendons against surrounding structures ulnarly at the distal CT. It is possible that differences in the magnitude of frontal displacements in each direction were linked to differences in the ROM achieved in either direction; participants supinated their forearm approximately 52°, and pronated 20°. Furthermore, the lack of frontal displacement between mid-pronation and pronation may be an indication of radial constraints when the forearm is pronated. These constraints in turn may indicate radial compression of the median nerve and synovial tissue. However, the FDS2/3 displacements observed may be of particular clinical relevance, because these tendons may come into direct contact with the median nerve.

At both the MS and RS, the FDS tendons displaced more than the FDP tendons. However, the average amount of frontal movement observed distal to the CT, across all FDS and FDP tendons, was considerably smaller than that seen at the RS (1.1 mm vs 2.5 mm respectively). The reduced frontal movement at the MS compared to the RS could be a reflection of constraining effects medio-laterally, due to the smaller cross-section of the distal tunnel compared to the proximal end (Bower, et al.; Keir, 2006); recall that the MS is just distal to the tunnel. Both the smaller cross-section and the rigid adjacent carpal walls may contribute to medio-lateral motion constraints, which can affect medio-lateral contact forces within the tunnel.

In forearm-deviated postures, tendons may be pressed against adjacent structures; the addition of tendon excursions elicited by repetitive finger and/or wrist flexion/extension may lead to frictional work between the tendons and the surrounding structures, contributing to histological changes and subsequent pathologies. Similarly, medio-lateral frictional work can also be elicited by combining sustained wrist flexion/extension with repetitive forearm pronation/supination (such as when using a wrench on a horizontal surface).

6.2.2 Sagittal Displacements

Recall that all tendons were located more volarly in flexion compared to both neutral and extension, and that displacements between neutral and extension were not significantly different. Because sagittal displacements represented movement with respect to the radial CS, a follow-up analysis was performed to obtain a better estimate of tendon sagittal displacements at the level of the MS: for each tendon, the x coordinate of the MS location was subtracted from the x coordinate of the antero-posterior location. The results revealed average displacements within the hand of 4.6 mm between flexion and extension (3.4 mm of which occurred between flexion and neutral, and 1.3 mm between neutral and extension). Although these findings provide a better representation of sagittal displacements at the hand, displacements were measured along the radial antero-posterior axis—thus were not actually perpendicular to the metacarpal. However, the results were similar to findings by Keir and Wells (1999) (5 mm), particularly when taking into account two differences: the current study evaluated a smaller range of motion during scan acquisition than theirs did (24.9° vs 57°), and the two studies measured displacement differently.

The current study, as well as others (Keir & Wells, 1999; Chapter 5, this thesis), has found volar flexor displacements with increased flexion (for tendon locations proximal, within, and

distal to the CT), which may increase volar contact forces between tendons and anterior surroundings. In addition, gradual deformation of the median nerve with increased wrist flexion has been observed (Zeiss, et al., 1989). It is possible that median nerve deformation could be influenced by tendon movement, potentially demonstrating a mechanism of injury for CTS. However, the current study did not evaluate either nerve deformation or the location of the flexor retinaculum with respect to tendons.

In addition, anterior displacements at both the tunnel's proximal and distal ends may suggest that somewhere within the tunnel there is a point of high volar contact, given that the tendons may be contained volarly by the flexor retinaculum—a concept supported by Armstrong et al. (1984), who identified greater vascular, synovial, and nerve damage near the wrist crease, which approximately corresponds to the mid-carpal joints in the tunnel.

Furthermore, volar contact forces with wrist flexion (or dorsal contact forces with wrist extension), in combination with other movements, may increase frictional work (for tendons moving medio-laterally when combined with forearm pronation/supination, and axially when combined with finger movements), between tendons and anterior or posterior tissues. Frictional work in turn may lead to histological changes in tissues, potentially leading to conditions such as tendonitis, tenosynovitis, and tendinosis.

The effect of forearm pronation/supination on the sagittal motion of the FDS2 tendons consisted of a small dorsal movement (1.9 mm) from pronation to supination. The FDS2 is the only muscle bundle originating on the anterior mid-radius, thus it is possible that the dorsal displacements occurred due to increased tendon tension as the forearm moved into supination. Due to the magnitude and direction of the displacement, it may not have clinical relevance;

although it will probably increase contact force against the trochlear surface of the carpals, this surface has a large radius of curvature—so it is an unlikely source of injurious MSK loading.

6.2.3 Frontal Angular Deviations

Almost all tendons were affected by forearm posture, and some were affected by wrist posture as well. The magnitude and direction of the angular deviation of each tendon in each forearm posture varied according to the tendons' locations in the medio-lateral direction (Figure 6.7). Tendons angles are generally more radially curved in pronation, and shifted ulnarly with supination. The most radial tendons (of digits second and third) showed large radial angular deviations in pronation, and became straighter in supination, whereas the more ulnar tendons (of fourth and fifth digits) exhibited large ulnar deviations in supination, but these angles reduced as the forearm moved into pronation. The tendons of the fourth digit were nearly straight in supination, whereas the FDP5 remained at an ulnar angle. These findings suggest that supinated postures are favourable for tendons of the second and third digits, but not for tendons of the fourth and fifth digits, and pronation may be favourable for tendons of the fourth and fifth digits, but not to those of the second and third digits.

In pronated postures, increased radial angles of the tendons of the second and third digits may increase the contact forces against the radial carpals wall and other more radial structures. The forces may be further increased when the tendons are under tension. Given the close proximity of the FDS2/3 to the median nerve (Zeiss et al., 1989), the radial contact force they elicit may compress the median nerve radially; the compression may be further increased if combined with volar contact forces from wrist flexion, both of which can potentially increase the risk of developing CTS.

Activities requiring repetitive finger movements of the middle and index fingers would cause their tendons to glide axially during normal tendon excursion. Frictional work on the radial side may occur when these movements are combined with radial contact forces elicited by radial angles of these same tendons, perhaps increasing the risk of tissue damage radially.

Sustained pronation, which occurs in activities such as flute playing (top hand) may require, finger exertions, and wrist flexion. In these activities, the median nerve may face tendon contact from anterior tendon displacement caused by wrist flexion, and radial contact from radial angular shifts in pronation—along with frictional work due the combination of (volar and radial) normal forces and movement (e.g., finger tendon excursions during finger actions). Thus, such activities may result in a high risk of developing CTS, due to the additive effects of these tendon movements.

Supinated postures, on the other hand, may increase MSK loading at the ulnar end, particularly on the tendons of the fourth and fifth digits. Sustained supination with repetitive movement of these digits, (seen in violinists or guitar players, for example), increases the MSK loading at the ulnar side of the tunnel. The combined effects of ulnar contact forces, possible volar contact if wrist flexion is present, and tendon excursions due to repetitive finger movements may lead to increased frictional work at the ulnar/volar aspect of the common tendon sheath, posing a risk of developing tendonitis and tenosynovitis in that area.

Additionally, the loading of tendons with greater angular deviations in the frontal plane from forearm deviated postures may pose a risk of muscle overexertion. For example, a sustained pinch grip, with the second and third digits in pronation, may require increased activity of ulnar deviators to maintain wrist posture due to the added radial deviation torque potential elicited by the change in the moment arm of those tendons at the wrist in pronation.

The angular sweep of all tendons ranged from 8.0-11.5°, with the tendons of the second and fourth digits showing a larger relative angular sweep than the other tendons of the same muscle (FDS or FDP). Recall that medio-lateral tendon linear displacements at the MS were only significant for the FDS3, and nearly so for FDS2. Although linear displacements were small, the medio-lateral angular sweep of most tendons suggests that somewhere along the tendons, further away from the CT, larger medio-lateral movement may have occurred between forearm postures (Figure 6.9). This tendon movement could lead to an increase in medio-lateral frictional work within the tunnel with repetitive pronation/supination.

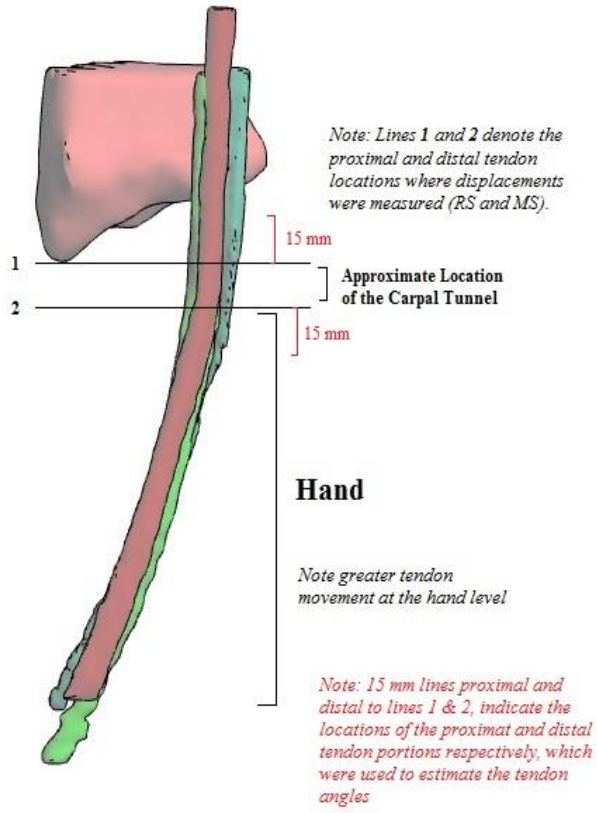

Figure 6.9. Anterior view of a radius and a tendon, in three forearm postures: pro (pink), mid (green), and sup (blue), indicating with the two horizontal lines the levels of proximal and distal displacement measurements. Proximal and distal angles were measured proximally and distally to the RS and MS respectively. It can be observed that most movement occurs outside of the carpal tunnel.

6.2.4 Sagittal Angular Deviations

The sagittal angles of all tendons deviated volarly with wrist flexion, and dorsally (to a lesser extent) with extension, as illustrated in Figure 6.8. Angular changes were more pronounced between neutral and flexion, than between neutral and extension.

Most tendons tended to deviate more palmarly in all postures compared to their respective joint angles, as illustrated in Figure 6.10. In wrist flexion, distal tendon deviation angles with respect to their proximal portion ranged from 86.1-116.9% of joint angle. The only tendons unable to reach 100% of the joint angle were the FDS2, FDS3, and the FDP2 (falling short by 1.6°, 0.03°, and 2.0°, respectively). In extension, tendon angles were 60.6-107% of the joint angles, with only the FDP2, and FDP3 slightly exceeding their respective joint angle by 0.7° and 0.6° respectively (Figure 6.10). Conversely, Keir and Wells reported that FDS and FDP tendons of the second and third digits achieved anywhere between 50-65% of joint angle in both flexion and extension. Their observed tendon deviations with respect to joint angle were somewhat smaller (more dorsal) than in the current study for the tendons of those two digits. Although both studies estimated tendon angles using two straight lines on either side of the CT, it appears that in their study the joint angles were been manually measured from scans; however, they did not explicitly report what method they used. Differences in posture angle calculation methodology could have contributed to the discrepancies in the findings. Furthermore, it is possible that the greater range of motion achieved in their study (24.9° vs 57° in the current study) had an effect on those differences.

The larger palmar angles of most finger flexor tendons, when compared to joint angles, may have occurred for two reasons. One explanation is that the tendon at the proximal end is coming from a volar location in the forearm, and becoming more dorsal as it enters the CT, further

increasing the volar angle of the tendon trajectories. Second, it is possible that tendons may be raised by volar, deep, musculature (such as the transverse and oblique heads of the adductor pollicis and lumbrical muscles) at the level of the MS. Note that the lumbricals may have affected only the FDS tendon angles, and not the FDP—because these muscles are deep to the FDS tendons and lie at the same depth as the FDP tendons. The bulky palmar musculature could have contributed to increased tendon angular deviations at the distal end. Furthermore, larger palmar deviations in more ulnar tendons could have been due to the increased metacarpal mobility of the most ulnar digits as they held the hand grip dynamometer during the scans. This observed palmar tendon angle bias with respect to joint angle may be advantageous in extension, but it is detrimental in flexion; it would decrease the tendon's angular deviation in extension, but increase it in flexion.

The main effect of volar tendon angular shifts with wrist flexion on MSK loading appears to be the increased volar contact forces of tendons against the sub-synovial tissue and more anterior structures. This finding further supports a possibility previously discussed in the sagittal displacement section: that a point of high antero-posterior contact force may exist somewhere within the tunnel in flexion, since the tendons appear to be contained volarly by the flexor retinaculum—creating a pulley system. Activities requiring sustained flexion, in combination with repetitive forearm pronation/supination and/or finger movement, could increase the frictional work done by tendons against nearby structures, and potentially lead to tissue damage.

Finally, increased palmar angular deviations represent an increased moment arm of the finger flexors, producing a flexor torque at the wrist. The main purpose of the finger flexors is to produce flexion at the metacarpophalangeal and proximal interphalangeal joints, with wrist flexion being a by-product of the FDS and FDP action; they both have to cross the wrist to reach

their respective digits. Because wrist flexion is produced by the activity of the finger flexors, a counteracting force is required by the extensors to maintain wrist posture during manual activities. Thus, increased palmar angles in wrist flexion, which result in an increased moment arm for wrist flexor torque, may in turn increase the exertional demand of the extensor side. This increased demand could increase the risk of muscle fatigue during prolonged activities, potentially increasing the risk of developing epicondylitis and extensor muscle pain.

Note: In most tendons, $T\theta > P\theta$ **in Flexion** *and* $T\theta < P\theta$ **in Extension**

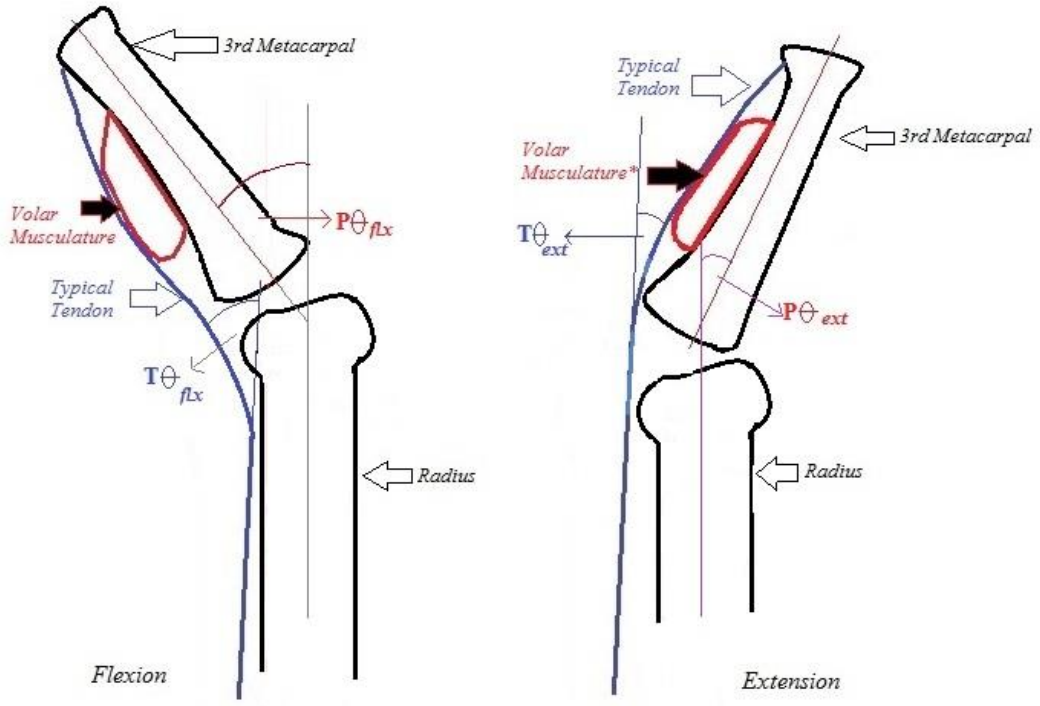

		Tendon-Posture Angle Proportion						
		FDS2	*FDS3*	*FDS4*	*FDP2*	*FDP3*	*FDP4*	*FDP5*
Flexion	***%***	88.7	99.7	111.4	86.1	114.4	107.5	116.9
	deg	*-12.7*	*-14.3*	*-16.0*	*-12.4*	*-16.4*	*-15.5*	*-16.8*
Extension	***%***	85.5	65.7	86.2	107.1	105.6	87.8	60.6
	deg	*12.4*	*9.8*	*5.3*	*10.3*	*9.8*	*3.3*	*3.8*

Posture	*Flexion*	-14.4
	Neutral	0.0
	Extension	10.5

Figure 6.10. Average ratios of tendon-joint angular deviations from neutral across participants, for individual tendons. Most tendons deviated more palmarly than their respective joint angle, except FDS2/3, FDP2 **in flexion**, and FDP2/3 **in extension**. Tendon palmar orientation proximal to the CT and musculature under the FDS may contribute to this tendon palmar shift. Average wrist postures are given below the table.

6.3 Limitations

This study shares some limitations with Study II: Proximal Results and Discussion (Chapter 5). First, some participants were unable to maintain full force towards the end of the scan. It is unclear if this induced noise in the scans, and whether it could have affected tendon trajectories. Additionally, the registration process reduced within-subject variability, by essentially maintaining the same CS for each bone across conditions for each participant. However, between-subject variability should be acknowledged; it may be responsible for the increased variability of the CS orientation with respect to the bone (and thus on the magnitude of posture and tendon measurements). Finally, it is unclear if scanning the forearm off axis (with respect to the long axis of the scanner) could have had affected the forearm centroid calculations, since the centroids were calculated as the centers of fitted circles through proximal and distal forearm surfaces, which were perpendicular to the scanner's long axis—not necessarily to the forearm.

The following limitations pertain only to findings of the distal end. First, tendons were represented by two lines, measured outside the tunnel. There was no information about tendon trajectories within the tunnel, or about instantaneous curvatures along the tendon. Because of this, the identification of sites with smaller radius, hence higher contact forces, were not identified. Tracking of the flexor retinaculum was difficult, thus the current study was unable to uncover the nature of the relationship between the tendons and the flexor retinaculum.

Second, movement of the fifth metacarpal (and maybe the fourth) could have occurred when accommodating to reach the handgrip dynamometer during image acquisition. Although participants were instructed to maintain a straight hand, sagittal metacarpal movement was not controlled, thus some metacarpal movement could have occurred while pushing the dynamometer, potentially affecting the trajectories of those tendons.

Recall that tendon displacements were measured with respect to the radial CS. Frontal displacements in the radial CS were assumed to represent frontal plane movement at the level of the MS. Although radial/ulnar movement was minimal, it was not taken into account for frontal displacement measurements. Although the antero-posterior tendon displacements were adjusted to better estimate sagittal tendon movement with respect to the metacarpal, displacements remained expressed with respect to the radial CS, thus displacement measurements did not represent movement perpendicular to the metacarpal. Information about the sagittal angular changes provided a better understanding of the implications of tendon kinematics on MSK loading at the wrist.

Lastly, recall that wrist flexion/extension posture had an effect on frontal tendon angles. This movement does not appear to have anatomical relevance, because tendons moved in the same direction with flexion and extension. This finding could be the result of planar perception on the yz plane, an effect which we were unable to control, rather than actual rotation of the tendon about the antero-posterior axis.

6.4 Conclusions and Future Directions

This study shed light on the combined effects of forearm pronation/supination and wrist flexion/extension postures on frontal and sagittal flexor tendon movement, which may affect MSK loading within the CT. Its unique contribution lies in taking into account the effect of forearm posture on anatomical changes within the CT, and the forearm posture effect on MSK loading. Although forearm pronation/supination often accompanies manual activities, and has been previously linked to injury, its role in injury development had not been investigated. The current study quantified the effect of forearm pronation/supination and wrist flexion/extension postures on tendon locations at the level of the MS, and on tendon orientations within the tunnel. The implications of these changes on contact forces, frictional work, and exertional demands were discussed.

In summary, there were no interactions of forearm and wrist posture on tendon movement. Rotation only affected frontal plane displacements and angular changes, whereas wrist flexion/extension only affected antero-posterior displacements and angular changes. Tendon frontal angles shifted ulnarly with supination, and radially with pronation. Small tendon ulnar displacements with supination from pronation and mid-pronation were observed, whereas radial displacements with pronation from mid-pronation was negligible. The magnitude of the angular deviations of each tendon varied per digit. Pronation caused greater angular deviations of the second and third digit tendons radially, while only small deviations of the tendons of the fourth and fifth digits were seen. Supination caused the opposite effect, with greater ulnar angles of the fourth and fifth digit tendons, and smaller angular deviations of the second and third digit tendons. Wrist flexion elicited volar tendon displacements and angles, whereas extension elicited smaller dorsal displacements and angular deviations.

Future directions include investigating tendon trajectories within the tunnel and instantaneous curvatures, in order to identify tighter bends along tendons. Additionally, an evaluation of the relationship of tendons to nearby structures in the tunnel, including the flexor retinaculum and median nerve, may be necessary to better understand the loading effects of tendons on such structures. Lastly, given that tendons did not displace much medio-laterally, particularly between pronation and mid-pronation, it would be interesting to evaluate the proximity of the carpal walls with respect to the tunnel, and determine whether the internal geometry of the tunnel changes with forearm posture.

In conclusion, radial angular shifts of tendons of the second and third digits and small radial tendon displacements were seen with pronation. Thus, activities requiring sustained pronation may add radial contact force and radial compression to the median nerve; these changes may be aggravated by volar contact, in sustained flexion. Furthermore, ulnar angular deviations of tendons of the fourth and fifth digits were observed with supination. Thus, activities requiring sustained supination may increase loading of tissues on the ulnar side. In both forearm deviated postures, because of the increased lateral contact force, repetitive tendon excursions caused by finger and/or wrist movement may elicit frictional work of tendons on adjacent structures (i.e., on the median nerve radially, and on the synovium on both the radial and the ulnar sides). Activities requiring repetitive forearm pronation/supination, on the other hand, when combined with increased anterior or dorsal contact (with flexion or extension, respectively) may lead to medio-lateral frictional work at the site of contact, which could lead to histological changes and subsequent pathologies (e.g., tendonitis, tenosynovitis). Lastly, changes in the direction of the torque potential induced by tendon angular deviations of the second and third digits in pronation,

and of the fourth and fifth digits in supination, may increase antagonist muscular demand (ulnar and radial deviators, respectively) to maintain wrist posture.

7 CHAPTER 7. STUDY IV

Frontal tendon angle estimates during a task involving repetitive forearm pronation/supination

7.1 Introduction

Earlier studies from this dissertation were able to: a) provide insight into the potential for Xsens IMUs to provide forearm pronation/supination measurements in the workplace, and b) quantify the amount of tendon movement associated with postural change at the forearm and wrist. Now that the effect of forearm rotation on finger flexor tendon trajectories has been measured, tendon trajectories during continuous manual activities may be predicted from forearm rotation measurements. Since the angle at which a tendon wraps around a joint affects the force of the tendon exerted on a trochlear surface, tendon trajectories can provide valuable information to estimate MSK loading associated with different activities (Armstrong & Chaffin, 1979). Thus a main contribution of this research lies in its potential for improving the modeling of MSK loading at the wrist during continuous manual activities.

Models that involve the finger flexor tendons often consider the tendon-joint relationship analogous to a belt-pulley system (Armstrong & Chaffin, 1978; 1979). For example, Armstrong and Chaffin (1979) developed a model to estimate the normal force (F_R) that a tendon exerts over the entire contact area of a trochlear surface as a function of the tendon force (F_T) and the angle at which the tendon wraps the joint (θ) (Eq. 7.1). In this model, the tendon wrap angle is treated as analogous to the joint's angular deviation from straight. An adaptation of this model could allow the estimate of changes in the contact forces of tendons exerted on radial and ulnar carpal walls as a function of forearm pronation/supination posture and hand force. The model's requirement of tendon angular displacement from neutral as a function of joint angle means that

to implement a similar model as a function of pronation/supination requires a method of converting joint angle to tendon angle. A method to quantify the frontal wrap tendon angle could be derived from the observed relationship between frontal tendon angular deviation and forearm posture from study III.

$$F_R = 2F_t sin\left(\frac{\theta}{2}\right) \quad \text{(Eq. 7.1)}$$

Where: F_R is the total normal force of tendon on pulley
F_T is the tendon tension
θ is the wrist angle (in degrees from straight)

According to the results from study I, it appears that selecting the amplitude probability distribution function (APDF) levels (Jonsson, 1978) of forearm rotation measurements (e.g. 10^{th}, 50^{th}, and 90^{th} percentiles) during a continuous task may be appropriate for assessing forearm posture in the workplace. The 10th and 90th percentiles (APDF) of the continuous posture measurements can provide an approximation of the ROM associated with an activity, while the 50th percentile can provide an estimate of the mean posture during the entire task. Furthermore, as Lagree et al.'s findings (2016) showed, even when sensors were near metal the largest average error of pooled Xsens forearm posture measurements was only 3.9° (compared to the observed average RMSE error of 12.6° in study I).

Recall that forearm pronation/supination posture consistently affected the frontal plane angular trajectories of the finger flexors; angular shifts towards the radius were observed with increased forearm pronation, and shifts towards the ulna with increased supination. Also recall that the magnitude of the tendon angles and their direction of bend (i.e. radial or ulnar) depended on the tendons' respective digit; tendons of the 2^{nd} and 3^{rd} digits were deviated at greater radial

angles in forearm pronation, but were nearly straight in supination, whereas tendons of the 4th and 5th digits were deviated at greater ulnar angles in supination, but nearly straight in pronation.

Tendons of interest in the current study include the FDP2, FDS3, and FDS4, for several reasons. First, these tendons showed the largest angular sweep, with the FDP2 exhibiting the largest radial angular deviation in pronation, while the FDS4 demonstrated a large ulnar deviation in supination. These findings suggest that evaluating the frontal angles of these tendons may be important, as they may provide an estimate of the relatively large angular sweep fluctuations associated with a continuous, repetitive task. Additionally, because the FDP2 and FDS4 tendons are located near the radial and ulnar carpal walls (respectively), and because they reach large angular deviations towards the nearest carpal wall (medio-laterally), they are likely to wrap around the trochlear surface more tightly in certain postures, potentially leading to increased contact force, possibly impinging the synovial sheath. Lastly, angular deviations of the FDS3 may also be important, as they may be relevant to CTS development, because this tendon is commonly located just ulnar to the median nerve (Zeiss et al., 1998), and takes up most of the force (35%) in a power grip (Hazelton, 1975).

Thus, the goal of this study is to develop a regression model based on the observed relationship between forearm posture and frontal tendon angle of the FDP2, FDS3, and FDS4 tendons (from study III), and apply the model to continuous forearm posture measurements from Xsens, during a task requiring repetitive pronation/supination (from study I).

7.2 Methods

A simple linear regression was calculated in SPSS to predict tendon angle deviation in the frontal plane of each tendon (FDP2, FDS3, and FDS4) based on their respective forearm pronation/supination posture. MRI data from all four participants (1 female, 3 males) in chapter 4 (described in section 4.2.1), were used for the regression analyses (i.e. nine scans for each participant for a total of 36 observations per tendon).

A Matlab program was used to calculate the ROM and the APDF levels from Xsens' forearm posture measurements during all trials of the handle turning task in study I (Chapter 3), across all participants (19 male participants as described in section 3.2.1). In order to select two conditions with the largest difference in ROMs, a one-way repeated measures ANOVA was used to test the effect of trial number (each trial was numbered according to the specific combination of material, vertical and horizontal locations) (18 levels) on ROM across locations and materials. The Greenhouse-Geisser correction was used due to sphericity violation. Then, Bonferroni-corrected multiple comparisons were used to detect the largest significant difference in ROM between two trials across participants.

The APDF levels of the two trials with the largest significant difference in ROM, along with the regression equations, were used to estimate the percent time spent at and below different frontal tendon angles during a continuous task requiring repetitive forearm rotation. These trials involved forearm posture measurements from two metallic handle-turning trials (top and bottom rows within the middle column, as described in section 3.2.3), across all 19 participants in chapter 3 (section 3.2.1). A total of 38 (2 conditions x 19 participants from study I) posture measurement trials at the three APDF levels were transformed into frontal angles of each of the

three tendons. Finally, descriptive statistics were used to present the magnitude of the angular deviations of each tendon (FDP2, FDS3, and FDS4) in the two conditions with different ROMs.

7.3 Results

The ANOVA revealed that the ROM of forearm rotation among trials were different ($F(3.307, 59.533) = 2.772$, $p < 0.05$). Bonferroni-corrected multiple comparisons showed that two metallic trials had the largest significant difference in ROM (13.2°). The top middle handle elicited an average ROM of 103.9° (SD=14.2°), whereas the bottom middle handle elicited a larger ROM of 117.1° (SD=13.5°).

The simple linear regressions predicting the angles of the three tendons during the handle-turning task produced significant results ($F(1, 34) = 16.382$, $p < 0.05$), ($F(1, 34) = 31.385$, $p < 0.05$), and ($F(1, 34) = 42.609$, $p < 0.05$), with an R^2 of 0.325, 0.480, and 0.556, for the FDP2 (Figure 7.1), FDS3 (Figure 7.2), and FDS4 (Figure 7.3), respectively.

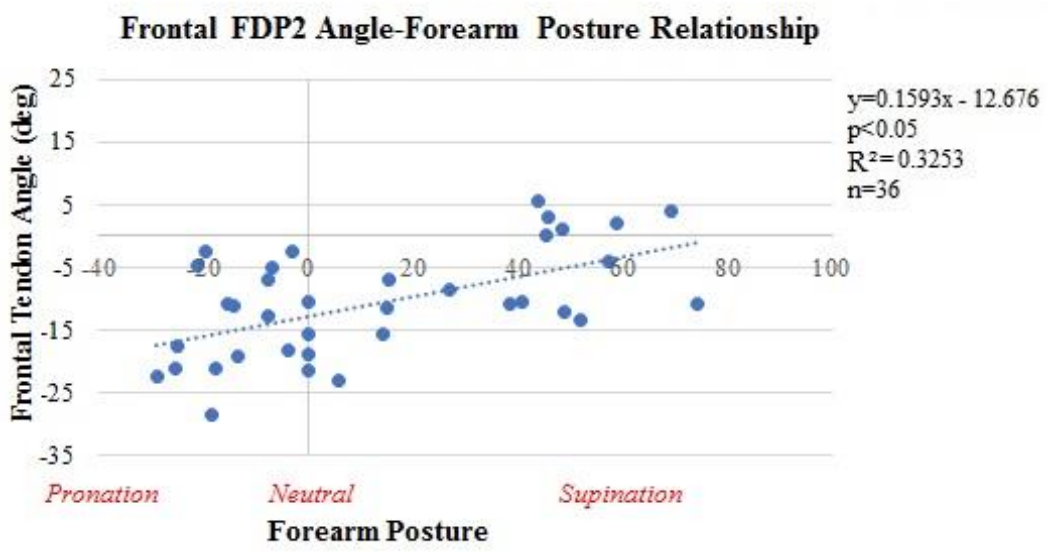

Figure 7.1. Linear model to predict frontal FDP2 tendon angle as a function of forearm pronation/supination posture.

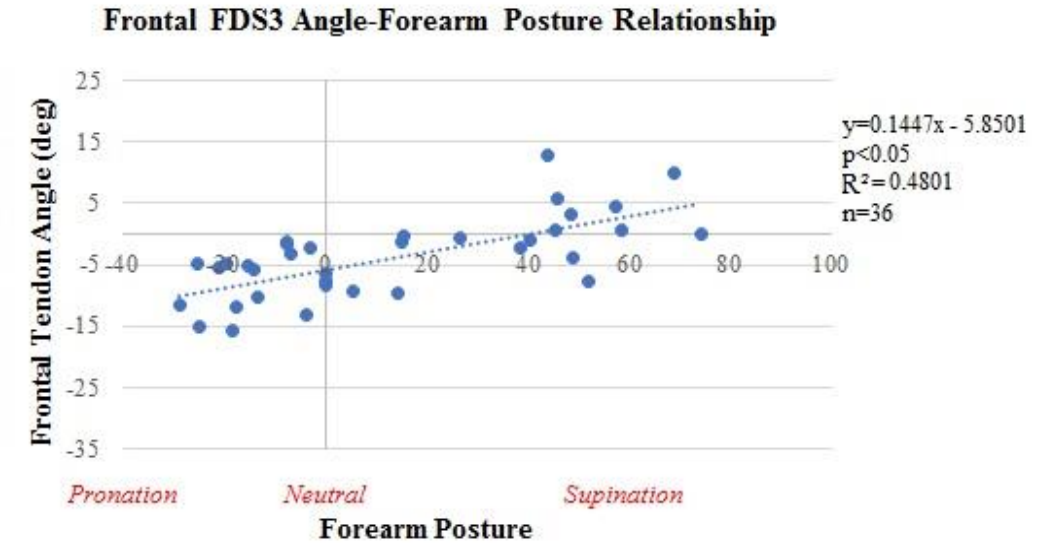

Figure 7.2. Linear model to predict frontal FDS3 tendon angle as a function of forearm pronation/supination posture.

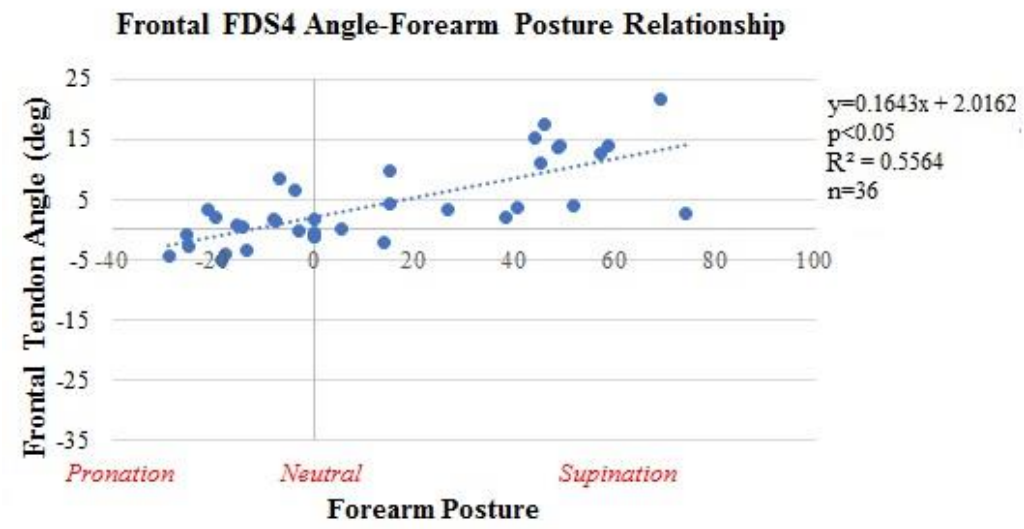

Figure 7.3. Linear model to predict frontal FDS4 tendon angle as a function of forearm pronation/supination posture.

Applying the regression models to the two trials identified above, provided frontal plane angles for each tendon. Figure 7.4 shows the results for each of the three tendons for one trial.

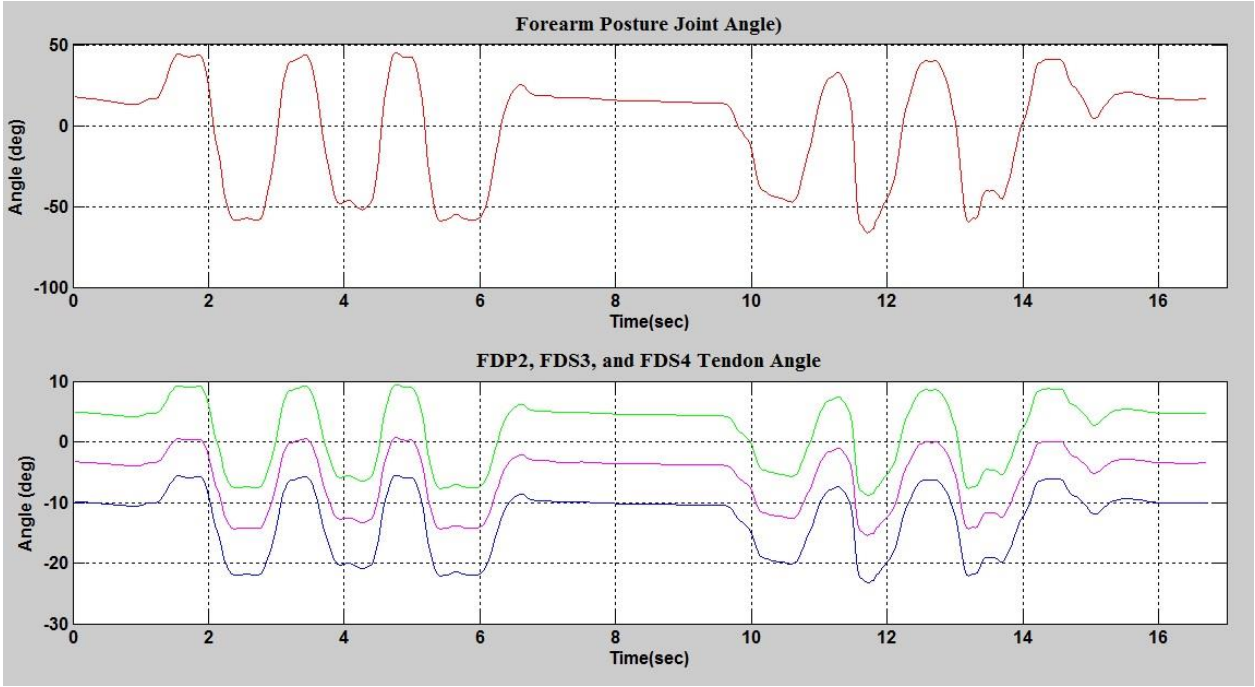

Figure 7.4. (Above) Forearm rotation angle measured with Xsens while turning a metallic handle placed at the top row, and middle column, from one participant in study I (Positive represents supination). (Below) Predicted FDP2 (blue), FDS3 (green), and FDS4 tendon.

The posture APDF levels (10th, 50th, and 90th percentiles) were estimated for both trials identified and summarized in Figure 7.5. In both conditions, participants achieved approximately 45° of pronation; the FDP2, FDS3, and FDS4, deviated radially 19.7° (SD= 1.3°), 12.2° (SD= 1.1°), and 5.3° (SD= 1.3°) respectively in the top handle, and 20.0° (SD= 1.2°), 12.5° (SD= 1.1°), and 5.5° (SD= 1.2°) in the bottom handle (Figure 7.4). The bottom handle elicited 51.6° of supination (SD= 10.6°), resulting in a small FDP2 radial deviation of 4.5° (SD = 1.7°), a nearly straight angle of the FDS3 (1.6° ulnarly, SD = 1.6°), and a pronounced ulnar angle of the FDS4 (10.5°, SD = 1.8°). A much smaller ROM in the supination direction was elicited by the top handle (36.4°, SD = 6.8°), resulting in the FDP2 slightly deviated radially (6.8°, SD= 1.3°), the

FDS3 nearly straight (0.6° radially, SD = 1.1°), and the FDS4 deviated ulnarly (8°, SD = 1.3°). The median forearm posture observed in the top handle was in slight supination (10.2°, SD = 7.8°), resulting in a radial deviation of the FDP2 (11.0°, SD = 0.8°), and to a lesser extent of the FDS3 (4.4°, SD = 0.7°), while the FDS4 had a small ulnar deviation (3.7°, SD = 0.9°). The median posture observed in bottom handle, however, was closer to neutral (2.1° of supination, SD = 9.8°), resulting in a relatively large radial angle of the FDP2 (12.2, SD = 0.8), a lesser radial deviation of the FDS3 (5.5°, SD = 0.8°), and a small ulnar deviation of the FDS4 (2.5°, SD = 1.5°) (Figure 7.5).

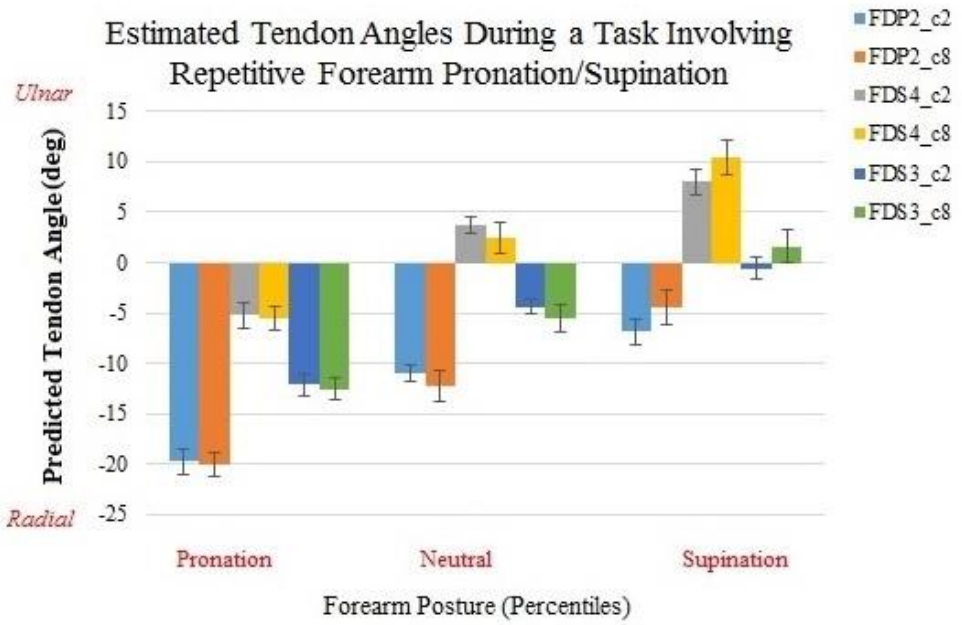

Metal Top Middle Handle				
	Joint Angle	***FDP2***	***FDS3***	***FDS4***
10th	-43.6 SD (7.4)	-19.7 SD (1.2)	-12.2 SD (1.07)	-5.2 SD (1.3)
50th	10.2 SD (5.1)	-11.0 SD (0.8)	-4.4 SD (0.7)	3.7 SD (0.9)
90th	36.4 SD (7.8)	-6.8 SD (1.3)	-0.6 SD (1.1)	8.0 SD (1.3)
Metal Bottom Middle Handle				
	Joint Angle	***FDP2***	***FDS3***	***FDS4***
10th	-46.2 SD (7.6)	-20.0 SD (1.2)	-12.5 SD (1.1)	-5.5 SD (1.2)
50th	2.1 SD (9.8)	-12.2 SD (1.5)	-5.5 SD (1.4)	2.5 SD (1.5)
90th	51.6 SD (10.9)	-4.5 SD (1.7)	1.6 SD (1.6)	10.5 SD (1.8)

Figure 7.5. Means and standard deviations of predicted frontal angles of the FDP2, FDS3, and FDS4 tendons, from estimated ROM measures (10^{th} and 90^{th} percentiles), and median posture (50^{th} percentile) calculated from Xsens measurements, during a handle turning task. C2 represents the top, middle row handle, and c8 the bottom, middle handle (Larger ROM compared to c2).

7.4 Discussion

The current study developed a model to estimate frontal angles of the FDP2, FDS3, and FDS4, from forearm posture measurements during a continuous task. Estimating frontal tendon angles as a function of forearm rotation can provide meaningful information in the quest to eventually estimate MSK loading. When modelling tendons as a pulley/belt system, tendon angular displacement from neutral (or straight) means that there must be loading on adjacent structures (i.e. increased Normal force) in the presence of axial tendon force, as illustrated in Figure 7.6. Any activities combining grasping (which involves finger flexors) with forearm postures eliciting deviations of tendons from neutral would be expected to increase MSK loading on adjacent structures—as the tendons wrap around the carpal walls in the direction of the movement.

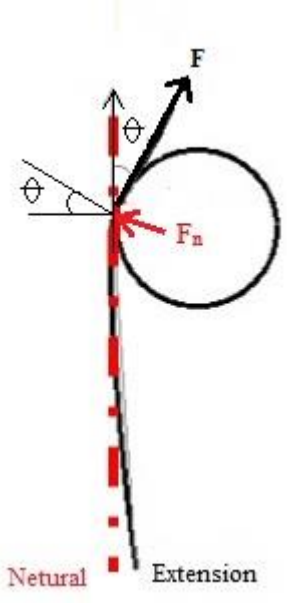

Figure 7.6. Illustration of two hypothetical tendons loaded axially: one straight (dotted line), and one deviated to the dorsal carpal wall in extension (continuous line). Note that a component of the axial force of the bent tendon results in a force exerted over the trochlear surface.

Findings revealed that forearm posture was a significant predictor of frontal tendon angle in all tendons, as forearm posture explained 33%, 48%, and 56% of the variance in frontal tendon angles of the FDP2, FDS3, and FDS4 respectively. The tendons deviated angularly similar magnitudes per degree of forearm posture: FDP2 deviated 0.164°/°, FDS3 deviated 0.159°/°, and FDS4 deviated 0.145°/° respectively. This information could be useful in evaluating frictional implications using the model by Moore et al. (1991), although it is recognized that more information (such as force in the tendon and radius of curvature within the tunnel) would be needed.

The models allowed to estimate the tendon angles that could be elicited at the ends of the ROM during a turning task. These results could be used in Armstrong and Chaffin's model (1979) to estimate the contact force of the tendon over the trochlea, if hand force was also measured. Figure 7.5 displays continuous forearm posture data along with the estimated angular deviations for each of the three tendons. It highlights how although each tendon shifts ulnarly with supination and radially with pronation, each has a predominant bias: FDS4 remains more ulnarly oriented than the other tendons, regardless of forearm posture; FDS3 shifts radially and ulnarly, while oscillating closer to zero; and the FDP2 remains predominantly shifted towards the radial side. The 10^{th} and 90^{th} percentiles of the tendon angles showed that the FDP2 had the largest deviation overall, in the radial direction in pronated postures (20°). The ulnar deviation of the FDS4 was approximately half of the FDP2's radial deviation (10.5°). These results suggest that the FDP2 is wrapping around the lateral carpal wall (trapezium and scaphoid bones), which may result in increased contact force between the FDP2 and the carpals, causing the tendon to impinge on the synovial sheath. As depicted in Eq. 7.1, according to Armstrong and Chaffin's model, an increase in angular deviation (for a given force) would result in increased contact force

(when the tendon is under tension). Additionally, because the FDS3 also showed relatively large radial deviations in pronation, and because of its close proximity to the median nerve ulnarly, pronated postures may result in radial compression of the median nerve.

The current findings involve the evaluation of a repetitive task which approximates full range of forearm rotation, as they were instructed to rotate a handle 180°. In this case, the increased normal force against the radial walls may not be as much of a concern as the sweep angle measured, given that the main source of friction may be the medio-lateral movement when the wrist is either flexed or extended and the tendons are under tension. Further information—about the wrist posture, tendon radius of curvature, hand force measurements, and coefficients of friction between the tendons and their respective sheaths—would be needed to estimate MSK loading (frictional work).

The 90th percentile posture observed in the current trials is comparable to the 42° of pronation observed in a mouse task by Quemelo et al. (2013). Based on our findings, and Armstrong and Chaffin's model, assuming a hypothetical axial force of 5 N on the FDP2 (based of Keir's findings (1995) of tendon tension of the FDP2 while the wrist was extended at 45°, with a straight index finger, a commonly adopted posture during mousing tasks) a reaction force of 1.7 N on the FDP2 would be expected. A task requiring sustained pronation appears to increase the risk of CTS, given that FDS3 would compress the nerve radially. Furthermore, if the mouse task was click-intensive, the task may result in increased frictional work, from both the tendon excursion associated with the clicking and the increased normal force against the radial carpal wall due to the sustained pronation.

7.5 Conclusions and Future Directions

The current research is one more step towards future research goals. An immediate goal is to evaluate a task using this model to estimate tendon angles in conjunction with hand force measurements, and then predict the contact force of tendons and the entire trochlear surface. Further evaluation about the radii of curvature as they pass through the tunnel (in terms of kinematic measures) is necessary to estimate frictional implications of medio-lateral tendon movement (Moore et al., 1991).

In conclusion, this study introduces a new model to estimate the frontal tendon angles of three finger flexor tendons from forearm pronation/supination measurements. It makes valid predictions over a continuous, repetitive task, allowing the estimation of angular sweep for each tendon, as well as the tendon angular deviations at the ends of the ROM in pronation and supination. These tendon angles may be used in further models to estimate MSK loading.

8 CHAPTER 8: SUMMARY

8.1 Discussion

Posture has been shown to alter the physical relationships among anatomical structures (Armstrong & Chaffin, 1979; Armstrong & Chaffin, 1978; Bower, Stanisz, & Keir, 2006; Keir & Wells, 1999; Loh, Nakashima, & Muraki, 2016; Moore, Wells, & Ranney, 1991). It is an important risk factor in the development of MSK injury, as it dictates the way force is experienced. A large part of the current evidence has centred on the effect of finger and wrist posture on loading of the distal upper limbs, disregarding loading effects associated with forearm pronation/supination.

Although forearm pronation/supination often accompanies distal upper limb functioning during manual activities and has been linked to MSK injury, it has frequently been disregarded in ergonomic evaluations. In fact, the associated mechanisms of injury have not been well understood. The current dissertation works on minimizing these gaps by addressing two goals: to identify a user-friendly methodology to measure forearm pronation/supination in the workplace, and to evaluate tendon movement, proximal and distal to the CT, as a function of wrist and forearm posture. Adding the knowledge of tendon anatomical changes within the wrist due to forearm pronation/supination to knowledge about wrist flexion/extension may facilitate a greater understanding of their combined loading effects.

The first study of this dissertation was geared towards finding an effective methodology to quantify forearm pronation/supination. Given that widely accepted motion capture systems (such as Vicon) are not feasible in the workplace, a search for a system which offered portability, measurement validity, and ease of use was necessary. The Xsens system is a type of inertial motion unit (IMU) equipped with 3D gyroscopes, 3D accelerometers, and 3D magnetometers.

Due to the presence of a magnetometer, the effect of metal on measurements needed to be studied. These IMUs offer portability and ease of use, and have been reported to demonstrate good agreement (maximum average difference of 3.9°) when comparing pooled data (10^{th}, 50^{th}, 90^{th} percentiles and number of turns) of forearm rotation measurements to Vicon measurements.

An experiment was designed to evaluate the instantaneous agreement between Xsens-Vicon forearm pronation/supination measurements during a handle turning task, with and without metal near the IMUs. It was determined that instantaneous Xsens-Vicon agreement for forearm pronation/supination measurements was lower than previously reported by Lagree et al. Although continuous posture signals were highly correlated in the current dissertation, an average RMSE error of 9° in the absence of metal, and 15° RMSE in the presence of metal were observed. Inconsistencies in the signal time-synchronization appeared to be a major contributor to such discrepancies. It should be recognized that these measurements were obtained during motions that included high velocities, large ranges of motion, and the presence of metal.

In the second part of the dissertation, changes in the tendon orientations and locations, proximal and distal to the CT, were evaluated, and changes in the tendons' trajectories at the CT were estimated by modelling tendon portions proximal and distal to the CT. In summary, wrist flexion/extension only affected antero-posterior movement, whereas forearm pronation/supination influenced medio-lateral tendon movement, proximal and distal to the CT. As proximal tendon angles in the sagittal plane were not affected by wrist posture, any sagittal wrist posture effects on whole tendon angular trajectories was mainly a consequence of the effects of wrist posture on distal angles. Frontal tendon displacements were considerably smaller than sagittal displacements, and the former were smaller at the distal end than that at the proximal end. Proximal frontal displacements were nearly triple the displacements seen at the

MS. Distal sagittal displacements, on the other hand, were smaller than those at the proximal end by nearly 1 mm.

A regression model was developed in the last study to estimate tendon angles of the FDP2, FDS3, and FDS4 from forearm posture measurements. These tendons were of particular importance because they presented the largest sweep (in study III), and also the FDP2 and FDS4 showed the largest angular bends to their respective lateral carpal wall (FDP2 – radial bend, and FDS4 – ulnar bend). Then the model was applied to forearm posture measurements of a continuous task of repetitive nature, and it allowed to determine frontal angle sweep and the more expected radial and ulnar deviations in pronation and supination of the three different tendons.

When modelling tendons as a pulley/belt system, tendon angular displacement from neutral means that there must be increased contact force on the adjacent structure (in the presence of axial tendon force). Any activities involving grasping along with forearm postures eliciting deviations of tendons from neutral may increase MSK loading on adjacent structures because deviated tendons would wrap around one of the carpal walls in the direction of the movement. Because the largest movement with wrist flexion was observed at the wrist, it appears that wrist flexion alone can elicit substantial mechanical loading. However, forearm pronation/supination can have a substantial additive effect on MSK loading when combined with wrist deviated postures. Recognizing the individual effects of each forearm and wrist posture, on MSK loading is important to understand their cumulative effect. Posture by itself can increase contact forces: flexion increases volar contact, extension increases dorsal contact (to a lesser extent), pronation increases radial contact, and supination increases ulnar contact. These increases are the result of displacements and/or tendon bends. Tension added to any bent tendon can further increase

contact forces. The addition of repetitive finger and/or wrist movement may result in frictional work caused by tendon excursions occurring in the presence of contact forces. Figure 8.2 summarizes various combinations of these loading mechanisms in sustained forearm and wrist postures, and describes specific sample activities. Although not explicitly identified in the figures, any added excursions with finger and/or wrist repetitive motions will always add frictional work, a risk factor for abrasive tissue damage.

For example, loading of the median nerve may involve several mechanisms. Certain wrist postures have been recognized as risk factors for CTS, but loading on the median nerve can be exacerbated through other mechanisms associated with the forearm. For instance, volar displacements and angular deviations in wrist flexion may be responsible for increased anterior contact forces around the median nerve and its blood supply (Figure 8.1). Thus, wrist flexed postures alone pose an increased risk for developing CTS, because compression to the median nerve is known to decrease neural conduction and has been recognized as a potential mechanism for neuropathy development (Keir & Rempel, 2005). Moreover, this effect can be aggravated by sustained pronation, which may add further direct compression to the median nerve radially (Figure 8.1, 8.2). Furthermore, the increased contact forces, volar and/or radial, may increase normal forces between tendons and the median nerve, sub-synovial connective tissue (SSCT), and their common sheath radially (Figure 8.1). Increased normal forces in turn increase the potential for frictional work during normal tendon excursions in repetitive finger movement, particularly in the second and third digits. Subsequently, frictional work on such structures may lead to abrasive damage of the tissues involved and associated pathologies (e.g., CTS, tendinitis, and tenosynovitis). Note that mechanical loading is likely to affect a general area, thus cluster pathologies are not uncommon.

In addition to the effects of posture on contact force, posture deviations resulting in large tendon bends may also increase muscular demands by increasing moment arms for movements which are not necessarily the functional goal. For instance, pronation elicits great angular deviations of the FDS and FDP tendons of the second and third digits over the radial carpal wall, inducing torque potential radially. Wrist flexion increases the moment arm of all finger flexors to flex the wrist. If the goal of a task is to pinch something with the first three digits while in pronation with a mildly flexed wrist, the functional goal of the finger flexors would be to flex the metacarpophalangeal, and the proximal and distal inter-phalangeal joints. The force generated by the muscle bundles of these tendons may create the desired flexor torque at the phalangeal joints, but it will also produce a flexor and a radial torque at the wrist. As a result, increased muscle activity of both ulnar deviators and wrist extensors is required to counteract the radial and flexor torques at the wrist, so that a functional wrist posture is maintained. Activities requiring comparable postures for substantial periods of time may increase the muscular demand to the extent of posing a risk of developing forearm muscle fatigue.

Finally, the effect of repetitive forearm pronation/supination is similar to that seen by tendon excursions in the presence of high contact force. Tendons in repetitive forearm pronation/supination tend to shift medio-laterally, thus have the potential for medio-lateral frictional work against structures in contact with moving tendons. The risk of abrasive wear is higher when the wrist is deviated from neutral, because the volar and dorsal shifts with flexion and extension create higher contact (normal) forces, against the anterior and posterior carpal walls respectively. Conversely, tendons are relatively straight in the sagittal plane in neutral wrist, thus tendons may only minimally contact the surrounding tissues. Frictional work on the median nerve during medio-lateral tendon shifts of repetitive forearm motion, even in neutral and

extended wrists, is a possibility, due to the contact of the median nerve with flexor tendons (Zeiss et al., 1989). Zeiss et al. studied the anatomical relationships of the median nerve and the finger flexors as a function of wrist flexion/extension postures, using MRI. They reported that with a neutral wrist, the median nerve was anterior to the FDS2 and in contact with the retinaculum; this position elicited antero-posterior compression of the nerve to a lesser extent than with flexion, as seen by some antero-posterior flattening. A similar relationship in extension was observed, although the amount of nerve flattening or deformation in extension was less than in the other two wrist postures. These findings imply that the median nerve may experience frictional work during repetitive forearm pronation/supination regardless of wrist flexion/extension—due to the medio-lateral tendon motion elicited with rotation, and contact in all wrist postures, as suggested by Zeiss et al. However, because more nerve deformation was observed in flexion and less in extension, greater frictional work may be experienced with increased wrist flexion. The combined effect of repetitive forearm pronation/supination with sustained wrist postures is illustrated in Figure 8.3.

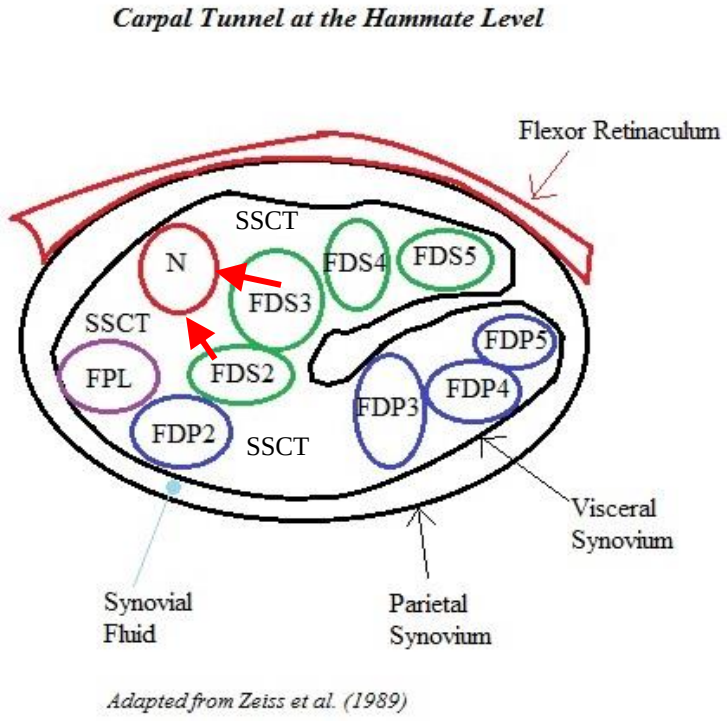

Figure 8.1. Transverse view of the carpal tunnel. All tendons are surrounded by sub-synovial connective tissue (SSCT) within the tunnel. The median nerve (N) is frequently in close proximity with or without contact with the FDS2/3. Small tendon shifts with flexion

This research represents an important cornerstone towards improving MSD risk estimates during manual occupational tasks, as findings are critical for incorporating the effect of forearm pronation/supination on MSD risk assessments of the upper limb. This research provided new knowledge, by contributing with numerous pieces of information to facilitate forearm rotation quantification, and to estimate finger flexor tendon kinematics associated with forearm posture – two areas which are crucial for determining why forearm rotation can be problematic, and which have been previously overlooked.

The forearm rotation quantification findings led us to conclude that measuring forearm postures with Xsens IMUs, and using their percentiles (Jonsson, 1978), provided accurate estimates of pronation and supination (with a maximum average error of 3.9°) during continuous manual tasks. This accuracy is better than other technologies previously reported in the literature, such as torsiometers, which have shown errors of up to 7° when aligned with the axis of rotation, and even greater errors if misaligned. Results from this research took into account a larger ROM (59° of pronation to 55° of supination) than those often reported in the literature (±45°) (Lowe, 2004; Spielholz et al. 2001, Flodgren et al. 2006), high angular velocities (approximately ± 500°/sec based on data of 9 participants), and magnetic disturbance (included errors associated with holding metal in the hands). Thus Xsens IMUs are a good choice to measure forearm postures in the workplace, where magnetic disturbance may be present.

The current findings on the evaluation of finger flexor tendon trajectories associated with forearm posture are of outstanding value, as they are a gateway to understanding forearm rotation's contribution to injury development, and to identifying potentially injurious forearm movements and postures – an area not been previously evaluated. More specifically, findings from the MRI studies can be used as inputs to kinetic models to estimate MSK loading. For example, assuming that tendon tension has been estimated from grip force, tendon angles in the frontal plane could replace the "wrist angle variable – a sagittal angle" in Armstrong and Chaffin's model (1979) (Eq. 7.1) in order to identify contact forces against an entire medio-lateral trochlear surface. In this proposed case, the tendon angle would be used to represent the angle at which the tendon wraps a trochlear surface medio-laterally, rather than antero-posteriorly as previously done, giving estimates of radio-ulnar contact forces.

Similarly, one of the models used by Moore et al. (1991) to estimate antero-posterior tendon pressure on surrounding structures (i.e. force per unit area) could be adapted to determine the effect of axial tendon movement on tendon medio-lateral pressure on other structures (e.g. during typing – where the forearm is pronated (radial contact) and the index finger hits the keys repetitively). In this proposed scenario, the "wrist angle variable" would be replaced by the frontal tendon angle (estimated from forearm rotation posture), as pressure estimates are based on tendon axial excursion velocity (based on Armstrong and Chaffin, 1978) tendon force, wrist joint angle, tendon width, and synovium-tendon coefficient of friction. Eventually, the knowledge of the normal pressure, assuming changes in muscle length of the FDS and/or FDP tendons were known, frictional work could also be estimated (Moore et al. 1991).

Major contributions:

1. A new methodology to quantify forearm rotation of continuous tasks, using Xsens IMUs, with an accuracy of 3.9° if comparing percentile levels (Jonsson, 1978), with or without metal.
2. Effect of forearm and wrist posture on locations and orientations of finger flexor tendons proximal to the CT, and relevant implications in the forearm.
3. Effect of forearm and wrist posture on locations of finger flexor tendons distal to the CT, and orientations through the tunnel, and relevant implications in the CT.

Lastly, in the process of pursuing the main goals of this thesis, a series of new methodologies emerged, which had not been previously known. These include the following:

1. *A new arm Vicon model:*

To measure forearm pronation/supination, a new marker configuration was created to build two forearm segments, so that the distal forearm segment could rotate with respect to the proximal segment about a fixed axis (long forearm's axis). The model was fully customized in Visual 3D because the software did not provide options to measure forearm rotation. The proximal segment was created using the medial and lateral epicondylar markers, and a mid-point calculated between the radial and ulnar styloids. The distal segment was created using the markers of the radial and ulnar styloids, and a mid-point between the medial and lateral epicondyles.

2. *Methodologies to create anatomical coordinate systems (CS) for the radius, ulna, and metacarpal using Mimics and 3Matics:*

These methodologies created CSs on three separate bones, by creating 3D segmental models of each bone and the forearm using Mimics, and digitizing selective anatomical landmarks on 3Matics. Digitization was done on the neutral wrist and forearm scan. For each neutral scan, bony landmarks were digitized on each bone. A registration process was used to super-impose the digitized landmarks onto each of the other eight scans of the same participant, in order to minimize within subject variability. Lastly, landmarks were used to create the medio-lateral axes in all bones using a customized Matlab program. Longitudinal axes of the radius and ulna for each scan were shared, and were determined by identifying the proximal and distal axial centroids of segmented forearms. The longitudinal axes of the metacarpals were obtained using centroids of their respective shaft. The 3rd axes and orthogonality corrections were done through the use of cross-product calculations. This

method was observed to be inter-tester (from 0.812-.972) and intra-tester reliable (ICC 0.871-0.993), when measuring wrist flexion/extension, and forearm pronation/supination.

3. *A methodology to generate tendon trajectories, and express them with respect to a radial CS.*

Because tendon trajectories had to be expressed in anatomical terms, 3D models of eight finger flexor tendons were first segmented, and their centerlines generated in Mimics. A customized Matlab program was created to adapt a transformation (rotation and translation) method from Winter (2004) to translate and rotate tendons' centerlines in order to express them with respect to the radial CS. This method was initially used to transform Vicon markers' global coordinates into an anatomical CS.

4. *A methodology to fit a 3D line through centerline coordinates*

Tendons had to be defined as lines in order to measure their angular trajectories. Thus, lines were fitted through the proximal and distal tendon portions of interest. This iterative process systematically translated and rotated a line, joining all possible connections between two grids of $\pm$5 mm along the antero-posterior x and medio-lateral z axes around each of the identified proximal and distal tendon centerline points, in 1 mm increments, and then in 0.1 mm increments. The fit was tested by averaging the perpendicular deviations of all original centerline points from the line.

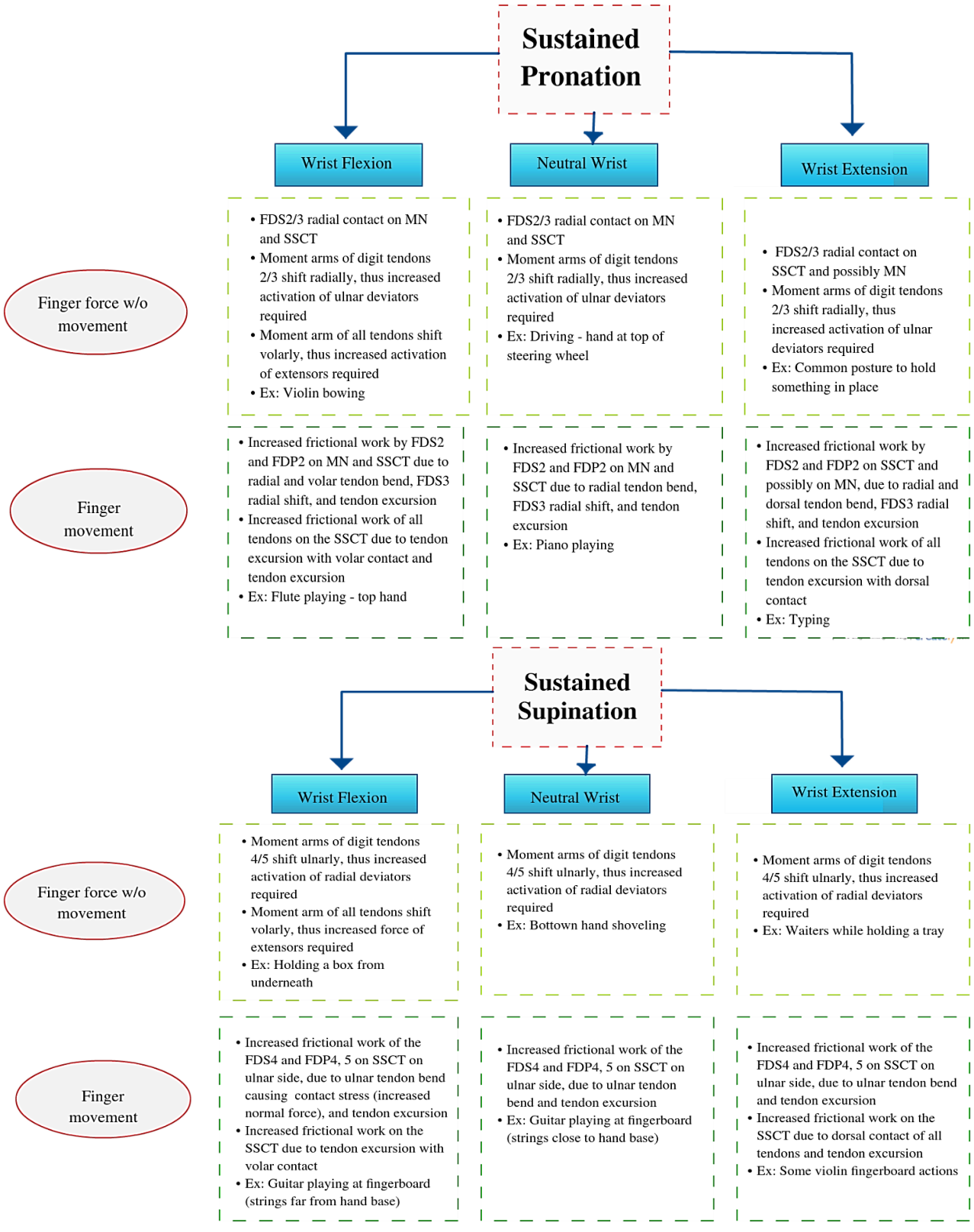

Figure 8.2. Summary of potential injury mechanisms associated with sustained forearm posture deviated from neutral, with three wrist postures, with finger static force or movement.

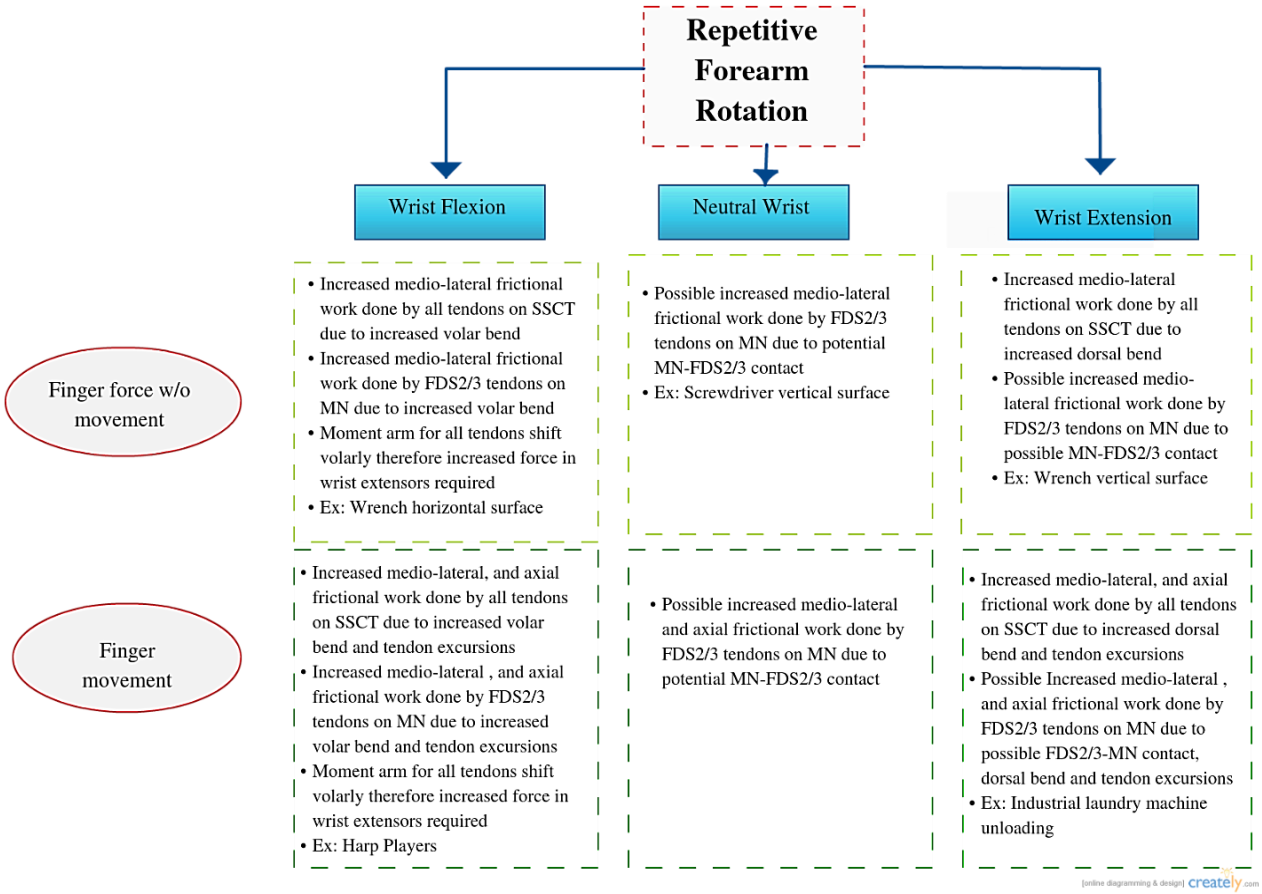

Figure 8.3. Summary of potential injury mechanisms associated with repetitive forearm pronation/supination, with three wrist postures, with finger static force or movement.

8.2 **Future Directions**

Further work is called for, with the continued aim of modeling internal MSK loading with pronation and supination. As this dissertation only took tendon movement outside the CT into account, investigating tendon trajectories within the tunnel is the next logical step. This work will include measuring the radii of curvature associated with the tendon in the tunnel and linking these measurements to the shape of the tunnel. Additionally, evaluations will be performed on the effect of forearm pronation/supination on kinetic relationships between structures, possibly taking into account tissues' mechanical properties, CT pressure, and additional tendon force.

Studying the effects of forearm pronation/supination on MSK loading in terms of injury mechanisms at the forearm and elbow should include the evaluation of trajectories of tendons that do not pass through the tunnel, such as finger and wrist extensor muscles and wrist flexors. Furthermore, changes in muscle length and muscle moment arms may provide meaningful insight about the muscular demand associated with different forearm postures.

8.3 **Conclusions**

In conclusion, wrist flexion and forearm postures away from neutral increase MSK loading through various mechanisms. Although relating external exposures to internal loading is highly challenging due to the numerous contributing factors, the current study has provided important knowledge relating combined forearm pronation/supination and wrist flexion/extension postures on tendon movement, which may impact MSK loading at the wrist and forearm.

The combined knowledge from these studies brings the current state of research closer to the goal of modelling the mechanical loading associated with postural requirements of particular manual tasks. This dissertation presents a method for the quantification of forearm pronation/supination in the workplace, reveals the most accurate variables (percentiles and turns analysis) to use in a potential model, and recognizes the extent of motion capture system errors in the presence of metal. In addition, these studies have gathered new knowledge about the combined effects of forearm pronation/supination and posture flexion/extension on tendon kinematics, and have outlined possible MSK loading implications. Thus, there are new, relevant tools to improve the estimation of MSK loading associated with work tasks.

REFERENCES

Armstrong, T. J. & Chaffin, D. B. (1979). Some biomechanical aspects of the carpal tunnel. *J Biomech*, *12*(7), 567–570.

Armstrong, T. J., Castelli, W. A., Evans, G., and Diaz-Perez, R. (1984). Some histological changes in carpal tunnel contents and their biomechanical implications. *Journal of Occupational Medicine*, *26*(3), 197–201. Retrieved from http://www.ncbi.nlm.nih.gov/pubmed/6716187

Armstrong, T. J, & Chaffin, D. B. (1978). An investigation of the relationship between displacements of the finger and wrist joints and the extrinsic finger flexor tendons. *Journal of Biomechanics*, *11*(1), 119–128.

Armstrong T. J., Foulke, J., Joseph, B., and Goldstein, S. (1982). Investigation of cumulative trauma disorders in a poultry processing plant. *American Industrial Hygiene Association Journal*, *43*(2), 103–116. https://doi.org/10.1080/15298668291409433

Birkfellner, W., Hummel, J., Wilson, E., and Cleary, K. (2008). Tracking devices. In T. Peters & K. Cleary (Eds.), *Tracking Devices BT - Image-Guided Interventions: Technology and Applications* (pp. 23–44). Boston, MA: Springer US. https://doi.org/10.1007/978-0-387-73858-1_2

Bower, J., Stanisz, G., and Keir, P. (2006). An MRI evaluation of carpal tunnel dimensions in healthy wrists: Implications for carpal tunnel syndrome. *Clinical Biomechanics*, *21*(8), 816–825. https://doi.org/10.1016/j.clinbiomech.2006.04.008

Browning, R., Kurtz, R., and Kerherve, H. (2012). Biomechanics of walking with snowshoes. *Sports Biomech*, *11*(1), 73–84. https://doi.org/10.1080/14763141.2011.637129

Cuesta-Vargas, A., Galán-Mercant, A., and Williams, J. M. (2010). The use of inertial sensors system for human motion analysis. *Physical Therapy Reviews : PTR*, *15*(6), 462–473. https://doi.org/10.1179/1743288X11Y.0000000006

Dang, A., Salas, E. A., and Moore, A. E. (2016). Intra and inter rater reliability of identifying bony landmarks of distal forearm and wrist bones to calculate joint angles. In *CRE-MSD*. Toronto.

Denbeigh, K., Slot, T. R. and Dumas, G. A. (2013). Wrist postures and forces in tree planters during three tree unloading conditions. *Ergonomics*, *56*(10), 1599–1607. https://doi.org/10.1080/00140139.2013.824615

Descatha, A., Leclerc, A., Chastang, J. F., and Roquelaure, Y. (2003). Medial Epicondylitis in Occupational Settings: Prevalence, Incidence and Associated Risk Factors. *Journal of Occupational and Environmental Medicine*, *45*(9), 993–1001. https://doi.org/10.1097/01.jom.0000085888.37273.d9

Domizio, J. D. & Keir, P. (2010). Forearm posture and grip effects during push and pull tasks, *Ergonomics*, *53*(3), 336–343. https://doi.org/10.1080/00140130903389076

Drake, R.L., Vogl, W. and Mitchell, A. (2005). *Gray's anatomy for students*. (Vogl, Mitchell, & Grey, Eds.). Philadelphia: Elsevier/Churchill Livingstone.

Eichelberger, Ferraro, Minder, Denton, Blasimann, Krause, & Baur. (2016). Analysis of accuracy in optical motion capture – A protocol for laboratory setup evaluation. Journal of Biomechanics, 49(10), 2085–2088. https://doi.org/10.1016/j.jbiomech.2016.05.007

El-Gohary, M., & McNames, J. (2012). Shoulder and elbow joint angle tracking with inertial sensors. *IEEE Transactions on Biomedical Engineering*, *59*(9), 2635–2641. https://doi.org/10.1109/TBME.2012.2208750

Flodgren, G., Heiden, M., Lyskov, E., & Crenshaw, A. G. (2007). Characterization of a laboratory model of computer mouse use-Applications for studying risk factors for musculoskeletal disorders. *Applied Ergonomics*, *38*(2), 213–218. https://doi.org/10.1016/j.apergo.2006.03.001

Garrett. J. W. (1970). *Anthropometry of the hands of male air force flight personnel.* Ohio, U.S.A.

Goldstein, S. A., Armstrong, T. J., Chaffin, D. B., & Matthews, L.. (1987). Analysis of cumulative strain in tendons and tendon sheaths. *Journal of Biomechanics*, *20*(1), 1–6. https://doi.org/10.1016/0021-9290(87)90261-2

Grevsten, S., & Sjögren, B. (1996). Symptoms and sickleave among forestry machine operators working with pronated hands. *Applied Ergonomics*, *27*(4), 277–280. https://doi.org/10.1016/0003-6870(95)00058-5

Günther, C. M., Bürger, A., Rickert, M., Crispin, A., & Schulz, C. U. (2008). Grip Strength in Healthy Caucasian Adults: Reference Values. *Journal of Hand Surgery*, *33*(4), 558–565. https://doi.org/10.1016/j.jhsa.2008.01.008

Hughes, R., Silverstein, B., & Evanoff, B. A. (1997). Risk Factors for Work-Related Musculoskeletal Disorders in an Aluminum Smelter, *32*, 66–75.

Jones, T. & Kumar, S. (2006). Assessment of physical demands and comparison of multiple exposure definitions in a repetitive high risk sawmill occupation: Saw-filer. *International Journal of Industrial Ergonomics*, *36*(9), 819–827. https://doi.org/10.1016/j.ergon.2006.07.004

Jonsson, B. (1978). Kinesiology: with special reference to electromyographic kinesiology. *Electroencephalography and Clinical Neurophysiology. Supplement*, (34), 417–428. https://doi.org/10.2519/jospt.2010.3025

Keir, P. J. & Rempel, D. M. (2005). Pathomechanics of peripheral nerve loading: Evidence in carpal tunnel syndrome. *Journal of Hand Therapy*. https://doi.org/10.1197/j.jht.2005.02.001

Keir, P. J. & Wells, R. (1999). Changes in geometry of the finger flexor tendons in the carpal tunnel with wrist posture and tendon load: An MRI study on normal wrists. *Clinical Biomechanics*, *14*(9), 635–645. https://doi.org/10.1016/S0268-0033(99)00012-1

Khan, A. A.,O'Sullivan, L., & Gallwey, T. J. (2009a). Effects of combined wrist deviation and forearm rotation on discomfort score. *Ergonomics*, *52*(3), 345–61. https://doi.org/10.1080/00140130802376018

Khan, A. A.,O'Sullivan, L., & Gallwey, T. J. (2009b). Effects of combined wrist

flexion/extension and forearm rotation and two levels of relative force on discomfort. *Ergonomics*, *52*(10), 1265–1275. https://doi.org/10.1080/00140130903040208

Kociolek, A. M. & Keir, P. J. (2016). Relative motion between the flexor digitorum superficialis tendon and paratenon in zone V increases with wrist flexion angle. *Journal of Orthopaedic Research*, *34*(7), 1248–1255. https://doi.org/10.1002/jor.23133

Kroemer, K. H. E. (1989). Cumulative trauma Their recognition and measures to avoid them. *Applied Ergonomics*, *20*(December), 274–280. https://doi.org/http://dx.doi.org/10.1016/0003-6870(89)90190-7

Lagree, A., Salas, E., & Moore. A. E. (2016). Factors affecting the use of IMUs in forearm rotation assessment. In *Ninth International Scientific Conference on the Prevention of Work-Related Musculoskeletal Disorders (PREMUS)* (p. 283). Toronto.

Loh, P.Y., Nakashima, H., Muraki, S. (2016). The effect of full finger flexion on the deformation of median nerve at carpal tunnel. In *Ninth International Scientific Conference on the Prevention of Work-Related Musculoskeletal Disorders (PREMUS).* (p. 244). Toronto.

Loudon, J.K., Manske, R.C., Reiman. (2013). *Clinical Mechanics and Kinesiology*. United States of America: Human Kinetics.

Lowe, B. (2004). Accuracy and validity of observational estimates of shoulder and elbow posture. *Applied Ergonomics*, *35*(2), 159–171. https://doi.org/10.1016/j.apergo.2004.01.003

Luinge, H. J., Veltink, P. H., & Baten, C. T. M. (2007). Ambulatory measurement of arm orientation. *Journal of Biomechanics*, *40*(1), 78–85. https://doi.org/10.1016/j.jbiomech.2005.11.011

Manal, K. T., & Buchanan, T. S. (2004). Standard handbook of biomedical engineering and design. Biomechanics of Human Movement (Chapter 5). In Kurtz (Ed.), *Standard Handbook of Biomedical Engineering and Design* (pp. 1–26). Newark: McGraw-Hill. https://doi.org/10.1

Marklin, R. W., & Monroe, J. F. (1998). Quantitative biomechanical analysis of wrist motion in bone-trimming jobs in the meat packing industry. *Ergonomics*, *41*(2), 227–37. https://doi.org/10.1080/001401398187279

Marras, W. S., & Schoenmarklin, R. W. (1993). Wrist motions in industry. *Ergonomics*, *36*(4), 341–51. https://doi.org/10.1080/00140139308967891

Mcatamney, L., & Corlett, E. N. (1993). RULA: a survey method for the investigation of world-related upper limb disorders. *Applied Ergonomics*, *24*(2), 91–99. https://doi.org/10.1016/0003-6870(93)90080-S

McGill, S. M., Juker, D., Axler, D. & Axler, C. (1996). Correcting trunk muscle geometry obtained from MRI and CT scans of supine postures for use in standing postures. *Journal of Biomechanics*. https://doi.org/10.1016/0021-9290(95)00119-0

McKinley, M. & O'Loughlin. (2006). *Human Anatomy*. New York: The McGraw-Hill Companies Inc.

Mogk, J. P. & Keir, P. J.. (2003). The effects of posture on forearm muscle loading during gripping. *Ergonomics*, *46*(9), 956–975. https://doi.org/10.1080/0014013031000107595

Mohankumar, D., Garner, H., Ruff, R., Ramirez, F. C., Fleischer, D., Wu, Q. W., & Santello, M.. (2014). Characterization of right wrist posture during simulated colonoscopy: An application of kinematic analysis to the study of endoscopic maneuvers. *Gastrointestinal Endoscopy*, *79*(3), 480–489. https://doi.org/10.1016/j.gie.2013.11.023

Moore, A., Wells, R., & Ranney, D. (1991). Quantifying exposure in occupational manual tasks with cumulative trauma disorder potential. *Ergonomics*, *34*(12), 1433–53. https://doi.org/10.1080/00140139108964888

Moore, J. S., & Garg, A. (1995). The Strain Index: a proposed method to analyze jobs for risk of distal upper extremity disorders. *Am Ind Hyg Assoc J*, *56*(768414177), 443–458. https://doi.org/10.1080/15428119591016863

Mukhopadhyay, P., O'Sullivan, L., & Gallwey, T. J. (2007). Estimating upper limb discomfort level due to intermittent isometric pronation torque with various combinations of elbow angles, forearm rotation angles, force and frequency with upper arm at 90° abduction. *International Journal of Industrial Ergonomics*, *37*(4), 313–325. https://doi.org/10.1016/j.ergon.2006.11.007

Occupational Health and Safety Council of Ontario (OHSCO). (2008). MSD prevention toolbox: Getting started. *Musculoskeletal Disorders Prevention Series*, *3*, 1–58.

Polhemus Innovation in Motion. (2012). 3Space Fastrak User Manual. Colchester, Vermont.

Park, H. S., Kim, J. Y., Kim, J. G., Choi, S. W. & Kim, Y. (2013). A New Position Measurement System Using a Motion-Capture Camera for Wind Tunnel Tests, *Sensors*, 12329–12344. https://doi.org/10.3390/s130912329

Quemelo, P. & Vieira, E. (2015). Biomechanics and performance when using a standard and a vertical computer mouse, *139*(September). https://doi.org/10.1080/00140139.2013.805251

Rempel, D., Bach, J. M., Gordon, L. & So, Y. (1998). Effects of forearm pronation/supination on carpal tunnel pressure. *The Journal of Hand Surgery*, *23*(1), 38–42. Retrieved from http://www.ncbi.nlm.nih.gov/pubmed/9523952

Robbins. H. (1963). Anatomical Study of the Median Nerve in the Carpal Tunnel and Etiologies of the Carpal-Tunnel Syndrome. *J Bone of Joint Surg Am., 45,953-966.*

Schoenmarklin, R., Marras, W., & Leurgans, S. (1994). Industrial wrist motions and incidence of hand/wrist cumulative trauma disorders. *Ergonomics*, *37*(9), 1449–1459. https://doi.org/10.1080/00140139408964925

Shiratsu, A. & Coury, H.J. (2003). Reliability and accuracy of different sensors of a flexible electrogoniometer, *18*, 682–684. https://doi.org/10.1016/S0268-0033(03)00110-4

Shublaq, N., Smith, P., & Stebbins. J. (2009). Informing patient, career and professional in

improved stroke rehabilitation: Feedback in exercise rehabilitation regime. In *The 5th UK & RI Postgraduate Conference in Biomedical Engineering & Medical Physics* (p. 47). Oxford.

Silverstein, B., Fine, L. & Armstrong, T. (1986). Hand wrist cumulative trauma disorders in industry. *British Journal of Industrial Medicine*, *43*(11), 779–784. https://doi.org/10.1136/oem.43.11.779

Spielholz, P., Silverstein, B., Morgan, M., Checkoway, H., & Kaufman, J. (2001). Comparison of self-report, video observation and direct measurement methods for upper extremity musculoskeletal disorder physical risk factors. *Ergonomics*, *44*(6), 588–613. https://doi.org/10.1080/00140130118050

Statistics. (2008). *Nonfatal Occupational Injuries and Illnesses Requiring Days Away From Work, 2007*. Washington, D.C.

O'Sullivan, L., & Gallwey, T. (2005). Forearm torque strengths and discomfort profiles in pronation and supination, *Ergonomics*, *48*(6), 703–721. https://doi.org/10.1080/00140130500070954

O'Sullivan, L. & Gallwey, T. (2002). Upper-limb surface electro-myography at maximum supination and pronation torques : the effect of elbow and forearm angle, *Journal of Electromyography and Kinesiology*, *12*, 275–285.

Welch, G. & Bishop, G. (2006). An Introduction to the Kalman Filter. In Practice, 7(1), 1–16. https://doi.org/10.1.1.117.6808

Wells, R; Moore, A. E., Ranney, D. (1990). Evaluation of hand-intensive tasks using biomechanical load factors. In *Work Design in Practice* (pp. 183–190). London: Tylor & Francis.

Werner, R., Armstrong, T., & Aylard, M. (1997). Intracarpal canal pressures: The role of finger, hand, wrist and forearm position. *Clinical Biomechanics*, *12*(1), 44–51.

Windolf, M., Götzen N. & Morlock, M. (2008). Systematic accuracy and precision analysis of video motion capturing systems — exemplified on the Vicon-460 system. *Journal of Biomechanics*, *41*, 2776–2780. https://doi.org/10.1016/j.jbiomech.2008.06.024

Winter, D. (2004). *Biomechanics and Motor Control of Human Movement: Anthropometry*. (3rd ed.). Hoboken, NY: John Wiley & Sons, Inc.

Woodman, O. (2007). *An Introduction to Inertial Navigation*. *University of Cambridge*. https://doi.org/10.1017/S0373463300036341

Xsens motion technologies. (2008). MTi and MTx User Manual and Technical Documentation. Netherlands.

Zeiss, J., Skie, M., Ebraheim, N., & Jackson, W.T. (1989). Anatomic relations between the median nerve and flexor tendons in the carpal tunnel: MR evaluation in normal volunteers. *American Journal of Roentgenology*, *153*, 533–536.

Zhou, H., Stone, T., Hu, H., & Harris, N. (2008). Use of multiple wearable inertial sensors in

upper limb motion tracking. *Medical Engineering and Physics*, *30*(1), 123–133. https://doi.org/10.1016/j.medengphy.2006.11.010

APPENDIX A – LANDSMEER'S MODELS I AND II

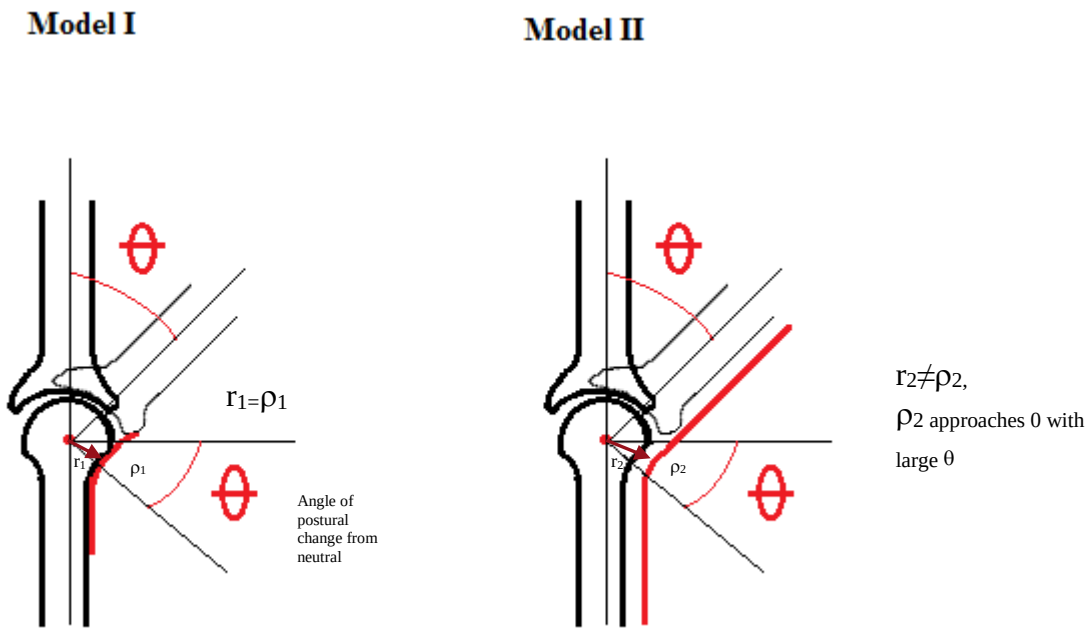

Figure A.1. Illustration of the 1st and 2nd Landsmeer models. **Model I** assumes that the tendon crosses the joint along the bone surface, thus the tendon's radius of curvature ρ1 is the same as the distance from the center of rotation to the tendon r_1 (moment arm). **Model II** on the other hand, assumes the tendon is restrained at a point, thus the angle of curvature ρ_2 of the tendon corresponds to the angle between two straight lines on either side of the restraint.

APPENDIX B

1) ICC Pairwise comparisons.

Bonferroni-Adjusted Pairwise Comparisons of ICC Means among Vertical Locations by Material							
Material	(i) Vertical Location	(j) Vertical Location	Mean Difference (i-j)	Std. Error	Sig[b]	95% CI for Difference	
						Lower Bound	Upper Bound
Metal	*Top*	*Middle*	0.014	0.006	0.093	-0.002	0.03
	Top	*Bottom*	0.037	0.008	0.001*	0.016	0.058
	Middle	*Bottom*	0.023	0.007	0.011*	0.005	0.042
Plastic	*Top*	*Middle*	-0.001	0.001	1.000	-0.005	0.003
	Top	*Bottom*	0.006	0.002	0.057	0.000	0.012
	Middle	*Bottom*	0.007	0.002	0.001*	0.003	0.011

Based on estimated marginal means

*The mean difference is significant at the .05 level.

[b]**Adjustment for multiple comparisons: Bonferroni.**

Bonferroni-Adjusted Pairwise Comparisons of ICC Means							
Vertical Locations	(i) Material	(j) Material	Mean Difference (i-j)	Std. Error	Sig[b]	95% CI for Difference	
Top	*Metal*	*Plastic*	-0.015	0.004	0.002	-0.023	-0.006
Middle	*Metal*	*Plastic*	-0.03	0.006	0.000	-0.043	-0.017
Bottom	*Metal*	*Plastic*	-0.047	0.008	0.000	-0.063	-0.03

Based on estimated marginal means

*The mean difference is significant at the .05 level.

[b]**Adjustment for multiple comparisons: Bonferroni.**

2) RMSE Pairwise comparisons

Bonferroni-Adjusted Pairwise Comparisons of RMSE Means among Vertical Locations by Material							
Material	(i) Vertical Location	(j) Vertical Location	Mean Difference (i-j)	Std. Error	Sig[b]	95% CI for Difference	
						Lower Bound	Upper Bound
Metal	*Top*	*Middle*	-3.543	0.788	0.001*	-5.622	-1.465
	Top	*Bottom*	-5.126	0.522	0.000*	-6.504	-3.747
	Middle	*Bottom*	-1.582	0.948	0.337	-4.083	0.919
Plastic	*Top*	*Middle*	-0.24	0.158	0.442	-0.658	0.178
	Top	*Bottom*	-1.1	0.281	0.003*	-1.843	-0.358
	Middle	*Bottom*	-0.86	0.203	0.002*	-1.397	-0.324

Based on estimated marginal means

*The mean difference is significant at the .05 level.

[b]**Adjustment for multiple comparisons: Bonferroni.**

Bonferroni-Adjusted Pairwise Comparisons of RMSE Means							
Vertical Locations	(i) Material	(j) Material	Mean Difference (i-j)	Std. Error	Sig[b]	95% CI for Difference	
Top	*Metal*	*Plastic*	1.62	0.428	0.001	0.721	2.52
Middle	*Metal*	*Plastic*	4.924	0.791	0.000	3.262	6.585
Bottom	*Metal*	*Plastic*	5.645	0.732	0.000	4.108	7.183

Based on estimated marginal means

*The mean difference is significant at the .05 level.

[b]**Adjustment for multiple comparisons: Bonferroni.**

APPENDIX C

RMSE Bonferroni Pairwise Comparisons with Four Locations (Floor included), in metal only.

Bonferroni-Adjusted Pairwise Comparisons of ICC Means						
(i) Vertical Location	(j) Vertical Location	Mean Difference (i-j)	Std. Error	Sig[b]	95% CI for Difference	
					Lower Bound	Upper Bound
Top	*Middle*	-2.73	1.04	0.103	-5.82	0.35
	Bottom	-5.886*	1.52	0.007*	-10.40	-1.37
	Floor	-5.495*	1.51	0.011*	-9.97	-1.02
Middle	*Top*	2.73	1.04	0.103	-0.35	5.82
	Bottom	-3.15	1.34	0.183	-7.13	0.82
	Floor	-2.76	1.71	0.746	-7.84	2.32
Bottom	*Top*	5.886*	1.52	0.007*	1.37	10.40
	Middle	3.15	1.34	0.183	-0.82	7.13
	Floor	0.39	1.85	1.000	-5.08	5.86
Floor	*Top*	5.495*	1.51	0.011*	1.02	9.97
	Middle	2.76	1.71	0.746	-2.32	7.84
	Bottom	-0.39	1.85	1.000	-5.86	5.08

APPENDIX D

INFORMED CONSENT FORM

School of Kinesiology and Health Science, York University

Study Title: Evaluation of Finger Flexor Tendon Trajectories at the Wrist, as a Function of Forearm and Wrist Postural Change, Using MRI.

Upper limb injuries are prevalent in the workplace and costly. Understanding of upper limb injury mechanisms that are associated with work tasks is of crucial importance to reduce their incidence in the workplace. Epidemiological evidence has shown that that sustained pronated postures and repetitive pronation and supination have been associated with upper limb injury. However, it is unknown how forearm pronation/supination, in combination with wrist posture, contributes to musculoskeletal loading of the forearm and wrist. Thus, the purpose of this study is to set a cornerstone to better understand forearm and wrist loading as a function on forearm pronation/supination postures, by measuring the magnitude of the deviations of tendons passing though the wrist with different forearm pronation/supination postures.

You will be asked to answer two questionnaires: In the first one, you will be asked questions to gather information on height, weight, handedness, and musculoskeletal health. In the second one we will ask you questions to screen whether it is safe for you to access the MRI room. You will be asked to remove any metallic objects you may be carrying. The anatomy of the your wrist will be imaged using MRI, while you sustain three forearm pronation/supination postures in combination with three wrist flexion/extension postures. During this process, you will be required to lie completely still on the patient bed that slides into the bore of the MRI scanner. No dye will be required. You will be able to communicate with the MRI technologist and researcher through an intercom, and will have an emergency bulb that you can squeeze at anytime if you need to come out of the scanner during the procedure. During the collection, you will be required to wear a splint to hold your wrist in the desired posture. At the same time, you will be required apply a constant light grip force hand dynamometer, connected to a monitor to give you feedback on the amount of force that you will need to keep constant during each sequence. Your estimated participation will take approximately 1.5 hours, one of which will be inside the scanner at the neuroimaging laboratory at York University.

It is important to inform you that these images are not intended to reveal any disease state, in part because this MRI protocol is not designed for clinical diagnosis. Thus, your wrist images will not be routinely examined by a clinical radiologist. The personnel at the Neuroimaging Laboratory are not qualified to medically evaluate your images. However, if in the course of collecting the images we have any concerns, we may show your scans to a clinical radiologist, who may suggest that you obtain further diagnostic tests.

At the investigator's discretion, you may view your wrist images and receive digital copies of them. However, you should be aware that structural images within the normal population can be highly variable, and that it is difficult to draw any conclusions from your images; you should be

aware of the potential distress or discomfort that may occur by viewing your own images. Do not rely on this research MRI to detect or screen for any abnormalities.

Risks and Benefits

This study has been reviewed and approved by the Human Participants Review Sub-Committee, York University's Ethics Review Board, and conforms to the standards of the Canadian Tri-Council Research Ethics guidelines. The risks associated with this study involve the following risks:

Metal: The MRI scanner produces a constant strong magnetic field, which may cause any metal implants and/or clips within your body to shift position. The magnetic field may also cause any implanted medical devices to malfunction. Thus, if you have any implanted metal, clips or devices, it is hazardous to your health to participate in this study. Please provide us with as much information as you can, for example if you had surgery in the past, so that we may decide whether it is safe for you to be a subject. Metallic objects brought into the MRI environment can become hazardous projectiles. Metal earrings, body piercings, and necklaces must be removed prior to the study.

Pregnancy: Exposure to MRI scanning might be harmful to a pregnant female or an unborn child. Although there are no established guidelines at this time about MR and pregnancy, you should be informed that there is a possibility of a yet undiscovered pregnancy related risk. If you know or suspect you may be pregnant or if you do not want to expose yourself to this risk, we recommend that you do not participate in this study.

Inner ear damage: MRI scanning produces loud noises that can cause damage to the inner ear if appropriate sound protection is not used. Earplugs and/or headphones will be provided to protect your ears.

Claustrophobia: When you are inside the MRI scanner, the MRI scanner surrounds your body and your head will also be positioned inside a close-fitting scanning coil. If you feel anxious in confined spaces you may not want to participate. If you decide to participate and begin to feel claustrophobic later, you will be able to tell us via the intercom and we will discontinue the study immediately.

Burns: In rare cases, contact with the MRI transmitting and receiving coil, conductive materials such as wires or other metallic objects, or skin-to-skin contact that forms conductive loops may result in excessive heating and burns during the experiment. The operators of the MRI scanner will take steps, such as using foam pads when necessary, to minimize this risk. Tattoos with metallic inks can also potentially cause burns. Any heating or burning sensations during a scan in progress should be reported to the operators immediately and we will discontinue the scan.

Besides the risks listed above, there are no other known risks from the magnetic field or radio waves at this time. Although functional MRI scanning has been used for more than 15 years,

long-term effects are unknown. If new findings about the risks of the MRI technique become available within a year of your participation, we will let you know about them.

All information obtained during the study will be held in strict confidence to the fullest extent possible by law. In no case will your personal information be shared with any other individuals or groups without your expressed written consent. Your images will be stored on secured computer servers and will be archived indefinitely. The experimental data acquired in this study may, in an anonymized form that cannot be connected to you, be used for teaching purposes, be presented at meetings, published, shared with other scientific researchers or used in future studies. Your name or other identifying information will not be used in any publication or teaching materials without your specific permission.

Consent of Participant

I have read this form about the nature and procedures of the study have received a copy and understand it in full. I agree to serve as a participant in the study. I have been assured that Elizabeth Salas will respond appropriately to any questions that I may have. I understand that

participation is entirely voluntary and I can refuse to answer any question, item, etc., and may withdraw my consent at any time by verbal declaration without prejudice to me either now or in the future. I know that if I withdraw my consent any data already obtained will be destroyed. Before giving my consent, I know that there would be no advantages or disadvantages for me depending on my decision and refusal to participate or withdrawal from participation will not jeopardize current or future relationships with the researchers or York University. I know that the university and those conducting this project subscribe to the ethical conduct of research and to the protection at all times to the dignity, rights, interest and safety of its participants. I know that any concerns or comments regarding my participation in this study can be addressed, anonymously if I wish, to Alison Collins-Mrakas, York University's Manager of Research Ethics, acollins@yorku.ca, 416-736-5914, York Research Tower, 5th Floor, or Dr. Anne Moore, Biomechanics Professor, amoore@yorku.ca, (416)736-2100 x 40498, School of Kinesiology and Health Science, Sherman Health Science Research Centre 2024.

_____ _____

Print Name Signature of Participant

_____ _____

Dated at Toronto, Ontario Witnessed

APPENDIX E

York University Neuroimaging Laboratory

Magnetic Resonance (MR) Safety Screening Form

Name _____ Weight _____
Last First MI Height _____

Date of Birth _____/_____/_____ ☐ Male ☐ Female
Month Day Year

Do you have: **Cardiac pacemaker or implantable cardioverter defibrillator (ICD)** ☐ Yes ☐ No
Aneurysm clip ☐ Yes ☐ No
Are you: Claustrophobic ☐ Yes ☐ No
Are you currently taking any medications? ☐ Yes ☐ No
List: _____

Have you ever had an injury to the eye involving a metallic object or fragment? ☐ Yes ☐ No
Have you ever worked in a metal shop? ☐ Yes ☐ No
Possibility of pregnancy? ☐ Yes ☐ No ☐ Not applicable

Brain/Head Surgery ☐ Yes ☐ No
List type/date
_____

Heart/Chest Surgery ☐ Yes ☐ No
List type/date *Retained pacer wires* ☐ Yes ☐ No
_____

Ear Surgery ☐ Yes ☐ No
List type/date
_____

Eye Surgery ☐ Yes ☐ No
List type/date
_____

Artificial Implants/Mechanical Devices
List type/date ☐ Yes ☐ No
_____

Other Surgery
List type/date ☐ Yes ☐ No
_____

Pierced body parts (earrings, etc.) ☐ Yes ☐ No
Hearing aid or cochlear implant ☐ Yes ☐ No
Permanent retainer or braces ☐ Yes ☐ No
Dentures or partials ☐ Yes ☐ No
History of bullets, shrapnel or BBs ☐ Yes ☐ No
History of seizures ☐ Yes ☐ No
Hair piece, wig or hair extensions ☐ Yes ☐ No
Medication or transdermal patch ☐ Yes ☐ No
Tattoo or permanent makeup ☐ Yes ☐ No
Stent, filter ☐ Yes ☐ No

WARNING: Certain implants, devices, or objects may be hazardous to you and/or may interfere with the MR procedure (i.e., MRI, MR angiography, functional MRI, MR spectroscopy). Do not enter the MR system room or MR environment if you have any questions or concerns regarding an implant, device, or object. Consult the MRI Technologist or Researcher BEFORE entering the MR system room. The MR system magnet is ALWAYS on.

I attest that the above information is correct to the best of my knowledge. I have read and understood the contents of this form and had the opportunity to ask questions regarding the information on this form and regarding the MRI procedure that I am about to undergo.

Signature of person completing form: _____ **Date** ___/___/____
M D Y

Form completed by: ☐ MRI participant ☐ Other (specify)_____

Reviewed by: _____ **PI of study** _____

APPENDIX F

Date: _____

Initial Questionnaire

Participant #: _____

Demographic Information

1. Date of Birth (mm/d/yr): _____
2. Sex: Female ☐ Male ☐
3. Handedness: _____
4. Height: _____m _____cm or _____ft _____in
5. Weight: _____Kg or _____Lb

Health and Injury Information

1. Do you currently have any health condition that could potentially be aggravated with physical activity (e.g. cardiovascular problems, high blood pressure, joint problems, etc.)?
   Y ☐ N ☐
   If yes, please explain: _____
2. Have you ever been diagnosed with neurological disorders (e.g. carpal tunnel syndrome, pronator teres syndrome)? Y ☐ N ☐
   - If yes, please explain: _____
     _____
3. Have you ever received treatment for any of the following, please specify:
   - Fractures - body part: _____
   - Dislocations –body part: _____
   - Muscle Strains or sprains - _____
   - Upper Back pain - _____

- Lower back pain - _____
- Tendonitis/tenosynovitis - _____
- Other musculoskeletal disorder - _____

4. In the past year, have you had treatment for any musculoskeletal injury or disorder? Please specify:

   _____

5. Do you currently have any physical discomfort/pain? Y ☐ N ☐

   If yes, please indicate in the figure where you feel the discomfort/pain

APPENDIX G

Mimics and 3-Matics Software commands for segmentation, digitization, registration, centerline and centroid calculations

4.3.a. Commands used on Mimics for structure segmentation, and creation of tendon centerlines. Centerlines and segmented models were exported for post processing in 3matics.

			Action	Result
Mimics	*Mask*	1)	"3D livewire" to create mask contours	Contours
			Created contours around structure of interest in 2 planes Click "segment"	Raw mask
		2)	Mask editing: i) "Erode"/"dilate" through morphology operations menu (1 pixel) Used to fill holes on mask or shrink mask leakage onto other structures	
			ii) Manual editing using a pen/eraser, as well as multiple slice editing (Note this step is repeated with new masks created through the process of dilation and erosion)	
			iii) Mask smoothing with "smooth mask" (Note this step is repeated with new masks created through the process of dilation and erosion)	Finished mask
	3 D model	3)	"Calculate 3D" through segmentation menu	Raw 3D model
		4)	3D model smoothing: "Wrap" then "smooth" operations through 3D tools	Smoothed 3D model
	Centerline	5)	Centerline creations of tubular structures - "Fit centerline function"	Centerline Coordinates text file
		6)	Export centerline coordinates - "Centerline properties", "Export"	
		7)	Export 3D models to 3Matic - "Export to 3-Matic"	

4.3.b. 3Matics was used to digitize, register, and export landmark coordinates used to create local coordinate systems.

3-Matic	*Digitization*	1)	Digitized points on anatomical landmarks on NM scan - "Analyze" then "Create Point", and digitize points of interest	Digitized landmarks
	Registration	2)	Copy and paste NM digitized structures on the same participant's scan	Segmented structures of 2 scans on the same work space
		3)	"3-Point registration" - select the NM structures as moving entities along with digitized landmarks to align with the same structure on other scans. This is done through the "align menu"	Superimposed structures of 2 different scans of the same participant along with digitized landmarks
			Note that 3 points have to be digitized for this function on both structures.	
		4)	"Global registration" - Select NM structures as moving entities along with digitized points. This works to fine tune the registration process	
		5)	"Export Curves and Primitives" to export digitized landmarks as .igs files	Landmark coordinate files

APPENDIX H

Details specific to the calculation of the CS of each bone: Radius, ulna, and metacarpal

1. Radial CS

The interim vector of the medio-lateral axis of the radius z'_r was calculated using equation 1, and normalized by dividing each of its xyz coordinates by its magnitude (Eq. 3), which was calculated using the Pythagorean Theorem (Eq. 2). The normalization procedure was done to create unit vectors so that rotation matrices could be created.

$$z'_r = RS_{xyz} - UN_{xyz} \qquad \text{(Eq. 1)}$$

Where:
z'_r = interim medio-lateral axis of the radius pointing radially
RS_{xyz}= xyz of radial styloid (Global or Scanner Coordinates)
UN_{xyz}= xyz of ulnar notch (Global or Scanner Coordinates)

$$z'_{rMag} = \sqrt{(z'_{rx})^2 + \left(z'_{ry}\right)^2 + (z'_{rz})^2} \qquad \text{(Eq. 2)}$$

Where:
$z'_{r\text{-}Mag}$ = magnitude of z'_r
z'_{rxyz} = xyz coordinates of z'_r

$$z'_{rNorm} = \frac{z'_r}{z'_{rMag}} \qquad \text{(Eq. 3)}$$

Where:
z'_{rNorm} = the normalized interim medio-lateral axis of the radius pointing radially

The longitudinal axis of the radius was calculated using the forearm centroids (Eq. 4), along with a similar approach as Eq. 2 & 3 for normalization yielding (y_{rNorm}).

$$y_r = PFC_{xyz} - DFC_{xyz} \qquad \text{(Eq. 4)}$$

Where:
y_r = longitudinal axis of the forearm pointing proximally
PFC_{xyz} = xyz of proximal forearm centroid (Global or Scanner Coordinates)
DFC_{xyz} = xyz of distal forearm centroid (Global or Scanner Coordinates)

The anteroposterior axis x_r was calculated as the cross-product between the normalized vectors z'_{rNorm} (normalized interim mediolateral axis) and y_{rNorm} (normalized forearm long axis) (Eq. 5). The x_r vector was also normalized using the approach previously mentioned x_{rNorm} (Eq. 2 & 3).

$$= z'_{rNorm} \, x \, y_{rNorm} \qquad \text{(Eq. } 5x_r\text{)}$$

Where:
x_r = anteroposterior axis of the radius pointing dorsally
z'_{rNorm}= normalized interim mediolateral axis pointing radially
y_{rNorm}= normalized longitudinal axis of the forearm pointing proximally

After these steps, a final correction of the radius CS must be done so that all axes are orthogonal to each other. Note that even though the vector $x_{rNorm}$is perpendicular to the yz' plane, the vectors z'_{rNorm} and y_{rNorm} are not necessarily orthogonal to each other. To do this, a new mediolateral axis z_r was created by obtaining the cross product of x_{rNorm} and y_{rNorm} (Eq. 6), and normalized with the same approach as above (Eq. 2 & 3). This last correction created a right-hand rule LCS of the radius, with three axes that were orthogonal to each other. Dot products were used to confirm orthogonality.

$$z_r = x_{rNorm}\, x\, y_{rNorm} \qquad \text{(Eq. 6)}$$

Where:
z_r = mediolateral axis of the radius pointing ulnarly
x_{rNorm}= normalized anteroposterior axis of the radius pointing dorsally
y_{rNorm}= normalized longitudinal axis of the forearm pointing proximally

A rotation matrix was created using the unit vectors of the components of the radial CS as follows:

$$R_r = \begin{bmatrix} x_{rNormx} & x_{rNormy} & x_{rNormz} \\ y_{rNormx} & y_{rNormy} & y_{rNormz} \\ z_{rNormx} & z_{rNormy} & z_{rNormz} \end{bmatrix}$$

Where:
Each row represents a component of the radial CS, and each column represents the normalized xyz coordinates of such components.

2. Ulnar CS

A similar approach to the calculations of the CS of the radius was used to create the ulna CS. Note that both, the radius and ulna shared the same long axis y_{rNorm} , which was the normalized version of the vector calculated in Eq. 4. The interim mediolateral axis x'_u of the ulna was created using the ulnar styloid and the radio-distal prominence across from it (Eq. 7), and normalized by dividing it by its own magnitude, similar to the previous approach (Eq. 2 & 3).

$$x'_u = RDP_{xyz} - US_{xyz} \qquad \text{(Eq. 7)}$$

Where:
x'_u = interim mediolateral axis of the ulna pointing radially
RDP= xyz of radio-ulnar prominence of ulna across from the ulnar styloid (Global or Scanner Coordinates)
US= xyz of ulnar styloid of ulna (Global or Scanner Coordinates)

The anteroposterior axis z_u was calculated as the cross product of the normalized interim mediolateral axis x'_{uNorm} and the normalized long axis y_{rNorm} vectors (Eq. 8), and normalized as above.

$$z_u = x'_{uNorm} \, x \, y_{rNorm} \qquad \text{(Eq. 8)}$$

Where:
z_u = anteroposterior axis of the ulna pointing dorsally
x'_{uNorm}= normalized interim mediolateral axis of the ulna pointing radially
y_{rNorm}= normalized longitudinal axis of the forearm pointing proximally

The corrected mediolateral axis x_u was calculated as the cross product between the normalized vectors y_{rNorm} and z_{uNorm}, and normalized as above. Dot products were used to ensure for orthogonality between axes.

$$x_u = y_{rNorm} \, x \, z_{uNorm} \qquad \text{(Eq. 9)}$$

Where:
x_u = mediolateral axis of the ulna pointing radially
y_{rNorm}= normalized longitudinal axis of the forearm pointing proximally
z_{uNorm}= normalized anteroposterior axis of the ulna pointing dorsally

A rotation matrix was created using the unit vectors of the components of the ulnar CS as follows:

$$R_u = \begin{bmatrix} x_{uNormx} & x_{uNormy} & x_{uNormz} \\ y_{rNormx} & y_{rNormy} & y_{rNormz} \\ z_{uNormx} & z_{uNormy} & z_{uNormz} \end{bmatrix}$$

Where:
Each row represents a component of the ulnar CS, and each column represents the normalized xyz coordinates of such components.

3. Metacarpal CS

A similar approach as above was used to create the CS of the 3rd metacarpal. The interim medio-lateral axis z'_m of the metacarpal was created using the metacarpal styloid and the proximal dorso-ulnar corner of the bone (Eq. 10), and normalized by dividing it by its own magnitude (Eq. 2 & 3).

$$z'_m = MST_{xyz} - MDU_{xyz} \qquad \text{(Eq. 10)}$$

Where:

z'_m = interim mediolateral axis of the metacarpal pointing radially
MST = xyz of the styloid of the 3rd metacarpal (Global or Scanner Coordinates)
MDU= xyz of the dorso-ulnar corner of the 3rd metacarpal's head (Global or Scanner Coordinates)

The longitudinal axis of the metacarpal y_{mNorm} was created using the two points selected from the centerline along the shaft of the metacarpal (Recall section 2.5.3.) (Eq. 11).

$$y_m = PMC_{xyz} - DMC_{xyz} \qquad \text{(Eq. 11)}$$

Where:
y_m = longitudinal axis of the metacarpal pointing proximally
PMC_{xyz} = xyz of proximal metacarpal centroid (Global or Scanner Coordinates)
DMC_{xyz} = xyz of distal metacarpal centroid (Global or Scanner Coordinates)

The anteroposterior axis x_m was calculated as the cross product of the normalized interim mediolateral axis z'_{mNorm} and the normalized long axis y_{mNorm} vectors (Eq. 12), and normalized as above.

$$x_m = z'_{mNorm}\, x\, y_{mNorm} \qquad \text{(Eq. 12)}$$

Where:
x_m = anteroposterior axis of the metacarpal pointing dorsally
z'_{mNorm}= normalized interim mediolateral axis of the metacarpal pointing radially
y_{mNorm}= normalized longitudinal axis of the metacarpal pointing proximally

The mediolateral axis z_m was corrected by calculating the cross product between the normalized vectors x_{mNorm} and y_{mNorm} (Eq. 13), and normalized as above. Dot products were used to ensure for orthogonality between axes.

$$z_m = x_{mNorm}\, x\, y_{mNorm} \qquad \text{(Eq. 13)}$$

Where:
z_m = mediolateral axis of the 3rd metacarpal pointing ulnarly
y_{rNorm}= normalized longitudinal axis of the metacarpal pointing proximally
x_{mNorm}= normalized antero-posterior axis of the metacarpal pointing dorsally

A rotation matrix was created using the unit vectors of the components of the metacarpal CS (Eq. 14) as follows:

$$R_m = \begin{bmatrix} x_{mNormx} & x_{mNormy} & x_{mNormz} \\ y_{mNormx} & y_{mNormy} & y_{mNormz} \\ z_{mNormx} & z_{mNormy} & z_{mNormz} \end{bmatrix} \qquad \text{(Eq. 14)}$$

Where:
Each row represents a component of the metacarpal CS, and each column represents the normalized xyz coordinates of such components.

APPENDIX I

Details specific to posture calculations

1. Wrist Posture

Euler angles were calculated using a custom made Matlab program to describe the posture of the hand with respect to the radius. A rotation matrix needed to align the metacarpal CS with the radial CS R_{mr} was calculated, by obtaining the product of the two matrices that represented their respective coordinates in the global reference system (Eq. 15) as follows:

$$R_{mr} = \begin{bmatrix} x_{mNormx} & x_{mNormy} & x_{mNormz} \\ y_{mNormx} & y_{mNormy} & y_{mNormz} \\ z_{mNormx} & z_{mNormy} & z_{mNormz} \end{bmatrix} * \begin{bmatrix} x_{rNormx} & x_{rNormy} & x_{rNormz} \\ y_{rNormx} & y_{rNormy} & y_{rNormz} \\ z_{rNormx} & z_{rNormy} & z_{rNormz} \end{bmatrix}' \quad \text{(Eq. 15)}$$

$$\text{Yielding: } R_{mr} = \begin{bmatrix} R_{11} & R_{12} & R_{13} \\ R_{21} & R_{22} & R_{23} \\ R_{31} & R_{32} & R_{33} \end{bmatrix}$$

Where: R_{mr} represents the rotation matrix to rotate the metacarpal to the radial CS.

The Euler angles were calculated using a xyz sequence, which means that each transformation of any point from the metacarpal CS $x_0y_0z_0$ to the radial CS, must first have gone through a rotation around the x axis to yield $x_1y_1z_1$, then a second rotation around the y_1 axis to yield $x_2y_2z_2$, and finally a third rotation around the z_2 axis to yield $x_3y_3z_3$. This series of rotations can be represented by the following three equations (Eqs. 16-18) (Winter, 2004).

$$\begin{bmatrix} x_1 \\ y_1 \\ z_1 \end{bmatrix} = \begin{bmatrix} 1 & 0 & 0 \\ 0 & c_1 & s_1 \\ 0 & -s_1 & c_1 \end{bmatrix} \begin{bmatrix} x_0 \\ y_0 \\ z_0 \end{bmatrix} \quad \text{(Eq. 16)}$$

$$\begin{bmatrix} x_2 \\ y_2 \\ z_2 \end{bmatrix} = \begin{bmatrix} c_1 & 0 & -s_1 \\ 0 & 1 & 0 \\ s_2 & 0 & c_2 \end{bmatrix} \begin{bmatrix} x_1 \\ y_1 \\ z_1 \end{bmatrix} \quad \text{(Eq. 17)}$$

$$\begin{bmatrix} x_3 \\ y_3 \\ z_3 \end{bmatrix} = \begin{bmatrix} c_3 & s_3 & 0 \\ -s_3 & c_3 & 0 \\ 0 & 0 & 1 \end{bmatrix} \begin{bmatrix} x_2 \\ y_2 \\ z_2 \end{bmatrix} \qquad \text{(Eq. 18)}$$

All rotations can be combined into one large equation yielding Eq. 19. The 3x3 matrix portion allowed for determining the Euler angles of the relative orientations of the two CS, θ_1, θ_2, and θ_3 (Table VI.a) (Winter, 2004). Recall that θ_1, θ_2, and θ_3 were the rotations about the x,y,z axes, which corresponded to the anteroposterior, longitudinal, and mediolateral axes respectively. Thus θ_1 and θ_3 represented wrist radio/ulnar deviation and wrist flexion/extension respectively.

$$\begin{bmatrix} x_3 \\ y_3 \\ z_3 \end{bmatrix} = \begin{bmatrix} c_2c_3 & s_3c_1 + s_1s_2c_3 & s_1s_3 - c_1s_2c_3 \\ -c_2s_3 & c_1c_3 - s_1s_2s_3 & s_1c_3 + c_1s_2s_3 \\ s_2 & -s_1c_2 & c_1c_2 \end{bmatrix} \begin{bmatrix} x_0 \\ y_0 \\ z_0 \end{bmatrix} \qquad \text{(Eq. 19)}$$

A. Sample calculation used to determine wrist flexion/extension posture, using Euler angles to describe orientation of the metacarpal CS with respect to the radial CS.

Used the following terms	**To calculate:**	**Notes:**	**Example** $R = \begin{bmatrix} R_{11} & R_{12} & R_{13} \\ R_{21} & R_{22} & R_{23} \\ R_{31} & R_{32} & R_{33} \end{bmatrix}$ $R = \begin{bmatrix} 0.9507 & 0.3074 & -0.0398 \\ -0.3096 & 0.9483 & -0.0704 \\ 0.0161 & 0.0792 & 0.9967 \end{bmatrix}$
R_{31}	$R_{31}=s_2$	$\theta_2=(s_2)^{-sin}$	s_2= 0.0161, θ_2=.9212° or -0.9212°
θ_2	$c_2=\cos\theta_2$	c_2 was always assumed to be positive, thus θ_2 could only be on quadrants (Q) I or IV	c_2=0.9999*, thus θ_2=.9212°
R_{33} and c_2 Note: $R_{33}=c_1c_2$	$c_1 = R_{33}/ c_2$ and θ_1	c_1 = 0.9967/ 0.9999 c_1 >0, thus θ_1 in Q I or IV	c_1=0.9968, thus θ_1=4.59 or -4.59°
R_{32}, c_2, and c_1 Note that $R_{32}=-s_1c_2$	$s_1= -(R_{32}/ c_2)$ and θ_1	s_1=-(0.0792/0.9999) If c_1>0, then $\theta_1=(s_1)^{-sin}$ (θ_1 in Q I or IV) If c_1<0, then θ_1=180-$(s_1)^{-sin}$ (θ_1=Q II or III)	s_1 = -0.0792, thus θ_1= -4.59°
R_{11} and c_2 Note that $R_{11}=c_2c_3$	$c_3=R_{11}/c_2$	c_3=0.9507/0.9999 c_3 >0 thus θ_3 in Q I or IV	c_3= 0.9509, thus θ_1=18.03 or -18.03°
R_{21} and c_2, and c_3 Note that $R_{21}=-c_2s_3$	$s_3=-(R_{21}/c_2)$	s_3=-(-0.3096/0.9999) If c_3>0 then $\theta_3=(s_3)^{-sin}$ (θ_3 in Q I or IV) If c_3<0 then θ_3=180- $(s_3)^{-sin}$ (θ_3=Q II or III)	s_3=0.3096, thus θ_3= 18.03°

*Note: *Calculations involving c2 always checked that $c_2 \neq 0$ because it would cause gimbal lock. Numbers used in this example are from the scan in wrist extension with forearm mid-pronation.*

2. Forearm Pronation/Supination Posture

A custom made Matlab program was used to describe forearm pronation/supination posture. This was done by describing the orientation of the ulnar CS with respect to the radial CS. A rotation matrix R_{ur} was calculated to align the ulnar CS with the radial CS, by obtaining the product of the two matrices that represented their respective coordinates in the global reference system (Eq. 20) as follows:

$$R_{ur} = \begin{bmatrix} x_{uNormx} & x_{uNormy} & x_{uNormz} \\ y_{uNormx} & y_{uNormy} & y_{uNormz} \\ z_{uNormx} & z_{uNormy} & z_{uNormz} \end{bmatrix} * \begin{bmatrix} x_{rNormx} & x_{rNormy} & x_{rNormz} \\ y_{rNormx} & y_{rNormy} & y_{rNormz} \\ z_{rNormx} & z_{rNormy} & z_{rNormz} \end{bmatrix}' \quad \text{(Eq. 20)}$$

Where: R_{ur} represents the rotation matrix to rotate the ulna to the radial CS.

The same xyz Euler angle sequence for wrist posture was used, thus Eq. 19 served to solve for θ_1, θ_2, and θ_3. . Note that only θ_2 was of interest because it represented rotation of the forearm (Table V.b).

B. Sample calculation used to determine forearm pronation/supination posture, using Euler angles to describe orientation of the ulnar CS with respect to the radial CS.

Used the following terms	**To calculate:**	**Notes:**	**Example** $R = \begin{bmatrix} R_{11} & R_{12} & R_{13} \\ R_{21} & R_{22} & R_{23} \\ R_{31} & R_{32} & R_{33} \end{bmatrix}$ $R = \begin{bmatrix} 0.7724 & 0.0000 & -0.6352 \\ 0.0000 & 1.0000 & 0.0000 \\ 0.6352 & 0.0000 & 0.7724 \end{bmatrix}$
$R_{31}=s_2$	s_2		s_2= 0. 6352
R_{11}	$c_2=R_{11}*c_3$	Note that c_3=1 due to shared y axis, thus $c_2=R_{11}$	c_2=0.7724
s_2 and c_2	θ_2	If c_2 and $s_2>0$ then $\theta_2=Sin^{-1}(s_2)$ (in Q I) if $c_2>0$ and $s_2<0$ then $\theta_2=Sin^{-1}(s_2)$ (Q IV). If $c_2<0$ and $s_2>0$ then $\theta_2=180 – Sin^{-1}(s_2)$ (Q II) if c_2 and $s_2<0$ then $\theta_2=-180-Sin^{-1}(s_2)$ (θ_2 in QIII).	θ_2=39.43°
R_{33} and c_2 Note: $R_{33}=c_1c_2$	$c_1 = R_{33}/ c_2$	c_1 = 0.7724/ 0.7724	c_1 =1
R_{32}, c_2, and c_1 Note that $R_{32}=-s_1c_2$	$s_1= -(R_{32}/ c_2)$ and θ_1	s_1=-(0.0000/0.7724) If $c_1>0$, then $\theta_1=Sin^{-1}(s_1)$ (θ_1 in QI or IV) If $c_1<0$, then $\theta_1=180-Sin^{-1}(s_1)$ (θ_1=Q II or III)	s_1 = 0.0000, thus θ_1= 0°
R_{11} and c_2 Note that $R_{11}=c_2c_3$	$c_3=R_{11}/c_2$	c_3=0.7724/0.7724 c_3 =1	c_3 =1, thus θ_3 =0°
R_{21} and c_2, and c_3 Note that $R_{21}=-c_2s_3$	$s_3=-(R_{21}/c_2)$	s_3=-(-0.3096/0.9999) If $c_3>0$ then $\theta_3=Sin^{-1}(s_3)$ (θ_3 in QI or IV) If $c_3<0$ then $\theta_3=180-Sin^{-1}(s_3)$, ($\theta_3$=Q II or III)	s_3=0.3096, thus θ_3= 18.03°

Note: Calculations involving c2 always checked that c2≠0 because it would cause gimbal lock. Numbers used in this example are from the scan in wrist extension with prone forearm.

3. Forearm Pronation/Supination Posture Normalization

Sample calculation to normalize each condition to the NM scan for each participant:

$$\theta_{2EP\_norm} = \theta_{2NM} - \theta_{2EP} \qquad \text{(Eq. 21)}$$

Where:

θ_{2EP_norm} represents the *normalized* forearm pronation/supination angle when the wrist *is extended with prone forearm*.

θ_{2NM} represents the *raw* forearm pronation/supination angle when the wrist *is straight with the forearm in mid-pronation*.

θ_{2EP} represents the *raw* forearm pronation/supination angle when the wrist *is extended with prone forearm*.

APPENDIX J

Calculations for centerline transformations from the global to the radial CS

In order to express tendon deviations anatomically, tendon centerlines were first translated to the radial CS's origin (RS) (Eq. 22) and then rotated to the radial CS (Eq. 23).

$$x_t y_t z_t = x_0 y_0 z_{0\_ct} - x_{rs} y_{rs} z_{rs} \qquad \text{(Eq. 22)}$$

Where:
$x_t y_t z_t$ represent the translated xyz centerline coordinates from the global CS to the radial CS.
$x_0 y_0 z_{0\_ct}$ represent the xyz centerline coordinates in the global CS of the MRI scanner.
$x_{rs} y_{rs} z_{rs}$ represent global coordinates of the radial styloid (RS), which is the origin of the radial CS.

$$\begin{bmatrix} x_{rt} \\ y_{rt} \\ z_{rt} \end{bmatrix} = \begin{bmatrix} x_{rNormx} & x_{rNormy} & x_{rNormz} \\ y_{rNormx} & y_{rNormy} & y_{rNormz} \\ z_{rNormx} & z_{rNormy} & z_{rNormz} \end{bmatrix} \begin{bmatrix} x_t \\ y_t \\ z_t \end{bmatrix} \qquad \text{(Eq. 23)}$$

Where:
$x_{rt} y_{rt} z_{rt}$ represent the translated and rotated xyz centerline coordinates from the global CS to the radial CS.
R_r represents the rotation matrix from the global to the radial CS, where each row of the matrix represents a component of the radial CS and each column represents the normalized xyz coordinates of such components.
$x_{rs} y_{rs} z_{rs}$ represent global coordinates of the radial styloid (RS), which is the origin of the radial CS.

APPENDIX K

Expanded explanation of line fitting through tendon centerlines

The initial line of fit was calculated as a line going from y=0 to y=15 along the tendon centerline. This was accomplished by developing parametric equations to identify the position vectors associated with each of these points as follows.

First, a direction vector was created from the tendon coordinate closest to the RS at y=0 (just proximal to it) to the closest tendon coordinate to y=15 (just distal from it) (~15mm proximal to the RS along the longitudinal axis of the forearm) (Eq. 24).

$$mdir = p_{cy15} - d_{cy0} \qquad \text{(Eq. 24)}$$

Where:
$mdir$ represents the direction vector between the two end points closest to y=0 and y=15 (pointing to y=15)
p_{cy15} represents the xyz coordinates of the point on the tendon centerline closest to y=15 (just distal from y=15)
d_{cy0} represents the xyz coordinates of the point on the tendon centerline closest to y=0 (just proximal from RS)

Secondly, two scalars (t) corresponding with points at y=0 and 15 along the tendon centerline were calculated using parametric equations, with the most proximal point on the centerline p_{cy15} and the direction vector ($mdir_y$) as inputs (Eq. 25a,b).

$$t_0 = -p_{cy15y}/mdir_y \quad \text{(Eq. 25a)}$$

$$t_{15} = p_{cy15y} - 15/mdir_y \quad \text{(Eq. 25b)}$$

Where:
t represents a scalar along the direction vector (subscripts 0 and 15 represent the scalar of the distal and proximal points respectively)
p_{cy15y} represents the y coordinate of the tendon centerline point identified closest to y=15
$mdir_y$ represents the y coordinate of the direction vector
Both, the scalars and the direction vector were used to identify the x and z coordinates at y=0 and 15 with other series of parametric equations as follows:

$$p_{0x} = p_{cy15x} + t_0 * mdir_x \quad \text{(Eq. 26a)}$$

$$p_{0z} = p_{cy15z} + t_0 * mdir_z \quad \text{(Eq. 26b)}$$

$$p_{15x} = p_{cy15x} + t_{15} * mdir_x \quad \text{(Eq. 26c)}$$

$$p_{15z} = p_{cy15z} + t_{15} * mdir_z \quad \text{(Eq. 26d)}$$

Where:
$p_{0x,0z,15x,15z}$ represent the x and z coordinates at y=0 and y=15 (defined by subscripts)
p_{c15} represent the tendon centerline x and z coordinates (defined by subscripts) of the point closest to y=15
t represents a scalar along the direction vector
$mdir_y$ represents the y coordinate of the direction vector

Subsequently, two 11x11mm grids were created (with 1mm squares) along the xz plane, at y=0 and y=15. The grids were created as $\pm$5mm along the x and z axes, from the points identified along the tendon centerline at y=0 and y=15. Then, the line was systematically translated and rotated, by connecting each of the points on the 1stgrid at y=0 to all of the points of the 2nd grid at y=15 (1mm increments along the x and z in both directions of each grid). This procedure required 11*11*11*11 iterations. For each line, the perpendicular deviations of each of the points of the original centerline from the segmented structure between y=0 and y=15 mm to the potential line of best fit were calculated using the Pythagorean Theorem. The average deviation of all points from the line (sum/# of points) was used as an estimate of the fit of each line. The xz coordinate pairs at y=0 and y=15 of the line with the lowest error were selected as the starting points for a second set of grids. The iterative procedure was repeated to translate and rotate the line using a finer grid, this time in 0.1mm increments from -0.5-0.5mm in the x and z directions around the beginning and end points of the line. The line with the lowest error was selected to calculate tendon displacements and changes in orientation.

APPENDIX L

Bonferroni pairwise comparisons per digit

Note: Pairwise comparisons of the effect of forearm and wrist posture on: sagittal displacements (x@y0), frontal displacements (z@y0), and frontal angular changes (yz frontal angle), for each digit, where significance was found. Measure 1 is equivalent to wrist posture effects, and Measure 2 equivalent to forearm posture effects.

FPL						
yz frontal angle						
Measure: MEASURE_2						
(I) forearm	(J) forearm	Mean Difference (I-J)	Std. Error	Sig.a	95% CI for Differencea	
					Lower Bound	Upper Bound
1	2	-0.328	2.221	1	-11.114	10.459
	3	-6.356	1.877	0.129	-15.471	2.76
2	1	0.328	2.221	1	-10.459	11.114
	3	-6.028	0.651	0.008	-9.191	-2.866
3	1	6.356	1.877	0.129	-2.76	15.471
	2	6.028	0.651	0.008	2.866	9.191
Based on estimated marginal means						
a Adjustment for multiple comparisons: Bonferroni.						
Measure 1= Wrist, 2= forearm						

FDS2						
x@y0						
Pairwise Comparisons						
Measure: MEASURE_1						
(I) wrist	(J) wrist	Mean Difference (I-J)	Std. Error	Sig.b	95% CI for Differenceb	
					Lower Bound	Upper Bound
1	2	1.365	0.588	0.309	-1.49	4.22
	3	4.703	0.956	0.048	0.057	9.348
2	1	-1.365	0.588	0.309	-4.22	1.49
	3	3.338	0.372	0.009	1.529	5.146
3	1	-4.703	0.956	0.048	-9.348	-0.057
	2	-3.338	0.372	0.009	-5.146	-1.529
Based on estimated marginal means						
* The mean difference is significant at the .05 level.						
b Adjustment for multiple comparisons: Bonferroni.						
Measure 1= Wrist, 2= forearm						
yz frontal angle						
Measure: MEASURE_2						
(I) forearm	(J) forearm	Mean Difference (I-J)	Std. Error	Sig.a	95% CI for Differencea	
					Lower Bound	Upper Bound
1	2	-1.427	1.513	1	-8.773	5.92
	3	-7.665	1.782	0.069	-16.322	0.992
2	1	1.427	1.513	1	-5.92	8.773
	3	-6.238	0.531	0.004	-8.815	-3.662
3	1	7.665	1.782	0.069	-0.992	16.322
	2	6.238	0.531	0.004	3.662	8.815
Based on estimated marginal means						
a Adjustment for multiple comparisons: Bonferroni.						
Measure 1= Wrist, 2= forearm						

FDP2						
yz frontal angle						
Pairwise Comparisons						
Measure: MEASURE_2						
(I) forearm	(J) forearm	Mean Difference (I-J)	Std. Error	Sig.a	95% CI for Differencea	
					Lower Bound	Upper Bound
1	2	-0.504	1.588	1	-8.217	7.209
	3	-4.581	1.771	0.244	-13.18	4.019
2	1	0.504	1.588	1	-7.209	8.217
	3	-4.077	0.567	0.017	-6.828	-1.325
3	1	4.581	1.771	0.244	-4.019	13.18
	2	4.077	0.567	0.017	1.325	6.828
Based on estimated marginal means						
a Adjustment for multiple comparisons: Bonferroni.						
Measure 1= Wrist, 2= forearm						

FDS3						
x@y0						
Pairwise Comparisons						
Measure: MEASURE_1						
(I) wrist	(J) wrist	Mean Difference (I-J)	Std. Error	Sig.b	95% CI for Differenceb	
					Lower Bound	Upper Bound
1	2	1.715	1.105	0.656	-3.653	7.083
	3	5.064	1.158	0.066	-0.558	10.687
2	1	-1.715	1.105	0.656	-7.083	3.653
	3	3.349	0.226	0.002	2.254	4.444
3	1	-5.064	1.158	0.066	-10.687	0.558
	2	-3.349	0.226	0.002	-4.444	-2.254
Based on estimated marginal means						
* The mean difference is significant at the .05 level.						
b Adjustment for multiple comparisons: Bonferroni.						
Measure 1= Wrist, 2= forearm						
z@y0						
Measure: MEASURE_2						
(I) forearm	(J) forearm	Mean Difference (I-J)	Std. Error	Sig.a	95% CI for Differencea	
					Lower Bound	Upper Bound
1	2	0.653	0.242	0.222	-0.523	1.829
	3	-2.777	0.632	0.065	-5.845	0.291
2	1	-0.653	0.242	0.222	-1.829	0.523
	3	-3.43	0.467	0.016	-5.699	-1.161
3	1	2.777	0.632	0.065	-0.291	5.845
	2	3.43	0.467	0.016	1.161	5.699
Based on estimated marginal means						
a Adjustment for multiple comparisons: Bonferroni.						
Measure 1= Wrist, 2= forearm						
yz frontal angle						
Measure: MEASURE_2						
(I) forearm	(J) forearm	Mean Difference (I-J)	Std. Error	Sig.a	95% CI for Differencea	
					Lower Bound	Upper Bound
1	2	-1.418	1.778	1	-10.054	7.219
	3	-7.978	1.836	0.067	-16.894	0.937
2	1	1.418	1.778	1	-7.219	10.054
	3	-6.561	0.418	0.002	-8.589	-4.533
3	1	7.978	1.836	0.067	-0.937	16.894
	2	6.561	0.418	0.002	4.533	8.589
Based on estimated marginal means						
a Adjustment for multiple comparisons: Bonferroni.						
Measure 1= Wrist, 2= forearm						

FDP3						
x@y0						
Pairwise Comparisons						
Measure: MEASURE_1						
(I) wrist	(J) wrist	Mean Difference (I-J)	Std. Error	Sig.b	95% CI for Differenceb	
					Lower Bound	Upper Bound
1	2	1.731	0.84	0.394	-2.349	5.811
	3	-0.05	0.591	1	-2.92	2.82
2	1	-1.731	0.84	0.394	-5.811	2.349
	3	-1.781	0.315	0.033	-3.311	-0.251
3	1	0.05	0.591	1	-2.82	2.92
	2	1.781	0.315	0.033	0.251	3.311
Based on estimated marginal means						
* The mean difference is significant at the .05 level.						
b Adjustment for multiple comparisons: Bonferroni.						
Measure 1= Wrist, 2= forearm						

FDS4						
x@y0						
Pairwise Comparisons						
Measure: MEASURE_1						
(I) wrist	(J) wrist	Mean Difference (I-J)	Std. Error	Sig.b	95% CI for Differenceb	
					Lower Bound	Upper Bound
1	2	1.209	0.624	0.445	-1.823	4.241
	3	3.897	0.908	0.07	-0.512	8.307
2	1	-1.209	0.624	0.445	-4.241	1.823
	3	2.688	0.345	0.013	1.012	4.364
3	1	-3.897	0.908	0.07	-8.307	0.512
	2	-2.688	0.345	0.013	-4.364	-1.012
Based on estimated marginal means						
* The mean difference is significant at the .05 level.						
b Adjustment for multiple comparisons: Bonferroni.						
Measure 1= Wrist, 2= forearm						
z@y0						
Measure: MEASURE_2						
(I) forearm	(J) forearm	Mean Difference (I-J)	Std. Error	Sig.a	95% CI for Differencea	
					Lower Bound	Upper Bound
1	2	-0.181	0.213	1	-1.213	0.852
	3	-3.356	0.465	0.016	-5.616	-1.096
2	1	0.181	0.213	1	-0.852	1.213
	3	-3.176	0.556	0.032	-5.875	-0.476
3	1	3.356	0.465	0.016	1.096	5.616
	2	3.176	0.556	0.032	0.476	5.875
Based on estimated marginal means						
a Adjustment for multiple comparisons: Bonferroni.						
Measure 1= Wrist, 2= forearm						
yz frontal angle						
Measure: MEASURE_2						
(I) forearm	(J) forearm	Mean Difference (I-J)	Std. Error	Sig.a	95% CI for Differencea	
					Lower Bound	Upper Bound
1	2	-0.378	1.43	1	-7.324	6.568
	3	-10.15	1.979	0.043	-19.761	-0.539
2	1	0.378	1.43	1	-6.568	7.324
	3	-9.772	0.623	0.002	-12.798	-6.746
3	1	10.15	1.979	0.043	0.539	19.761
	2	9.772	0.623	0.002	6.746	12.798
Based on estimated marginal means						
a Adjustment for multiple comparisons: Bonferroni.						
Measure 1= Wrist, 2= forearm						

FDP4						
x@y0						
Pairwise Comparisons						
Measure: MEASURE_1						
(I) wrist	(J) wrist	Mean Difference (I-J)	Std. Error	Sig.b	95% CI for Differenceb	
					Lower Bound	Upper Bound
1	2	0.454	0.618	1	-2.548	3.455
	3	2.716*	0.547	0.047	0.061	5.371
2	1	-0.454	0.618	1	-3.455	2.548
	3	2.263*	0.345	0.022	0.589	3.936
3	1	-2.716*	0.547	0.047	-5.371	-0.061
	2	-2.263*	0.345	0.022	-3.936	-0.589
Based on estimated marginal means						
* The mean difference is significant at the .05 level.						
b Adjustment for multiple comparisons: Bonferroni.						
Measure 1= Wrist, 2= forearm						
yz frontal angle						
Measure: MEASURE_2						
(I) forearm	(J) forearm	Mean Difference (I-J)	Std. Error	Sig.a	95% CI for Differencea	
					Lower Bound	Upper Bound
1	2	0.295	1.092	1	-5.01	5.6
	3	-6.931	1.623	0.071	-14.814	0.952
2	1	-0.295	1.092	1	-5.6	5.01
	3	-7.226	0.577	0.003	-10.026	-4.426
3	1	6.931	1.623	0.071	-0.952	14.814
	2	7.226	0.577	0.003	4.426	10.026
Based on estimated marginal means						
a Adjustment for multiple comparisons: Bonferroni.						
Measure 1= Wrist, 2= forearm						

FDP5						
x@y0						
Pairwise Comparisons						
Measure: MEASURE_1						
(I) wrist	(J) wrist	Mean Difference (I-J)	Std. Error	Sig.b	95% CI for Differenceb	
					Lower Bound	Upper Bound
1	2	1.384	0.776	0.517	-2.383	5.15
	3	4.708	1.066	0.065	-0.47	9.886
2	1	-1.384	0.776	0.517	-5.15	2.383
	3	3.324	0.439	0.014	1.194	5.454
3	1	-4.708	1.066	0.065	-9.886	0.47
	2	-3.324	0.439	0.014	-5.454	-1.194
Based on estimated marginal means						
* The mean difference is significant at the .05 level.						
b Adjustment for multiple comparisons: Bonferroni.						
Measure 1= Wrist, 2= forearm						
yz frontal angle						
Measure: MEASURE_2						
(I) forearm	(J) forearm	Mean Difference (I-J)	Std. Error	Sig.a	95% CI for Differencea	
					Lower Bound	Upper Bound
1	2	-0.371	1.275	1	-6.561	5.819
	3	-6.175	0.948	0.022	-10.779	-1.57
2	1	0.371	1.275	1	-5.819	6.561
	3	-5.804	1.233	0.054	-11.791	0.184
3	1	6.175	0.948	0.022	1.57	10.779
	2	5.804	1.233	0.054	-0.184	11.791
Based on estimated marginal means						
a Adjustment for multiple comparisons: Bonferroni.						
Measure 1= Wrist, 2= forearm						

APPENDIX M

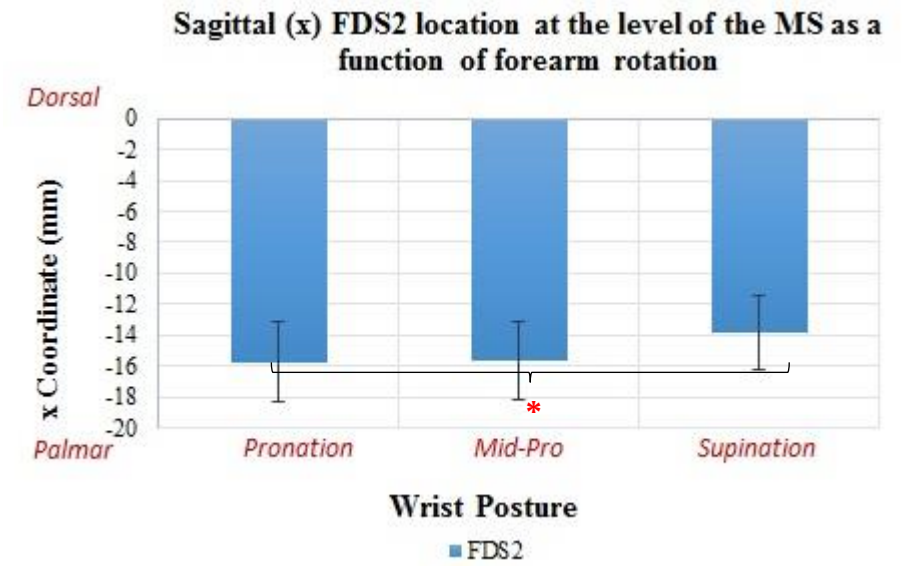

Figure M.1. Significant effects of forearm posture on sagittal FDS2 location at the level of the MS. Asterisk denotes significance at $p<0.05$ Bonferroni corrected for multiple comparisons. Error bars represent SD.

APPENDIX N

Bonferroni pairwise comparisons per digit

Note: Pairwise comparisons of the effect of forearm and wrist posture on: sagittal displacements (x at the level of MS), frontal displacements (z at the level of MS), and whole tendon angular changes in the frontal and sagittal planes, for each digit, where significance was found. Ordered per digit.

FDS2						
x@y of MS						
Pairwise Comparisons						
Measure: Wrist						
(I) wrist	(J) wrist	Mean Difference (I-J)	Std. Error	Sig.[b]	95% CI for Difference[b]	
					Lower Bound	Upper Bound
Ext	*Neut*	2.568	0.958	0.225	-2.084	7.221
	Flx	7.803	1.322	0.029	1.382	14.223
Neut	*Flx*	5.234	0.586	0.009	2.389	8.08
Based on estimated marginal means						
* The mean difference is significant at the .05 level.						
b Adjustment for multiple comparisons: Bonferroni.						
x@y of MS						
Measure: Forearm						
(I) forearm	(J) forearm	Mean Difference (I-J)	Std. Error	Sig.[a]	95% CI for Difference[a]	
					Lower Bound	Upper Bound
Pro	*Mid*	-0.125	0.308	1	-1.62	1.37
	Sup	-1.907	0.332	0.031	-3.517	-0.297
Mid	*Sup*	-1.782	0.556	0.148	-4.482	0.919
Based on estimated marginal means						
a Adjustment for multiple comparisons: Bonferroni.						

FDS2						
z@y of MS						
Pairwise Comparisons						
Measure: Forearm						
(I) forearm	(J) forearm	Mean Difference (I-J)	Std. Error	Sig.[b]	95% CI for Difference[b]	
					Lower Bound	Upper Bound
Pro	*Mid*	0.613	0.182	0.131	-0.273	1.499
	Sup	-2.137	0.516	0.077	-4.643	0.37
Mid	*Sup*	-2.75	0.654	0.074	-5.925	0.425
Based on estimated marginal means						
* The mean difference is significant at the .05 level.						
b Adjustment for multiple comparisons: Bonferroni.						

FDS2						
Sagittal Tendon Angle						
Pairwise Comparisons						
Measure: Wrist						
(I) wrist	(J) wrist	Mean Difference (I-J)	Std. Error	Sig.[b]	95% CI for Difference[b]	
					Lower Bound	Upper Bound
Ext	*Neut*	8.983	1.992	0.061	-0.691	18.658
	Flx	21.725	2.564	0.01	9.272	34.178
Neut	*Flx*	12.742	1.534	0.011	5.29	20.193
Based on estimated marginal means						
* The mean difference is significant at the .05 level.						
b Adjustment for multiple comparisons: Bonferroni.						

FDS2						
Frontal Tendon Angle						
Pairwise Comparisons						
Measure: Wrist						
(I) wrist	(J) wrist	Mean Difference (I-J)	Std. Error	Sig.[b]	95% CI for Difference[b]	
					Lower Bound	Upper Bound
Ext	*Neut*	7.108	0.419	0.001	5.073	9.144
	Flx	4.45	1.703	0.238	-3.82	12.72
Neut	*Flx*	-2.658	1.301	0.401	-8.978	3.661
Based on estimated marginal means						
* The mean difference is significant at the .05 level.						
b Adjustment for multiple comparisons: Bonferroni.						
Frontal Tendon Angle						
Measure: Forearm						
(I) forearm	(J) forearm	Mean Difference (I-J)	Std. Error	Sig.[b]	95% CI for Difference[b]	
					Lower Bound	Upper Bound
Pro	*Mid*	-3.492	1.506	0.31	-10.806	3.822
	Sup	-9.2	2.189	0.074	-19.833	1.433
Mid	*Sup*	-5.708	0.921	0.025	-10.182	-1.234
Based on estimated marginal means						
* The mean difference is significant at the .05 level.						
b Adjustment for multiple comparisons: Bonferroni.						

FDP2						
x@y of MS						
Pairwise Comparisons						
Measure: Wrist						
(I) wrist	(J) wrist	Mean Difference (I-J)	Std. Error	Sig.[b]	95% CI for Difference[b]	
					Lower Bound	Upper Bound
Ext	*Neut*	1.933	1.016	0.46	-3.002	6.867
	Flx	7.449	1.533	0.05	0.004	14.895
Neut	*Flx*	5.517	0.815	0.02	1.56	9.474
Based on estimated marginal means						
* The mean difference is significant at the .05 level.						
b Adjustment for multiple comparisons: Bonferroni.						

FDP2						
Sagittal Tendon Angle						
Pairwise Comparisons						
Measure: Wrist						
(I) wrist	(J) wrist	Mean Difference (I-J)	Std. Error	Sig.[b]	95% CI for Difference[b]	
					Lower Bound	Upper Bound
Ext	*Neut*	11.242	1.794	0.025	2.528	19.956
	Flx	23.617	2.159	0.005	13.133	34.1
Neut	*Flx*	12.375	1.784	0.018	3.709	21.041
Based on estimated marginal means						
* The mean difference is significant at the .05 level.						
b Adjustment for multiple comparisons: Bonferroni.						

FDP2						
Frontal Tendon Angle						
Pairwise Comparisons						
Measure: Forearm						
(I) forearm	(J) forearm	Mean Difference (I-J)	Std. Error	Sig.[b]	95% CI for Difference[b]	
					Lower Bound	Upper Bound
Pro	*Mid*	-2.683	2.201	0.93	-13.375	8.008
	Sup	-11.475	3.003	0.095	-26.057	3.107
Mid	*Sup*	-8.792	1.962	0.062	-18.323	0.739
Based on estimated marginal means						
* The mean difference is significant at the .05 level.						
b Adjustment for multiple comparisons: Bonferroni.						

FDS3						
x@y of MS						
Pairwise Comparisons						
Measure: Wrist						
(I) wrist	(J) wrist	Mean Difference (I-J)	Std. Error	Sig.[b]	95% CI for Difference[b]	
					Lower Bound	Upper Bound
Ext	*Neut*	2.468	1.512	0.60	-4.875	9.812
	Flx	8.069	1.434	0.03	1.103	15.036
Neut	*Flx*	5.601	0.411	0.00	3.604	7.598
Based on estimated marginal means						
* The mean difference is significant at the .05 level.						
b Adjustment for multiple comparisons: Bonferroni.						

FDS3						
z@y of MS						
Pairwise Comparisons						
Measure: Forearm						
(I) forearm	(J) forearm	Mean Difference (I-J)	Std. Error	Sig.[b]	95% CI for Difference[b]	
					Lower Bound	Upper Bound
Pro	*Mid*	0.451	0.312	0.73	-1.064	1.966
	Sup	-2.49	0.61	0.08	-5.453	0.473
Mid	*Sup*	-2.941	0.513	0.03	-5.43	-0.452
Based on estimated marginal means						
* The mean difference is significant at the .05 level.						
b Adjustment for multiple comparisons: Bonferroni.						

FDS3						
Sagittal Tendon Angle						
Pairwise Comparisons						
Measure: Wrist						
(I) wrist	(J) wrist	Mean Difference (I-J)	Std. Error	Sig.[b]	95% CI for Difference[b]	
					Lower Bound	Upper Bound
Ext	*Neut*	6.9	1.989	0.12	-2.76	16.56
	Flx	21.217	3.051	0.02	6.4	36.034
Neut	*Flx*	14.317	1.117	0.00	8.891	19.742
Based on estimated marginal means						
* The mean difference is significant at the .05 level.						
b Adjustment for multiple comparisons: Bonferroni.						

FDS3						
Frontal Tendon Angle						
Pairwise Comparisons						
Measure: Wrist						
(I) wrist	(J) wrist	Mean Difference (I-J)	Std. Error	Sig.[b]	95% CI for Difference[b]	
					Lower Bound	Upper Bound
Ext	*Neut*	4.633	1.035	0.06	-0.392	9.658
	Flx	1.333	1.026	0.85	-3.649	6.316
Neut	*Flx*	-3.3	1.222	0.22	-9.235	2.635
Based on estimated marginal means						
* The mean difference is significant at the .05 level.						
b Adjustment for multiple comparisons: Bonferroni.						
Frontal Tendon Angle						
Measure: Forearm						
(I) forearm	(J) forearm	Mean Difference (I-J)	Std. Error	Sig.[b]	95% CI for Difference[b]	
					Lower Bound	Upper Bound
Pro	*Mid*	-3.533	1.759	0.42	-12.077	5.01
	Sup	-10.425	2.47	0.07	-22.423	1.573
Mid	*Sup*	-6.892	1.306	0.04	-13.233	-0.551
Based on estimated marginal means						
* The mean difference is significant at the .05 level.						
b Adjustment for multiple comparisons: Bonferroni.						

FDP3						
x@y of MS						
Pairwise Comparisons						
Measure: Wrist						
(I) wrist	(J) wrist	Mean Difference (I-J)	Std. Error	Sig.[b]	95% CI for Difference[b]	
					Lower Bound	Upper Bound
Ext	*Neut*	1.743	1.096	0.63	-3.577	7.064
	Flx	6.53	1.065	0.03	1.358	11.702
Neut	*Flx*	4.787	0.257	0.00	3.538	6.035
Based on estimated marginal means						
* The mean difference is significant at the .05 level.						
b Adjustment for multiple comparisons: Bonferroni.						

FDP3						
Sagittal Tendon Angle						
Pairwise Comparisons						
Measure: Wrist						
(I) wrist	(J) wrist	Mean Difference (I-J)	Std. Error	Sig.[b]	95% CI for Difference[b]	
					Lower Bound	Upper Bound
Ext	*Neut*	11.075	3.58	0.16	-6.311	28.461
	Flx	27.492	4.769	0.03	4.332	50.651
Neut	*Flx*	16.417	1.457	0.00	9.341	23.492
Based on estimated marginal means						
* The mean difference is significant at the .05 level.						
b Adjustment for multiple comparisons: Bonferroni.						

FDP3						
Frontal Tendon Angle						
Pairwise Comparisons						
Measure: Wrist						
(I) wrist	(J) wrist	Mean Difference (I-J)	Std. Error	Sig.[b]	95% CI for Difference[b]	
					Lower Bound	Upper Bound
Ext	*Neut*	5.25	0.911	0.03	0.826	9.674
	Flx	0.908	1.619	1.00	-6.956	8.773
Neut	*Flx*	-4.342	0.99	0.07	-9.147	0.464
Based on estimated marginal means						
* The mean difference is significant at the .05 level.						
b Adjustment for multiple comparisons: Bonferroni.						
Frontal Tendon Angle						
Measure: Forearm						
(I) forearm	(J) forearm	Mean Difference (I-J)	Std. Error	Sig.[b]	95% CI for Difference[b]	
					Lower Bound	Upper Bound
Pro	*Mid*	0.375	1.159	1.00	-5.254	6.004
	Sup	-8.842	1.754	0.05	-17.363	-0.321
Mid	*Sup*	-9.217	1.061	0.01	-14.369	-4.064
Based on estimated marginal means						
* The mean difference is significant at the .05 level.						
b Adjustment for multiple comparisons: Bonferroni.						

FDS4						
x@y of MS						
Pairwise Comparisons						
Measure: Wrist						
(I) wrist	(J) wrist	Mean Difference (I-J)	Std. Error	Sig.[b]	95% CI for Difference[b]	
					Lower Bound	Upper Bound
Ext	*Neut*	2.103	0.994	0.37	-2.726	6.933
	Flx	7.146	1.168	0.03	1.472	12.82
Neut	*Flx*	5.043	0.515	0.01	2.539	7.546
Based on estimated marginal means						
* The mean difference is significant at the .05 level.						
b Adjustment for multiple comparisons: Bonferroni.						

FDS4						
z@y of MS						
Pairwise Comparisons						
Measure: Forearm						
(I) forearm	(J) forearm	Mean Difference (I-J)	Std. Error	Sig.[b]	95% CI for Difference[b]	
					Lower Bound	Upper Bound
Pro	*Mid*	0.133	0.276	1.00	-1.207	1.472
	Sup	-1.225	0.472	0.24	-3.517	1.067
Mid	*Sup*	-1.358	0.464	0.18	-3.613	0.898
Based on estimated marginal means						
* The mean difference is significant at the .05 level.						
b Adjustment for multiple comparisons: Bonferroni.						

FDS4						
Sagittal Tendon Angle						
Pairwise Comparisons						
Measure: Wrist						
(I) wrist	(J) wrist	Mean Difference (I-J)	Std. Error	Sig.[b]	95% CI for Difference[b]	
					Lower Bound	Upper Bound
Ext	*Neut*	9.058	2.656	0.13	-3.843	21.96
	Flx	25.067	3.273	0.01	9.173	40.96
Neut	*Flx*	16.008	1.153	0.00	10.409	21.608
Based on estimated marginal means						
* The mean difference is significant at the .05 level.						
b Adjustment for multiple comparisons: Bonferroni.						

FDS4						
Frontal Tendon Angle						
Pairwise Comparisons						
Measure: Wrist						
(I) wrist	(J) wrist	Mean Difference (I-J)	Std. Error	Sig.[b]	95% CI for Difference[b]	
					Lower Bound	Upper Bound
Ext	*Neut*	3.642	1.714	0.37	-4.685	11.968
	Flx	-1.075	1.803	1.00	-9.834	7.684
Neut	*Flx*	-4.717	0.87	0.04	-8.944	-0.49
Based on estimated marginal means						
* The mean difference is significant at the .05 level.						
b Adjustment for multiple comparisons: Bonferroni.						
Frontal Tendon Angle						
Measure: Forearm						
(I) forearm	(J) forearm	Mean Difference (I-J)	Std. Error	Sig.[b]	95% CI for Difference[b]	
					Lower Bound	Upper Bound
Pro	*Mid*	-1.192	1.516	1.00	-8.552	6.169
	Sup	-10.792	1.918	0.03	-20.104	-1.479
Mid	*Sup*	-9.6	1.123	0.01	-15.055	-4.145
Based on estimated marginal means						
* The mean difference is significant at the .05 level.						
b Adjustment for multiple comparisons: Bonferroni.						

FDP4						
x@y of MS						
Pairwise Comparisons						
Measure: Wrist						
(I) wrist	(J) wrist	Mean Difference (I-J)	Std. Error	Sig.[b]	95% CI for Difference[b]	
					Lower Bound	Upper Bound
Ext	*Neut*	2.636	1.207	0.35	-3.224	8.496
	Flx	7.698	1.162	0.02	2.052	13.343
Neut	*Flx*	5.062	0.494	0.01	2.664	7.46
Based on estimated marginal means						
* The mean difference is significant at the .05 level.						
b Adjustment for multiple comparisons: Bonferroni.						

FDP4						
Sagittal Tendon Angle						
Pairwise Comparisons						
Measure: Wrist						
(I) wrist	(J) wrist	Mean Difference (I-J)	Std. Error	Sig.[b]	95% CI for Difference[b]	
					Lower Bound	Upper Bound
Ext	*Neut*	9.233	3.06	0.17	-5.628	24.095
Neut	*Ext*	-9.233	3.06	0.17	-24.095	5.628
	Neut	-15.45	1.548	0.01	-22.967	-7.933
Based on estimated marginal means						
* The mean difference is significant at the .05 level.						
b Adjustment for multiple comparisons: Bonferroni.						

FDP4						
Frontal Tendon Angle						
Measure: Forearm						
(I) forearm	(J) forearm	Mean Difference (I-J)	Std. Error	Sig.[b]	95% CI for Difference[b]	
					Lower Bound	Upper Bound
Pro	*Mid*	0.008	1.237	1.00	-6.001	6.017
	Sup	-9.558	0.791	0.00	-13.399	-5.718
Mid	*Sup*	-9.567	0.537	0.00	-12.173	-6.96
Based on estimated marginal means						
* The mean difference is significant at the .05 level.						
b Adjustment for multiple comparisons: Bonferroni.						

FDP5						
x@y of MS						
Pairwise Comparisons						
Measure: Wrist						
(I) wrist	(J) wrist	Mean Difference (I-J)	Std. Error	Sig.[b]	95% CI for Difference[b]	
					Lower Bound	Upper Bound
Ext	*Neut*	2.922	1.215	0.29	-2.981	8.824
	Flx	8.092	1.372	0.03	1.43	14.754
Neut	*Flx*	5.17	0.607	0.01	2.22	8.12
Based on estimated marginal means						
* The mean difference is significant at the .05 level.						
b Adjustment for multiple comparisons: Bonferroni.						

FDP5						
Sagittal Tendon Angle						
Pairwise Comparisons						
Measure: Wrist						
(I) wrist	(J) wrist	Mean Difference (I-J)	Std. Error	Sig.[b]	95% CI for Difference[b]	
					Lower Bound	Upper Bound
Ext	*Neut*	6.367	2.422	0.24	-5.394	18.128
	Flx	23.167	4.926	0.06	-0.757	47.09
Neut	*Flx*	16.8	4.28	0.09	-3.988	37.588
Based on estimated marginal means						
* The mean difference is significant at the .05 level.						
b Adjustment for multiple comparisons: Bonferroni.						

FDP5						
Frontal Tendon Angle						
Measure: Forearm						
(I) forearm	(J) forearm	Mean Difference (I-J)	Std. Error	Sig.[b]	95% CI for Difference[b]	
					Lower Bound	Upper Bound
Pro	*Mid*	-1.342	1.915	1.00	-10.643	7.959
	Sup	-8.042	0.655	0.00	-11.225	-4.859
Mid	*Sup*	-6.7	2.153	0.16	-17.155	3.755
Based on estimated marginal means						
* The mean difference is significant at the .05 level.						
b Adjustment for multiple comparisons: Bonferroni.						